ABSTRACT

Title of dissertation: A MACROSCALE PERSPECTIVE OF NEAR-EQUILIBRIUM RELAXATION OF STEPPED CRYSTAL SURFACES

John Quah, Ph.D. 2009

Dissertation directed by: Professor Dionisios Margetis
Department of Mathematics
Institute for Physical Science and Technology

Crystal surfaces serve a crucial function as building blocks in small electronic devices, especially for mobile communications technology and photovoltaics. In the history of computing, for example, a crucial innovation that hastened the demise of vacuum tube computers was the etching of patterns on surfaces of semiconductor materials, which led to the integrated circuit. These early procedures typically worked with the materials at very high temperatures, where the thermally rough surface could be modeled from the perspective of continuum thermodynamics. More recently, with the drive towards smaller devices and the accompanying reduction of the lifetime of surface features, manufacturing conditions for the shaping of crystal surfaces have shifted to lower temperatures. At these lower temperatures the surface is no longer rough. In order to describe an evolving surface under typical experimental conditions today, we need to consider the processes that take place at the nanoscale.

Nanoscale descriptions of surface evolution start with the motion of adsorbed atoms (adatoms). Because of their large numbers, the concentration of adatoms is a meaningful object to study. Restricted to certain bounded regions of the surface, the adatom concentration satisfies a diffusion equation. At the boundaries between these regions, the hopping of adatoms is governed by kinetic laws. Real-time obser-

vation of these nanoscale processes is difficult to achieve, and experimentalists have had to devise creative methods for inferring the relevant energy barriers and kinetic rates. In contrast, the real-time observation of macroscale surface evolution can be achieved with simpler imaging techniques. Motivated by the possibility of experimental validation, we derive an equation for the macroscale surface height, which is consistent with the motion of adatoms. We hope to inspire future comparison with experiments by reporting the novel results of simulating the evolution of the macroscale surface height.

Many competing models have been proposed for the diffusion and kinetics of adatoms. Due to the difficulty of observing adatom motion at the nanoscale, few of the competing models can be dismissed outright for failure to capture the observed behavior. This dissertation takes a few of the nanoscale models and systematically derives the corresponding macroscopic evolution laws, of which some are implemented numerically to provide data sets for connection with experiments. For the modeling component of this thesis, I study the effect of anisotropic adatom diffusion at the nanoscale, the inclusion of an applied electric field, the desorption of adatoms, and the extension of linear kinetics in the presence of step permeability. Analytical conjectures based on the macroscale evolution equation are presented. For the numerical component of this thesis, I select a few representative simulations using the finite element method to illustrate the most salient features of the surface evolution.

A MACROSCALE PERSPECTIVE OF NEAR-EQUILIBRIUM RELAXATION OF STEPPED CRYSTAL SURFACES

by

John Quah

Dissertation submitted to the Faculty of the Graduate School of the
University of Maryland, College Park in partial fulfillment
of the requirements for the degree of
Doctor of Philosophy
2009

Advisory Committee:
Professor Dionisios Margetis, Chair/Advisor
Professor Ricardo Nochetto
Professor Manoussos Grillakis
Professor Theodore Einstein
Professor Janice Reutt-Robey

Dedication

To M. Z., who taught me to leave bridges intact and encouraged me to repair the ones I burned in moments of impulsiveness.

Acknowledgments

I owe my gratitude to all the people who have made this thesis possible and without whom my perseverence in the graduate program might not have endured six turbulent years.

First and foremost I'd like to thank my advisor, Professor Dionisios Margetis (Dio), who presented me with challenging research problems and equipped me with the specialized techniques needed to solve them. If I had not been daring enough to enroll in his course on advanced analytical methods the first time he taught it at Maryland (Spring 2007), this collaboration and the resulting thesis might never have taken off. Apart from being an invaluable source of mathematical knowledge, Dio also made a special effort to involve me in the conferences and workshops he organized. These meetings brought me in contact with a larger network of research scientists and mathematicians, whose examples inspired me to pursue my own thesis problem with more alacrity. The professional training I received under Dio's supervision greatly exceeded any expectations I had upon entering the graduate program.

Other faculty at the University of Maryland deserve credit for their role in the development of this thesis. Thanks to Professor Georg Dolzmann, whose course in numerical analysis imparted an appreciation for the beauty of the field. Thanks to Professors Eugenia Kalnay, Da-Lin Zhang, and Jim Carton for making accessible to applied mathematics students the world of atmospheric and oceanic science, along with the quantitative tools needed to understand the interactions among processes

at different time and length scales. Professors Stuart Antman, Manoussos Grillakis, and Matei Machedon conveyed their knowledge of partial differential equations and nonlinear analysis with exceptional clarity.

I am particularly indebted to several faculty in physics, chemistry, and materials science. Professor Ted Einstein of the Physics Department co-organized a research interaction team (RIT) with Dio and Professor Tzavaras in the spring of 2008. This series featured many informative lectures and also gave me the opportunity to practice my own blackboard presentation skills. Professor Einstein continued to provide guidance and physical intuition as my thesis research progressed into new areas. Similarly, conversations with Professor John Weeks of the Chemistry Department and IPST[1], and with Professor Ray Phaneuf of the Materials Science and Engineering Department, helped point out some of the problems I would face in connecting my theoretical investigations with real materials. Professor Janice Reutt-Robey of the Chemistry Department has been gracious with her time by offering to serve as the Dean's Representative on my thesis defense committee.

I also appreciate the financial support of the Monroe Martin Graduate Fellowship in summer 2008, which would not have come to my attention were it not for Professor Jim Yorke of the Mathematics Department and IPST. Professors Einstein and Margetis wrote the letters to nominate me for this stipend. During that summer, collaboration with Dio and the REU student Jerrod Young led to my first publication in Physical Review E.

My own undergraduate research experience, working out a problem in the

[1]Institute of Physical Science and Technology

mathematics of composite materials under the guidance of Professor Yury Grabovsky of Temple University, was decisive in encouraging me to pursue a graduate degree in applied mathematics. Little did I know at the time that a colleague of one of Professor Grabovsky's collaborators would eventually supervise my thesis, after first introducing me to interesting mathematical problems motivated by a different branch of materials science. Other faculty who deserve mention for their helpful discussions are Bob Kohn of New York University, Joachim Krug of the Institute for Theoretical Physics (Universität Köln), John Venables of Arizona State University, Jonah Erlebacher of Johns Hopkins University, Jim Evans of Iowa State University, and Richard James of the University of Minnesota.

I am grateful to Dr. Alex Prasertchoung of MRSEC[2] for pushing me to be a mentor for the AIP[3] Student Science Conference (a truly rewarding experience, not least because I got to see how much talent and fluid intelligence today's middle school students possess), and for pushing me around on the tennis court. I also had the good fortune of receiving financial support from MRSEC through grant NSF-MRSEC DMR0520471 during the spring of 2009, for which I thank Professor Ellen Williams, director of the UMD MRSEC. By sheer coincidence, I happened to be finalizing my thesis precisely when the NSF[4] was scheduled to conduct a site visit at the UMD MRSEC. Professor Williams invited me to present a poster at the site visit, which gave me the rare opportunity to have my work scrutinized in person by scientists from outside Maryland.

[2]Materials Research Science and Engineering Center

[3]American Institute of Physics

[4]National Science Foundation

Among all the faculty behind this thesis, Professor Ricardo Nochetto deserves recognition for sharing his extensive knowledge of the finite element method, both in private discussions and in a formal classroom context. For his patience with me in the latter setting, in a semester which challenged my management of time among such disparate tasks as thesis writing, teaching and grading, work at the food co-op, organizing numerical simulations, and finishing up a paper for publication, Professor Nochetto can hardly be thanked enough. Collaboration with him and his former postdoc, Andrea Bonito, always went smoothly, despite the differing perspectives we brought as mathematical modelers and numerical analysts.

The staff of the math department also offered just the right degree of support, without drowning me in paperwork or other bureaucratic hurdles. Alverda McCoy of the AMSC[5] program has been ever helpful with registration issues and completion of forms along the road to graduation. Mark Tilmes graciously applied his computer expertise to maintain all the software I needed for the numerical portion of this thesis. Bill Schildknecht accommodated several last-minute requests to change my teaching assignment, no small feat considering how many courses and other graduate teaching assistants were potentially affected.

For their support in my personal life, the following people deserve a word of thanks. David Shoup, Carter Price, J. C. Flake, Charles Glover, Chris Manon, Jeff Heath, Avanti Athreya, Ryan Janicki, Toni Watson, I-Kun Chen, and other occupants of "the Zoo" in 2003 helped with my acclimation to graduate life. Chris Zorn, David Bourne, Seba Pauletti, J. T. Halbert, and other more advanced graduate stu-

[5]Applied Mathematics, Statistics, and Scientific Computation

dents showed by example how to balance work and play while still making adequate progress toward a finished thesis. Dr. Jonathan Kandell of the Counseling Center offered some much-needed relief when relations among peers became strained. Under the care of Dr. Stephen Feinberg, my astigmatic eyes received the proper corrective lenses and vision therapy to enable two years of intense near-focus work. Dr. Robert Delong and the neurosurgeons at Duke University Medical Center were instrumental in curing me of epilepsy. Dr. James Wainer of Raleigh, NC, and Dr. Eric Griffey of Lewiston, ME, kept me on psychotropic drugs long enough to delay until graduate school the broadening of social and intellectual horizons that I should have experienced in my undergraduate years.

I also thank the badminton club and its dedicated faculty sponsor, Professor Peter Teuben, for providing access to a fun-filled team sport and a supportive environment on the many occassions when I needed to release frustrations. On my very first visit to the badminton club, I made contact with one person in particular, whose friendship led to many learning experiences in disciplines ranging from the humanities to the fine arts. This friendship finally culminated in the healing of a rift between me and the Maryland Food Co-op, where I have worked or volunteered since summer 2007. The community of workers and volunteers at the food co-op has kept me anchored and well-nourished throughout the hectic two years of working on my thesis.

Finally, I'd like to thank my family for providing a loving and nurturing environment throughout my formative years. Their continued support during graduate school has not gone unnoticed, although I have not always made the time to recip-

rocate and keep in touch with them. When I emerge from the tunnel vision that will allow me to see the thesis through to the end, my parents deserve to be the first to hear that I'm still alive.

Table of Contents

List of Abbreviations

symbol	**meaning**	**dimensions**
α	aspect ratio of a biperiodic height profile	
λ_x, λ_y	characteristic lengths at the macroscale	length
a	atomic height	length
h	macroscale surface height	length
$\mathbf{r}$	position vector in the (x, y) plane	length
η	transverse step coordinate	
η_i	transverse coordinate of the ith step	
σ	longitudinal step coordinate	
ξ_η	metric coefficient along η	length
ξ_σ	metric coefficient along σ	length
m_i	discrete step density	
E	surface free energy	energy
γ	free energy density	energy/length^2
β	step stiffness	energy/length
g_1	line tension coefficient	energy/length^2
g_3	step interaction coefficient	energy/length^2
C_i	adatom density on the ith terrace	1/length^2
C	macroscale adatom density	1/length^2
C_i^{eq}	equilibrium adatom density at the ith step	1/length^2
C_s	straight step equilibrium adatom density	1/length^2
D, D^{ad}	terrace adatom diffusivity (boldface=tensor)	length^2/time
D^{ed}	edge atom diffusivity	length^2/time
J^{ad}	terrace adatom flux	1/(length·time)
J^{ed}	edge atom flux	1/(length·time)
J	macroscale adatom flux	1/(length·time)
k, k_u, k_d	kinetic rates of attachment/detachment	length/time
M	macroscale mobility (boldface=tensor)	length^2/(energy·time)
$\mathbf{\Lambda}$	dimensionless mobility tensor	
μ_i	chemical potential of the ith step	energy
μ	macroscale chemical potential	energy
q	material parameter comparing diffusion to attachment/detachment	
T	temperature	temperature
$\mathbf{v}$	adatom drift velocity	length/time
$\mathbf{u}$	nondimensionalized drift velocity	
$\mathbf{E}$	electric field	energy/(charge·length)
Z^*e	effective charge of adatoms	charge
Ω	atomic volume	length^3

Chapter 1

Introduction

1.1 Chapter overview

In this chapter, we will introduce the basic principles of the near-equilibrium morphological evolution of crystal surfaces. Depending on the length scale under consideration, these surfaces present different physical pictures to the viewer. To capture the relevant physics of these experimental pictures, mathematical models make certain simplifying assumptions about the operative mechanisms at each length scale. The different mathematical models are typically analyzed independently of one another. In this chapter, we emphasize the *connections* between models at different length scales. These connections constitute the primary focus of the next few chapters. Finally, we outline the main results of this thesis, indicating how this work contributes to the ongoing effort to understand and exploit the physical mechanisms that govern the evolution of crystal surfaces.

1.2 Physical description of surfaces at various length scales

There are three distinct scales for crystal surfaces: atomistic scale, nanoscale, and macroscale. A typical picture on the atomistic scale has individually distinguishable atoms arranged periodically in a crystal lattice. The atomistic picture

of a *surface* has atoms with missing bonds at the solid-vapor interface. The more missing bonds these surface atoms have, the rougher the resulting height profile looks.

At the nanoscale, the viewer can identify not the individual atoms, but only the extended surface features they form in aggregate. Just as a viewer from an airplane can see the Great Wall of China but not its individual stones, the nanoscale viewer of crystal surfaces can see the meandering lines formed by a large number of surface atoms at one height, adjacent to a large number of surface atoms at a different height. These line defects are called *steps*, since they appear at the boundary between two regions whose heights differ by a lattice constant. From the perspective of the nanoscale viewer, the steps resemble smooth curves. For this viewer, the fact that steps can be counted individually is the only clue that the microscope is showing an essentially discrete object.

At the macroscale, all clues of discreteness are taken away, and the viewer is left with what looks like a smooth topography. Until the mid-20th century, this resolution was the only one accessible to experimentalists. However, the *mental* picture of a discrete lattice structure was always available, and it helped establish a framework for thinking about crystal surfaces.

1.3 Mathematical models of various length scales

One possible mathematical approach to the atomistic scale is to seek approximate solutions of the many-body Schroedinger equation for electrons and nuclei

[121]. These approximate solutions are valid over prohibitively short time scales, which impedes most attempts to reconcile the motion of individual atoms with coarser descriptions of the surface. By allowing for atomic motions governed by classical mechanics, rather than quantum mechanics, Vvedensky and Haselwandter [121] sought a connection between atomistic models and the nanoscale. This connection lies outside our present scope.

In this thesis, we study analytical and numerical aspects of the connection between nanoscale and macroscale. The nanoscale model assumes that steps move in response to (i) adatom attachment/detachment at step edges, (ii) diffusion of adatoms on terraces, and (iii) energetic interactions between steps. This description of the microscopic physics, introduced in a simplified form by Burton, Cabrera, and Frank (BCF) [10], serves as the basis for our present discussion of surface morphological evolution. The BCF model and its generalizations support a rich variety of step dynamics. The patterns that emerge during surface evolution have motivated analytical and numerical attempts to understand what experimentalists observe based on the behavior of steps.

The temperature below which the BCF model applies is called the roughening temperature, T_R. Thermal wandering of steps is allowed below T_R, but the steps themselves are stable objects, not momentary deviations from surface flatness. Above T_R, creation of a step has zero free energy cost, and steps are created and destroyed spontaneously. Not only steps, but also point defects such as vacancies can be present on the surface. This roughening indicates that a description of the surface in terms of steps is not appropriate. A rough surface is more easily visualized

Figure 1.1: The stepped surface of Si(001) as seen through an STM, taken from [99].

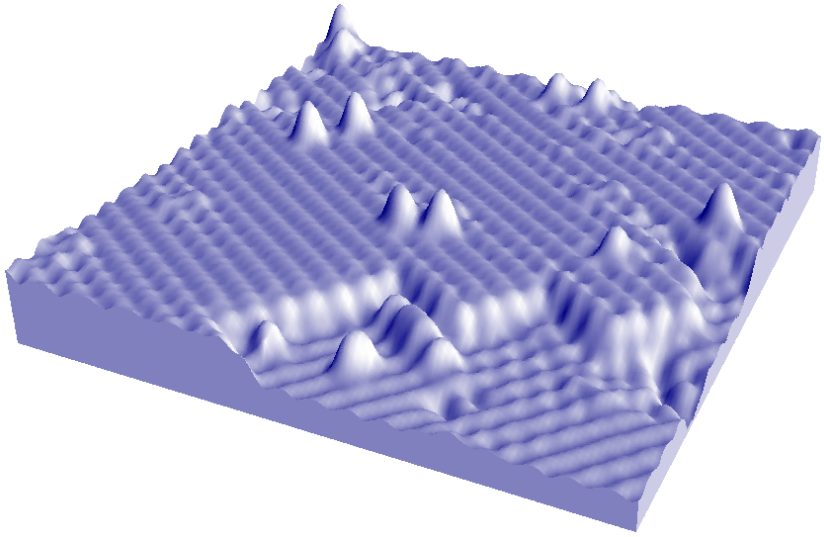

at the atomistic scale, where bonds between atoms at the surface are broken and formed at random.

The macroscopic theory of Herring and Mullins [34, 75], based on continuum thermodynamics and mass conservation, accurately predicts the observed behavior of surfaces above the roughening temperature. However, the fabrication of crystal surface morphologies is no longer restricted to temperatures above T_R, which challenges the validity of the continuum theory of Herring and Mullins.

Following the trend toward miniaturization of semiconductor devices, the length scales on which crystal surfaces are patterned have grown smaller, necessitating lower temperatures so that the desired pattern is more stable. These lower temperatures require a macroscale theory consistent with the flow of thermally stable steps.

Figure 1.1 shows the surface of Si(001) as seen through a Scanning Tunneling Microscope (STM). We can identify terraces where the surface is locally flat, except

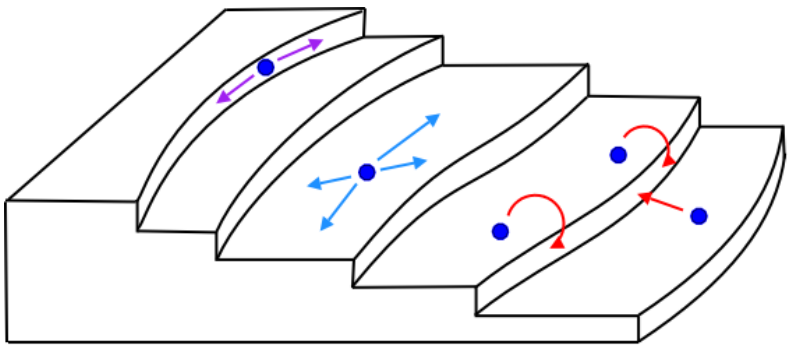

Figure 1.2: Schematic of curved crystal steps on a vicinal surface. The arrows represent the different physical processes through which adatoms affect the flow of steps.

for a few isolated bumps and vacancies of size about 3 Å(one lattice constant). The line defects bounding the terraces are steps about one lattice constant high. The widths of terraces range from one to a thousand lattice constants.

The presence of kinks and edge atoms, visible in Figure 1.3, reminds us that continuum steps are only an approximation of a fundamentally discrete phenomenon. To use an image with the same resolution as Figure 1.3 to generate initial conditions for a simulation of continuum steps, one would have to smooth out the kinks and edge atoms. Jeong and Williams [43] suggest the use of an integral mollifier for this purpose. The result is a representation of the surface by smooth steps as in Figure 1.2.

In Figure 1.2, the relevant near-equilibrium physical processes are (i) adatom diffusion on terraces, (ii) diffusion of edge adatoms along steps, and (iii) attachment/detachment of adatoms at step edges. Diffusion processes such as (i) and (ii) arise when each terrace or edge adatom is assumed to perform a random walk; the

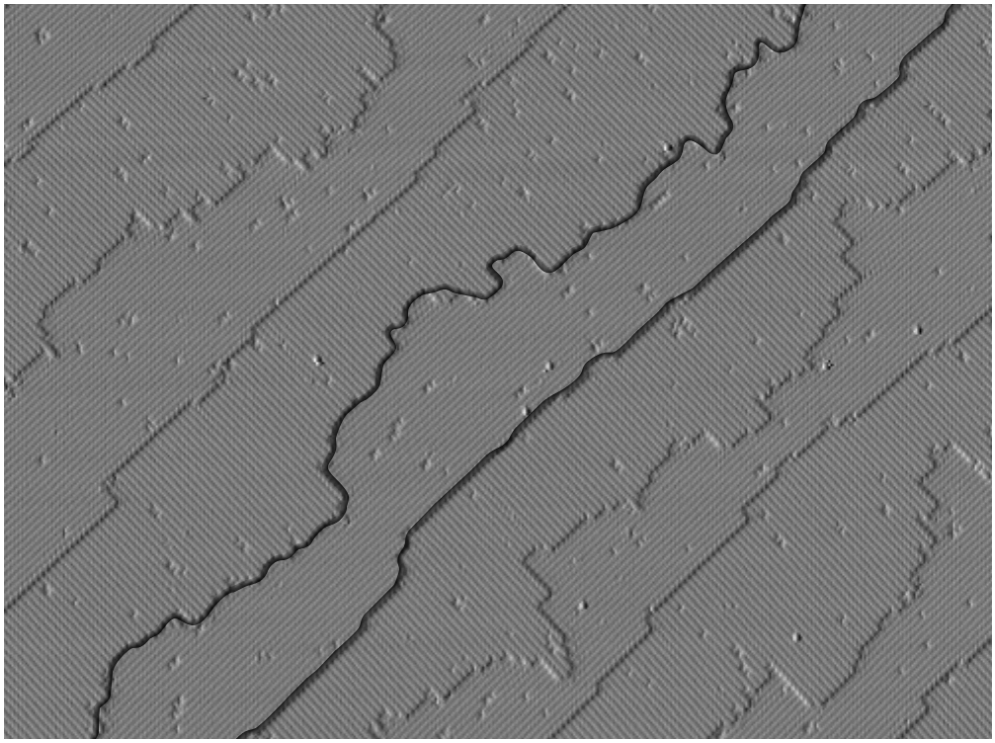

Figure 1.3: Image of a silicon (100) surface, taken from [99], showing kinks and edge atoms over many steps. Solid curves along the diagonal have been superimposed to illustrate the approximation of smooth steps. Note two kinds of steps on this surface.

resulting step-continuum equations represent the homogenized (averaged) effect of a large number of these adatoms moving stochastically throughout their domains. The overall evolution of nanoscale averages, such as the adatom density, is predictable according to the law of large numbers. The kinetic process (iii) is a manifestation of a near-equilibrium law, whose forcing term is similar to those that appear in differential equations for chemical reaction rates. In the case of surface steps, the rate at which adatoms attach or detach at step edges is proportional to a difference of concentrations. A step advances when adatoms attach to the step edge; it retreats when adatoms detach from the step edge.

We now discuss a few of the atomic processes that change the shape of a step. A curved step, such as those depicted by the solid diagonal paths in Figure 1.3, actually features kinks that 'zig-zag' along the step edge. The expansion of kinks can result from nucleation of terrace adatoms, if the difference of concentrations is favorable to adatom attachment at the ends of a kink. The opposite effect, when concentration differences favor adatom detachment, consists of a step emitting adatoms. This change in the step shape reduces the free energy associated with unbonded edge atoms. Such energy-minimizing mass transport can be interpreted as an effect of *step line tension*. In general, a step can change its shape by adsorbing or emitting adatoms. It remains to explain how the equilibrium shape of a step is communicated to the adatoms.

Absorption and emission of adatoms depend on the differences between concentrations. One of these, the terrace adatom concentration, is in principle directly observable. The other concentration is an equilibrium quantity that depends on the

surface geometry via the step curvature and energetics of interacting steps. Intuitively, steps with high curvature and small separations from their nearest neighbors have higher energy than straight steps widely separated from their nearest neighbors. We expect a highly curved step to require more energy because a greater number of broken bonds are associated with regions of high curvature, as one can see in Figures 1.1 and 1.3. The effect of step separation is more subtle and involves two different kinds of interaction, as we see shortly.

The energy of a step train is conveniently analyzed using the concept of *step chemical potential*. The step chemical potential, reflecting the contribution of step line tension and step-step interactions, measures the propensity of a step to incorporate adatoms. This physical interpretation follows from the monotone relation between adatom equilibrium density and step chemical potential; see the discussion around (3.10).

Interactions between steps of the same sign (both either step-up or step-down) are of two types, entropic and elastic-dipole. Entropic repulsions enforce the noncrossing of steps, by restricting how far each step at nonzero temperature can deviate from its average position. This *thermal wandering* is an unavoidable consequence of nonzero temperature. However, the presence of other steps imposes a penalty for any wandering that brings a step into collision with one of its neighbors. This penalty takes the form of a loss in entropy, making the step's free energy greater than it would be in the absence of neighboring steps. Elastic-dipole interactions are mediated by the strain fields that steps produce in the crystal [63, 76]. Any defect on the surface, including a step, induces a force distribution that in principle

has a multipole expansion of all orders. Comparison between predictions of this multipole expansion and data from classical atomistic simulations led Najafabadi and Srolovitz [76] to conclude that the dipole-dipole interaction is dominant over higher-order contributions for the typical range of terrace widths. The combination of elastic-dipole and entropic interactions yields the step chemical potential as the superposition of two terms, each term reflecting an inverse-square dependence on the distance between the step and one of its neighbors. This superposition is not linear, appearing in the equation for interaction energy as a renormalized parameter for the strength of repulsions [43].

The approximation of continuum steps, as noted above, deliberately glosses over the details of point defects on the steps themselves. Kinks and edge atoms, always present to some extent on steps at nonzero temperature, are not directly incorporated into the formula for step chemical potential. Some variations of the BCF model account for kinks and edge atoms by introducing auxiliary fields, such as kink density. Equations for these auxiliary fields are coupled with the other equations for step motion in a way that respects mass conservation [3, 11, 68]. We do not treat coupled field equations in this thesis, instead opting for the simplicity of a semi-empirical formula for the step chemical potential. By "semi-empirical" we mean that the *scaling* of the step chemical potential with nearest-neighbor distance can be derived analytically, but in general the *prefactor* can only be approximated by comparisons with data, numerical or experimental.

1.4 Connecting step models to experiments

The feedback loop between step models and experiments began with an observation that puzzled the mid-20th century crystal growth community. According to the accepted models of crystal nucleation and growth in solution, the concentration of crystal atoms had to be sufficiently large in order for crystals to precipitate on the growing surface. When the threshold concentration was observed to be much lower than predicted, Burton, Cabrera, and Frank [10] hypothesized a new mechanism for crystal growth in solution to explain the discrepancy. This explanation proposed the existence of steps, which serve as convenient nucleation sites for the atoms adsorbed from solution. In the BCF model, step motion is governed by the diffusion of adatoms across terraces and the attachment/detachment of adatoms at step edges. Their formulation of equilibrium density differs from the one we adopt following [37, 64, 113], in that the BCF model omits step interactions. The simple picture inspired by the BCF model enabled many successful predictions of surface phenomena, such as Spohn's prediction of step density in the neighborhood of a facet [109], and the inverse linear decay of peak-to-valley distances found by Rettori and Villain [98] for certain biperiodic profiles.

More recently, the BCF model has been expanded to account for step-step interactions and anisotropies in the material parameters. These extensions of the BCF model are often introduced to provide better interpretations of the observations of crystal surfaces. For example, the experimental determination of certain coefficients in the formula for surface free energy leads to interesting analogies between the ter-

race width distribution and other probabilistic phenomena. The successful interplay between step models and experiments confirms that step-based models still hold a valuable place among the various approaches to surface science.

1.5 Macroscale limit

Advances in imaging techniques since the early investigations of epitaxial phenomena have expanded the range of time and length scales over which we can study crystal surfaces. Today with Atomic-Force Microscopy (AFM) and other imaging devices, it is common to observe samples with characteristic lengths of the order of 100 μm or larger for durations of minutes, hours or more. Samples of this size comprise hundreds or thousands of steps, and the AFM probe will not resolve all the details fast enough to follow the individual steps as the surface relaxes. A meaningful connection between observations at this scale and the predictions of a step-based theory requires a systematic way to bridge the gap between the limited capabilities of an AFM probe and the difficulties of understanding large-scale surface morphological evolution via the flow of steps. In applications it is also often desired to control the evolution of crystal surfaces, and this control is more readily achieved at larger scales. Because of the below-roughening temperatures under which modern small devices are made, the presence of steps at the nanoscale must be taken into account when attempting to control the surface evolution at the macroscale.

It turns out that we can bypass a complete simulation of step motion in 2+1 dimensions by using a formal procedure known as coarse-graining. This method

regards the equations of step flow as a discrete scheme for some evolution law governing macroscale quantities, such as the surface height. In the same way that decompilation of computer code reconstructs a plausible version of the higher-level source code, coarse-graining takes the low-level "instructions" given by a nanoscale model and determines a consistent macroscale "program" for which the nanoscale equations are one implementation. This analogy fails in several ways, most importantly by suggesting that the output of a coarse-graining procedure is not unique (up to isomorphism), since different computer code decompilers can yield structurally different source code programs. In fact, coarse-graining is a well-defined operation, producing a unique partial differential equation (PDE) given a deterministic system for the finer-scale variables.

The PDE generated by a coarse-graining operation describes the relation between space and time derivatives of the surface height. This PDE is also known as the *full continuum limit* (or macroscale limit) of the nanoscale equations. This terminology reflects the facts that (i) a limit is taken when going to the coarser scale, and (ii) the resulting PDE is a fully continuum equation, making no explicit reference to the nanoscale variables from which it was derived. After verifying the hypotheses that justify using the macroscale limit, one might make direct comparisons between the predictions of this PDE and the experimental results.

In the case of surface relaxation, the macroscale limit is a fourth-order parabolic nonlinear PDE for the height decay in the region of space where $\nabla h \neq 0$ [37, 64, 96]. If the complementary region $\{\mathbf{x} : \nabla h(\mathbf{x}) = 0\}$—i.e., the set of macroscopically flat *facets*—has positive measure, then we need to determine the appropriate bound-

ary conditions at facet edges to obtain a well-posed problem from the macroscale limit [31, 109]. The choice of boundary conditions must weigh the sometimes conflicting demands of easy numerical implementation on the one hand, and accurate microscale physics on the other hand.

1.6 Overview of this thesis

The main results of this thesis are fully continuum equations for the surface height based on step models, and investigation of these equations from numerical and analytical perspectives. In Chapter 2, we introduce the basic ideas common to all macroscopic theories, and we review the numerical method we apply later to approximate the solutions of macroscale equations. In Chapter 3, we introduce the assumptions of near-equilibrium step flow in the context of one-dimensional step trains, to lay the groundwork for subsequent generalizations in 2+1 dimensions. In Chapter 4, we take a brief detour to derive the formula for elastic interaction energy between steps. The generalization of this formula is used in Chapter 5, where we review the (2+1)-dimensional macroscopic limit of [66].

The modeling component of this thesis extends the (2+1)-dimensional setting of [66] in several ways. First, the diffusion of adatoms on terraces is allowed to be anisotropic, which allows for a more realistic representation of surfaces where adatoms hop more readily perpendicular to steps than parallel to them, or vice versa. Second, we include the effect of step edge diffusion, where mass transport along the step edge is modeled as the result of longitudinal variations in the step

chemical potential. The macroscale limit with anisotropic terrace diffusion and step edge diffusion is presented in Chapter 6. Different scalings of approximate, separable solutions of the PDE are made possible by the additional parameters corresponding to step edge diffusion and anisotropic terrace diffusion.

In Chapter 7, we generalize the boundary conditions at step edges to address the possibility of permeable steps. Adatoms approaching a permeable step are free to hop directly to the next terrace. In principle, step permeability can lead to nonlocal effects, as adatoms diffuse over many terraces before attaching to a step edge. The macroscale limit, however, reflects step permeability only through a renormalized kinetic rate. Our derivation in 2+1 dimensions generalizes the work of Pierre-Louis [88] for straight steps.

Another extension of (2+1)-dimensional step models introduces a drift velocity in the terrace diffusion equation, which corresponds physically to an applied electric field. The study of crystal surfaces evolving under the influence of an electric field began with an experiment by Latyshev et al. [59], who reported the onset of step bunching. This surface instability is characterized by wide terraces between clusters of closely-spaced steps. Electromigration-induced step bunching has been used as a practical method for fabricating quantum wires. More recently, the application of an electric field parallel to step edges has been shown to produce a step meandering instability. This phenomenon features the growth of harmonic perturbations of straight steps, as predicted by Dufay et al. [15] and observed by Degawa et al. [14]. Motivated by these possible applications, we introduce in Chapter 8 the physics of electromigration at the nanoscale. Then we use the BCF-type model with

electromigration to derive the corresponding macroscale equation.

In Chapter 9, we discuss the inclusion of facets in the macroscopic theory. A relaxing surface with a facet can be modeled as a free-boundary problem [64, 109]. The influence of step-step interactions on the slope profile depends on the distance from the facet edge. We apply boundary-layer ideas, similar to those employed in [64], to determine how the slope profile behaves near a facet edge in 2+1 dimensions. The boundary-layer solution is qualitatively different if we introduce an appreciably large electric field. We study this effect analytically in the case of straight steps, axisymmetry, and also more general step geometries with slowly varying curvature.

In Chapter 10, we use the finite element method to simulate the macroscopic equations. Numerical simulations of the PDEs derived in Chapters 5–8 illustrate the rich variety of relaxation phenomena predicted by the model. The first noteworthy result, evident even in the case of isotropic terrace diffusion, is the morphological transition exhibited by an initially biperiodic profile, which relaxes to become almost one-dimensional [7]. We discuss the plausible mechanisms behind this transition. To isolate the effect of longitudinal fluxes, we simulate the macroscopic equation with electromigration for an initially biperiodic profile. In this case, the accelerated transition to an almost one-dimensional profile offers insight into the driving mechanism behind the observed morphological changes.

Chapter 2

Macroscopic equations and numerical solutions

In this chapter, we provide the necessary background for the subsequent investigation of macroscale crystal surface evolution. Our research relies on PDEs for the macroscale surface variables, as well as numerical simulations of these PDEs. These components of our research program build on previous work in modeling and numerics. In the following review of the relevant background material, we make special note of the limitations of previous macroscopic theories and simulations, in order to motivate the new topics of the following chapters.

2.1 Macroscopic theories of crystal surfaces

In a fully continuum picture of crystal surfaces, we smooth out the kinks and approximate the discrete height by a continuous graph. The immediate advantage of this approach is the reduced number of dependent variables. The height profile in the macroscopic model is a single function of time and the two spatial variables. The PDE satisfied by the macroscale height function lends itself more readily to numerical simulations on modest hardware, whereas atomistic models require much more memory to store the positions of all the atoms in a sample. Fully continuum theories also have the advantage of enabling global predictions, such as scaling laws and similarity solutions, more easily than discrete models. These global predictions

are better suited for comparisons with experimental results, because the time scale of experimental observation is realized by macroscopic simulations but is typically unattainable by atomistic methods.

Macroscopic theories are not without their limitations, however. One should be cautious in applying a fully continuum theory when detailed resolution of atomistic or nanoscale processes is desired. The configuration of kinks and edge atoms, for example, cannot be recovered from a macroscopic simulation. Moreover, kinetic rates manifest themselves in macroscopic theories only through combinations of material parameters. To determine any particular kinetic rate is outside the scope of our fully continuum models.

2.1.1 Effect of different mass transport mechanisms

In total, four different physical mechanisms have been identified for mass transport in a crystal material. In [33], Herring considers separately the processes of (i) viscous flow, (ii) evaporation and condensation, (iii) volume diffusion, and (iv) surface diffusion. Each of these processes leads to a different scaling between the lifetime and size of a surface feature. For example, two geometrically similar surface features with characteristic length scales L_1 and L_2 will change their shape by evaporation/condensation with lifetimes τ_1 and τ_2, which satisfy $\tau_2/\tau_1 = (L_2/L_1)^2$. The exponent 2 appears because evaporation/condensation works at the solid-vapor interface, where total surface area (proportional to the square of the characteristic length) is relevant. In general, a surface feature with characteristic length λL_1 de-

caying via one of the mechanisms (i)—(iv) has a lifetime τ given by $\tau = \tau_1 \lambda^p$, where $p \in \{1, 2, 3, 4\}$ is associated with the operative mechanism of mass transport. The largest possible power, $p = 4$, is associated with surface diffusion.

At a given temperature, any of the four possible mass transport mechanisms may be present in a crystal material. The lifetime of a structure varies most rapidly with characteristic size when surface diffusion is present. The trend toward fabricating ever smaller surface features, as required for mobile electronic devices, would impose severe time constraints at the temperatures commonly used in previous decades for crystal surface patterning. For example, a miniaturized surface feature, half as large as one produced currently, might decay 16 times faster at the same temperature. To mitigate the difficulties of shorter lifetimes in structures subject to surface diffusion, experimentalists and manufacturers have brought their equipment to lower operating temperatures. At these lower temperatures, the continuum thermodynamic description of crystal surface evolution is challenged. The appropriate theory, based on the motion of steps below roughening, is thus enjoying a resurgence in the research community.

2.1.2 Macroscopic theory above the roughening temperature

Before describing the extension of macroscale theories to temperatures below roughening, we review the ingredients of surface evolution models that first appeared in descriptions above the roughening temperature. Macroscale descriptions of crystal surfaces above roughening apply the ideas of continuum thermodynamics and mass

conservation, obtaining PDEs or variational principles for the surface height. A classic example is the fourth-order PDE,

$$\partial_t h \propto \text{div}\nabla(\Delta h), \tag{2.1}$$

derived by Mullins and Herring. This result holds if

1. the chemical potential μ is proportional to the mean curvature, $\mu \propto \kappa_1 + \kappa_2$,
2. the surface flux is proportional to the gradient of chemical potential, $\mathbf{J} \propto \nabla\mu$, and
3. mass conservation is enforced via $\partial_t h \propto -\text{div}\mathbf{J}$.

In this derivation, Mullins introduces only one chemical potential, μ, which is associated with the surface geometry through the mean curvature. A second chemical potential for the vapor phase would be needed in the case of evaporation/condensation, but Mullins assumes only surface diffusion in his analysis. As noted in Chapter 1, it is reasonable to expect the mean curvature to determine the likelihood of adatom attachment/detachment on the surface. In the regime of small slope ($|\nabla h| \ll 1$), the mean curvature definition of chemical potential yields

$$\mu \propto \Delta h, \tag{2.2}$$

where Δ is the 2D Laplacian. An alternative formulation of the chemical potential is in terms of the surface energy E, via the variational formula

$$\mu = \frac{\delta E}{\delta h}, \tag{2.3}$$

where

$$E = \int_{\mathbb{R}^2} \gamma(|\nabla h|)\mathrm{d}\mathbf{x}, \quad \gamma = g_0 + \frac{1}{2} g_2 |\nabla h|^2 + o(|\nabla h|^2). \tag{2.4}$$

We remark that the above-roughening free energy density γ is smooth for any surface slope $|\nabla h|$.

The relation between surface flux and the gradient of chemical potential is the macroscale analog of Fick's law[1]. At the level of steps and terraces we have a flux $\mathbf{J}^{\mathrm{ad}}$ defined by $\mathbf{J}^{\mathrm{ad}} = -\mathbf{D}^{\mathrm{ad}} \cdot \nabla C$, where C is the adatom concentration and $\mathbf{D}^{\mathrm{ad}}$ is the adatom diffusivity. At the macroscale we have the similar relation

$$\mathbf{J} \propto -\mathbf{M} \cdot \nabla \mu, \tag{2.5}$$

where $\mathbf{M}$ is the mobility. Both $\mathbf{D}^{\mathrm{ad}}$ and $\mathbf{M}$ are in principle tensor-valued functions of the slope, restricted on physical grounds to be positive definite. The case of scalar $\mathbf{D}^{\mathrm{ad}}$ and $\mathbf{M}$ is perhaps easiest to understand intuitively, but we shall soon encounter regimes where this intuition is challenged.

Finally, the law of mass conservation is written so that a net flux of adatoms across a level set for h is exactly balanced by the local time derivative of the height. In the absence of deposition, the material derivative (or total derivative) of the level set $h = \text{const.}$ yields the mass conservation law,

$$\partial_t h \propto -\operatorname{div} \mathbf{J}. \tag{2.6}$$

When deposition is present, a forcing term must be added to the right hand side of (2.6). This case is not studied in this thesis.

[1]See the discussion around (5.3).

2.1.3 Macroscopic theory below the roughening temperature

The three ingredients of macroscale models of surface morphological evolution, first introduced in the study of materials above roughening, also carry over to temperatures below T_R. Care must be taken in writing the analogs of (2.2)–(2.6) below roughening, in order to respect the presence of steps. For example, according to the BCF model, there are N different step chemical potentials for an array of N steps. It is not immediately obvious how one would obtain a fully continuum chemical potential μ in this setting, much less a relation analogous to (2.2). Similarly, the dependence of terrace flux $\mathbf{J}^{\mathrm{ad}}$ on adatom concentration is not readily connected with the macroscale relation (2.5). In Chapter 5 we review the details of this macroscale limit procedure for the simple case of isotropic terrace diffusion, where $\mathbf{D}^{\mathrm{ad}}$ is a scalar constant.

The idea of a *macroscale limit* has a long history in the literature, producing PDEs based on BCF models alone [2, 51, 86, 94, 119], BCF models coupled with adatom density [16, 62, 104], or kinetic Monte Carlo models [120]. We follow the first approach and consider BCF models alone, allowing for some interesting generalizations to account for different possible physics at the nanoscale. In Chapter 6 we include the effects of step edge diffusion and anisotropic terrace diffusion. In Chapter 7 we derive the macroscale limit for permeable steps, which allow adatoms to jump from one terrace to its neighbor without first attaching to the step between them. In Chapter 8 we include the effects of a drift velocity caused by an applied electric field, and desorption of adatoms from a terrace into the vapor phase. These

effects are easily accommodated in the below-roughening analogs of (2.2)–(2.6) without disrupting the structure of the macroscopic equations. In every case we study here, the macroscale limit can be written in the form

$$\partial_t h = \operatorname{div}(\mathbf{M} \cdot \nabla \mu), \tag{2.7}$$

$$\mu = \frac{\delta E}{\delta h} \tag{2.8}$$

for some appropriate mobility $\mathbf{M}$ and surface energy E.

Below roughening, the singular surface energy E can be expanded as a series in $|\nabla h|$:

$$E = g_0 + g_1 |\nabla h| + \frac{g_3}{3} |\nabla h|^3. \tag{2.9}$$

By interpreting $|\nabla h|$ as the macroscale analog of the discrete step density, the coefficients of the expansion for E reflect the relative contribution of energies (i) proportional to the number of steps (g_1 term), (ii) independent of the number of steps (g_0 term), or (iii) stemming from interactions that decay as the inverse square of step separation (g_3 term).

Because μ is not directly observable, but only serves as an auxiliary variable in the fully continuum PDE, it will sometimes be convenient to change variables so that the variational structure (2.7),(2.8) remains intact.

2.2 Numerical simulations

In this section, we discuss the numerical treatment of evolution equations for the macroscale surface height. Our approach takes advantage of the variational structure (2.7),(2.8) to implement a weak form of the macroscale PDE using finite

elements. If the mobility $\mathbf{M}$ and surface energy E are chosen appropriately, we expect the solution of the macroscale PDE to approximate the near-equilibrium motion of steps. However, a full comparison between the predictions of nanoscale and macroscale models is outside the scope of this research. Lacking a numerical implementation of step flow equations in 2+1 dimensions, the only data available for comparison come from simulations of the coupled differential equations for the positions of straight or concentric circular steps [25, 45].

We now turn to the implementation of fully continuum models for the surface height. To simulate these macroscale PDEs, we must decide on a discretization, which introduces computable quantities to approximate the fully continuum data. The vector of step positions is, of course, one such discretization. However, the equations of step flow are in general too unwieldy to simulate directly. We take advantage of the flexibility afforded by the fact that any given differential equation has more than one possible discretization.

Among the possible discretization choices available to us, two in particular have proven useful for the simulation of crystal surface relaxation. The first (Galerkin) method approximates the surface height by an expansion in trigonometric basis functions [108], which yields coupled differential equations for the coefficients after substitution in (2.7),(2.8). This system of ordinary differential equations is then integrated numerically. Due to its easy formulation and capacity to accommodate higher-order discretizations in time, the Galerkin method is a natural choice for simulating the evolution equation.

We adopt the finite element method, which partitions the domain into non-

overlapping elements (e.g., triangles) and approximates at time n the surface height h^n and the macroscale chemical potential μ^n as a sum of basis functions ϕ_i (sometimes called hat functions), each of which is supported on a finite, contiguous cluster of elements, viz.,

$$h^n = \sum_i H_i^n \phi_i, \tag{2.10}$$

$$\mu^n = \sum_i m_i^n \phi_i. \tag{2.11}$$

The approximations (2.10),(2.11) can only resolve the spatial dependence of h and μ over distances not less than the mesh size. By choosing the mesh size appropriately, we can resolve all the physically meaningful spatial variations in h, without introducing unmanageably many degrees of freedom in the triangulation $\mathcal{T}$. We denote by $\mathbb{V}_\mathcal{T}$ the finite element space spanned by the hat functions ϕ_i for the triangulation $\mathcal{T}$. The weak formulation of the evolution law, expressed in the space $\mathbb{V}_\mathcal{T}$, will finally allow us to find approximate solutions of (2.7),(2.8). In order to write this weak formulation, we must first choose a discretization for the time derivative.

The finite element method works by solving a linear system for the coefficients H_i^n and m_i^n in (2.10),(2.11). The exact definition of μ in terms of h is, in general, nonlinear, so the first task of a time discretization is to find an approximate, linear version of the relation (2.8). We choose a semi-implicit Euler time step [32, 77], replacing (2.7) by

$$\frac{h^n - h^{n-1}}{\Delta t} = \mathrm{div}\mathbf{M}(h^{n-1}) \cdot \nabla \mu^n, \tag{2.12}$$

$$\mu^n = \left.\frac{\delta E}{\delta h}\right|_{h^{n-1}}. \tag{2.13}$$

This discretization allows us to find the unknown coefficients at any time by solving a matrix equation. To determine which linear system the coefficients H_i^n and μ_i^n satisfy, we take the inner product of (2.12) with an arbitrary test function $g \in \mathbb{V}_{\mathcal{T}}$, and also the inner product of (2.13) with an arbitrary test function $\psi \in \mathbb{V}_{\mathcal{T}}$. Because $\mathbb{V}_{\mathcal{T}}$ is spanned by the basis functions ϕ_j, it suffices to consider inner products with each ϕ_j individually. The linear system that emerges is

$$\sum_i (H_i^n - H_i^{n-1}) \int_{\mathcal{B}} \phi_i \phi_j = \Delta t \sum_i m_i^n \int_{\mathcal{B}} \mathbf{M}(h^{n-1}) \nabla \phi_i \cdot \nabla \phi_j, \tag{2.14}$$

$$\sum_i m_i^n \int_{\mathcal{B}} \phi_i \phi_j = \int_{\mathcal{B}} \left. \frac{\delta E}{\delta h} \right|_{h^n} \phi_j, \quad \forall \phi_j, \tag{2.15}$$

where $\mathcal{B}$ is the domain over which the PDE (2.7),(2.8) is assumed to hold.

The integral on the right-hand side of (2.15) is more commonly rewritten using integration by parts, as we shall see in Chapter 5 when considering the formula for macroscale chemical potential in more detail. Integration by parts has already been performed on the right-hand side of (2.14), with vanishing boundary terms[2].

We alert the reader that the surface energy E has a singularity at $|\nabla h| = 0$. For the integration in (2.15) to make sense, we add a regularization parameter $\varepsilon \ll 1$ to the denominator $|\nabla h|$ that appears in the g_1 term of $\delta E / \delta h$. The qualitative behavior of the approximate solution is not significantly affected by ε [7].

Finally, the tensor mobility in the fixed coordinate system might also have a singularity at $|\nabla h| = 0$. Different regularization schemes are possible to remove this singularity. For mathematical consistency we might wish that the regularized

[2]Namely, $\partial_t h$ and the flux $\mathbf{J}$ are both zero on the boundary of $\mathcal{B}$; or, we apply periodic boundary conditions (assuming steps lie on a torus in $\mathbb{R}^2$).

mobility approaches a scalar as $\nabla h \to 0$. However, we find that the approximate solution is rather robust with respect to the mobility regularization, as discussed in Chapter 10.

A number of linear solvers are available to compute the coefficients H_i^n, μ_i^n using (2.14),(2.15). Once a solution is obtained, we can quantify its usefulness by estimating the size of the truncation errors and interpolation errors (due to discretization in time, the choice of mesh, and the choice of polynomial space for the basis functions). In the present work, we do not focus on a posteriori analysis in this vein. Our emphasis is on the global behavior of solutions to the PDE (2.7),(2.8), which we expect to be well captured by any reasonable numerical solution of (2.14),(2.15).

The preceding illustration of the finite element method gives only a flavor of the mathematics behind this powerful tool. A much richer description appears in [9]. Evans [24] serves as a good reference for the necessary background in Sobolev spaces.

Chapter 3

One-dimensional nanoscale models of interacting steps

In this chapter we review an extended version of the BCF step model. This classical picture of step motion, updated to include entropic and elastic-dipole step interactions, describes the relevant nanoscale physics of stepped surfaces. Here *nanoscale* reminds us that the motion of steps, which we use to derive a macroscale limit, is itself a coarse approximation of atomistic processes.

3.1 Geometry of straight steps

We consider a descending train of steps with atomic height a, separated by flat regions called terraces; see Figure 3.1. The step positions x_i are treated as moving boundaries for the adatom diffusion of each terrace. To account for the fact that no overhangs or step crossings are allowed, we require that at each time t, the step position $x_i(t)$ increase monotonically with the step number i, $x_{i+1}(t) > x_i(t)$. If this condition is satisfied for the initial step positions $x_i(0)$, then the subsequent evolution is expected to respect the monotonicity, due to the repulsive step-step interactions introduced in the equations below. We regard the monotonicity of step positions for $t > 0$ as a basic assumption, although an elementary proof is

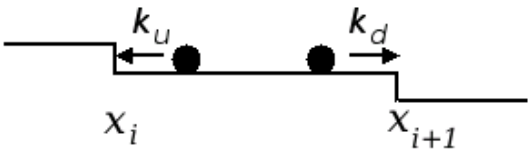

Figure 3.1: Geometry of straight steps.

possible for certain mass transport mechanisms.[1] For each time t, the ith terrace $\{x : x_i < x < x_{i+1}\}$ is a well-defined domain on which we seek solutions of the equation of motion for adatom diffusion. For the present case of one independent spatial variable, the elliptic problem corresponding to adatom diffusion reduces to an ordinary differential equation that admits an explicit solution.

3.2 BCF model for interacting straight steps

A quantitative discussion of the BCF theory begins with the adatom density, C_i, on the ith terrace, $x_i < x < x_{i+1}$. This C_i satisfies the diffusion (or heat) equation [10],

$$\partial_t C_i = \partial_x (D^{\mathrm{ad}} \cdot \partial_x C_i) \ , \tag{3.1}$$

where D^{ad} is the diffusivity for adsorbed atoms on the terrace. Note that we have omitted from (3.1) terms that describe atom desorption, electromigration and material deposition from above, considering only the effect of surface relaxation. Equation (3.1) can be simplified significantly by elimination of the time derivative, for the following reason. The time scale for step motion is much larger than the time scale

[1] For instance, by considering mass transport dominated by evaporation-condensation, we obtain a second-order PDE for the slope, to which the maximum principle applies.

for terrace diffusion. Thus, we simplify (3.1) via the "quasi-steady approximation", $\partial_t C_i \approx 0$; the time dependence in C_i enters through the boundary conditions at step edges. Solving the resulting differential equation for C_i by successive integrations yields

$$C_i = A_i(x - x_i) + B_i, \quad x_i < x < x_{i+1}. \tag{3.2}$$

The approximation $\partial_t C_i \approx 0$ might break down in the case of fast-moving steps, for example, in a surface grown by molecular beam epitaxy using a large deposition flux [29]. Since we discuss only surface relaxation, material deposition from above is not relevant, and the quasi-steady approximation can safely be invoked.

The adatom flux on the ith terrace is defined by

$$J_i^{\mathrm{ad}} = -D^{\mathrm{ad}} \partial_x C_i, \tag{3.3}$$

which is Fick's law of diffusion.

Mixed (or Robin) boundary conditions at the step edges $x = x_i$ and $x = x_{i+1}$ complement (3.1) to yield a unique solution for C_i. These conditions emerge from linear kinetics [10, 37, 43]:

$$-J_i^{\mathrm{ad}}(x_i, t) = k_u[C_i(x_i, t) - C_i^{\mathrm{eq}}(t)] \ , \tag{3.4}$$

$$J_i^{\mathrm{ad}}(x_{i+1}, t) = k_d[C_i(x_{i+1}, t) - C_{i+1}^{\mathrm{eq}}(t)] \ , \tag{3.5}$$

where k_u, k_d are kinetic rates that account for the Ehrlich-Schwoebel barrier [17, 105], and $C_i^{\mathrm{eq}}(t)$ is the equilibrium density at the ith step edge. Substituting for C_i and J_i using (3.2) and (3.3), we find a linear system of equations for the integration

constants.

$$\begin{bmatrix} D^{\mathrm{ad}} & -k_u \\ -D^{\mathrm{ad}} - k_d \delta x_i & -k_d \end{bmatrix} \cdot \begin{pmatrix} A_i \\ B_i \end{pmatrix} = - \begin{pmatrix} k_u C_i^{\mathrm{eq}} \\ k_d C_{i+1}^{\mathrm{eq}} \end{pmatrix}. \tag{3.6}$$

This matrix equation is solved for A_i and B_i to obtain

$$\begin{pmatrix} A_i \\ B_i \end{pmatrix} = \frac{1}{D^{\mathrm{ad}}(k_u + k_d) + k_u k_d \delta x_i} \begin{pmatrix} k_u k_d (C_{i+1}^{\mathrm{eq}} - C_i^{\mathrm{eq}}) \\ D^{\mathrm{ad}}(k_u C_i^{\mathrm{eq}} + k_d C_{i+1}^{\mathrm{eq}}) + k_u k_d \delta x_i C_i^{\mathrm{eq}} \end{pmatrix} \tag{3.7}$$

Knowing the explicit values of A_i and B_i, we write the formula for the mass flux J_i on the ith terrace:

$$\begin{aligned} J_i^{\mathrm{ad}} &= -D^{\mathrm{ad}} A_i \\ &= -D^{\mathrm{ad}} \frac{k_u k_d (C_{i+1}^{\mathrm{eq}} - C_i^{\mathrm{eq}})}{D^{\mathrm{ad}}(k_d + k_u) + k_u k_d \delta x_i}, \end{aligned} \tag{3.8}$$

where $\delta x_i := x_{i+1} - x_i$ is the terrace width.

We then compute the velocity of the ith step according to the law of mass conservation:

$$\dot{x}_i = \frac{\mathrm{d}x_i}{\mathrm{d}t} = \frac{\Omega}{a}[J_{i-1}^{\mathrm{ad}} - J_i^{\mathrm{ad}}]. \tag{3.9}$$

Together with the initial step positions and a formula for determining C_i^{eq} based on the step geometry, the system (3.8),(3.9) governs the subsequent motion of steps.

3.3 1D interaction energy and the step chemical potential

In order to render (3.8)–(3.9) a closed system of equations for the step positions, we need a formula for the equilibrium densities in terms of the x_i. Our

starting point is the near-equilibrium thermodynamics law [37, 43]

$$C_i^{\text{eq}} = C_s \exp \frac{\mu_i}{k_B T} \sim C_s \left[1 + \frac{\mu_i}{k_B T} \right] , \tag{3.10}$$

where μ_i is the chemical potential of the ith step. We consider this μ_i to depend on the energy of interactions with other steps [37, 43, 66], in contrast to the original BCF model [10], which omitted step interactions. The linearization in (3.10) is permissible under typical experimental conditions, where $|\mu_i| \ll k_B T$ [114].

The usual interpretation of *chemical potential* refers to the change in a system's energy upon addition or removal of a single atom. In the case of a straight step, we can only add or remove atoms one row at a time. The *step chemical potential* accounts for this geometric restriction by appropriate scaling of the relevant energy changes.

We denote by $V_{i,j}$ the repulsive interaction energy between steps i and j. This interaction is *repulsive* if the steps have the same sign, e.g., both are step-down. The mechanisms underlying this repulsion between steps of the same sign deserve some attention. We build towards an understanding of elastic interactions between one-dimensional line defects (steps) by starting with the strain field of zero-dimensional point defects (e.g., vacancies or impurities). Then we address entropic interactions using ideas from statistical physics.

From the theory of crystal lattice mechanics [50], we know that a point defect in the bulk (e.g., a vacancy or an impurity) creates an elastic strain field that acts over distances far from the point defect. This elastic strain field can be modeled by

a point distribution of forces

$$F_i = A_{ik}\frac{\partial}{\partial x_k}\delta(\mathbf{r}), \quad i,k = 1,2,3; \tag{3.11}$$

where $\mathbf{r}$ is a three-dimensional radius vector and the point defect is located at $\mathbf{r} = 0$; A_{ik} is some symmetric tensor; the overall effect of such a distribution is zero total force and zero moment.

The analogous point distribution formula in the case of a point defect located on the surface is

$$f_\mu = A_{\mu\nu}\frac{\partial}{\partial x_\nu}\delta(\rho), \quad \mu,\nu = 1,2, \tag{3.12}$$

where the indices μ, ν correspond to a coordinate system in the tangential plane; ρ is a two-dimensional radius vector in the plane of the surface (the defect is located at $\rho = 0$), and $A_{\mu\nu}$ is some symmetric tensor. The calculation of elastic interaction energy between two such point defects [58] uses the field of elastic strains resulting from the force distribution (3.12). In an isotropic solid those defects with isotropic force distributions ($A_{\mu\nu} = A\delta_{\mu\nu}$) exert on each other a mutual repulsive force F given by [63]

$$F(\rho) = \frac{1-\zeta^2}{\pi Y}\frac{A^2}{\rho^3}, \tag{3.13}$$

where Y is the Young modulus and ζ is the Poisson ratio. The ρ^{-3} decay is predicted even in the case of an arbitrary symmetric tensor $A_{\mu\nu}$.

An isolated step differs from a point defect in that its associated force distribution has nonzero total moment. To analyze the step-step interactions using continuum elasticity, we model the displacement field associated with an isolated step by an array of force dipoles oriented normal to the step in the plane of the

terrace [63]:

$$u_x(x, z = 0) = f_x \frac{\partial}{\partial x} \delta(x), \tag{3.14}$$

where f_x is the strength of the dipole force and the step is identified with the y-axis. This formula greatly oversimplifies the true force distribution, which in fact has finite width, has components normal the surface plane, and has in-plane components which are not pure dipoles [76]. Rather than include all these effects systematically, Najafabadi and Srolovitz [76] take an empirical approach and invoke a multipole expansion for the true force distribution due to an isolated step. The coefficients of this multipole expansion are fit to data from simulations of interacting steps. To compare the data with the theory, we need to know what repulsive forces are predicted by the multipole expansions.

The interaction between two steps is calculated in a manner similar to the calculation of repulsive forces between point defects. Using a multipole expansion for the force distribution due to each step, Najafabadi and Srolovitz derived an expansion for the total interaction energy in a one-dimensional step train. The starting equation is a volume integral of the elastic interactions between the strain fields ϵ due to individual steps.

$$E_{\text{int}} = \frac{1}{2} \int \mathbf{C} \left[\sum_i \epsilon_i(\mathbf{r}) \right] \left[\sum_j \epsilon_j(\mathbf{r}) \right] \mathrm{d}V \tag{3.15}$$

By distributing the product over the sums inside the integral, Najafabadi and Srolovitz expand (3.15) to separate the contributions from self-energy and interaction energy:

$$E_{\text{int}} = N[\gamma_{\text{self}}(w) + \gamma_{\text{int}}], \tag{3.16}$$

where the interaction energy is found by summing over all steps,

$$\gamma_{\text{int}}(w) = \sum_{j=1}^{\infty} \gamma_{\text{s-s}}(jw) \tag{3.17}$$

and the contribution from steps of separation jw is given by the multipole expansion

$$\gamma_{\text{s-s}}(w) = \sum_{k=1}^{\infty} \zeta_k \left(\frac{a}{w}\right)^k. \tag{3.18}$$

The substitution of (3.18) into (3.17) yields

$$\begin{aligned} \gamma_{\text{int}}(w) &= \sum_{j=1}^{\infty} \left[\sum_{k=1}^{\infty} \zeta_k \left(\frac{a}{jw}\right)^k\right] \\ &= \sum_{k=1}^{\infty} \zeta_k \beta_k \left(\frac{a}{w}\right)^k, \end{aligned} \tag{3.19}$$

where $\beta_k = \sum_{j=1}^{\infty} j^{-k}$ are material independent and easily calculated. In this formula for total interaction energy, series truncation and curve fitting suffice to determine the coefficients in the multipole expansion of a typical step's force distribution.

By fitting the coefficients of this expansion to the step simulation data, Najafabadi and Srolovitz conclude that for step spacings w larger than $3a$, the dominant term is the dipole-dipole interaction energy. Truncating the series for interaction energy at a higher power of a/w does not significantly improve the fit between (3.19) and the simulation data [76]. Therefore, the repulsive interaction between steps is, for all practical purposes, the same as if each step were viewed as an array of force dipoles. Considering, for example, the pair of neighboring steps indexed by i and $i+1$, we find an elastic interaction energy per unit length $V_{i,i+1}$ given by

$$V_{i,i+1} = \frac{g}{3}\left(\frac{a}{x_i - x_{i+1}}\right)^2, \tag{3.20}$$

where $g > 0$ measures the strength of *repulsive* elastic interactions between steps.

Another reason for steps to repel each other is the fact that steps are thermally rough. Just as steps are line defects on the surface, steps themselves can have point defects (edge atoms) or kinks, which slightly perturb their straight shape. The formation of an edge atom requires only the energy ϵ_κ associated with broken bonds, while the creation of an entire step requires energy in proportion to its length. At any nonzero temperature T, it is more energetically favorable for a step to wander (due to formation of kinks and edge atoms) than to advance or retreat as a whole. This thermal wandering does not proceed unimpeded. Invoking the non-crossing condition for steps, Gruber and Mullins [30] observed that collisions with neighbors would restrict the thermal wandering of a given step in an array of parallel steps. This restriction leads to a smaller entropy for the step in question, which then has larger free energy. The overall effect is that of entropic repulsion between steps.

To quantify the entropic interaction between steps, it is helpful to consider the in-plane correlation function

$$\langle |x(y) - x(y')|^2 \rangle = \frac{k_B T}{\tilde{\delta}} |y - y'|, \tag{3.21}$$

where the angle brackets denote a thermal average with respect to the equilibrium distribution, the steps are aligned with the y-axis, and $\tilde{\delta}$ is the step stiffness derived from the Ising lattice gas model [73],

$$\tilde{\delta} = \frac{k_B T}{a} e^{\epsilon_\kappa / k_B T}. \tag{3.22}$$

Neighboring steps are assumed to have an average separation w (measured in the x-direction), and the average distance between collisions is L_c (measured in the

y-direction). Setting the left hand side of (3.21) equal to w^2 and substituting L_c for $|y - y'|$, we find $L_c \approx w^2\tilde{\delta}/(k_BT)$. If each collision decreases the entropy by a fixed amount k_BC, then the step's free energy per unit length is increased by the amount

$$\Delta\delta \approx \frac{Ck_BT}{L_c} = \frac{C(k_BT)^2}{w^2\tilde{\delta}}. \tag{3.23}$$

To determine the coefficient C, it is useful to think of the steps as world lines of non-interacting fermions, with the y-axis playing the role of time [42, 44]. This representation yields $C = \pi^2/6$.

The decay of entropic repulsion strength as w^{-2} is the same scaling we found for elastic-dipole interactions. The combination of both forces is easily accommodated in (3.20) by renormalizing the coefficient g.

Here we consider μ_i stemming from nearest-neighbor step interactions. Thus, μ_i depends only on the distances $|x_i - x_{i\pm1}|$. (In the macroscopic limit, adding up all the pairwise interactions has the same effect as renormalizing the parameter of interaction strength when considering only nearest-neighbor forces [66].) To determine the chemical potential of the ith step, it suffices to compute the elastic-dipole forces exerted by neighboring steps only, not taking into account any interactions beyond nearest-neighbor.

Suppose the ith step advances by an amount Δx_i. This step advance requires the attachment of an additional $\Delta N = a\Delta x_i/\Omega$ atoms per unit length, where Ω is the atomic volume. By analogy with the usual definition of chemical potential, we define the *step chemical potential* as the change in interaction energy upon addition

or removal of ΔN atoms per unit length. Formally letting $\Delta x_i \to 0$, we write

$$\mu_i := \frac{\Omega}{a} \frac{\mathrm{d}}{\mathrm{d}x_i} [V_{i,i+1} + V_{i,i-1}]. \tag{3.24}$$

The formulas (3.20) and (3.24), together with (3.8) and (3.9), constitute a system of ordinary differential equations governing the flow of straight steps.

A typical question of interest for this system is whether an equilibrium solution (i.e., that for equally-spaced steps or constant surface slope) is stable. If not, we try to characterize the types of instabilities that emerge as the surface relaxes. Stability analysis of the step flow equations in this geometry employs techniques from perturbation theory, such as the phase equation method [49], which studies the evolution equation satisfied by the phase ϕ of a given initial pattern. Research in this vein has led to general conclusions about the properties of steady state solutions for a large class of nonlinear PDEs [95]. The focus of our work is on step systems in 2+1 dimensions, where such a stability analysis is not practical. The reader is directed to [15, 95] for more details about the dynamics of (1+1)-dimensional step trains.

3.4 BCF model for interacting concentric circular steps

The restriction that step positions be expressible in terms of only one spatial variable allows yet another geometry. Whereas the geometry of straight steps emerges from translational invariance, we obtain the geometry of concentric circular steps (Figure 3.2) by requiring rotational invariance. Polar coordinates (r, θ) are appropriate in this setting, where the dependence on the angular variable θ is

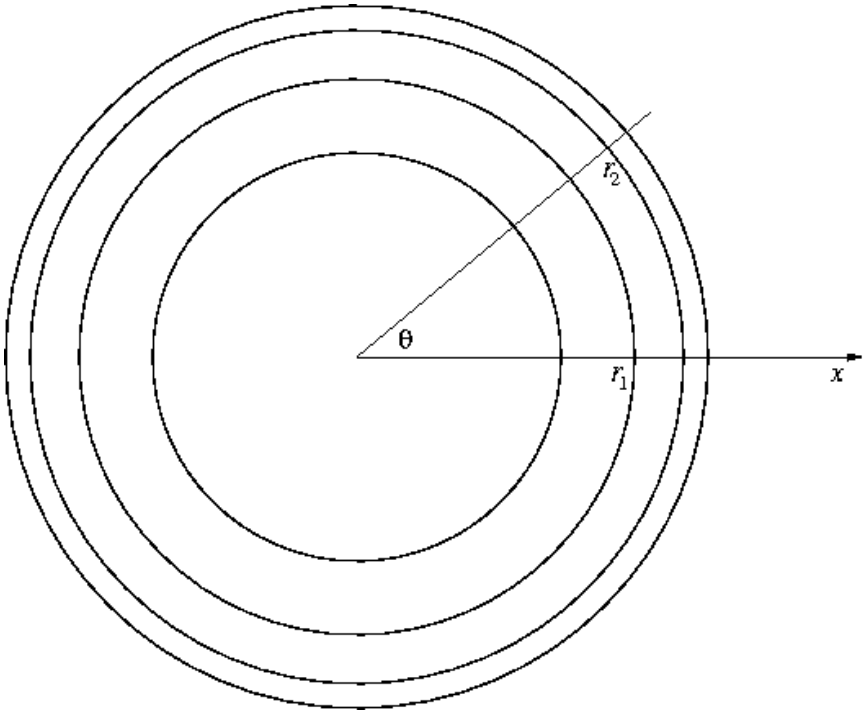

Figure 3.2: Geometry of concentric circular steps.

eliminated due to the assumed axisymmetry.

The point $r = 0$ is singled out as the center of the mound or valley. To establish some parallelism with the case of straight steps, we restrict our attention to axisymmetric structures where the height is a decreasing function of r (mounds). At any position inside the innermost step, in particular at $r = 0$, the height is a constant; $h(r,t) = h_f(t)$ for $0 < r < r_0$, where r_0 is the radius of the innermost step. The subscript f recalls the picture of a *facet*, a macroscopically flat region about $r = 0$ characterized by a length scale significantly larger than the typical terrace width.

The analog of (3.1) for axisymmetric surface profiles reads

$$\frac{\mathrm{d}^2 C_i}{\mathrm{d}r^2} + \frac{1}{r}\frac{\mathrm{d}C_i}{\mathrm{d}r} = 0, \tag{3.25}$$

where again we have invoked the quasi-steady approximation, $\partial_t C_i \approx 0$.

We solve (3.25) by successive integrations to find

$$C_i(r) = B_i + A_i \ln(r/r_i), \quad r_i < r < r_{i+1}. \tag{3.26}$$

The terrace adatom flux, directed radially outward to satisfy the symmetry constraints, is calculated using $J_i^{\mathrm{ad}} = -D^{\mathrm{ad}} \partial_r C_i$. In terms of the integration constants, the adatom flux is

$$J_i^{\mathrm{ad}} = -\frac{D^{\mathrm{ad}} A_i}{r}, \quad r_i < r < r_{i+1}. \tag{3.27}$$

Boundary conditions analogous to (3.4) and (3.5) complement (3.25) to yield the adatom density field on the ith terrace. Again assuming linear kinetics at step edges, we have

$$-J_i^{\mathrm{ad}}(r_i, t) = k_u [C_i(r_i, t) - C_i^{\mathrm{eq}}(t)], \tag{3.28}$$

$$J_i^{\mathrm{ad}}(r_{i+1}, t) = k_d [C_i(r_{i+1}, t) - C_{i+1}^{\mathrm{eq}}(t)], \tag{3.29}$$

where C_i^{eq} is the equilibrium adatom density at the ith step edge.

Substituting (3.26),(3.27) for C_i and J_i, we find the integration constants by solving the matrix equation

$$\begin{bmatrix} -\frac{D^{\mathrm{ad}}}{k_u r_i} & 1 \\ \frac{D^{\mathrm{ad}}}{k_d r_{i+1}} + \ln \frac{r_{i+1}}{r_i} & 1 \end{bmatrix} \begin{pmatrix} A_i \\ B_i \end{pmatrix} = \begin{pmatrix} C_i^{\mathrm{eq}} \\ C_{i+1}^{\mathrm{eq}} \end{pmatrix}. \tag{3.30}$$

Solving for A_i and B_i allows us to write the explicit solution of the requisite

boundary value problem on each terrace.

$$A_i = \frac{C_{i+1}^{\mathrm{eq}}}{D^{\mathrm{ad}}\left(\frac{1}{k_u r_i} + \frac{1}{k_d r_{i+1}}\right) + \ln\frac{r_{i+1}}{r_i}} \tag{3.31}$$

$$B_i = \frac{C_{i+1}^{\mathrm{eq}} + C_i^{\mathrm{eq}}\left(1 + \frac{k_u r_i}{k_d r_{i+1}} + \frac{k_u r_i}{D^{\mathrm{ad}}}\ln\frac{r_{i+1}}{r_i}\right)}{1 + \frac{k_u r_i}{k_d r_{i+1}} + \frac{k_u r_i}{D^{\mathrm{ad}}}\ln\frac{r_{i+1}}{r_i}}. \tag{3.32}$$

In these coefficients for the solution of the diffusion equation, we identify certain fractions that indicate the rate-limiting process. The kinetics are called attachment-detachment limited (ADL) if $D^{\mathrm{ad}}(k_u^{-1} + k_d^{-1})/a \gg 1$, i.e., adatoms diffuse much faster than they attach and detach at step edges. The kinetics are called diffusion limited (DL) if $D^{\mathrm{ad}}(k_u^{-1} + k_d^{-1})/a \ll 1$, i.e., adatoms diffuse much slower than they attach and detach at step edges. "Mixed kinetics" is the intermediate regime where $D^{\mathrm{ad}}(k_u^{-1} + k_d^{-1})/a = O(1)$. Simplifications of (3.31),(3.32) in the regimes of DL or ADL kinetics will be useful when discussing scaling laws in Chapter 5.

The difference of fluxes from neighboring terraces at the ith step edge yields the step velocity $\dot{r}_i = \frac{\mathrm{d}r_i}{\mathrm{d}t}$ according to the law of mass conservation:

$$\dot{r}_i = \frac{\Omega}{a}[J_{i-1}^{\mathrm{ad}}(r_i) - J_i^{\mathrm{ad}}(r_i)]. \tag{3.33}$$

3.5 Interaction energy and step chemical potential for circular steps

It remains to derive the dependence of C_i^{eq} on step positions. This calculation reveals one key difference between the axisymmetric geometry and the straight-step geometry. In the axisymmetric setting, the equilibrium density C_i^{eq} contains information not only about the energetic interactions analogous to those of straight

steps, but also the energetic cost of step curvature. For the circular step with radius r_i, the equilibrium density is given by (3.10) and the inclusion of curvature in the formula for step chemical potential:

$$\mu_i = \frac{\Omega}{a}\left[\frac{\beta}{r_i} + \frac{1}{r_i}\partial_{r_i}(r_i U_i^{\text{int}})\right], \tag{3.34}$$

$$U_i^{\text{int}} = [V(r_i, r_{i+1}) + V(r_i, r_{i-1})], \tag{3.35}$$

$$V(r, r') = \frac{g}{3}\frac{2r'}{r + r'}\left(\frac{a}{r - r'}\right)^2, \tag{3.36}$$

where β is the step line tension (energy/length) and U_i^{int} is the interaction energy per unit length of the ith step.

A geometric argument for the appearance of step curvature and line tension (the term β/r_i in (3.34)) is as follows. Again we measure the change in the system's energy ΔU_i and count the number ΔN of additional atoms that must attach to the step at $r = r_i$ to accomplish this energy change. For circular steps, the length of the ith step is $2\pi r_i$, which imposes an energetic cost of $2\pi\beta r_i$ due to line tension. To advance the ith step by a distance Δr_i will increase the line tension energy by an amount $\Delta U_i = 2\pi\beta\Delta r_i$. The number ΔN of additional atoms required to advance this step is proportional to the area of an annulus, approximately $2\pi r_i \Delta r_i$ in the limit $\Delta r_i \to 0$. To be precise, $\Delta N = 2\pi r_i \Delta r_i/(\Omega/a)$, where Ω/a is the cross-sectional area of an atom. Taking the ratio $\Delta U_i/\Delta N$, we find that the change in line tension energy for each added atom is $(\Omega/a)(\beta/r_i)$.

We remark that formula (3.36) for the interaction energy has the same dependence on the local step density as in the case of straight steps, but with a shape-dependent prefactor $\frac{2r'}{r+r'}$. This shape factor appears when we calculate the

interaction energy between concentric arrays of dipoles by integrating along each step. To our knowledge, (3.36) first appeared in [113], with little explanation of its origin. An independent derivation of this formula, emphasizing the geometric assumptions under which it holds, is given in Chapter 4. The presence of a shape factor arising from integration of the dipole energy formula is characteristic of 2-dimensional steps, as we see in section 4.3 when considering arbitrary step geometry.

Equations (3.10),(3.36),(3.31), and (3.33) suffice to determine the subsequent evolution of the step positions in the axisymmetric setting.

Due to the inclusion of step curvature in the formula for the step chemical potential, an axisymmetric surface profile can exhibit step bunching instabilities [26]. This phenomenon results from the competition between nearest-neighbor repulsions and the tendency of an isolated circular step to minimize its line tension energy by expanding. Step bunching has been proposed as a possible means of growing nanowires, a setting in which the axisymmetric model applies.

Chapter 4

Elastic-dipole interactions between steps in 2 dimensions

In this chapter, we pause to examine the origin of formula (3.36) for the elastic-dipole interaction energy between two steps. As noted above, equation (3.36) first appeared in [113], accompanied only by a brief plausibility argument. Subsequent uses of the formula in [25, 36, 37, 64, 118] offered neither a derivation nor a clear set of assumptions under which (3.36) is expected to hold. The purpose of this chapter is to derive equation (3.36) starting from an interaction energy formula based on linear elasticity. In the course of this derivation it will become apparent to what extent (3.36) is an approximation, and under which conditions we can expect it to provide correct values for the interaction energy. Finally, this calculation is extended to more general step configurations by appropriate local definitions of the relevant geometric parameters. We use the result of this derivation when describing the fully (2+1)-dimensional relaxation problem in the next chapter.

4.1 From electrostatics to linear elasticity

The presence of a line defect (step) in a crystal surface introduces an elastic strain field, as noted in Chapter 3. This field can be understood as stemming from a line of force dipoles normal to the step. In this section we appeal to knowledge of electrostatics to motivate the expression for the field of an elastic force dipole.

We caution the reader not to expect an exact analogy between the equations of electrostatics and those of linear elasticity. In contrast to electric fields, an elastic displacement field cannot exist without a medium. This medium introduces material-dependent quantities, such as the Young modulus and the Poisson ratio, which might lead to correction terms in the formula for dipole interaction energy. It turns out that we find the same leading-order term as if the steps consisted of *electric* dipoles, since the characteristic scaling of the field strength as the inverse cube of separation is common to both types of dipoles. We begin by reviewing the electrostatic equations required to describe interacting dipoles.

4.1.1 Field and potential of an electric dipole

A common calculation in electrostatics is the long-range behavior of the electric potential due to a collection of point charges q_α. The expression for this potential is a series in negative powers of the distance r from the center of the distribution, which is known as a *multipole expansion* [40]. This series is only expected to yield correct values at distances r much greater than the finite extent R of the charge distribution. Often only the first two terms in the series make a significant contribution to the electric potential. The *monopole* term decays as r^{-1} and is proportional to the total charge. The *dipole* term decays as r^{-2} and depends on the magnitude and direction of the *dipole moment* $\mathbf{p}$. This dipole moment is calculated by [40]

$$\mathbf{p} = \sum_\alpha q_\alpha \mathbf{R}_\alpha, \tag{4.1}$$

where $\mathbf{R}_\alpha$ is the position of charge q_α in some appropriate coordinate system.

At positions $\mathbf{r}$ far from the center of the dipole, the potential Φ can be written as

$$\Phi = \frac{\mathbf{r} \cdot \mathbf{p}}{r^3}. \tag{4.2}$$

Note that we choose CGS units, where the usual SI prefactor $(4\pi\epsilon_0)^{-1}$ is set to 1, so that the eventual transition to *elastic* interactions is not hindered by lingering dimensional constants.

To calculate the electric field $\mathbf{E}$ at position $\mathbf{r}$, we apply the gradient operator to (4.2).

$$\mathbf{E} = -\nabla\Phi = \frac{1}{r^3}[3\hat{\mathbf{r}}(\mathbf{p} \cdot \hat{\mathbf{r}}) - \mathbf{p}]. \tag{4.3}$$

The analog of the electric field in the context of continuum mechanics is the strain field, which exerts a force on point and line defects in the surface. We determine the energy associated with a given configuration of surface defects by computing a volume integral over a region where the potential Φ admits an expansion in Taylor series.

4.1.2 Energy of a charge distribution in an electric field

Assembling a given collection of charges in an ambient electric field requires an amount of work given by

$$W = \int_\Omega \rho\Phi \mathrm{d}^3\mathbf{x}, \tag{4.4}$$

where ρ is the charge density defined at each point in the domain Ω, Φ is the electric potential, and $\mathrm{d}^3\mathbf{x}$ is the volume element.

We assume that the spatial variation of Φ within Ω is accurately captured by

a Taylor series expansion about $\mathbf{x}_0 \in \Omega$:

$$\Phi(\mathbf{x}) = \Phi(\mathbf{x}_0) + (\mathbf{x} - \mathbf{x}_0) \cdot \nabla\Phi|_{\mathbf{x}_0} + \mathcal{O}(|\mathbf{x} - \mathbf{x}_0|^2), \quad \mathbf{x} \in \Omega. \tag{4.5}$$

Because the energy of a charge configuration does not depend on the origin of the coordinate system, we choose $\mathbf{x}_0 = \mathbf{0}$ for convenience. Substituting (4.5) into (4.4), we find

$$W = \int_\Omega \mathrm{d}^3\mathbf{x}\rho\Phi(\mathbf{0}) + \rho\mathbf{x} \cdot \nabla\Phi(\mathbf{0}) + \mathcal{O}(|\mathbf{x}|^2). \tag{4.6}$$

The evaluation of the electric potential and its derivatives at $\mathbf{0}$ can now be taken outside the integral.

$$W = q\Phi(\mathbf{0}) + \mathbf{p} \cdot \nabla\Phi(\mathbf{0}) + \ldots, \tag{4.7}$$

where $q = \int_\Omega \rho \mathrm{d}^3\mathbf{x}$ is the total charge, $\mathbf{p} = \int_\Omega \rho\mathbf{x}\mathrm{d}^3\mathbf{x}$ is the dipole moment about the origin of the given charge distribution, and the omitted terms account for energy contributions from higher-order poles.

In combining formula (4.3) for the field of an electric dipole and (4.7) for the work done to assemble a collection of charges, we need to distinguish the two dipole moments, even though they play symmetric roles in the final formula for interaction energy. We use $\mathbf{p}_A$ for the dipole that creates the ambient electric field, and $\mathbf{p}_B$ for another dipole that we bring to a desired location within this field. Using (4.7), the term accounting for dipole-dipole interactions is

$$W_{dip} = \frac{1}{r_{AB}^3}[\mathbf{p}_A \cdot \mathbf{p}_B - 3(\mathbf{p}_A \cdot \hat{\mathbf{r}}_{AB})(\hat{\mathbf{r}}_{AB} \cdot \mathbf{p}_B)], \tag{4.8}$$

where $\mathbf{r}_{AB}$ is the separation vector between dipoles A and B.

4.1.3 Interaction energy of two force dipoles

To check whether a direct adaptation of (4.8) would yield plausible results, we consider first the special one-dimensional case of *electric* dipoles A and B aligned with the separation vector $\mathbf{r}_{AB}$. If $\mathbf{p}_A$ and $\mathbf{p}_B$ are parallel and point in *opposite* directions, then the force between them is repulsive, and we should expect that a positive amount of work is needed to assemble this charge configuration. Indeed, the overall sign of (4.11) is positive in this case. However, if $\mathbf{p}_A$ and $\mathbf{p}_B$ are parallel and point in the *same* direction, then they experience an attractive force, so it should take a negative amount of work to assemble this charge configuration. The sign predicted by (4.8) is again consistent with this intuition.

The nature of *elastic* step-step interactions implies that two steps of the same sign exert a repulsive force on each other. To illustrate this effect, it helps to think of a stepped surface as a continuous elastic medium. In the absence of any other steps, a single step on such a medium would decay to a smoother, flat profile, just as an initial injection of dye into a clear solution would eventually diffuse to uniform concentration. The relaxation of a single step is frustrated by the presence of neighboring steps. Effectively, each pair of same-sign steps experiences a mutually repulsive force. This repulsive interaction between steps of the same sign, in marked contrast to the attractive interaction between parallel electric dipoles, indicates that (4.8) needs to be replaced by its counterpart from linear elasticity before proceeding.

The reader who is already familiar with the theory of defect interactions in linear elasticity should consult [21, 56, 93] to find a more thorough discussion of the

correct formulas describing interacting line defects on a crystal surface. We appeal to the calculation given by Pimpinelli and Villain [93] for the interaction energy of two force dipoles. By analogy with (4.1), they define a *force dipole moment* m resulting from a set of forces $\mathbf{F}_R$ acting at points $\mathbf{R}$:

$$m_{\alpha\gamma} = \sum_R R_\alpha F_R^\gamma \quad (\alpha, \gamma = x, y, z). \tag{4.9}$$

Two such force dipoles, m and m', are calculated to have an interaction energy

$$W_{\text{int}} = \frac{1-\zeta^2}{\pi Y r^3}\left[mm' - \frac{\zeta}{1-\zeta}(mm'_{zz} + m_{zz}m') + \left(\frac{\zeta}{1-\zeta}\right)^2 m_{zz}m'_{zz}\right], \tag{4.10}$$

where Y is the Young modulus, ζ is the Poisson coefficient, and r is the separation between the two dipoles. The dominant term in (4.10) is the product mm', since the Poisson coefficient is always smaller than 1/2 [93]. This inequality suggests that (4.10) can be viewed as a series expansion in powers of the small material parameter $\zeta/(1-\zeta)$. For the purposes of calculating the total interaction energy between two steps, we restrict our attention to the truncated version of (4.10), which reads

$$W_{\text{int}} = \frac{1-\zeta^2}{\pi Y r^3} mm' + \mathcal{O}[\zeta/(1-\zeta)]. \tag{4.11}$$

In order to apply (4.11), the dipole moments m and m' are measured with respect to a fixed coordinate system. In particular, the interaction energy between non-parallel step segments involves the projection (or inner product) of one dipole moment onto the other.

4.2 Integral for the energy of interacting steps

In light of the rotational symmetry (see Figure 3.2), it suffices to fix our attention on the interaction between a line element on the inner step and the net strain field induced by the outer step. By superposition, we can calculate the energy per unit length of the inner step by applying (4.11) for each line element on the outer step. We recall that the dipole moment is proportional to the length of the line element, and its contribution to elastic interactions arises through the step-normal component (radially outward). Using Cartesian coordinates, the interacting dipoles are located at $(r_1, 0)$ and $(r_2 \cos\theta_2, r_2 \sin\theta_2)$. Their respective xx dipole moments are

$$\begin{aligned} m &= P r_1 \mathrm{d}\theta_1 \\ m' &= P \cos\theta_2 r_2 \mathrm{d}\theta_2, \end{aligned} \tag{4.12}$$

where P is the dipole moment per unit length associated with an atomic-height step.

The squared distance between the two dipoles is

$$r^2 = r_1^2 + r_2^2 - 2 r_1 r_2 \cos\theta_2. \tag{4.13}$$

We calculate the product required by (4.11) for step-step interactions:

$$m m' = P^2 \cos\theta_2 r_1 \mathrm{d}\theta_1 r_2 \mathrm{d}\theta_2. \tag{4.14}$$

The interaction energy per unit length is given by the integral

$$\frac{\mathrm{d}W}{r_1 \mathrm{d}\theta_1} = P^2 \int_{-\pi}^{\pi} \frac{\cos\theta_2 \cdot r_2 \mathrm{d}\theta_2}{(r_1^2 + r_2^2 - 2 r_1 r_2 \cos\theta_2)^{3/2}}. \tag{4.15}$$

Motivated by the physically reasonable assumption that the step separation is much less than the two individual step radii, we seek a simplified integral in which the dependence on step separation becomes more obvious. We set $r_2 = r_1 + \rho$, where the inner radius $r_1 = \epsilon^{-1}$ defines a "large" length scale, and the step separation ρ is considered only $\mathcal{O}(1)$. Our task now is to compute

$$I = 2\int_0^\pi \frac{\cos\theta_2}{(\epsilon^{-2} + (\epsilon^{-1}+\rho)^2 - 2\epsilon^{-1}(\epsilon^{-1}+\rho)\cos\theta_2)^{3/2}} r_2 \mathrm{d}\theta_2. \tag{4.16}$$

In the following calculation we omit the subscript of θ_2 for brevity, keeping in mind that the only varying angle refers to the position on the step of radius r_2. We expand the denominator of (4.16), arriving at the simplified formula

$$I = \int_0^\pi \frac{\cos\theta}{[\rho^2 + 2(\epsilon^{-2}+\epsilon^{-1}\rho)(1-\cos\theta)]^{3/2}} r_2 \mathrm{d}\theta. \tag{4.17}$$

Note that this integral can be computed in terms of complete elliptic integrals, but the resulting formulas are not instructive for our purposes.

Now we use the substitution $s := \sin(\theta/2)$, so that

$$\cos\theta = 1 - 2s^2, \tag{4.18}$$

$$\mathrm{d}\theta = \frac{2\mathrm{d}s}{\sqrt{1-s^2}}. \tag{4.19}$$

After this change of variables, the interaction energy is given by

$$I = 2r_2 \int_0^1 \frac{\mathrm{d}s}{\sqrt{1-s^2}} \frac{1-2s^2}{[4(\epsilon^{-2}+\epsilon^{-1}\rho)s^2 + \rho^2]^{3/2}}. \tag{4.20}$$

We define the macroscopic length parameter λ by

$$\lambda^2 := 4(\epsilon^{-2} + \epsilon^{-1}\rho). \tag{4.21}$$

Notice that in the limit of small step separation ($\epsilon\rho \ll 1$), applying the binomial expansion to the square root of (4.21) yields

$$\begin{aligned}\lambda &= 2\epsilon^{-1}(1+\epsilon\rho)^{1/2} \\ &\approx 2\epsilon^{-1}(1+\epsilon\rho/2) \\ &= 2\epsilon^{-1}+\rho = r_1 + r_2. \end{aligned} \tag{4.22}$$

Already we see a possible origin of the denominator $r_1 + r_2$ in the formula (3.36), and the geometric condition under which the replacement for λ is valid. We proceed with the calculation by substituting λ into (4.20).

$$I = 2r_2 \int_0^1 \frac{\mathrm{d}s}{\sqrt{1-s^2}} \frac{1-2s^2}{[\lambda^2 s^2 + \rho^2]^{3/2}} \tag{4.23}$$

$$= 2r_2 \int_0^1 \frac{\mathrm{d}s}{\sqrt{1-s^2}} \frac{1-2s^2}{\lambda^3 \left[s^2 + \left(\frac{\rho}{\lambda}\right)^2\right]^{3/2}}. \tag{4.24}$$

Now we introduce the small parameter $\delta := \rho/\lambda$. The integral becomes

$$\begin{aligned} I &= \frac{2r_2}{\lambda^3} \int_0^1 \frac{\mathrm{d}s}{\sqrt{1-s^2}} \frac{1-2s^2}{[s^2+\delta^2]^{3/2}} \\ &= \frac{2r_2}{\lambda^3} \int_0^1 \frac{\mathrm{d}s}{\sqrt{1-s^2}} \frac{-2(s^2+\delta^2)+2\delta^2+1}{[s^2+\delta^2]^{3/2}} \\ &= \frac{2r_2}{\lambda^3} \int_0^1 \frac{\mathrm{d}s}{\sqrt{1-s^2}} \left[\frac{2\delta^2+1}{(s^2+\delta^2)^{3/2}} - \frac{2}{(s^2+\delta^2)^{1/2}}\right]. \end{aligned} \tag{4.25}$$

Notice that by regarding δ and s as independent, the partial fraction decomposition (4.25) reduces our problem to that of calculating a single integral, namely,

$$I_c(\delta^2) = \int_0^1 \frac{\mathrm{d}s}{\sqrt{1-s^2}} \frac{1}{\sqrt{s^2+\delta^2}}. \tag{4.26}$$

The subscript c recalls the underlying circular geometry. The desired interaction energy per unit length is then given by the identity

$$I = \frac{2r_2}{\lambda^3}\left[-2(2\delta^2+1)\frac{\mathrm{d}}{\mathrm{d}(\delta^2)} - 2\right] I_c(\delta^2). \tag{4.27}$$

Our motivation for writing I in this way stems from the method of asymptotic expansion we want to use in the limit $\delta \to 0$. The integral for elastic interaction between circular steps can actually be given in terms of complete elliptic integrals, which have well-studied asymptotic expansions for small values of the parameter δ [19]. Keeping in mind the eventual application of our method to settings without axisymmetry, we opt to follow a more general procedure, using the Mellin transform with respect to δ^2. When we apply this technique, we must evaluate double integrals with respect to s and δ^2. The calculation of these double integrals using the Fubini theorem (coming next) is greatly simplified if we omit at the very beginning any trivial δ-dependence, such as multiplicative factors.

4.2.1 Mellin transform of the axisymmetric integral

To approximate the behavior of $I_c(\delta^2)$ for $\delta \ll 1$, we resort to the Mellin transform in δ^2. This variant of the Laplace transform has proved useful in many fields of applied mathematics since the 1980s, especially in asymptotic evaluation of integrals; see [100] for a review. The Mellin transform $\hat{f}(\zeta)$ of a function $f(x)$ is given by

$$\hat{f}(\zeta) = \int_0^\infty x^{-\zeta} f(x) \mathrm{d}x, \qquad a < \mathrm{Re}\zeta < b, \tag{4.28}$$

where the domain of $\hat{f}$ is restricted to ensure convergence of the integral; see Appendix A for details.

The inversion formula is

$$f(x) = \frac{1}{2\pi\imath} \int_{\alpha-\imath\infty}^{\alpha+\imath\infty} x^{\zeta-1} \hat{f}(\zeta) \mathrm{d}\zeta, \tag{4.29}$$

where $a < \alpha < b$ so that $\hat{f}$ is defined for ζ along the integration path.

We apply these formulas to the function I_c as follows.

$$\hat{I}_c(\zeta) = \int_0^\infty \mathrm{d}\delta^2 I_c(\delta^2)(\delta^2)^{-\zeta} \tag{4.30}$$

$$= \int_0^\infty \mathrm{d}\delta^2 (\delta^2)^{-\zeta} \int_0^1 \frac{\mathrm{d}s}{\sqrt{1-s^2}} \frac{1}{\sqrt{s^2+\delta^2}} \tag{4.31}$$

$$= \int_0^1 \frac{\mathrm{d}s}{\sqrt{1-s^2}} \left(\int_0^\infty \mathrm{d}\delta^2 \frac{(\delta^2)^{-\zeta}}{\sqrt{s^2+\delta^2}} \right). \tag{4.32}$$

For the inner integral, we pull out a factor of s from the denominator and let $\xi := \delta^2/s^2$, treating s^2 as a *fixed* nonzero parameter. This change of variables leads to

$$\hat{I}_c(\zeta) = \int_0^1 \frac{\mathrm{d}s}{\sqrt{1-s^2}} (s^2)^{1/2-\zeta} \int_0^\infty \mathrm{d}\xi \frac{\xi^{-\zeta}}{\sqrt{1+\xi}}, \tag{4.33}$$

and the rightmost integral can be evaluated in terms of Gamma functions [1]. We have the formula

$$\int_0^\infty \mathrm{d}\xi \frac{\xi^{-\zeta}}{\sqrt{1+\xi}} = B(1-\zeta, \zeta - 1/2), \tag{4.34}$$

where the Beta function B is more conveniently written as

$$B(z,w) = \frac{\Gamma(z)\Gamma(w)}{\Gamma(z+w)}, \tag{4.35}$$

and Γ denotes the Gamma function.

Applying these formulas to the Mellin transform $\hat{I}_c$ yields

$$\hat{I}_c(\zeta) = \frac{\Gamma(1-\zeta)\Gamma(\zeta-1/2)}{\Gamma(1/2)} \int_0^1 \mathrm{d}s \frac{(s^2)^{1/2-\zeta}}{\sqrt{1-s^2}} \tag{4.36}$$

$$= \frac{\Gamma(1-\zeta)\Gamma(\zeta-1/2)}{\Gamma(1/2)} \int_0^1 \frac{\mathrm{d}(s^2)}{2s} \frac{(s^2)^{1/2-\zeta}}{\sqrt{1-s^2}} \tag{4.37}$$

$$= \frac{\Gamma(1-\zeta)\Gamma(\zeta-1/2)}{\Gamma(1/2)} \int_0^1 \mathrm{d}(s^2) \frac{(s^2)^{-\zeta}}{\sqrt{1-s^2}}, \tag{4.38}$$

and again the rightmost integral admits a representation in terms of the Beta function. From p. 258 of [1],

$$\int_0^1 \mathrm{d}t \frac{t^{-\zeta}}{\sqrt{1-t}} = B(1-\zeta, 1/2) = \frac{\Gamma(1-\zeta)\Gamma(1/2)}{\Gamma(3/2-\zeta)}. \tag{4.39}$$

So the Mellin transform of $I_c(\delta^2)$ is concisely expressed as

$$\hat{I}_c(\zeta) = \frac{1}{2}\frac{\Gamma(1-\zeta)^2\Gamma(\zeta-1/2)}{\Gamma(3/2-\zeta)}, \tag{4.40}$$

a *meromorphic* function of ζ. The fundamental strip where the integral (4.32) converges is found to be $\frac{1}{2} < \mathrm{Re}\zeta < 1$.

4.2.2 Asymptotic expansion using the inverse Mellin transform

Recall that the only singularities of $\Gamma(z)$ are poles at the nonpositive integers. Thus, the line integral prescribed by the *inverse* Mellin transform can be found by applying the residue theorem. The sum of these residues is a power series in δ^2, with the possible presence of logarithmic terms.

The inverse Mellin transform applied to $\hat{I}_c$ reads

$$I_c(\delta^2) = \frac{1}{2\pi\imath}\int_{\alpha-\imath\infty}^{\alpha+\imath\infty} \mathrm{d}\zeta (\delta^2)^{\zeta-1}\hat{I}_c(\zeta), \qquad \frac{1}{2} < \alpha < 1. \tag{4.41}$$

The leading-order term comes from the residue at the closest pole to the right of the fundamental strip, or $\zeta = 1$ in the present case. To approximate the Gamma functions near $\zeta = 1$, we make the substitution $\epsilon = 1-\zeta \Leftrightarrow \zeta = 1-\epsilon$. Then

$$\hat{I}_c(\zeta) = \frac{\Gamma(\epsilon)^2\Gamma(\frac{1}{2}-\epsilon)}{\Gamma(\frac{1}{2}+\epsilon)}. \tag{4.42}$$

As $\epsilon \to 0$, we have

$$(\delta^2)^{-\epsilon}\hat{I}_c(\zeta) \sim (1-\epsilon\ln\delta^2)\left(\frac{1}{\epsilon}-\gamma\right)^2 \frac{\Gamma(\frac{1}{2})[1-\epsilon\Psi(\frac{1}{2})]}{\Gamma(\frac{1}{2})[1+\epsilon\Psi(\frac{1}{2})]} \tag{4.43}$$

$$\sim (1-\epsilon\ln\delta^2)\left(\frac{1}{\epsilon^2}-\frac{2\gamma}{\epsilon}\right)[1-2\epsilon\Psi(\frac{1}{2})] \tag{4.44}$$

$$\sim (1-\epsilon\ln\delta^2)\left[\frac{1}{\epsilon^2}-2\frac{\Psi(\frac{1}{2})+\gamma}{\epsilon}\right], \tag{4.45}$$

where γ is Euler's constant and Ψ denotes the logarithmic derivative of Γ, i.e., $\Psi(z) = \mathrm{d}/\mathrm{d}z(\ln\Gamma(z))$ [1].

Reading off the coefficient of ϵ^{-1} in the Laurent series given by (4.45), we find the residue contribution from $\zeta = 1$ to be $-2\Psi(\frac{1}{2}) - 2\gamma - \ln\delta^2 = 4\ln 2 - \ln\delta^2 = \ln(16/\delta^2)$. To leading order, the original integral I_c behaves like $\ln(16/\delta^2)$ for small values of δ.

Substituting $\ln(16/\delta^2)$ for I_c in (4.27), we find

$$I(\delta^2) \sim -\frac{4r_2}{\lambda^3}\left[\ln\frac{16}{\delta^2}-\frac{1}{\delta^2}-2\right] \sim \frac{4r_2}{\lambda_3\delta^2}. \tag{4.46}$$

In terms of the step radii, (4.46) reads

$$\frac{\mathrm{d}W}{r_1\mathrm{d}\theta_1} \sim \frac{4P^2r_2}{(r_2+r_1)(r_2-r_1)^2}, \tag{4.47}$$

in agreement with the inverse-square dependence on $r_2 - r_1$ and the shape factor $r_2/(r_2+r_1)$ given in [113].

4.2.3 Corrections to the leading-order term under axisymmetry

It is of interest to note that corrections to the leading-order term (4.47) in principle arise from several different places. First, the inverse Mellin transform

could be better approximated by including the residues from poles beyond $\zeta = 1$. This direction is summarized below. Secondly, by retaining higher-order terms in (4.10) or (4.46), we obtain other corrections, whose magnitude in relation to the first correction is not known a priori. Finally, the superposition of strain fields from different line elements on the two steps is justified only in the context of linear elasticity. We have not addressed the validity of this linear regime in real crystal surfaces.

The contribution from the pole $\zeta = 2$ is found by writing expansions in $\epsilon := 2 - \zeta$, which parallel the derivation above. We find

$$\begin{aligned}\frac{\Gamma(1-\zeta)^2\Gamma(\zeta-\frac{1}{2})}{\Gamma(\frac{3}{2}-\zeta)} &\sim \left[\frac{1}{\epsilon^2}+\frac{2(1-\gamma)}{\epsilon}\right]\frac{\Gamma(\frac{3}{2})[1-\epsilon\Psi(\frac{3}{2})]}{\Gamma(-\frac{1}{2})[1+\epsilon\Psi(-\frac{1}{2})]} \\ &\sim -\frac{1}{4}\left[\frac{1}{\epsilon^2}+\frac{2(1-\gamma)}{\epsilon}\right](1-\epsilon[\Psi(3/2)+\Psi(-1/2)]) \\ &\sim -\frac{1}{4\epsilon^2}-\frac{2\ln 2-1}{2\epsilon}. \end{aligned} \tag{4.48}$$

Multiplying (4.48) by $(\delta^2)^{\zeta-1} = (\delta^2)^{1-\epsilon} \sim \delta^2 \cdot (1 - \epsilon \ln \delta^2)$ furnishes the residue contribution from $\zeta = 2$. This residue contribution,

$$\frac{1}{4}\delta^2\left(\ln\frac{\delta^2}{16}+2\right), \tag{4.49}$$

is added to the previous expansion for I_c, which upon substitution in (4.27) yields

$$I \sim \frac{4r_2}{\lambda^3\delta^2}+\frac{5r_2}{\lambda^3}-\frac{4r_2\delta^2}{\lambda^3}-\frac{3r_2\delta^2}{\lambda^3}\ln\frac{\delta^2}{16}+\frac{3r_2}{\lambda^3}\ln\frac{\delta^2}{16}. \tag{4.50}$$

We see that in addition to the inverse-square dependence on δ, *algebraic and logarithmic* correction terms are needed to characterize the asymptotic behavior of the integral for interaction energy between concentric circular steps. We alert

the reader that pursuing further corrections may be inappropriate: higher-order corrections may be comparable or smaller in magnitude than the terms omitted from our starting point, (4.10). Thus we choose not to seek more corrections of the integral I at this point.

4.3 Elastic interaction energy between steps without axisymmetry: A brief discussion

Our Mellin transform manipulations of the axisymmetric integral (4.26) could have been bypassed in favor of elliptic integrals and their asymptotic expansions, if our only goal was to compare the result with the interaction energy formula given in [113]. The worth of the Mellin transform is better demonstrated by indicating how this transform can be applied to the integral for elastic dipole interactions between steps of reasonably general shape, i.e., *without axisymmetry*. We still regard the steps as small perturbations of a circle, which allows them to be described as polar graphs $r = r(\sin(\theta/2))$, θ: polar angle. The substitution $s := \sin(\theta/2)$ is used exactly as above to simplify the integrand. In Figure 4.1 we illustrate two neighboring steps restricted to a circular sector around $\theta = 0$. The inner step admits the polar representation $r = r_1(s)$, while the outer step is given by $r = r_2(s)$.

In order to quantify the deviation of these steps from circles, we let

$$r_2(s) = r_1(s) + \rho r(s), \tag{4.51}$$

$$r_1(s) = \epsilon^{-1}\psi(s), \tag{4.52}$$

where $\rho = \mathcal{O}(1) > 0$, $r(s) = \mathcal{O}(1)$, $\psi(s) = \mathcal{O}(1)$, and $\epsilon \ll 1$. Here ϵ^{-1} denotes

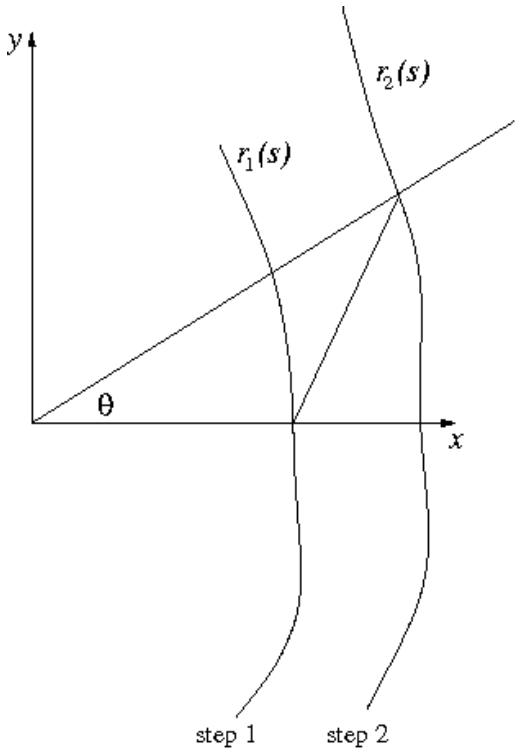

Figure 4.1: Geometry of neighboring steps *without* axisymmetry, parametrized by $r_1(s)$ and $r_2(s)$. We define $s := \sin(\theta/2)$ to convert trigonometric functions of θ into algebraic functions of s.

the characteristic length scale, roughly analogous to the radius of circular steps. In addition, we assume $\psi(s), r(s) \in C^1(-1,1)$, so that the tangent vector at each point on the two steps is well defined.

A crucial quantity to calculate is the distance R between points on the two steps, which enters as R^3 in the denominator of the elastic interaction energy integrand. We have

$$R^2 = r_2(s)^2 + r_1(0)^2 - 2r_1(0)r_2(s)\cos\theta \tag{4.53}$$

$$= \epsilon^{-2}\{[\psi(s) - \psi(0)]^2 + 4s^2\psi(0)\psi(s)\} + 2\epsilon^{-1}\rho r(s)[\psi(s) - \psi(0) + 2\psi(0)s^2] + \rho^2 r(s)^2. \tag{4.54}$$

Because ψ, r are assumed to be C^1, using Taylor series about $s = 0$ we can define the C^0 functions $\overline{\psi}, \overline{r}$ by

$$\psi(s) - \psi(0) =: s\overline{\psi}(s), \tag{4.55}$$

$$r(s) - r(0) =: s\overline{r}(s). \tag{4.56}$$

After adding and subtracting $\psi(0), r(0)$ as needed, we find

$$R^2 = \epsilon^{-2}4\psi(0)^2 s^2 + 4\epsilon^{-1}\rho r(0)\psi(0)s^2 + \rho^2 r(0)^2$$
$$+ \epsilon^{-2}[\overline{\psi}(s)^2 + 4s\overline{\psi}(s)\psi(0)]s^2 + 2\epsilon^{-1}\rho s\{\overline{r}(s)[s\overline{\psi}(s) + 2\psi(0)s^2] + r(0)\overline{\psi}(s)\}$$
$$+ \rho^2 s[2r(0)\overline{r}(s) + s\overline{r}(s)^2]. \tag{4.57}$$

In order to factor out the coefficient of s^2, we define

$$A(s) := \{4[\epsilon^{-2}\psi(0) + \epsilon^{-1}\rho r(0)]\psi(0)\}^{-1}\times$$
$$\big(\epsilon^{-2}[\overline{\psi}(s)^2 + 4s\overline{\psi}(s)\psi(0)]s + 2\epsilon^{-1}\rho\{\overline{r}(s)[s\overline{\psi}(s) + 2\psi(0)s^2] + r(0)\overline{\psi}(s)\}$$
$$+ \rho^2[2r(0) + s\overline{r}(s)]\overline{r}(s)\big). \tag{4.58}$$

Then

$$R^2 = 4[\epsilon^{-2}\psi(0)+\epsilon^{-1}\rho r(0)]\psi(0)\left\{s^2 + sA(s) + \frac{\rho^2 r(0)^2}{4\psi(0)[\epsilon^{-2}\psi(0) + \epsilon^{-1}\rho r(0)]}\right\}, \quad (4.59)$$

where $A(s) \leq \mathcal{O}(1)$.

To follow as closely as possible the notation of the axisymmetric case, we define the parameters

$$\delta^2 := \frac{\rho^2 r(0)^2}{4\psi(0)[\epsilon^{-2}\psi(0) + \epsilon^{-1}\rho r(0)]}, \quad (4.60)$$

$$\lambda^2 := 4[\epsilon^{-2}\psi(0) + \epsilon^{-1}\rho r(0)]\psi(0), \quad (4.61)$$

which feature in the asymptotic expansion of the integral for elastic interaction energy. In terms of δ and λ, the squared distance between points with (s, r) coordinates $(0, r_1(0))$, $(s, r_2(s))$ is

$$R^2 = \lambda^2\{s^2 + \delta^2 + sA(s)\}. \quad (4.62)$$

We note that the breaking of axisymmetry enters here through the term $sA(s)$, which accounts for the curvature variation when steps deviate from circles. The geometry of Figure 4.1 is deceptive in its simplicity. We have chosen a coordinate system such that the vector normal to step 1 at $s = 0$ is aligned with the x-axis. By following the procedure of the axisymmetric case, we still obtain an elastic interaction energy per unit length, but now we cannot immediately generalize the resulting formula to other points along step 1. In principle, a different calculation with different definitions of $A(s), \delta$, and λ is required for each point on step 1. Despite this shortcoming, we expect the qualitative features of our interaction energy formula, in particular the inverse-square dependence on local step separation, to persist no matter which

point on the inner step is used to orient the Cartesian coordinate system.

Below we outline the calculation for reasonably general 2D steps. A complete exposition of all the details would distract from the main point of this thesis (and chapter) and is hence omitted for the sake of clarity.

For simplicity, we write the integral over step 2 (which in principle requires s to range over $[-1,1]$) as two separate integrals,

$$\frac{\mathrm{d}W_{\mathrm{int}}}{r_1\mathrm{d}\theta_1} = \frac{1-\zeta^2}{\pi Y}P^2\left(\int_0^{\pi}+\int_{-\pi}^{0}\right)\frac{\sin\theta\mathrm{d}r_2/\mathrm{d}\theta + r_2\cos\theta}{(r_1^2+r_2^2-2r_1r_2\cos\theta)^{3/2}}\mathrm{d}\theta, \tag{4.63}$$

where P is the dipole moment per unit length of an atomic-height step. The first integral considers the energetic contributions given by (4.11) for θ ranging from 0 to π. The evaluation of the second integral is essentially not different and is therefore omitted. We now face the task of calculating

$$I_{2D} = \int_0^{\pi}\frac{\sin\theta\mathrm{d}r_2/\mathrm{d}\theta + r_2\cos\theta}{(r_1^2+r_2^2-2r_1r_2\cos\theta)^{3/2}}\mathrm{d}\theta, \tag{4.64}$$

The numerator in (4.64) stems from the inner product of the two vectors normal to step 1 at $s=0$ and normal to step 2 at $s=\sin(\theta/2)$.

We expand the numerator in (4.64), substituting the definitions of δ^2,λ^2, and $A(s)$ wherever possible. After grouping terms according to the highest power of s they contain as a factor, we reduce our problem to calculating integrals of the form

$$I_k(\rho^2) := 2\int_0^1 \frac{s^k B_k(s)}{[A(s)s^2+\rho^2 r(s)^2]^{3/2}}\frac{\mathrm{d}s}{\sqrt{1-s^2}}, \tag{4.65}$$

where $B_k(s\downarrow 0)\neq 0$ and $A(s\downarrow 0)\neq 0$ and $r(s\downarrow 0)\neq 0$.

We alert the reader that (4.65), unlike (4.26), in general cannot be evaluated in terms of elliptic integrals, especially since we don't know much about the behavior

of $A(s)$, $r(s)$, or $B_k(s)$. However, the Mellin transform with respect to ρ^2 does not need to know about these functions, since the main dependence on ρ^2 is already accounted for in (4.65). We apply (4.28) to (4.65), which yields

$$\hat{I}_k(\zeta) = 2\int_0^\infty \mathrm{d}(\rho^2)(\rho^2)^{-\zeta} \int_0^1 \frac{s^k B_k(s)}{[A(s)s^2 + \rho^2 r(s)^2]^{3/2}} \frac{\mathrm{d}s}{\sqrt{1-s^2}}. \tag{4.66}$$

We apply Fubini's theorem to (4.66) in order to switch the order of integration. The integral with respect to ρ^2 can be evaluated in terms of Gamma functions, which entails

$$\hat{I}_k(\zeta) = 2\frac{\Gamma(1-\zeta)\cdot\Gamma(\frac{3}{2}+\zeta)}{\Gamma(\frac{5}{2})} \int_0^1 \frac{\mathrm{d}s}{\sqrt{1-s^2}} s^{k-2\zeta-3} \frac{B_k(s)A(s)^{-\zeta-3/2}}{[r(s)^2]^{-\zeta+1}}. \tag{4.67}$$

This integral converges for

$$\{\zeta \in \mathbb{C} : \mathrm{Re}(-k+2\zeta+3) < 1\} = \{\zeta \in \mathbb{C} : \mathrm{Re}\zeta < -1 + k/2\}, \tag{4.68}$$

assuming that $A(s), r(s) \neq 0$ as $s \uparrow 1$ and similarly for B_k, A, r as $s \downarrow 0$. For each integral I_k, the leading-order term comes from expanding the Mellin transform near $\zeta = \alpha_k = \frac{k-2}{2}$. In the case where $\hat{I}_k$ has a *simple* pole at α_k, we have to compute the residue at the *next* pole on the right. This residue requires us to find an analytical continuation of $\hat{I}_k$ *outside* the fundamental strip of convergence, which is achieved via integration by parts.

After the required residues have been computed, we apply the inverse Mellin transform to determine the expansion of I_k as an extended power series in ρ. We find again that to leading order $\mathrm{d}W_{\mathrm{int}}/r_1\mathrm{d}\theta_1$ depends on ρ^{-2}, the inverse square of nearest-neighbor separation between steps. The correction terms involve logarithms and higher powers of ρ. We reiterate that the magnitude of these corrections in

relation to the omitted terms in (4.10) involving the Poisson ratio is not known a priori. Adding the corrections from the residues at more distant poles of $\hat{I}_k$ might not be enough to ensure agreement of our formula with the elastic energy of a stepped surface. The cross-terms of (4.10) might prove more important in the correction of our leading-order result.

For the purposes of this thesis, it is sufficient to note that the elastic interaction energy between two neighboring steps decays as the inverse square of their separation along the transverse direction. The prefactor of this leading-order term depends only on the values of the local coordinates and their derivatives, e.g., the factor $B_0(0)A(0)^{-1/2}/r(0)^4$ which appears in the expansion of $I_0(\rho)$ [71]. This result is similar to the step interaction formula used by Margetis and Kohn [66], who postulated a geometrical factor $\Phi(\cdot,\cdot)$ to account for the possible variation of step curvature. Here we do not attempt to make an explicit connection between the Φ of [66] and the corresponding coefficient of our extended power series in ρ. This coefficient in our extended power series depends in principle on which point of step 1 we use to orient our Cartesian coordinates. In contrast, the Φ of [66] depends only on the transverse coordinates $\eta_i, \eta_{i\pm1}$. Compatibility conditions between these two formulas are not pursued further, since the macroscopic limit eventually averages out any microscopic discrepancies in the interaction energy.

In this section we have summarized a rather substantial calculation, which derives the leading-order term of the elastic interaction energy between reasonably arbitrary 2D steps. The macroscale limits we derive in the next three chapters are not sensitive to the exact coefficient of this leading-order term. It suffices to note

that the calculations above offer a convincing demonstration of the *step separation dependence* typically assumed for elastic interaction energy. This inverse-square dependence is used in Chapter 5 to derive a formula for the macroscale chemical potential, which remains invariant under changes in the kinetic processes operating at the nanoscale.

Chapter 5

Review of equations for interacting steps in 2+1 dimensions, and macroscale limit[1]

In this chapter, we describe a model of interacting steps in 2+1 dimensions when the adatom diffusion is isotropic on each terrace. Then, we review the derivation of a macroscale evolution equation for the relaxation of a stepped crystal surface. A remarkable feature of the macroscopic description is that the effective surface mobility (or diffusivity) is strictly a tensor. The step-normal and step-parallel components of the macroscale surface flux scale differently as functions of the corresponding components of the chemical potential gradient. This prediction of a tensor mobility appears only as a result of coarse-graining the equations for step flow. Proceeding by analogy with the macroscale equation of 1-dimensional stepped surfaces would suggest a scalar mobility instead [64, 108].

We note that the tensor character of the mobility only manifests itself in the regimes of attachment-detachment limited (ADL) or mixed kinetics. Our predictions for surface relaxation subject to diffusion-limited (DL) kinetics would be indistinguishable from the predictions of a theory with scalar mobility.

[1]Material in this chapter appeared previously in Quah and Margetis, J. Phys. A: Math. Theor. **41**, 235004/1–18.

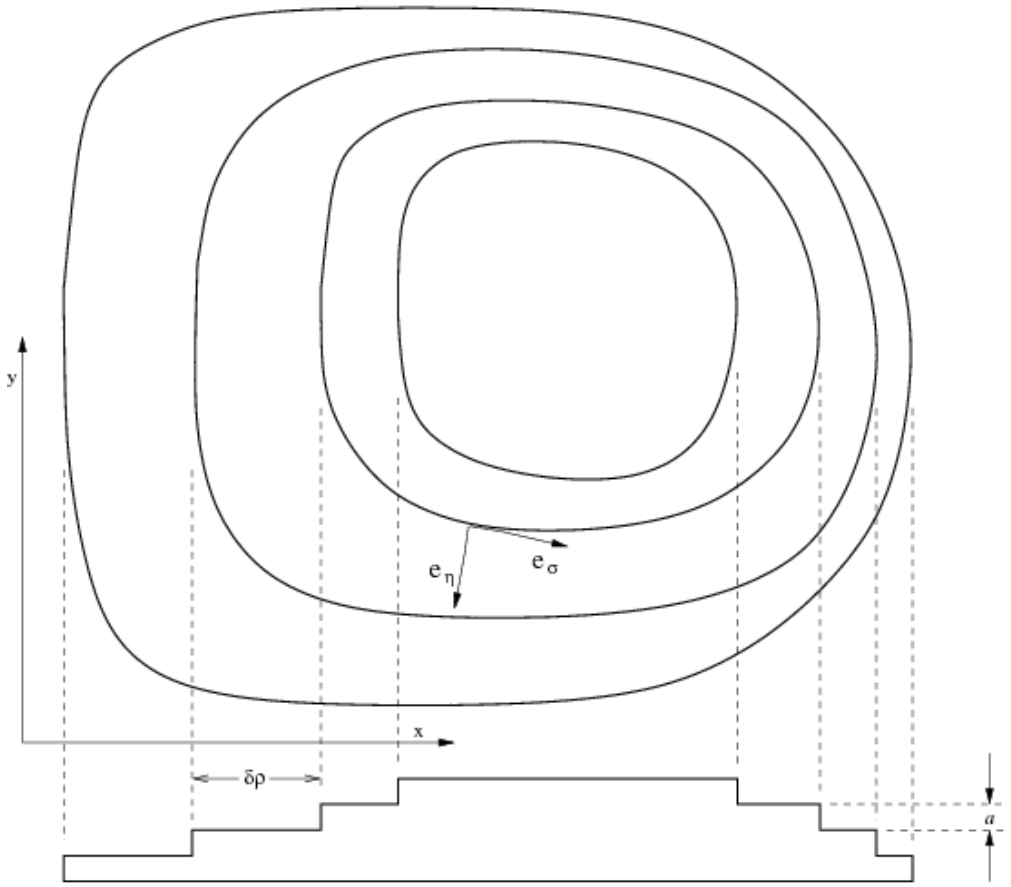

Figure 5.1: Orthogonal projection of step edges.

5.1 Geometry of a step train in 2+1 dimensions

In the spirit of the BCF theory [10], the edges of steps are projected to closed, noncrossing, and non-self-intersecting curves in a reference (*basal*) plane, where positions are indicated using fixed coordinates (x, y); see Fig. 5.1. These curves must possess x- and y-derivatives up to second order, so that the curvature, tangent vector, and normal vector are well-defined at each point on a curve. We treat the curves corresponding to step edges as moving boundaries for the adatom diffusion of each terrace.

Numbering the steps $i = 0, 1, 2, \ldots$, starting from the topmost step, we identify

the ith step with the boundary of the compact set $\{(x, y) : h(x, y, t) \geq h_f(t) - ia\}$. (Recall that $h_f(t)$ denotes the maximum height at time t, whether achieved at an isolated point or on a facet.) The ith step is in general a one-dimensional level set, and defining it in terms of fixed coordinates x and y is not always the most convenient option. We introduce local coordinates (η, σ) associated with the steps to describe the surface profile. The local coordinate η is roughly analogous to the radius in polar coordinates and increases monotonically as we descend the step train. In these new coordinates, the ith step corresponds to the set $\{\eta = \eta_i\}$ in the basal plane. The variable η serves as a continuous analog of the discrete step index i. Positions between step i and step $i + 1$ can be assigned η-coordinates from the set $\eta_i < \eta < \eta_{i+1}$, which is a local-coordinate description of the ith terrace. The local coordinate σ, analogous to the polar angle θ, measures the distance along a step edge; to be definite, we choose σ to increase counterclockwise (top view). By construction, the level sets of η and σ intersect at right angles; the associated unit vectors $\mathbf{e}_\eta$ and $\mathbf{e}_\sigma$ are orthogonal, $\mathbf{e}_\eta \cdot \mathbf{e}_\sigma = 0$. The reader is referred to [66] for more details.

For a fixed surface height profile, positions in the basal plane can be specified by their η and σ coordinates. If the height profile evolves in time, the mapping from local coordinates to fixed coordinates via $\mathbf{r} : (\eta, \sigma) \mapsto (x, y) \in \mathbb{R}^2$ can be viewed as a function of the time t. From this coordinate transformation we obtain two scale factors (metric coefficients) associated with the step coordinates. These metric coefficients, which appear when we compute spatial derivatives in (η, σ), are

[5]

$$\xi_\eta := |\partial_\eta \mathbf{r}|, \quad \xi_\sigma := |\partial_\sigma \mathbf{r}|. \tag{5.1}$$

A typical geometry of interest occurs when a mound or valley described by a given collection of steps projects onto a bounded rectangular region $\mathcal{B}$ in the basal plane. Periodically extending the height profile from $\mathcal{B}$ to all of $\mathbb{R}^2$ creates a mathematical representation of a regular surface corrugation. In this periodic setting, the monotonicity of the step train is violated in certain regions. We expect on physical grounds that solutions of the macroscale evolution law, known to be valid where the step train is monotonic, can be connected continuously across regions where monotonicity is violated. We consider periodic surface profiles in our subsequent numerical investigations in Chapter 10. The step geometry outlined here remains unaltered when we consider terrace anisotropy in Chapter 6.

5.2 BCF model with step interactions in 2+1 dimensions

Proceeding in the same vein as in the case of everywhere parallel steps, we denote by C_i the adatom density on the ith terrace, $\eta_i < \eta < \eta_{i+1}$. This C_i satisfies a diffusion equation, which under the quasi-steady approximation reads

$$0 = \operatorname{div}(\mathbf{D}^{\mathrm{ad}} \cdot \nabla C_i), \tag{5.2}$$

where $\mathbf{D}^{\mathrm{ad}}$ is in principle a tensor (2×2 matrix) diffusivity and $\nabla = \mathbf{e}_\eta \xi_\eta^{-1} \partial_\eta + \mathbf{e}_\sigma \xi_\sigma^{-1} \partial_\sigma)$ is the gradient on the basal plane. We define the adatom flux as

$$\mathbf{J}_i^{\mathrm{ad}} = -\mathbf{D}^{\mathrm{ad}} \cdot \nabla C_i, \tag{5.3}$$

which is Fick's law of diffusion in the absence of drift.

Note that (5.2) amounts to the most elementary description of surface relaxation by adatom diffusion, leaving out the effects of atom desorption, electromigration, and material deposition from above. These effects can be modeled by additive terms in (5.2), as we discuss in Chapter 8 (for desorption and electromigration). For the purposes of this chapter, (5.2) along with requisite boundary conditions at step edges are enough to illustrate the contrast between (1+1)- and (2+1)-dimensional surface morphological evolution.

Robin boundary conditions at the boundaries (step edges) of the ith terrace complement (5.2) to yield a unique solution for C_i. By analogy with the boundary conditions for everywhere parallel steps, we expect that the flux normal to a step edge is proportional to the difference between the actual adatom density and the equilibrium adatom density. So, we consider only the component $J^{\rm ad}_{i,\perp} := \mathbf{e}_\eta \cdot \mathbf{J}^{\rm ad}_i$ when writing the linear kinetic boundary conditions:

$$-J^{\rm ad}_{i,\perp}(\eta_i, \sigma, t) = k_u[C_i(\eta_i, \sigma, t) - C^{\rm eq}_i(\sigma, t)], \tag{5.4}$$

$$J^{\rm ad}_{i,\perp}(\eta_{i+1}, \sigma', t) = k_d[C_i(\eta_{i+1}, \sigma', t) - C^{\rm eq}_{i+1}(\sigma', t)], \tag{5.5}$$

where k_u, k_d are kinetic rates that account for the Ehrlich-Schwoebel barrier [17, 105] and $C^{\rm eq}_i(\sigma, t)$ is the equilibrium density at the ith step edge.

The relation between $C^{\rm eq}_i$ and the chemical potential of the ith step is precisely the same as in 1+1 dimensions, but now the chemical potential μ_i depends on the coordinate σ as well:

$$C^{\rm eq}_i(\sigma) = C_s \exp \frac{\mu_i(\sigma)}{k_B T} \sim C_s \left[1 + \frac{\mu_i(\sigma)}{k_B T}\right]. \tag{5.6}$$

The step chemical potential formula for arbitrary surface morphology, derived in [66] by a differential geometry calculation, expresses in 2+1 dimensions the combination of interaction energy and step line tension, which we first saw together in the axisymmetric setting. The result reads [66]

$$\mu_i = \frac{\Omega}{a}\left(\frac{1}{\xi_\eta}\partial_{\eta_i} U_i + \kappa_i U_i\right), \tag{5.7}$$

where Ω is the atomic volume, U_i is the total energy per length of the ith step edge and κ_i is the step edge curvature. We identify two contributions to U_i [66]:

$$U_i = \beta + U_i^{\text{int}}, \tag{5.8}$$

where β is the step line tension, assumed here to be constant, and U_i^{int} is the interaction term which depends on σ and the step positions $\{\eta_j\}$. For a surface with sufficiently small slope and nearest-neighbor interactions that decay as the inverse square of the terrace width, U_i^{int} is [66]

$$U_i^{\text{int}} = V_{i,i+1} + V_{i,i-1}, \tag{5.9}$$

$$V_{i,i+1} = \frac{g}{3} m_i^2 \Phi(\rho_i, \rho_{i+1}), \quad \rho_i := \int_{\eta_0}^{\eta_i} \xi_\eta \mathrm{d}\eta, \quad m_i := \frac{a}{\rho_{i+1} - \rho_i}, \tag{5.10}$$

where $g > 0$ is a constant quantifying the strength of step interactions, ρ_i corresponds to the radial distance in polar coordinates, m_i is the discrete step density, and Φ is a shape factor; note that $\Phi(\rho_i, \rho_i)$ is a constant, independent of the distance ρ_i [66]. The important feature of (5.10) is the inverse-square dependence on step separation, which follows from the elastic interaction formulas of Chapter 4. As we saw in Chapter 4, the calculation of a shape factor even in the special case of axisymmetry requires a substantial amount of analysis. We alert the reader that

(5.10) is an approximation, omitting the σ dependence of the prefactor to avoid unwarranted complications in the subsequent coarse-graining.

An alternative definition of the step chemical potential invokes the total energy, E^{steps}, of a step train in 2+1 dimensions. Each step contributes a line tension energy in proportion to its total arclength, because it takes energy to create the line defect of a step on a crystal surface. Moreover, the repulsive interaction between a step and its same-sign neighbors also adds to the total energy E^{steps}. Recall from Chapter 3 that the existence of a step introduces a mechanical strain field in the crystal. This strain field can be modeled as the result of a force dipole located at each point along the step. Each pair of neighboring step segments contributes an elastic interaction energy given by the energy of two interacting force dipoles, for example the dipoles $\mathrm{d}s_i\mathbf{e}_\eta|_i$, $\mathrm{d}s_{i+1}\mathbf{e}_\eta|_{i+1}$. In addition, neighboring steps exert an entropic repulsion on each other. We consolidate these contributions into a single integral over the ith step, and then sum over the step train to obtain

$$E^{\text{steps}} = \sum_i \int_{L_i} (\beta + V_{i,i+1})\mathrm{d}s. \tag{5.11}$$

To determine the step chemical potential μ_i, we need to know the number of additional atoms required at the ith step to effect a given change in step train energy. The normal displacement $v_i(\sigma)\Delta t$ at each position σ along the ith step will require the addition of enough atoms to cover an area of $\int_{L_i} v_i(\sigma)\Delta t\mathrm{d}s$. The typical cross-sectional area of an atom is Ω/a. According to the definition of step chemical potential, these additional atoms at the ith step will change the total energy by an amount $\frac{1}{\Omega/a}\int_{L_i} v_i(\sigma)\mu_i(\sigma)\mathrm{d}s\Delta t$. Summing up the contributions from every step to

determine the change in total energy, $\Delta E = \dot{E}^{\text{steps}}\Delta t$, yields a weak formulation of the step chemical potential, μ_i. We equate the sum over all steps with the direct calculation of $\dot{E}^{\text{steps}}$ using (5.11). The result is

$$\dot{E}^{\text{steps}} = \frac{1}{\Omega/a}\sum_i \int_{L_i} v_i \mu_i(\sigma)\mathrm{d}s. \tag{5.12}$$

We will use this weak formulation of the step chemical potential when deriving the macroscale limit in Section 5.4.2.

Before giving the final equations connecting the chemical potential to the step velocities, we take a moment to identify which of the preceding relations will carry through unchanged when we consider extensions of the terrace adatom kinetics. The definitions of local coordinates and metric coefficients, as noted above, will persist in their present form. In addition, the definitions of C_i^{eq} and μ_i are independent of the adatom kinetics on terraces, so their formulation here will carry through unaltered to the study of anisotropic terrace diffusion (Chapter 6) and electromigration (Chapter 8).

Lastly, we present the step velocity law in 2+1 dimensions. By including diffusion of atoms along the step edge with constant edge diffusivity D^{ed}, the normal velocity of the ith step edge is [82]

$$v_i = \mathbf{e}_\eta \cdot \frac{\mathrm{d}\mathbf{r}_i}{\mathrm{d}t} = \frac{\Omega}{a}(J^{\text{ad}}_{i-1,\perp} - J^{\text{ad}}_{i,\perp}) + a\partial_s\left(D^{\text{ed}}\partial_s \frac{\mu_i}{k_B T}\right), \tag{5.13}$$

where ∂_s is the space derivative along a step edge; $\partial_s = \xi_\sigma^{-1}\partial_\sigma$. The first term in (5.13) is the contribution of terrace adatom fluxes. The second term is due to step edge diffusion and stems from the variation of the step chemical potential, μ_i. We reason that the same μ_i has to be used both in edge diffusion and in C_i^{eq} by

virtue of the fact that μ_i controls the equilibrium shape of a step. This equilibrium shape should be the same regardless of which kinetic pathway (edge diffusion or attachment-detachment) is operative in the deformation of the step shape. So, if mass exchange with the terrace is turned off and relaxation occurs via edge diffusion, the step attains the same shape as in the case where edge diffusion is turned off and relaxation is allowed only by attachment-detachment kinetics. This property implies that the thermodynamic driving force has to be the same chemical potential, μ_i, in both cases [54].

Equations (5.2)–(5.13) in principle constitute a system of coupled differential equations for the step positions. As a discrete scheme of step flow, this system has been implemented numerically only in the case of straight or axisymmetric step trains. In this chapter we focus on (2+1)-dimensional settings where

$$D^{\mathrm{ed}} = 0 \tag{5.14}$$

and $\mathbf{D}^{\mathrm{ad}}$ is a scalar constant.

5.3 Approximations for slowly varying step train

We see from (5.13) that the adatom flux $\mathbf{J}_i^{\mathrm{ad}}$ plays a pivotal role in connecting the step normal velocity v_i to the step chemical potential. By solving approximately the diffusion equation (5.2) following [66], we write an explicit formula for the adatom flux.

We review the assumptions underlying the approximate solution of (5.2) subject to (5.4),(5.5). We assume that the boundary data C_i^{eq} varies more rapidly with

the step index i than the longitudinal coordinate σ. The slow variation in σ should also be expected of the solution for adatom density. We treat the derivative ∂_σ as $O(\epsilon)$ in comparison to the derivative ∂_η, which is treated as $O(1)$; $\epsilon \ll 1$. A possible geometric interpretation of ϵ is the ratio a/R where $R = O(\lambda)$ is a typical radius of curvature for steps and λ is a suitable macroscopic length [66]. Once the macroscale surface flux is derived, the assumptions for the η and σ derivatives are relaxed: both derivatives are allowed to be $O(1)$.

By neglecting the σ derivatives in (5.2), for constant $\mathbf{D}^{\mathrm{ad}}$ the diffusion equation for C_i reduces to

$$\partial_\eta \left(\frac{\xi_\sigma}{\xi_\eta} \partial_\eta C_i \right) \approx 0 \ , \tag{5.15}$$

which has the explicit solution

$$C_i \approx A_i(\sigma, t) \int_{\eta_i}^{\eta} \frac{\xi_\eta}{\xi_\sigma} \, \mathrm{d}\eta' + B_i(\sigma, t) \qquad \eta_i < \eta < \eta_{i+1} \ , \tag{5.16}$$

where A_i and B_i are integration constants to be determined via the boundary conditions (5.4), (5.5). A more systematic description of this procedure is offered in Chapter 8.

For isotropic adatom diffusion [66] with (scalar) diffusivity D^{ad} the vector-valued adatom flux is computed by

$$\mathbf{J}_i^{\mathrm{ad}} = -D^{\mathrm{ad}} \nabla C_i \ . \tag{5.17}$$

By use of (5.4) and (5.5), the flux components evaluated at $\eta = \eta_i$ are

$$J^{\rm ad}_{i,\perp} = -\frac{D^{\rm ad}C_s}{k_BT}\,\frac{1}{\xi_\sigma|_i}\,\frac{\mu_{i+1}-\mu_i}{D^{\rm ad}\left(\frac{1}{k_u\xi_\sigma|_i}+\frac{1}{k_d\xi_\sigma|_{i+1}}\right)+\int_{\eta_i}^{\eta_{i+1}}\frac{\xi_\eta}{\xi_\sigma}{\rm d}\eta}, \tag{5.18}$$

$$J^{\rm ad}_{i,\parallel} = -\frac{D^{\rm ad}}{\xi_\sigma|_i}\partial_\sigma\left\{\frac{D^{\rm ad}\left(\frac{C^{\rm eq}_{i+1}}{k_u\xi_\sigma|_i}+\frac{C^{\rm eq}_i}{k_d\xi_\sigma|_{i+1}}\right)+C^{\rm eq}_i\int_{\eta_i}^{\eta_{i+1}}\frac{\xi_\eta}{\xi_\sigma}{\rm d}\eta}{D^{\rm ad}\left(\frac{1}{k_d\xi_\sigma|_{i+1}}+\frac{1}{k_u\xi_\sigma|_i}\right)+\int_{\eta_i}^{\eta_{i+1}}\frac{\xi_\eta}{\xi_\sigma}{\rm d}\eta}\right\}, \tag{5.19}$$

where $J^{\rm ad}_{i,\parallel} := \mathbf{e}_\sigma \cdot \mathbf{J}^{\rm ad}_i$.

An alternative yet equivalent derivation of the approximate solution to (5.2),(5.4),(5.5), based on Taylor expansions at adjacent step edges [67] is reviewed in Chapter 6.

5.4 Macroscale limit with isotropic diffusion in 2+1 dimensions

In this section we present the macroscale limit of the discrete model (5.2)–(5.13) when the physics of each terrace is isotropic ($\mathbf{D}^{\rm ad} = D^{\rm ad}$: scalar) and there is no step edge diffusion ($D^{\rm ed} = 0$). This macroscale limit is a PDE for the surface height, one of whose possible discretizations coincides with the equations of step flow, (5.2)–(5.13). The surface height will be shown to obey a nonlinear fourth-order PDE.

First, we summarize the main assumptions underlying the derivation in [66]. The macroscale limit corresponds formally to taking $a/\lambda \to 0$ where λ is a macroscopic length. We note that it is a dimensionless ratio whose magnitude tends to zero; the macroscale limit makes no claim about physical lengths in an absolute sense, only in relation to other lengths relevant to the crystal surface. The metric coefficients ξ_σ and ξ_η are $O(\lambda)$, while the terrace width $\delta\rho_i$ is $O(a)$. Therefore, we have $\delta\eta_i = \eta_{i+1} - \eta_i \sim \delta\rho_i\xi_\eta^{-1} = O(a/\lambda) \to 0$. In this limit, we must keep as fixed,

$O(1)$ quantities the step density $m_i = a/\delta\rho_i$ and the kinetic parameters $D^{\rm ad}/(k_l a)$ where $l = u$ or d.

To obtain the macroscale limit, we must identify any discrete variable Q_i defined at a step edge ($\eta = \eta_i$) with the evaluation of a continuous, sufficiently differentiable function $\widetilde{Q}(\eta)$ at $\eta = \eta_i$. Thus, $Q_{i+1} - Q_i \approx (\delta\eta_i)\,\partial_\eta \widetilde{Q}|_i$ where $\mathcal{A}|_i$ is used in place of $\mathcal{A}(\eta_i)$ throughout. The following geometric limits made in [66] carry through for the macroscale limit of Chapters 6, 7, and 8 as well.

(i) The step density approaches the surface slope,

$$m_i \to m = |\nabla h||_i = O(1).$$

(ii) The unit vector normal to the ith step edge becomes

$$\mathbf{e}_\eta|_i \to \mathbf{e}_\eta = -\frac{\nabla h}{|\nabla h|}.$$

(iii) The step curvature, $\kappa_i = \nabla \cdot \mathbf{e}_\eta|_i$, approaches

$$\kappa_i \to \kappa = -\nabla \cdot \left(\frac{\nabla h}{|\nabla h|} \right).$$

(iv) The step normal velocity, $v_i = \mathbf{e}_\eta \cdot \mathrm{d}\mathbf{r}_i/\mathrm{d}t$, becomes

$$v_i \to v(\mathbf{r}, t) = \frac{\partial_t h}{|\nabla h|},$$

the velocity of the level set with height h.

Just as in the case of relaxation above the roughening temperature, the macroscale evolution equation consistent with the behavior of steps has three ingredients. We consider separately (i) the macroscopic analog of Fick's law, (ii) the formula for

macroscale step chemical potential, and (iii) the macroscopic law of mass conservation. Combining these three ingredients yields the desired PDE for the surface height h.

5.4.1 Adatom flux

We derive the macroscale limit of the flux components (5.18) and (5.19). The terms on the right-hand sides of these equations are replaced by series expansions as $\delta\eta_i \to 0$. In particular, we use the expansions

$$\int_{\eta_i}^{\eta_{i+1}} \frac{\xi_\eta}{\xi_\sigma} \mathrm{d}\eta = \frac{\xi_\eta|_i}{\xi_\sigma|_i}\delta\eta_i + \mathcal{O}[(\delta\eta_i)^2], \tag{5.20}$$

$$\mu_{i+1}(\sigma) - \mu_i(\sigma) = \xi_\eta|_i \delta\eta_i \partial_\eta \mu|_i + \mathcal{O}(\delta\eta_i^2), \tag{5.21}$$

$$\frac{1}{k_u}\frac{1}{\xi_\sigma|_i} + \frac{1}{k_d}\frac{1}{\xi_\sigma|_{i+1}} = \left(\frac{1}{k_u} + \frac{1}{k_d}\right)\frac{1}{\xi_\sigma|_i}[1 + \mathcal{O}(\delta\eta_i)], \qquad \delta\eta_i = \eta_{i+1} - \eta_i \to 0. \tag{5.22}$$

The resulting macroscale limit has the form of a matrix equation involving the adatom mobility $\mathbf{M}^{\mathrm{ad}}$,

$$\mathbf{J}_i^{\mathrm{ad}}|_i \to \mathbf{J}^{\mathrm{ad}}(\mathbf{r}, t) = \begin{pmatrix} J_\perp^{\mathrm{ad}} \\ \\ J_\parallel^{\mathrm{ad}} \end{pmatrix} = -C_s \mathbf{M}^{\mathrm{ad}} \cdot \begin{pmatrix} \partial_\perp \mu \\ \\ \partial_\parallel \mu \end{pmatrix}, \tag{5.23}$$

where

$$\mathbf{M}^{\mathrm{ad}} = \frac{D^{\mathrm{ad}}}{k_B T} \begin{pmatrix} \dfrac{1}{1 + q|\nabla h|} & 0 \\ \\ 0 & 1 \end{pmatrix}, \tag{5.24}$$

$\partial_\perp = \xi_\eta^{-1}\partial_\eta$, $\partial_\parallel = \xi_\sigma^{-1}\partial_\sigma$ and the kinetic parameter q is defined by

$$q := \frac{2D^{\mathrm{ad}}}{ka}, \qquad k^{-1} := (k_u^{-1} + k_d^{-1})/2. \tag{5.25}$$

Evidently, normal and longitudinal variations in the chemical potential contribute with unequal weight to the respective components of the surface flux. The tensor

mobility $\mathbf{M}$ reflects the fact that adatom flux normal to steps is inhibited by the attachment-detachment process, whereas longitudinal fluxes face no such barrier. The mobility $\mathbf{M}$ in (5.24) has dimensions ((length)^2(time)$^{-1}$(energy)$^{-1}$), and the macroscale step chemical potential μ has dimensions (energy/length).

In the basal plane's Cartesian coordinate system, the matrix elements M_{ij} are found by applying the change-of-basis matrix [66, 67]

$$\mathbf{S} = (\mathbf{e}_\eta \mathbf{e}_\sigma) = \frac{1}{|\nabla h|} \begin{pmatrix} -\partial_x h & \partial_y h \\ -\partial_y h & -\partial_x h \end{pmatrix}, \tag{5.26}$$

which yields

$$M_{xx} = \frac{D^{\mathrm{ad}}}{k_B T} \frac{(\partial_x h)^2}{|\nabla h|^2} \left[\frac{1}{1 + q|\nabla h|} + \alpha^2 \right], \tag{5.27}$$

$$M_{xy} = M_{yx} = -\frac{D^{\mathrm{ad}}}{k_B T} \frac{q|\nabla h|}{1 + q|\nabla h|} \frac{(\partial_x h)^2}{|\nabla h|^2} \alpha, \tag{5.28}$$

$$M_{yy} = \frac{D^{\mathrm{ad}}}{k_B T} \frac{(\partial_x h)^2}{|\nabla h|^2} \left[\frac{\alpha^2}{1 + q|\nabla h|} + 1 \right], \tag{5.29}$$

where $\alpha := \frac{\partial_y h}{\partial_x h}$.

Equation (5.23) is complemented by a mass conservation statement for the height profile h and a formula for the macroscale step chemical potential μ.

5.4.2 Macroscale step chemical potential

Next, we invoke (5.11)–(5.12) for the step chemical potential μ_i. First we multiply both sides of (5.11) by the step height a:

$$aE^{\mathrm{steps}} = \sum_i a \int_{L_i} \mathrm{d}s \left[\beta + \frac{g}{3} m_i^2 \Phi(\rho_i, \rho_{i+1}) \right]. \tag{5.30}$$

The sum over all steps in (5.30) can be interpreted as a quadrature scheme for the following integral with respect to the surface height h:

$$\lim_{a\to 0} aE^{\text{steps}} = \int \mathrm{d}h \int_{h=\text{const.}} \mathrm{d}s \left[\beta + \frac{g}{3}\Phi_0 |\nabla h|^2\right]. \tag{5.31}$$

Notice that the integrand in (5.31) is a function of the step index i and position σ along the step. Because h depends monotonically on the step index, we could consider the integrand in (5.31) as a function of h and σ. The sum over all steps in (5.30) formally approaches the Riemann integral with respect to h as $a \to 0$. In addition, the integrand of (5.11) is recast into its macroscale height counterpart, with $|\nabla h|$ in place of m_i and Φ_0 in place of $\Phi(\rho_i, \rho_{i+1})$.

The integral in (5.31) can be evaluated more easily by a change of variables. We apply the "coarea formula" [24], which allows us to integrate with respect to the area element $\mathrm{d}A$ in the basal plane.

For any integrable function $\psi(\mathbf{r})$, we have

$$\int \mathrm{d}h \int_{h=\text{const.}} \mathrm{d}s \psi(\mathbf{r}) = \int\int \mathrm{d}A |\nabla h| \psi(\mathbf{r}). \tag{5.32}$$

Using (5.32) and (5.31), we find

$$\lim_{a\to 0} aE^{\text{steps}} = \int\int \mathrm{d}A [\beta |\nabla h| + \frac{g}{3}\Phi_0 |\nabla h|^3]. \tag{5.33}$$

Similarly, the sum over all steps in (5.12) can be interpreted as a quadrature scheme for the following integral with respect to surface height:

$$\dot{E}^{\text{steps}} = \frac{1}{\Omega} \sum_i a \int_{L_i} \mathrm{d}s v_i \mu_i(\sigma) \tag{5.34}$$

$$\lim_{a\to 0} \dot{E}^{\text{steps}} = \frac{1}{\Omega} \int_{h=const.} \mathrm{d}h \int_{L_i} \mathrm{d}s \frac{\partial_t h}{|\nabla h|} \mu \tag{5.35}$$

$$= \frac{1}{\Omega} \int\int \mathrm{d}A |\nabla h| \frac{\partial_t h}{|\nabla h|} \mu, \tag{5.36}$$

where the last equality follows from the coarea formula.

An alternative formula for $\dot{E}^{\text{steps}}$ is obtained by differentiating (5.33) with respect to time.

$$\begin{aligned}
\lim_{a\to 0} \dot{E}^{\text{steps}} &= \int\int \mathrm{d}A \frac{\partial}{\partial t} [\beta |\nabla h| + \frac{g}{3} \Phi_0 |\nabla h|^3] \\
&= \frac{1}{a} \int\int \mathrm{d}A \frac{\partial}{\partial m} [\beta m + \frac{g}{3} \Phi_0 m^3] \frac{\partial m}{\partial t}, \qquad m := |\nabla h| \\
&= \frac{1}{a} \int\int \mathrm{d}A \frac{\partial}{\partial m} [\beta m + \frac{g}{3} \Phi_0 m^3] \frac{\nabla h}{|\nabla h|} \cdot \nabla \partial_t h.
\end{aligned} \tag{5.37}$$

We integrate (5.37) by parts to separate space and time derivatives of h. The integration region extends to the far-field where $\partial_t h = 0$; hence, boundary terms vanish and (5.37) reduces to

$$\lim_{a\to 0} a\dot{E}^{\text{steps}} = -\int\int \mathrm{d}A \,\mathrm{div} \left\{ \partial_m [\beta m + \frac{g}{3} \Phi_0 m^3] \frac{\nabla h}{|\nabla h|} \right\} \partial_t h. \tag{5.38}$$

Now we compare (5.36) and (5.38), which must agree for any $\partial_t h$. We can view $\partial_t h$ as an arbitrary test function in $L^2(\mathcal{B})$ that vanishes on the boundary $\partial\mathcal{B}$. In none of these calculations did we assume that h solved a particular PDE. As far as the energetic formulas are concerned, $\partial_t h$ can vary independently of ∇h. In order

for the two formulas to agree, the macroscale chemical potential must be given by

$$\mu = -\frac{\Omega}{a}\,\mathrm{div}\left\{\beta\frac{\nabla h}{|\nabla h|} + g\Phi_0|\nabla h|\nabla h\right\}. \tag{5.39}$$

For ease of notation we define $g_1 := \beta/a$ and $g_3 := g\Phi_0/a$. An alternative derivation of (5.39) using differential geometry on the basis of (5.7) appears in [66].

5.4.3 Mass conservation for adatoms

For $D^{\mathrm{ed}} = 0$ the step velocity law (5.13) reduces to the usual mass conservation statement for adatoms [66]. As noted above, the step velocity v_i approaches $\partial_t h/|\nabla h|$ in the macroscale limit. To derive the mass conservation law in the limit $a/\lambda \to 0$, we first define a functional $I[\phi]$ which integrates the test function ϕ against the normal velocity v_i and sums over all steps:

$$I[\phi] := \sum_i \int_{L_i} \mathrm{d}s v_i \phi|_i. \tag{5.40}$$

Viewing the sum (5.40) as a quadrature scheme for an integral with respect to h, we apply the coarea formula (5.32) to obtain

$$I[\phi] \sim \frac{1}{a}\int\int \mathrm{d}A|\nabla h| v\phi = \frac{1}{a}\int\int \mathrm{d}A\partial_t h\phi, \qquad a/\lambda \to 0. \tag{5.41}$$

On the other hand, if in (5.40) we replace v_i by a difference of normal fluxes according to (5.13), the result is

$$I[\phi] = -\frac{\Omega}{a}\sum_i \int_{L_i} \mathrm{d}s[\mathbf{J}\cdot\mathbf{e}_\eta]|_i\phi|_i, \tag{5.42}$$

where $[\mathbf{J}\cdot\mathbf{e}_\eta]|_i$ denotes the jump $(\mathbf{J}_i(\eta_i,\sigma) - \mathbf{J}_{i-1}(\eta_i,\sigma))\cdot\mathbf{e}_\eta|_{i,\sigma}$. Recalling that the adatom surface current $\mathbf{J}(\mathbf{r},t)$ on the basal plane interpolates the nodal values $\mathbf{J}_i^{\mathrm{ad}}|_i$, and $\mathrm{div}\mathbf{J}_i^{\mathrm{ad}} = 0$ on each terrace, we have

$$I[\phi] = -\frac{\Omega}{a}\int\int \mathrm{d}A\, \mathrm{div}\mathbf{J}\phi. \tag{5.43}$$

Equating (5.41) and (5.43) for arbitrary test functions ϕ, we find the weak formulation of adatom mass conservation:

$$\partial_t h = -\Omega\, \mathrm{div}\mathbf{J}. \tag{5.44}$$

An alternative derivation of (5.44) proceeds by successive integration of $\mathrm{div}\mathbf{J}^{\mathrm{ad}}_{i-1} = 0$ over a path in the $(i-1)$th terrace from $(\eta_{i-1}, \sigma + \delta\sigma)$ to (η_i, σ), in order to substitute for $J_{i-1,\perp}|_{i,\sigma}$ in terms of $J_{i-1,\perp}|_{i-1,\sigma+\delta\sigma}$. The resulting formula for the jump in the normal flux is easily recognized as a discrete scheme for calculating the divergence of $\mathbf{J}^{\mathrm{ad}}$ in local coordinates, and the limit (5.44) follows in the strong sense [66].

5.4.4 Evolution equation for surface height

By combining the equations (5.23), (5.39), and (5.44), we find a PDE for the surface height $h(\mathbf{r}, t)$ [66, 67]:

$$\partial_t h = -B\, \mathrm{div}\left\{\mathbf{\Lambda}^{\mathrm{ad}} \cdot \nabla\left[\mathrm{div}\left(\frac{\nabla h}{|\nabla h|} + \frac{g_3}{g_1}|\nabla h|\nabla h\right)\right]\right\}, \tag{5.45}$$

where

$$\mathbf{\Lambda}^{\mathrm{ad}} := \frac{k_B T}{D^{\mathrm{ad}}}\mathbf{M}^{\mathrm{ad}}, \quad g_1 := \beta/a, \quad g_3 := 3g\Phi_0/a, \quad B := \frac{D^{\mathrm{ad}} C_s g_1 \Omega^2}{k_B T}. \tag{5.46}$$

The consolidation of constants is chosen so that B has dimensions $(\mathrm{length})^4/\mathrm{time}$ and $\mathbf{\Lambda}^{\mathrm{ad}}$ is dimensionless.

5.5 Scaling ansatz for the height profile

One of the motivations for deriving the macroscale limit (5.45) is its suitability for answering questions about the global surface morphological evolution under certain initial data for the surface height profile. In particular, we seek to classify the possible scaling laws permitted by the PDE for h. Here, the term "scaling law" describes the time-dependent part $A(t)$ of a separable solution,

$$h(\mathbf{r}, t) \approx H(\mathbf{r})A(t). \tag{5.47}$$

This variable separation, called a "scaling ansatz", is consistent with step simulations in 1D and kinetic Monte Carlo simulations in 2D , both for initial sinusoidal profiles. However, the scaling ansatz satisfies the PDE only approximately; we find a consistent equation by regarding as negligible some of the terms in μ and $\mathbf{M}^{\mathrm{ad}}$. It is not obvious that a single power of A will remain dominant in the equation for long times. Indeed, a given initial-boundary value problem with (5.45) need not have a separable solution. This property relies crucially on the initial data.

In order to extract a dominant power of A from the mobility matrix, we must compare the kinetic term $(1 + q\nu)^{-1}$ with the square of the aspect ratio α; here $\nu = \langle|\nabla h|\rangle$ is a typical slope. Depending on the relative magnitudes of these kinetic-geometric parameters, the elements of the mobility matrix might scale as A^0 or A^{-1}.

The macroscale step chemical potential μ scales with amplitude A according to which contribution to the energy dominates. If line tension (g_1 term) is dominant, then μ scales as A^0. If step interactions dominate, then μ scales as A^2. Combin-

Table 5.1: Decay laws for the amplitude $A(t)$ in ADL kinetics, taken from [67]. Top row: kinetic-geometric conditions on mobility. Leftmost column: dominant effects in μ. The constants $\mathcal{C}$, c, and $t^*(t^* > t)$ depend on $A(0) = A_0$ and H. The constant B_3 is defined by $B_3 := \frac{D^{\mathrm{ad}} C_s g_3 \Omega^2}{k_B T}$.

	$\alpha^2 \ll (1+q\nu)^{-1} \ll 1$	$(1+q\nu)^{-1} \ll \alpha^2 < 1$
Step interaction	$A_0 e^{-\mathcal{C}B_3 t}$	$A_0(1+cB_3A_0t)^{-1}$
Line tension	$A_0\sqrt{1-t/t^*}$	$A_0(1-t/t^*)$

ing these two possibilities with the kinetic-geometric conditions on the mobility, Margetis [67] obtained the possible scaling laws listed in Table 5.1.

We do not address analytically the spatial part of the approximate separable solution, $H(\mathbf{r})$, which solves a nonlinear PDE. Numerical solutions of the PDE, such as those given in Chapter 10, remain our most viable option for visualizing the spatial dependence of a separable solution.

5.6 Presence of facets in the variational formulation

The surface evolution law derived here conforms more closely to the behavior of steps than the PDEs obtained phenomenologically or by analogy with 1D macroscale models. However, the behavior of steps near a facet edge, where the surface energy has a singularity, is not respected by the PDE derived in this chapter. The variational formulation imposes its own *natural boundary conditions* at the facet edge, which in general are not identical to the boundary conditions stemming from

a microscale drop in height when the top step collapses [38]. We outline the natural boundary conditions in Chapter 9, in order to interpret the results of simulating the variational formulation in terms of strong PDE solutions informed by conditions at the free boundary. Only in the limiting case $g_1 \to 0$ can we expect the variational formulation to respect the flow of steps near $|\nabla h| = 0$. A hybrid approach, which informs the variational equations of the discrete height drop when the topmost step collapses, is beyond our scope in 2+1 dimensions, where an implementation of the step flow model is lacking. Comparison of the variational and hybrid approaches in the axisymmetric case [65] suggests that the discrepancy in boundary conditions is not likely to affect the observed scaling laws. To be cautious, however, we focus mainly on the case $g_1 = 0$ in our subsequent numerical simulations.

Chapter 6

Macroscale equation with terrace anisotropy and step edge diffusion[1]

In this chapter we extend the theory of chapter 5 to cases with a tensor-valued terrace diffusivity $\mathbf{D}^{\rm ad}$ and a nonzero edge diffusivity $D^{\rm ed}$. These extensions offer a more realistic description of diffusion processes on terraces and steps, while remaining firmly based in the framework of continuum steps. Again we seek a PDE for the surface height. The main contribution of this chapter is the surface mobility $\mathbf{M}$, which extends (5.24) by allowing for off-diagonal elements even in the local coordinate representation.

For convenience we rewrite the quasi-steady equation (5.2) describing adatom diffusion on the ith terrace:

$$\mathrm{div}(\mathbf{D}^{\rm ad} \cdot \nabla C_i) = 0 \ . \tag{6.1}$$

Equation (6.1) is complemented by the mixed boundary conditions dictated by linear kinetics:

$$-J_i^{\rm ad}(\eta_i, t) = k_u[C_i(\eta_i, t) - C_i^{\rm eq}(t)] \ , \tag{6.2}$$

$$J_i^{\rm ad}(\eta_{i+1}, t) = k_d[C_i(\eta_{i+1}, t) - C_{i+1}^{\rm eq}(t)] \ . \tag{6.3}$$

In this chapter the terrace diffusivity $\mathbf{D}^{\rm ad}$ is assumed to have the tensor form $\mathbf{D}^{\rm ad} = D_{11}\mathbf{e}_\eta\mathbf{e}_\eta + D_{12}\mathbf{e}_\eta\mathbf{e}_\sigma + D_{21}\mathbf{e}_\sigma\mathbf{e}_\eta + D_{22}\mathbf{e}_\sigma\mathbf{e}_\sigma$. For the sake of some generality,

[1]Material in this chapter appeared previously in Quah and Margetis, J. Phys. A: Math. Theor. **41**, 235004/1–18.

we do not impose the symmetry condition $D_{12} = D_{21}$, although in most physical settings this equality holds. The surface flux $\mathbf{J}_i^{\mathrm{ad}}$ depends on the adatom density C_i through the linear relation

$$\begin{pmatrix} J_{i,\perp}^{\mathrm{ad}} \\ J_{i,\parallel}^{\mathrm{ad}} \end{pmatrix} = - \begin{pmatrix} D_{11} & D_{12} \\ D_{21} & D_{22} \end{pmatrix} \cdot \begin{pmatrix} \xi_\eta^{-1} \partial_\eta C_i \\ \xi_\sigma^{-1} \partial_\sigma C_i \end{pmatrix} \qquad \eta_i < \eta < \eta_{i+1}, \tag{6.4}$$

which is Fick's law of diffusion in two spatial dimensions. This definition of surface flux is chosen so that the continuity relation

$$\oint_L \mathbf{J}_i^{\mathrm{ad}} \cdot \nu \mathrm{d}s = \frac{\mathrm{d}}{\mathrm{d}t} \int_{\mathrm{int}L} C_i \mathrm{d}A \tag{6.5}$$

holds for every closed loop L lying in the ith terrace.

6.1 Approximations for fast and slow step variables

In this subsection we provide relations for the adatom flux components at step edges for slowly varying step trains. The starting point is the boundary value problem for terrace adatom concentration C_i, which satisfies (6.1) subject to boundary conditions (6.2),(6.3). We note that the boundary conditions involve only the equilibrium concentrations at neighboring step edges, allowing us to solve the diffusion equation on each terrace independently. In local coordinates, the diffusion equation (6.1) becomes

$$\begin{aligned} &\frac{\partial}{\partial \eta} \left(\frac{\xi_\sigma D_{11}}{\xi_\eta} \frac{\partial C_i}{\partial \eta} \right) + \frac{\partial}{\partial \eta} \left(D_{12} \frac{\partial C_i}{\partial \sigma} \right) \\ &\quad + \frac{\partial}{\partial \sigma} \left(D_{21} \frac{\partial C_i}{\partial \eta} \right) + \frac{\partial}{\partial \sigma} \left(\frac{\xi_\eta D_{22}}{\xi_\sigma} \frac{\partial C_i}{\partial \sigma} \right) = 0 \ , \end{aligned} \tag{6.6}$$

where $\eta_i < \eta < \eta_{i+1}$.

For a slowly varying step train we invoke the separation of the variables (η, σ) into fast and slow as outlined in Chapter 5. A more rigorous justification of this procedure is postponed until Chapter 8, after we have developed some intuition about the solutions we obtain. Dropping σ derivatives in accordance with slow/fast variable separation, (6.6) reduces to

$$\partial_\eta \left(\frac{\xi_\sigma}{\xi_\eta} \partial_\eta C_i \right) \approx 0 \ , \tag{6.7}$$

which is solved by

$$C_i \approx A_i(\sigma, t) \int_{\eta_i}^{\eta} \frac{\xi_\eta}{\xi_\sigma} \, \mathrm{d}\eta' + B_i(\sigma, t) \qquad \eta_i < \eta < \eta_{i+1} \ , \tag{6.8}$$

for some η-independent functions A_i, B_i. In order to determine the integration constants A_i and B_i, we evaluate the flux components at the step edges and apply the boundary conditions (6.2),(6.3). The integration constants have a natural interpretation in terms of the adatom concentration and its gradient at the step edge. We eliminate A_i and B_i in favor of the more physical quantities $C_i|_i$, $\mathbf{J}|_i$ by applying Fick's law, (6.4).

Using (6.4), the corresponding flux components are

$$J^{\mathrm{ad}}_{i,\perp} \approx -\frac{D_{11}}{\xi_\sigma} A_i(\sigma, t) - \frac{D_{12}}{\xi_\sigma} \partial_\sigma \left[B_i(\sigma, t) + A_i(\sigma, t) \int_{\eta_i}^{\eta} \frac{\xi_\eta}{\xi_\sigma} \mathrm{d}\eta' \right] \ , \tag{6.9}$$

$$J^{\mathrm{ad}}_{i,\parallel} \approx -\frac{D_{21}}{\xi_\sigma} A_i(\sigma, t) - \frac{D_{22}}{\xi_\sigma} \partial_\sigma \left[B_i(\sigma, t) + A_i(\sigma, t) \int_{\eta_i}^{\eta} \frac{\xi_\eta}{\xi_\sigma} \mathrm{d}\eta' \right] \ . \tag{6.10}$$

Equations (6.9) and (6.10) are simplified when we evaluate $\mathbf{J}^{\mathrm{ad}}_i$ at $\eta = \eta_i$. The resulting matrix equation is

$$-\xi_\sigma|_i \begin{pmatrix} J^{\mathrm{ad}}_{i,\perp}|_i \\ \\ J^{\mathrm{ad}}_{i,\parallel}|_i \end{pmatrix} = \begin{pmatrix} D_{11} & D_{12} \\ \\ D_{21} & D_{22} \end{pmatrix} \begin{pmatrix} A_i \\ \\ \partial_\sigma B_i \end{pmatrix} \ . \tag{6.11}$$

By inspection of (6.11), the term $\partial_\sigma B_i$ must be treated on equal footing with A_i, since both terms make comparable contributions to the surface flux. We proceed to invert the matrix equation (6.11), viewing A_i and $\partial_\sigma B_i$ as integration constants that we have to eliminate from the boundary conditions (6.2) and (6.3). Thus, we obtain the formula

$$\begin{pmatrix} A_i \\ \\ \partial_\sigma B_i \end{pmatrix} = -\frac{\xi_\sigma|_i}{|\mathbf{D}^{\mathrm{ad}}|} \begin{pmatrix} D_{22} & -D_{12} \\ \\ -D_{21} & D_{11} \end{pmatrix} \begin{pmatrix} J^{\mathrm{ad}}_{i,\perp}|_i \\ \\ J^{\mathrm{ad}}_{i,\parallel}|_i \end{pmatrix} , \tag{6.12}$$

where $|\mathbf{D}^{\mathrm{ad}}| := D_{11}D_{22} - D_{12}D_{21}$ denotes the determinant of $\mathbf{D}^{\mathrm{ad}}$.

Next, we apply the boundary conditions (6.2) and (6.3) for atom attachment-detachment at step edges. By substituting the solution for the adatom density C_i into these conditions, we find the relations

$$-J^{\mathrm{ad}}_{i,\perp}(\eta_i,\sigma,t) = k_u[B_i(\sigma,t) - C^{\mathrm{eq}}_i(\sigma,t)] \tag{6.13}$$

$$J^{\mathrm{ad}}_{i,\parallel}(\eta_{i+1},\sigma',t) = k_d\left[B_i(\sigma',t) + A_i(\sigma',t)\int_{\eta_i}^{\eta_{i+1}} \frac{\xi_\eta}{\xi_\sigma}\,\mathrm{d}\eta - C^{\mathrm{eq}}_{i+1}(\sigma',t)\right]. \tag{6.14}$$

We eliminate B_i by setting $\sigma' = \sigma$ in equation (6.14), multiplying (6.13) by k_d/k_u and subtracting the resulting equation from (6.14). Substituting for A_i from (6.12), we arrive at the first desired relation between the surface flux components:

$$\begin{aligned}\left(\frac{1}{k_u} + \frac{\xi_\sigma|_i D_{22}}{|\mathbf{D}^{\mathrm{ad}}|}\int_{\eta_i}^{\eta_{i+1}} \frac{\xi_\eta}{\xi_\sigma}\mathrm{d}\eta\right) J^{\mathrm{ad}}_{i,\perp}|_i + \frac{1}{k_d}J^{\mathrm{ad}}_{i,\perp}|_{i+1} \\ - \frac{\xi_\sigma|_i D_{12}}{|\mathbf{D}^{\mathrm{ad}}|}\left(\int_{\eta_i}^{\eta_{i+1}} \frac{\xi_\eta}{\xi_\sigma}\mathrm{d}\eta\right) J^{\mathrm{ad}}_{i,\parallel}|_i = C^{\mathrm{eq}}_i - C^{\mathrm{eq}}_{i+1}\ .\end{aligned} \tag{6.15}$$

We obtain a second relation by exploiting variations in σ, which can be taken to be arbitrarily small; in contrast, changes in η are restricted by a and the requirement of finite slope. Therefore, we differentiate (6.13) with respect to σ and substitute for

$\partial_\sigma B_i$ from (6.12). Subsequently, we neglect $\partial_\sigma J^{\rm ad}_{i,\perp}$, consistent with the hypothesis of slowly varying step edge curvature. Thus, the second desired relation of the flux components reads

$$\frac{\xi_\sigma|_i}{|\mathbf{D}^{\rm ad}|}(D_{21}J^{\rm ad}_{i,\perp}|_i - D_{11}J^{\rm ad}_{i,\parallel}|_i) - \partial_\sigma C^{\rm eq}_i = 0 \ ,$$

which in turn becomes

$$D_{21}J^{\rm ad}_{i,\perp}|_i - D_{11}J^{\rm ad}_{i,\parallel}|_i = \frac{C_s|\mathbf{D}^{\rm ad}|}{\xi_\sigma|_i}\frac{\partial_\sigma \mu_i}{k_B T} = \frac{C_s|\mathbf{D}^{\rm ad}|}{k_B T}\partial_\parallel \mu_i \ . \tag{6.16}$$

Equations (6.15) and (6.16) suffice for the purpose of taking the macroscale limit.

6.2 Macroscale adatom flux

In this section we derive the analogue of (5.23) and (5.24), the relation between macroscale adatom flux and step chemical potential. The resulting mobility tensor, $\mathbf{M}^{\rm ad}$, accounts for the macroscale flux arising from adatom diffusion on terraces. An additional term, derived in Section 6.4, provides the mobility element corresponding to step edge diffusion.

First, we simplify relations (6.15) and (6.16) for $\mathbf{J}^{\rm ad}_i$. Considering $\delta\eta_i = \eta_{i+1} - \eta_i$ as small, we make the approximations

$$\frac{1}{k_u}J^{\rm ad}_{i,\perp}|_i + \frac{1}{k_d}J^{\rm ad}_{i,\perp}|_{i+1} = \left(\frac{1}{k_u} + \frac{1}{k_d}\right) J^{\rm ad}_{i,\perp}|_i\big[1 + O(\delta\eta_i)\big] \ , \tag{6.17}$$

$$\int_{\eta_i}^{\eta_{i+1}} \frac{\xi_\eta}{\xi_\sigma}{\rm d}\eta = \frac{\xi_\eta|_i}{\xi_\sigma|_i}\delta\eta_i\big[1 + O(\delta\eta_i)\big] \ . \tag{6.18}$$

We consolidate the kinetic rates k_u, k_d into the parameter $k = 2/(k_u^{-1} + k_d^{-1})$ of (5.25). Thus, (6.15) reduces to

$$\left[\left(\frac{2}{k} + \frac{\xi_\eta|_i D_{22}}{|\mathbf{D}^{\rm ad}|}\delta\eta_i\right) J^{\rm ad}_{i,\perp}|_i - \frac{\xi_\eta|_i D_{12}}{|\mathbf{D}^{\rm ad}|}\delta\eta_i J^{\rm ad}_{i,\parallel}|_i\right]\big[1 + O(\delta\eta_i)\big] = C^{\rm eq}_i - C^{\rm eq}_{i+1} \ . \tag{6.19}$$

We multiply (6.19) by $|\mathbf{D}^{\rm ad}|/(\xi_\eta|_i\delta\eta_i)$ and thereby obtain

$$\left(D_{22}+\frac{2|\mathbf{D}^{\rm ad}|}{k\xi_\eta|_i\delta\eta_i}\right)J^{\rm ad}_{i,\perp}|_i-D_{12}J^{\rm ad}_{i,\|}|_i=|\mathbf{D}^{\rm ad}|\frac{C^{\rm eq}_i-C^{\rm eq}_{i+1}}{\xi_\eta|_i\delta\eta_i}\ . \tag{6.20}$$

As $\delta\eta_i\to 0$, the right-hand side of (6.20) approaches $C_s|\mathbf{D}^{\rm ad}|\partial_\perp\mu/k_BT$. On the other hand, the ratio of parameters in the prefactor of $J^{\rm ad}_{i,\perp}|_i$ has the limiting value

$$\frac{2|\mathbf{D}^{\rm ad}|}{k\xi_\eta|_i\delta\eta_i}\to\frac{2|\mathbf{D}^{\rm ad}|}{ka}|\nabla h|=\mathcal{D}^{\rm ad}\,|\nabla h|\ ,\qquad \mathcal{D}^{\rm ad}:=\frac{2|\mathbf{D}^{\rm ad}|}{ka}\ , \tag{6.21}$$

where $\mathcal{D}^{\rm ad}$ has dimensions of diffusivity [(length)^2/time].

A matrix equation for the macroscale surface flux $\mathbf{J}^{\rm ad}=(J^{\rm ad}_\perp,J^{\rm ad}_\|)^T$ in terms of the step chemical potential μ comes from combining (6.16), (6.20) and (6.21):

$$\begin{pmatrix} D_{22}+\mathcal{D}^{\rm ad}|\nabla h| & -D_{12}\\ -D_{21} & D_{11}\end{pmatrix}\begin{pmatrix} J^{\rm ad}_\perp\\ J^{\rm ad}_\|\end{pmatrix}=-\frac{C_s|\mathbf{D}^{\rm ad}|}{k_BT}\begin{pmatrix}\partial_\perp\mu\\ \partial_\|\mu\end{pmatrix}\ . \tag{6.22}$$

By solving (6.22) for $\mathbf{J}^{\rm ad}$ we obtain

$$\mathbf{J}^{\rm ad}_i|_i\to\mathbf{J}^{\rm ad}(\mathbf{r},t)=\begin{pmatrix} J^{\rm ad}_\perp\\ J^{\rm ad}_\|\end{pmatrix}=-C_s\mathbf{M}^{\rm ad}\cdot\begin{pmatrix}\partial_\perp\mu\\ \partial_\|\mu\end{pmatrix}\ , \tag{6.23}$$

where the macroscale adatom mobility is

$$\mathbf{M}^{\rm ad}=\frac{1}{k_BT\,(1+q|\nabla h|)}\begin{pmatrix} D_{11} & D_{12}\\ D_{21} & D_{22}+\mathcal{D}^{\rm ad}|\nabla h|\end{pmatrix}\ ,\quad q:=\frac{2D_{11}}{ka}\ . \tag{6.24}$$

This formula reduces to the equation with diagonal $\mathbf{M}^{\rm ad}$ found in [66] when $D_{11}=D_{22}=D^{\rm ad}$ and $D_{12}=D_{21}=0$; cf (5.24). In contrast to the case with scalar diffusivity, all matrix elements of the mobility in (6.24) depend on the slope. This dependence is quite pronounced in the kinetic regime of attachment-detachment limited (ADL) kinetics, which we discuss in Section 6.6.

6.3 Alternative approach to macroscale limit: Taylor expansions

For the sake of completeness, we re-derive (6.23) and (6.24) via an alternative yet equivalent route. This is based on expansions of the boundary conditions (6.2) and (6.3) for atom attachment-detachment in appropriate Taylor series when $\delta\eta_i = \eta_{i+1} - \eta_i \to 0$ and $\delta\sigma = \sigma' - \sigma \to 0$. Instead of finding the general solution of (6.7) and imposing boundary conditions, we proceed directly to the physical variables $C_i|_i$ and $\mathbf{J}^{\rm ad}|_i$. By assuming sufficient differentiability, the values of C_i and $\mathbf{J}^{\rm ad}$ at η_{i+1}, σ' can be approximated using Taylor series about η_i, σ, as outlined in [67].

We first expand $C_i|_{i+1}$ and $J^{\rm ad}_{i,\perp}|_{i+1}$ in (3.5) to first order in $\delta\sigma$ and $\delta\eta_i$:

$$\begin{aligned} k_u\left(J^{\rm ad}_{i,\perp}|_i + \partial_\eta J^{\rm ad}_{i,\perp}|_i\delta\eta_i + \partial_\sigma J^{\rm ad}_{i,\perp}|_i\delta\sigma\right) &= k_u k_d\big[C_i|_i + \partial_\eta C_i|_i\delta\eta_i \\ &\quad +\partial_\sigma C_i|_i\delta\sigma - C_i^{\rm eq}(\sigma+\delta\sigma,t)\big]\ . \end{aligned} \tag{6.25}$$

Second, we multiply (6.2) by k_d and subtract the resulting equation from (6.25), so as to eliminate C_i. By neglecting the η- and σ-derivatives of $J^{\rm ad}_{i,\perp}$, we find

$$\begin{aligned} (k_u + k_d)J^{\rm ad}_{i,\perp}|_i &= k_u k_d\big\{\partial_\eta C_i|_i\delta\eta_i + \partial_\sigma C_i|_i\delta\sigma \\ &\quad -\frac{C_s}{k_BT}[\mu(\eta_{i+1},\sigma+\delta\sigma) - \mu(\eta_i,\sigma)]\big\}\ . \end{aligned} \tag{6.26}$$

Next, we solve for $\partial_\eta C_i$ and $\partial_\sigma C_i$ by applying the matrix equation (6.4). The substitution of $\partial_\eta C_i$ and $\partial_\sigma C_i$ into (6.26) and subsequent expansion of the difference $\mu(\eta_{i+1},\sigma+\delta\sigma) - \mu(\eta_i,\sigma)$ about (η_i,σ) yields a relation between $\mathbf{J}^{\rm ad}_i$ and the gradient of the macroscale step chemical potential $\mu(\mathbf{r},t)$:

$$\begin{aligned} &\left(\frac{1}{k_u} + \frac{1}{k_d} + \frac{D_{22}\,\xi_\eta\delta\eta_i}{|\mathbf{D}^{\rm ad}|}\right)J^{\rm ad}_{i,\perp}|_i - \frac{\xi_\eta D_{12}\delta\eta_i}{|\mathbf{D}^{\rm ad}|}J^{\rm ad}_{i,\parallel}|_i + \frac{C_s}{k_BT}\partial_\eta\mu|_i\delta\eta_i \\ &\quad = \left[\frac{\xi_\sigma}{|\mathbf{D}^{\rm ad}|}\big(D_{12}J^{\rm ad}_{i,\perp} - D_{11}J^{\rm ad}_{i,\parallel}\big)|_i - \frac{C_s}{k_BT}\partial_\sigma\mu|_i\right]\delta\sigma\ . \end{aligned} \tag{6.27}$$

Setting $\delta\sigma = 0$ in (6.27) and taking the macroscale limit provides our first equation for the components of the surface flux in terms of μ :

$$\left(1 + \frac{2|\mathbf{D}^{\mathrm{ad}}|}{kaD_{22}}|\nabla h|\right) J_{\perp}^{\mathrm{ad}} - \frac{D_{12}}{D_{22}} J_{\parallel}^{\mathrm{ad}} = -\frac{C_s|\mathbf{D}^{\mathrm{ad}}|}{k_B T D_{22}} \partial_{\perp}\mu \ . \tag{6.28}$$

The macroscale limit of (6.27) still applies when $\delta\sigma \neq 0$. By (6.28), we know that the left-hand side of (6.27) tends to zero in that limit. Therefore, the term proportional to $\delta\sigma$ must also vanish as $\delta\eta_i \to 0$. Thus, we have

$$D_{21} J_{\perp}^{\mathrm{ad}} - D_{11} J_{\parallel}^{\mathrm{ad}} = \frac{C_s|\mathbf{D}^{\mathrm{ad}}|}{k_B T} \partial_{\parallel}\mu \ . \tag{6.29}$$

By solving simultaneously (6.28) and (6.29) for the components of the macroscale surface flux, we find

$$\begin{pmatrix} J_{\perp}^{\mathrm{ad}} \\ \\ J_{\parallel}^{\mathrm{ad}} \end{pmatrix} = \frac{-C_s}{k_B T\,(1 + q|\nabla h|)} \begin{pmatrix} D_{11} & D_{12} \\ \\ D_{21} & D_{22} + \mathcal{D}^{\mathrm{ad}}\,|\nabla h| \end{pmatrix} \cdot \begin{pmatrix} \partial_{\perp}\mu \\ \\ \partial_{\parallel}\mu \end{pmatrix} \ , \tag{6.30}$$

which is directly identified with the combination of (6.23) and (6.24).

6.4 Mass conservation law and total surface flux

In this subsection we define the *total* surface flux $\mathbf{J}$ so that the mass conservation law for atoms is satisfied in the presence of step edge diffusion. The surface mobility is defined accordingly through the relation of $\mathbf{J}$ and μ.

At a given location σ on the ith step edge, the step normal velocity v_i must respect conservation of mass, taking into account all possible sources and sinks of atoms; see (5.13). By Section 5.4.3, in the macroscale limit (5.13) reduces to

$$\partial_t h = -\Omega\nabla\cdot\mathbf{J}^{\mathrm{ad}} + \frac{a|\nabla h|}{\xi_\sigma}\partial_\sigma\left\{\frac{D^{\mathrm{ed}}}{\xi_\sigma}\partial_\sigma\left(\frac{\mu}{k_B T}\right)\right\} \ , \tag{6.31}$$

where the adatom flux $\mathbf{J}^{\mathrm{ad}}$ is described by (6.23) and (6.24).

Since the terrace is a level set for the height, we have $h = H(\eta, t)$; in other words, h does not vary in the step-longitudinal (σ-) direction. Thus, $|\nabla h| = \xi_\eta^{-1}|\partial_\eta H|$ and the factor $|\partial_\eta H|$ can be passed through the σ derivative in (6.31). It follows that

$$\partial_t h = -\Omega \nabla \cdot \mathbf{J}^{\mathrm{ad}} + \frac{1}{\xi_\eta \xi_\sigma} \partial_\sigma \left\{ a D^{\mathrm{ed}} |\nabla h| \frac{\xi_\eta}{\xi_\sigma} \partial_\sigma \left(\frac{\mu}{k_B T} \right) \right\} \ . \tag{6.32}$$

We recognize the second term on the right-hand side of (6.32) as the divergence of $aD^{\mathrm{ed}}|\nabla h|\partial_\parallel(\mu/k_BT)\mathbf{e}_\sigma$. (Recall $\partial_\parallel = \xi_\sigma^{-1}\partial_\sigma$ as in Chapter 5.) Hence, we refer to the term $-\frac{aD^{\mathrm{ed}}}{\Omega}|\nabla h|\partial_\parallel(\mu/k_BT)\mathbf{e}_\sigma$ as the edge atom flux, denoted by $\mathbf{J}^{\mathrm{ed}}$. Combining the two divergence terms into one term, we obtain the mass conservation law

$$\partial_t h = -\Omega \nabla \cdot (\mathbf{J}^{\mathrm{ad}} + \mathbf{J}^{\mathrm{ed}}) = -\Omega \nabla \cdot \mathbf{J} \ , \tag{6.33}$$

where

$$\mathbf{J} = \mathbf{J}^{\mathrm{ad}} + \mathbf{J}^{\mathrm{ed}} \ , \qquad \mathbf{J}^{\mathrm{ed}} := -\frac{aD^{\mathrm{ed}}}{\Omega} |\nabla h| \, \partial_\parallel \left(\frac{\mu}{k_B T} \right) \mathbf{e}_\sigma \ . \tag{6.34}$$

Recall that μ here is the same macroscale chemical potential derived in Chapter 5, a function of the local slope according to the formula

$$\mu = -\Omega \, \mathrm{div} \left\{ g_1 \frac{\nabla h}{|\nabla h|} + g_3 |\nabla h| \nabla h \right\} , \tag{6.35}$$

which remains unchanged in the presence of terrace anisotropy and step edge diffusion.

The matrix equation (6.30) involving the mobility tensor can be updated to

reflect the additional source term in the overall surface flux:

$$\mathbf{J}(\mathbf{r},t) = \begin{pmatrix} J_\perp \\ \\ J_\parallel \end{pmatrix} = -C_s \begin{pmatrix} M_{\eta\eta} & M_{\eta\sigma} \\ \\ M_{\sigma\eta} & M_{\sigma\sigma} \end{pmatrix} \cdot \begin{pmatrix} \partial_\perp \mu \\ \\ \partial_\parallel \mu \end{pmatrix} = -C_s \mathbf{M} \cdot \nabla \mu, \qquad (6.36)$$

where

$$\mathbf{M} = \begin{pmatrix} M_{\eta\eta} & M_{\eta\sigma} \\ \\ M_{\sigma\eta} & M_{\sigma\sigma} \end{pmatrix} , \qquad (6.37)$$

$$\begin{aligned} M_{\eta\eta} &= \frac{D_{11}/(k_B T)}{1 + 2\dfrac{D_{11}}{ka}|\nabla h|} , \; M_{\eta\sigma} = \frac{D_{12}/(k_B T)}{1 + 2\dfrac{D_{11}}{ka}|\nabla h|} , \\ M_{\sigma\eta} &= \frac{D_{21}/(k_B T)}{1 + 2\dfrac{D_{11}}{ka}|\nabla h|} , \; M_{\sigma\sigma} = \frac{1}{k_B T} \left(\frac{D_{22} + \dfrac{2|\mathbf{D}^{\mathrm{ad}}|}{ka}|\nabla h|}{1 + 2\dfrac{D_{11}}{ka}|\nabla h|} + \frac{a D^{\mathrm{ed}}}{\Omega C_s}|\nabla h| \right) \end{aligned} \qquad (6.38)$$

This total mobility tensor expresses the geometric dependence of the macroscale surface flux on the chemical potential via (6.36), the continuum analog of Fick's law when step edge diffusion is present. In the above formulation, we assume that

$$\frac{D_{11}}{ka} = \mathcal{O}(1), \quad \frac{|\mathbf{D}^{\mathrm{ad}}|}{D_{22} ka} = \mathcal{O}(1), \quad \frac{a}{\Omega C_s}\frac{D^{\mathrm{ed}}}{D_{22}} = \mathcal{O}(1). \qquad (6.39)$$

6.5 Evolution equation for the surface height

We now combine the mass conservation law (6.33) with the effective surface flux (6.36) and the formula for the macroscale step chemical potential (5.39) in order to derive a PDE analogous to (5.45) for the surface height profile, $h(\mathbf{r},t)$. With the substitutions for μ and $\mathbf{J}$ by (5.39) and (6.36), the mass conservation law (6.33) becomes

$$\partial_t h = -\frac{\Omega^2 C_s}{a} \mathrm{div} \left\{ \mathbf{M} \cdot \nabla \left(\mathrm{div} \left[(\beta + 3g\Phi_0 |\nabla h|^2) \frac{\nabla h}{|\nabla h|} \right] \right) \right\} . \qquad (6.40)$$

To consolidate the physical parameters, we again use the definitions $g_1 = \beta/a$, $g_3 = 3g\Phi_0/a$, and $B = \Omega^2 C_s g_1$; see (5.46). Accordingly, we obtain (5.45) with $\mathbf{M}^{\mathrm{ad}}$ replaced by the effective total mobility $\mathbf{M}$.

6.6 New scaling laws with terrace anisotropy and edge diffusion

In this section we derive approximate, separable solutions of PDE (6.40). Our goal is to find plausible connections between macroscale solutions and decay laws observed in biperiodic profiles, e.g. observations reported in [4, 20, 48, 83]. Our discussion is heuristic; the relation of PDE solutions to experiments is not well understood at the moment. Questions to consider when comparing PDE solutions to experimental observations include (i) whether the experimental conditions satisfy the assumptions under which the PDE was derived, (ii) what values of the material parameters are appropriate for a given material and temperature, and (iii) what time scale is common to the PDE solution and the decay of the observed material. When seeking separable PDE solutions, the issue of material parameters is particularly relevant, as we see in the following argument when deciding which terms are negligible in the free energy formula and the mobility matrix elements.

We start with the scaling ansatz $h(\mathbf{r}, t) \approx A(t)H(\mathbf{r})$. This separation of variables is consistent with previously reported step flow simulations in 1D [38] and kinetic Monte Carlo simulations in 2D [108], both with initial sinusoidal profiles. The amplitude $A(t)$ can be obtained formally from an ordinary differential equation (ODE) by direct substitution in (6.40). We alert the reader that conditions on the

initial data and material parameters for having separable solutions and recovering an ODE for $A(t)$ are currently elusive, requiring detailed numerical studies. Such studies are not addressed in this thesis.

Additive terms in the driving force $\nabla\mu$ and in the total mobility $\mathbf{M}$ scale differently with A. We need to retain in the right-hand side of the PDE terms proportional to the same power of A and thus resort to approximations. It should be borne in mind that the nonlinearities in $\mathbf{M}$ and μ lead to spatial-frequency coupling for biperiodic height profiles; accordingly, evolution is in principle more complicated than the one implied here by our simple scaling scenario.

Depending on the powers of A that possibly prevail in the evolution equation, we find several plausible behaviors of h with time, including the exponential decay and inverse linear decay reported in related experiments [4, 20, 48, 83]. By (6.35) the driving force $\nabla\mu$ scales as A^0 if the dominant term is step line tension. If step interactions are dominant, then $\nabla\mu$ scales as A^2. To determine the scaling of the mobility tensor, it is convenient to introduce the "aspect ratio" $\alpha := \partial_y h/\partial_x h$; it is plausible yet not compelling to estimate α by λ_x/λ_y where λ_x and λ_y are wavelengths in the x and y directions. We also define the slope-dependent quantity $b := (1 + \frac{2D_{11}}{ka}|\nabla h|)^{-1}$. Note that α scales as A^0. When step edge diffusion is absent ($D^{\mathrm{ed}} = 0$), the possible scalings found for A with nonzero D_{12} and D_{21} are not different from those for isotropic adatom diffusion (where $D_{12} = D_{21} = 0$) [67].

With these definitions, the elements $M_{ij} = (k_B T)^{-1}|\nabla h|^{-2} b\widetilde{M}_{ij}$ $(i, j = x, y)$

from the Cartesian representation (5.27)–(5.29) of $\mathbf{M}$ read

$$\begin{aligned}
M_{xx} &= \frac{b\,(\partial_x h)^2}{k_B T|\nabla h|^2}\Big[D_{11} - \alpha(D_{12}+D_{21}) + \alpha^2 D_{22} \\
&\quad + \frac{2|\mathbf{D}^{\mathrm{ad}}|}{ka}\alpha^2|\nabla h| + \frac{aD^{\mathrm{ed}}\alpha^2|\nabla h|}{b\,\Omega C_s}\Big]\ , \\
M_{xy} &= \frac{b\,(\partial_x h)^2}{k_B T|\nabla h|^2}\Big[D_{12} + \alpha(D_{11} - D_{22}) - \alpha^2 D_{21} \\
&\quad - \frac{2|\mathbf{D}^{\mathrm{ad}}|}{ka}\alpha|\nabla h| - \frac{aD^{\mathrm{ed}}\alpha|\nabla h|}{b\,\Omega C_s}\Big]\ , \\
M_{yx} &= \frac{b\,(\partial_x h)^2}{k_B T|\nabla h|^2}\Big[D_{21} + \alpha(D_{11} - D_{22}) - \alpha^2 D_{12} \\
&\quad - \frac{2|\mathbf{D}^{\mathrm{ad}}|}{ka}\alpha|\nabla h| - \frac{aD^{\mathrm{ed}}\alpha|\nabla h|}{b\,\Omega C_s}\Big]\ , \\
M_{yy} &= \frac{b\,(\partial_x h)^2}{k_B T|\nabla h|^2}\Big[D_{22} + \alpha(D_{12}+D_{21}) + \alpha^2 D_{11} \\
&\quad + \frac{2|\mathbf{D}^{\mathrm{ad}}|}{ka}|\nabla h| + \frac{aD^{\mathrm{ed}}|\nabla h|}{b\,\Omega C_s}\Big]\ .
\end{aligned} \tag{6.41}$$

We restrict attention to ADL kinetics which closely correspond to relevant experimental situations [4, 20, 48, 83]. It follows that $b \ll 1$ where b scales as A^{-1}; by the scaling ansatz for h, the prefactor $\frac{b(\partial_x h)^2}{k_B T|\nabla h|^2}$ also scales as A^{-1}. For the sake of simplicity we consider weak anisotropy, $|\mathbf{D}^{\mathrm{ad}}| \approx D_{11}D_{22}$ (i.e., if the off-diagonal diffusivity elements D_{12}, D_{21} are small in comparison to the diagonal elements) and $|\mathbf{D}^{\mathrm{ad}}|/(ka) \gg aD^{\mathrm{ed}}/(b\,\Omega C_s)$. The dominant terms in $\mathbf{M}$ scale as:

(i) A^0 if $b \ll \min\{(D_{22}/D_{11})\alpha^2, (D_{22}/D_{11})\alpha^{-2}, D_{22}/D_{11}\}$; and

(ii) A^{-1} if $b \gg \max\{(D_{22}/D_{11})\alpha^2, (D_{22}/D_{11})\alpha^{-2}, D_{22}/D_{11}\}$.

In the presence of step edge diffusion with $|\mathbf{D}^{\mathrm{ad}}|/(ka) \ll aD^{\mathrm{ed}}/(b\,\Omega C_s)$, the dominant terms in the mobility tensor scale as A^1. Note that in all these cases the matrix $\mathbf{M}$ tends to become singular since the lowest eigenvalue acquires a small value. Hence, correction terms in $\mathbf{M}$, which strictly spoil the scalings reported here, are physically

important; solutions of the form $A(t)H(\mathbf{r})$ should be thought of as leading-order terms of appropriate asymptotic expansions for h.

Next, we combine the three possible scalings of $\mathbf{M}$ with the two possible scalings of $\nabla\mu$. Each combination yields an ODE of the form $\dot{A} \propto -A^p$ for some exponent p; the minus sign here is assumed for achieving profile decay. In the case of ADL kinetics, outlined above, we have $p \in \{-1, 0, 1\} \cup \{1, 2, 3\}$, where the first set corresponds to dominant step line tension and the second set corresponds to dominant step interactions in $\nabla\mu$. Since $p = 1$ is common to both sets, the associated scaling law $A = A_0 \exp(-t/\tau)$ could perhaps be observed in a wide range of experimental situations. On the other hand, the scaling law $A = A_0/\sqrt{1 + t/\tau}$ associated with $p = 3$ and dominance of step edge diffusion may not be physical; to our knowledge, this last decay law has not been observed.

We illustrate the procedure of finding A for weak anisotropy under condition (ii) above and dominant step interactions; thus, $p = 1$. The PDE has the form

$$\dot{A}(t)H(\mathbf{r}) \propto -A(t)\ \mathrm{div}\left\{ \frac{(\partial_x H)^2}{|\nabla H|^3} \begin{pmatrix} m_{xx} & m_{xy} \\ m_{yx} & m_{yy} \end{pmatrix} \cdot \nabla\big[\mathrm{div}\big(|\nabla H|\nabla H\big)\big] \right\}, \quad (6.42)$$

where the prefactor is positive and the elements $\{m_{ij}\}_{i,j=x}^{y}$ are constants that stem from $\mathbf{M}_{(x,y)}$ after factoring out A (but not H); the precise definition of m_{ij} is omitted here.

To satisfy (6.42) for all t and $\mathbf{r}$, we require that the time-dependent part $A(t)$ solve $\dot{A}(t) = -\mathcal{C}A$ for some positive constant $\mathcal{C}$ ($\mathcal{C} > 0$). The height profile $H(\mathbf{r})$

Table 6.1: Decay laws for height amplitude $A(t)$ in ADL kinetics. Leftmost column indicates plausible conditions. Next two columns list decay laws for line tension and step interaction dominated $\nabla\mu$. The time constant τ depends on $A(0)$ and H.

	Line tension	Step interaction
$\lvert\mathbf{D}^{\mathrm{ad}}\rvert \approx D_{11}D_{22}$		
$b \gg \max\{(D_{22}/D_{11})\alpha^2, D_{22}/D_{11}, (D_{22}/D_{11})\alpha^{-2}\}$	$A_0\sqrt{1-t/\tau}$	$A_0\exp(-t/\tau)$
$b \ll \min\{D_{22}/D_{11})\alpha^2, D_{22}/D_{11}, (D_{22}/D_{11})\alpha^{-2}\}$	$A_0(1-t/\tau)$	$A_0/(1+t/\tau)$
$\lvert\mathbf{D}^{\mathrm{ad}}\rvert/(ka) \ll aD^{\mathrm{ed}}/(b\Omega C_s)$	$A_0\exp(-t/\tau)$	$A_0/\sqrt{1+t/\tau}$

solves a nonlinear PDE of the form

$$\mathcal{C}\,H \propto \mathrm{div}\left\{ \frac{(\partial_x H)^2}{|\nabla H|^3} \begin{pmatrix} m_{xx} & m_{xy} \\ m_{yx} & m_{yy} \end{pmatrix} \cdot \nabla\big[\mathrm{div}\big(|\nabla H|\nabla H\big)\big] \right\}. \tag{6.43}$$

The solution for $A(t)$ is given in terms of the separation constant $\mathcal{C}$ and the initial amplitude A_0: $A(t) = A_0 e^{-\mathcal{C}t}$. Using a similar procedure, we derive other possible scaling laws for ADL kinetics under different restrictions. Our results are summarized in Table 6.1.

We do not address the issue of solving (6.43) in this analysis. Particularly interesting is the case with facets. The macroscale limit breaks down near facet edges, and associated boundary conditions for H must take into account the discrete step flow equations [65]. A numerical scheme to implement these boundary conditions within a macroscopic simulation is a worthy subject of future research.

A similar analysis can be carried out if terrace diffusion is the slowest process, i.e., $q|\nabla h| = |\nabla h|D_{11}/(ka) \ll 1$. Then, b is approximately a constant, $b \approx 1$. The

dominant terms in the mobility tensor scale as A^0 or A^1. Thus, we obtain $\dot{A} \propto -A^p$ for $p \in \{0, 1, 2, 3\}$, which yields four of the five decay laws already found for ADL kinetics.

6.7 Conclusion

By interpreting a (2+1)-dimensional step flow model for a relaxing surface as a discretization of a macroscale evolution equation, we derived the relevant PDE for the surface height profile. The starting point is a step velocity law that accounts for anisotropic adatom diffusion on terraces, diffusion of atoms along step edges and atom attachment-detachment at steps. In the macroscale limit we obtained a relation between the surface flux and the step chemical potential. This relation involves a tensor surface mobility with nonzero off-diagonal elements even in the local coordinate representation.

Combining the step velocity law with the constitutive relation between the surface flux and the step chemical potential resulted in a fourth-order nonlinear PDE for the surface height. Transforming the mobility tensor from local step coordinates to fixed coordinates introduced a dependence on the height partial derivatives. This dependence offers a plausible scenario of how an epitaxial surface can exhibit different decay laws. We found separable solutions for the height that approximately satisfy the evolution equation under certain conditions. These separable solutions exhibit different decay and may be used as a guide in interpreting experimental observations from a macroscale perspective.

Our PDE only accounts for a part of the possible microscopic physics. In Chapters 7–8 we discuss the macroscale consequences of additional effects, such as step permeability, adatom drift under the influence of an electric field, and desorption of adatoms. The calculations of this chapter serve as a prototypical example for later macroscale limits.

Chapter 7

Step permeability and macroscale limit [1]

In this chapter, we extend the model of continuum steps in 2+1 dimensions to include the possibility of permeable steps. Also known as step transparency, this phenomenological mechanism allows adatoms to jump from one terrace to a neighboring terrace without first attaching and detaching at the intervening step. In principle, step permeability can lead to *long-range* interactions, since an adatom might cross *many terraces* before attaching to a step and influencing the step motion. If such an effect is realized in the equations of step flow, we might naturally wonder whether the macroscopic limit also shows evidence of long-distance interactions. The main achievement of this chapter is the derivation of a macroscale limit consistent with permeable steps in 2+1 dimensions.

The macroscale PDE we derive here leaves unchanged the local character of step interactions, finding only a renormalized kinetic parameter as the result of including step permeability. This renormalized kinetic parameter generalizes to (2+1)-dimensions a formula in [88], which can be interpreted via an electric-circuit analog of the paths by which adatoms can jump between terraces.

In this chapter we continue to assume that mass transport on terraces is due to diffusion only. We omit from the diffusion equation terms corresponding to de-

[1] Material in this chapter appeared previously in Quah, Young and Margetis, Phys. Rev. E **78**, 042602/1–4.

position flux, electromigration current, and desorption of adatoms. The latter two effects will be addressed in Chapter 8. Here we discuss only the changed boundary conditions in the case of permeable steps.

7.1 Step permeability

According to the original BCF framework for studying step motion, mass transport of adatoms between adjacent terraces requires the intermediate processes of attaching and detaching at the common step edge. By decomposing the mass transport mechanism in this way and allowing for an Ehrlich-Schwoebel barrier, we have the freedom to choose two kinetic rates k_u and k_d, which in principle can explain such phenomena as the appearance of different island sizes during multilayer growth [23]. Motivated more by intellectual curiosity than by discrepancies between theory and experiment, Ozdemir and Zangwill imagined the possibility of direct exchange of adatoms and vacancies from one terrace to another with kinetic rate p [81]. This exchange mechanism is called *step permeability* or *step transparency*. Pierre-Louis used this theoretical construct in his attempt to resolve the question of temperature-dependent conditions for electromigration-induced step bunching [88].

The effect of step permeability is to change the linear kinetic boundary conditions (3.4) and (3.5) to

$$-J_{i,\perp} = k_u(C_i - C_i^{\text{eq}}) + p(C_i - C_{i-1}), \quad \eta = \eta_i, \tag{7.1}$$

$$J_{i,\perp} = k_d(C_i - C_{i+1}^{\text{eq}}) + p(C_i - C_{i+1}), \quad \eta = \eta_{i+1}, \tag{7.2}$$

where p is the permeability rate and $J_{i,\perp}$ is the adatom flux component in the step-

normal direction; see Chapter 5 to review the geometry and notation. The same p appears in both boundary conditions by Onsager reciprocity relations [89].

7.2 Macroscale limit

In order to derive a macroscale limit from (7.1),(7.2), and the terrace diffusion equation, we impose the same geometric conditions as in chapter 6, along with the conditions on the kinetic rates given in the preceding sections. The terrace widths are assumed to be much smaller than [66]: (i) the length λ over which the step density varies; and (ii) the step radius of curvature, if applicable. The discrete step density $a/\delta\rho_i$ with $\delta\rho_i = \xi_\eta|_{\eta_i}\delta\eta_i$ is assumed to remain fixed while we formally let $\delta\eta_i \to 0$. Recall that η is a dimensionless coordinate with discrete isolines corresponding to steps.

The restriction on the kinetic rates is that $D/(\nu a) = \mathcal{O}(1)$ for $\nu = k_u, k_d, p$. We used a similar assumption in Chapter 5 to derive our first macroscale limit. Here the condition $D/(\nu a) = \mathcal{O}(1)$ plays the same role, allowing us to keep fixed the dimensionless parameters $D/(\nu a)$ as various limits are taken.

If we wanted to proceed in the same vein as our first macroscale limit in Chapter 5, we would begin by solving the diffusion equation $\nabla^2 C_i = 0$ on the ith terrace, subject to the boundary conditions (7.1),(7.2). Immediately we notice that step permeability explicitly couples the resulting adatom concentration C_i with that of other terraces. For a step train with a finite number of terraces, the system of boundary conditions can be solved simultaneously by inverting a circulant matrix [43]. This

coupling at the step level suggests that the macroscopic limit of C_i must also be incorporated into the macroscale equation. A similar approach was taken in [16], although the authors provide only a brief discussion of the connection to the permeability rate p.

A direct solution of the terrace diffusion equation, in any case, would yield two integration constants that have to be found by applying the boundary conditions. We can bypass some tedious algebra by letting the values of adatom concentration and its normal derivative play the role of integration constants, for which the boundary conditions will serve as a linear system of equations. Accordingly, we assume the existence of the interpolating functions $\mathcal{C}$ and $\mathcal{J}$ for adatom concentration and transverse flux, respectively, which agree with C_i and $J_{i,\perp}$ when evaluated at the ith step edge. We take $\mathcal{C}$ and $\mathcal{J}$ as our primary variables. Whether we evaluate the terrace concentration and its derivative at the upper step edge (η_i) or the lower step edge (η_{i+1}) is irrelevant in the macroscale limit, since η_i and η_{i+1} approach the same value, corresponding to the transverse coordinate of a single level set. Our final goal is a system of equations for C and $J_\perp$, which emerge as the macroscale limits of $\mathcal{C}$ and $\mathcal{J}$, respectively.

7.2.1 Straight steps

In the straight step setting with no Ehrlich-Schwoebel barrier, the boundary conditions (7.1),(7.2) reduce to

$$-J_i = k(C_i - C_i^{\mathrm{eq}}) + p(C_i - C_{i-1}), \quad x = x_i \tag{7.3}$$

$$J_i = k(C_i - C_{i+1}^{\mathrm{eq}}) + p(C_i - C_{i+1}), \quad x = x_{i+1}. \tag{7.4}$$

We now identify C_i, C_{i+1}, C_{i-1} with values of a continuous adatom concentration function at the left step edge of the corresponding terrace. In particular, we define the interpolant $\mathcal{C}$ by $C_i|_{x_i} =: \mathcal{C}(i)$. As usual, the subscript x_i to the right of the vertical bar denotes the point of evaluation. Similarly, the flux $J_i|_{x_i}$ at the left step edge is identified with the value $\mathcal{J}(i)$ of an interpolating flux function. If a value of the terrace adatom concentration C_i at a point other than the left step edge is desired, then an approximation in terms of the concentration $\mathcal{C}(i)$ and flux $\mathcal{J}(i)$ can be found by applying a Taylor expansion along with Fick's law:

$$C_i|_x = \mathcal{C}(i) - D^{-1}\mathcal{J}(i)(x - x_i) + O[(x - x_i)^2]. \tag{7.5}$$

For the purposes of the macroscale limit, only the first-order term in the expansion (7.5) needs to be retained. Using (7.5) at $x = x_{i+1}$ and a similar expansion for $C_{i-1}|_{x_i}$, the boundary conditions now read

$$-\mathcal{J}(i) = k[\mathcal{C}(i) - C_i^{\mathrm{eq}}] + p[\mathcal{C}(i) - \mathcal{C}(i-1) + D^{-1}(x_i - x_{i-1})\mathcal{J}(i-1)] \tag{7.6}$$

$$\begin{aligned}\mathcal{J}(i) = {} & k[\mathcal{C}(i) - D^{-1}(x_{i+1} - x_i)\mathcal{J}(i) - C_{i+1}^{\mathrm{eq}}] \\ & + p[\mathcal{C}(i) - D^{-1}(x_{i+1} - x_i)\mathcal{J}(i) - \mathcal{C}(i+1)].\end{aligned} \tag{7.7}$$

In the absence of an Ehrlich-Schwoebel barrier, direct subtraction of (7.6) and (7.7) leads immediately to

$$-2\mathcal{J}(i) = k[C^{\mathrm{eq}}_{i+1} - C^{\mathrm{eq}}_i + D^{-1}(x_{i+1} - x_i)\mathcal{J}(i)]$$
$$+ p[\mathcal{C}(i+1) - \mathcal{C}(i-1) + D^{-1}(x_{i+1} - x_i)\mathcal{J}(i) + D^{-1}(x_i - x_{i-1})\mathcal{J}(i-1)]. \quad (7.8)$$

Bringing all the flux terms to the left side, we find

$$\mathcal{J}(i)\left[2 + \frac{k}{D}(x_{i+1} - x_i) + \frac{p}{D}(x_{i+1} - x_{i-1})\right]$$
$$+ \frac{p}{D}(x_i - x_{i-1})\mathcal{J}(i-1) = -k[C^{\mathrm{eq}}_{i+1} - C^{\mathrm{eq}}_i] - p[\mathcal{C}(i+1) - \mathcal{C}(i-1)]. \quad (7.9)$$

Assuming that $\mathcal{C}$ and the macroscale equilibrium concentration C^{eq} both admit Taylor series expansions about x_i, we can replace the differences $C^{\mathrm{eq}}_{i+1} - C^{\mathrm{eq}}_i$ and $\mathcal{C}(i+1) - \mathcal{C}(i-1)$ according to

$$C^{\mathrm{eq}}_{i+1} - C^{\mathrm{eq}}_i = (x_{i+1} - x_i)\left.\frac{\partial C^{\mathrm{eq}}}{\partial x}\right|_{x_i} + o(x_{i+1} - x_i), \quad (7.10)$$

$$\mathcal{C}(i+1) - \mathcal{C}(i-1) = (x_{i+1} - x_{i-1})\left.\frac{\partial \mathcal{C}}{\partial x}\right|_{x_i} + o(x_{i+1} - x_{i-1}). \quad (7.11)$$

Since the macroscale height profile is required to be differentiable, the mean-value theorem allows us to substitute $2a/|\partial_x h|$ for $x_{i+1} - x_{i-1}$ and $a/|\partial_x h|$ for $x_{i+1} - x_i$, where the evaluation point of the x-derivative is left unspecified for now. The constitutive relation (7.9) then becomes

$$\mathcal{J}(i)\left[2 + \frac{ka}{D|\partial_x h|} + \frac{2pa}{D|\partial_x h|}\right] + \frac{pa}{D|\partial_x h|}\mathcal{J}(i-1) = -\frac{ka}{|\partial_x h|}\partial_x C^{\mathrm{eq}} - \frac{2pa}{|\partial_x h|}\partial_x \mathcal{C}. \quad (7.12)$$

In the limit as $a/\lambda \to 0$, the positions of steps i and $i-1$ are assumed to tend to a common point x, so the equation for the macroscale flux J is

$$J(x)\left[2 + \frac{(k+2p)a}{D|\partial_x h|}\right] = \frac{ka}{|\partial_x h|}\partial_x C^{\mathrm{eq}} + \frac{2pa}{|\partial_x h|}\partial_x \mathcal{C}. \quad (7.13)$$

To eliminate the explicit dependence on $\mathcal{C}$, we take the macroscale limit of the boundary condition (7.6) directly and then substitute for $J(x)$ using (7.13). The macroscale limit of (7.6) reads

$$-J(x) = k(C - C^{\mathrm{eq}}) + p\left[\partial_x C \frac{a}{|\partial_x h|} + \frac{J(x)a}{D|\partial_x h|}\right]. \tag{7.14}$$

Combined with the macroscale flux from (7.13), we find an equation for $C - C^{\mathrm{eq}}$.

$$\begin{aligned} k(C - C^{\mathrm{eq}}) + \frac{pa}{|\partial_x h|}\partial_x C &= \frac{\frac{ka}{|\partial_x h|}\partial_x C^{\mathrm{eq}} + \frac{2pa}{|\partial_x h|}\partial_x C}{2 + \frac{(k+2p)a}{D|\partial_x h|}}\left[1 + \frac{pa}{D|\partial_x h|}\right] \\ \left(1 + \frac{(k+2p)a}{2D|\partial_x h|}\right)(C - C^{\mathrm{eq}}) &= \frac{a}{2|\partial_x h|}\left(1 + \frac{pa}{D|\partial_x h|}\right)\partial_x C^{\mathrm{eq}} + \frac{p^2 a^2}{kD|\partial_x h|^2}\partial_x C. \end{aligned} \tag{7.15}$$

In principle, we regard (7.15) as a series in powers of a, which holds identically as $a/\lambda \to 0$. By equating the coefficients of like powers of a, we obtain conditions on the coefficients. The dominant balance of terms in (7.15) indicates that we can take $C = C^{\mathrm{eq}}$ in the macroscopic limit. The factor multiplying $C - C^{\mathrm{eq}}$ on the left-hand side of (7.15) remains $\mathcal{O}(1)$ as $a/\lambda \to 0$, while the right-hand side vanishes since $p/k = \mathcal{O}(1)$ does not scale with a. Replacing C by C^{eq} in (7.13), we find

$$J(x) = -\frac{D\partial_x C}{1 + \frac{2D}{(k+2p)a}|\partial_x h|} = -\frac{DC_s}{k_B T}\frac{\partial_x \mu}{1 + q_{\mathrm{eff}}|\partial_x h|}, \tag{7.16}$$

where $q_{\mathrm{eff}} := 2D/(k_{\mathrm{eff}}a)$ and $k_{\mathrm{eff}} := k+2p$. *Thus, the effective attachment-detachment rate* k_{eff} *appears as an additive renormalization* of k to $k + 2p$.

We pause to mention a few previous derivations of this result in the literature. The unifying theme of these derivations is a replacement of the step-terrace system by a simpler mass transport mechanism with renormalized parameters. In this vein,

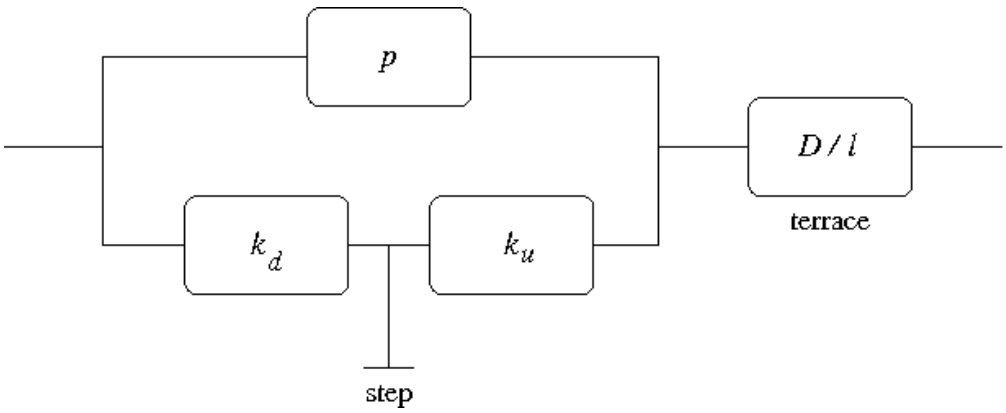

Figure 7.1: Electric circuit analogous to a terrace and a permeable step, adapted from [88].

Nozières proceeds by analogy with an electric circuit [78], where the attachment and detachment processes are regarded as a series of resistors, and the effect of step transparency is to provide a parallel resistor through which an adatom current can flow across the step. The simplest illustration of this analogy appears in the subsequent paper by O. Pierre-Louis [88], adapted here as Figure 7.1. A more complicated electric circuit analogy, incorporating several steps and terraces, is given by Jeong and Williams [43].

7.2.2 Circular steps with axisymmetry

We use the familiar setting of axisymmetry to introduce the additional algebra needed to deal with an Ehrlich-Schwoebel barrier. This bias of adatom flux toward a preferred direction appears in the boundary conditions as an inequality in the kinetic rates: $k_d > k_u$ if downhill drift is preferred, or $k_u > k_d$ if uphill drift is

preferred. The boundary conditions (7.1),(7.2) read

$$-J_i = k_u(C_i - C_i^{\mathrm{eq}}) + p(C_i - C_{i-1}), \quad r = r_i \tag{7.17}$$

$$J_i = k_d(C_i - C_{i+1}^{\mathrm{eq}}) + p(C_i - C_{i+1}), \quad r = r_{i+1}. \tag{7.18}$$

Again we identify C_i, C_{i+1}, C_{i-1} with values of a continuous interpolating function $\mathcal{C}$ at the inner step edge of the corresponding terrace. This convention says $\mathcal{C}(i) := C_i|_{r_i}$. Similarly, we define an interpolating flux function $\mathcal{J}(i)$ by $\mathcal{J}(i) := J_i|_{r_i}$. An approximation of the adatom concentration at the outer step edge can be found in terms of the concentration $\mathcal{C}(i)$ and flux $\mathcal{J}(i)$ by applying Fick's law:

$$C_i|_{r_{i+1}} = \mathcal{C}(i) - \frac{\mathcal{J}(i)}{D}(r_{i+1} - r_i) + o(r_{i+1} - r_i). \tag{7.19}$$

Retaining only the terms of the expansion (7.19) that are linear in $r_{i+1} - r_i$, the boundary conditions (7.17),(7.18) become

$$-\mathcal{J}(i) = k_u[\mathcal{C}(i) - C_i^{\mathrm{eq}}] \tag{7.20}$$

$$+ p[\mathcal{C}(i) - \mathcal{C}(i-1) + \frac{\mathcal{J}(i-1)}{D}(r_i - r_{i-1})], \tag{7.21}$$

$$\begin{aligned}\mathcal{J}(i) + \partial_r J_i|_{r_i}(r_{i+1} - r_i) = {} & k_d[\mathcal{C}(i) - \frac{\mathcal{J}(i)}{D}(r_{i+1} - r_i) - C_{i+1}^{\mathrm{eq}}] \\ & + p\left[\mathcal{C}(i) - \frac{\mathcal{J}(i)}{D}(r_{i+1} - r_i) - \mathcal{C}(i+1)\right].\end{aligned} \tag{7.22}$$

Eventually we plan to take a macroscale limit from these equations, which allows us to consider $a/r_i \ll 1$. The nondimensional parameter $k_d a/D$, however, remains $\mathcal{O}(1)$ in the macroscale limit. Hence we have the inequality

$$\frac{a}{r_i} \ll \frac{k_d a}{D}. \tag{7.23}$$

Multiplying (7.23) by $|\mathcal{J}(i)/a|$ and identifying the left-hand side as $\left|\partial_r J_i|_{r_i}\right|$ by use of the diffusion equation, we find

$$\left|\partial_r J_i|_{r_i}\right| \ll \left|k_d \frac{\mathcal{J}(i)}{D}\right|. \tag{7.24}$$

Therefore it is justified to neglect $\partial_r J_i|_{r_i}$ from (7.22), since our final goal is a macroscale limit relating the variables J and C. These macroscale variables satisfy

$$\mathcal{C}(i) - \mathcal{C}(i-1) = (r_i - r_{i-1})\partial_r C|_{r_i} + o(r_i - r_{i-1}), \tag{7.25}$$

$$\mathcal{C}(i+1) - \mathcal{C}(i) = (r_{i+1} - r_i)\partial_r C|_{r_i} + o(r_{i+1} - r_i), \tag{7.26}$$

$$\mathcal{J}(i) - \mathcal{J}(i-1) = o(1). \tag{7.27}$$

The discrete step density $a/(r_{i+1} - r_i)$ is assumed to approach the macroscale surface slope $|\nabla h|$. In fact, replacement of $r_{i+1} - r_i$ (or $r_i - r_{i-1}$) by $a/|\partial_r h|$ evaluated somewhere on $[r_i, r_{i+1}]$ (or $[r_{i-1}, r_i]$) is justified by the mean value theorem and the assumed smoothness of the macroscale surface height h. The desired system of equations for the macroscale variables is

$$-J\left(1 + \frac{p}{D}\frac{a}{|\partial_r h|}\right) = k_u(C - C^{\mathrm{eq}}) + \frac{pa}{|\partial_r h|}\partial_r C, \tag{7.28}$$

$$J\left(1 + \frac{p + k_d}{D}\frac{a}{|\partial_r h|}\right) = k_d(C - C^{\mathrm{eq}}) - \frac{k_d a}{|\partial_r h|}\partial_r C^{\mathrm{eq}} - \frac{pa}{|\partial_r h|}\partial_r C, \tag{7.29}$$

where C^{eq} is the macroscale limit of C_i^{eq}. To solve for the radial flux J, we divide (7.28) by k_u and (7.29) by k_d; the difference of the two resulting equations retains only the concentration gradients, not their pointwise values. We obtain the formula

$$J = -D\frac{(2p/k)\partial_r C + \partial_r C^{\mathrm{eq}}}{1 + 2p/k + q|\partial_r h|}, \tag{7.30}$$

where $k := 2(k_u^{-1} + k_d^{-1})^{-1}$ and $q := 2D/(ka)$; see section 5.4.1.

Unlike [16], we do not treat the macroscopic limit of adatom concentration as a variable in its own right. Indeed, we have seen above in the case of straight steps that the macroscale limit renders such a treatment unnecessary. A similar argument in the axisymmetric setting allows us to replace C by C^{eq} in (7.30). With this substitution, (7.30) becomes the desired relation between flux and chemical potential:

$$J = -D\frac{\partial_r C^{\text{eq}}}{1 + q_{\text{eff}}|\partial_r h|} = -\frac{DC_s}{k_B T}\frac{\partial_r \mu}{1 + q_{\text{eff}}|\partial_r h|}, \tag{7.31}$$

where $q_{\text{eff}} = D/(k_{\text{eff}}a)$ and $k_{\text{eff}} = k + 2p$. Evidently, the effect of step permeability in the axisymmetric setting is precisely the same renormalization of the kinetic parameter that we saw in the straight step case. The additional mass transport mechanism of adatoms hopping directly between terraces is reflected in the macroscale equations by a modified attachment-detachment coefficient. Under the conventional interpretation of step permeability, where $p > 0$, the new attachment-detachment coefficient is greater than k. However, no physical principle is violated if $p < 0$. This generalization has been suggested as a means of introducing different kinetic regimes as the temperature or the supersaturation is varied [90]. We discuss below the implications of negative p in relation to a two-region model of step dynamics by Weeks et al. [125].

7.2.3 Steps in 2+1 dimensions

The geometry considered here is identical to that of Chapter 5, where η is used as the transverse coordinate and σ is used as the longitudinal coordinate. Starting with the boundary conditions (7.1),(7.2), we replace the adatom concentrations and the normal flux components with either the macroscale interpolants, e.g., $\mathcal{C}(i)$, $\mathcal{J}_\perp(i)$, or series expansions about the upper step edge of the appropriate terrace. For example, the domain of the adatom concentration C_{i-1} is $\eta_{i-1} < \eta < \eta_i$, and in (7.1) we want to express this concentration at η_i in terms of the macroscale interpolant $\mathcal{C}(i-1)$. We use the expansion

$$C_{i-1}|_{\eta_i} = \mathcal{C}(i-1) + \delta\eta_{i-1}\partial_\eta C_{i-1}|_{\eta_{i-1}} + o(\delta\eta_{i-1}), \tag{7.32}$$

which now forces us to find an expression for $\partial_\eta C_{i-1}|_{\eta_{i-1}}$ in terms of the primary variables. Fortunately, Fick's law allows us to write this normal derivative as a multiple of the corresponding flux component. The resulting *microscale* expansion is

$$C_{i-1}|_{\eta_i} = \mathcal{C}(i-1) - \frac{\xi_\eta}{D}\mathcal{J}_\perp(i-1)\delta\eta_i + o(\delta\eta_{i-1}). \tag{7.33}$$

In the case of tensor diffusivity, we could still replace the normal derivative of C_{i-1} by a linear combination of flux components evaluated at the upper step edge. The flexibility of this series method offers a streamlined procedure to derive the macroscale limit even when an explicit solution of the terrace diffusion problem is inaccessible.

Similar series expansions apply to the other quantities that do not correspond

immediately to the macroscale interpolants. We have

$$C_i|_{\eta_{i+1}} = \mathcal{C}(i) + \delta\eta_i \partial_\eta C_i|_{\eta_i} + o(\delta\eta_i), \tag{7.34}$$

$$J_{i,\perp}|_{\eta_{i+1}} = \mathcal{J}_\perp(i) + \delta\eta_i \partial_\eta J_{i,\perp}|_{\eta_i} + o(\delta\eta_i). \tag{7.35}$$

Again, Fick's law allows us to replace the normal derivative in (7.34) by a multiple of the normal flux component. For the normal derivative in (7.35), appeal to the diffusion equation itself, along with the separation of variables into slow and fast; see Chapter 5. Keeping in mind these considerations and the eventual macroscale limit, we may safely neglect $\partial_\eta J_{i,\perp}$ from (7.35). After substituting the primary variables, the boundary conditions now read:

$$-\mathcal{J}_\perp(i) = k_u[\mathcal{C}(i) - C_i^{\text{eq}}] + p[\mathcal{C}(i) - \mathcal{C}(i-1) + \frac{\xi_\eta \delta\eta_{i-1}}{D}\mathcal{J}_\perp(i-1)], \tag{7.36}$$

$$\mathcal{J}_\perp(i) = k_d[\mathcal{C}(i) - C_{i+1}^{\text{eq}} - \frac{\xi_\eta \delta\eta_i}{D}\mathcal{J}_\perp(i)] + p[\mathcal{C}(i) - \mathcal{C}(i+1) - \frac{\xi_\eta \delta\eta_i}{D}\mathcal{J}_\perp(i)]. \tag{7.37}$$

Next, we introduce the (macroscale) variables C and $J_\perp$ via the expansions

$$\mathcal{C}(i) - \mathcal{C}(i-1) = \delta\eta_{i-1}\partial_\eta C|_{\eta_i} + o(\delta\eta_{i-1}), \tag{7.38}$$

$$\mathcal{C}(i+1) - \mathcal{C}(i) = \delta\eta_i \partial_\eta C|_{\eta_i} + o(\delta\eta_i), \tag{7.39}$$

$$\mathcal{J}_\perp(i) - \mathcal{J}_\perp(i-1) = o(1). \tag{7.40}$$

The discrete step density $a/(\xi_\eta \delta\eta)$ is assumed to approach the macroscale surface slope $|\nabla h|$, independent of the evaluation point (η_i or η_{i-1}). We therefore replace $\xi_\eta \delta\eta_i$ and $\xi_\eta \delta\eta_{i-1}$ by $a/|\nabla h|$. The desired system of equations for the macroscale

variables is

$$-J_\perp \left(1 + \frac{p}{D}\frac{a}{|\nabla h|}\right) = k_u(C - C^{\rm eq}) + \frac{pa}{|\nabla h|}\partial_\perp C, \tag{7.41}$$

$$J_\perp \left(1 + \frac{p + k_d}{D}\frac{a}{|\nabla h|}\right) = k_d(C - C^{\rm eq}) - \frac{k_d a}{|\nabla h|}\partial_\perp C^{\rm eq} - \frac{pa}{|\nabla h|}\partial_\perp C, \tag{7.42}$$

where $\partial_\perp = \xi_\eta^{-1}\partial_\eta$ and $C^{\rm eq}(\mathbf{r})$ is the macroscale limit of $C_i^{\rm eq}$. We solve this system of equations for $J_\perp$ to obtain the formula

$$J_\perp = -D\frac{(2p/k)\partial_\perp C + \partial_\perp C^{\rm eq}}{1 + 2p/k + q|\nabla h|}, \tag{7.43}$$

where $k := 2(k_u^{-1} + k_d^{-1})^{-1}$ and $q := 2D/(ka)$ as before.

We now need a relation between C and $C^{\rm eq}$. First, the sum of the boundary conditions (7.41),(7.42) yields

$$\frac{k_d a}{D|\nabla h|}J_\perp = (k_u + k_d)(C - C^{\rm eq}) - \frac{ka}{|\nabla h|}\partial_\perp C^{\rm eq}. \tag{7.44}$$

By substituting for $J_\perp$ according to (7.43), we find

$$0 = \left(1 + \frac{2p}{k} + \frac{2D}{ka}|\nabla h|\right)(C - C^{\rm eq}) + \frac{2pa}{k|\nabla h|}\frac{k_d}{k_u + k_d}\partial_\perp C. \tag{7.45}$$

In order to isolate the dominant terms, it helps to multiply by the $\mathcal{O}(1)$ quantity $ka/(2D|\nabla h|)$. The resulting equation,

$$0 = \left(1 + \frac{(k + 2p)a}{2D|\nabla h|}\right)(C - C^{\rm eq}) + \frac{a}{|\nabla h|^2}\frac{pa}{D}\frac{k_d}{k_u + k_d}\partial_\perp C, \tag{7.46}$$

can be viewed as an expansion in powers of a. For this equality to hold in the macroscale limit $a/\lambda \to 0$, the zeroth-order term must vanish, which implies $C = C^{\rm eq}$. Returning to (7.43), we have

$$J_\perp = -\frac{D\partial_\perp C^{\rm eq}}{1 + q_{\rm eff}|\nabla h|} = -\frac{DC_s}{k_B T}\frac{\partial_\perp \mu}{1 + q_{\rm eff}|\nabla h|}, \tag{7.47}$$

where $q_{\text{eff}} := 2D/(k_{\text{eff}}a)$ and $k_{\text{eff}} = k+2p$. Again, as far as the macroscale limit of the normal flux is concerned, the kinetic rate undergoes only an additive renormalization in the presence of permeability.

The parallel flux $J_\parallel$ is not expected to require modification in the case of permeable steps, which reduces the barrier only for the motion of adatoms across terrace boundaries. Motion of adatoms parallel to a step edge is an independent process, subject to the same fully continuum treatment as in Chapter 5. Accordingly, we differentiate the boundary condition (7.36) with respect to σ:

$$a\partial_\parallel \mathcal{J}_\perp(i) = \frac{k_u a}{D}[\mathcal{J}_\parallel(i)+D\partial_\parallel C_i^{\text{eq}}]+\frac{pa}{D}[\mathcal{J}_\parallel(i)-\mathcal{J}_\parallel(i-1)-\partial_\parallel(\xi_\eta\delta\eta_{i-1}\mathcal{J}_\perp(i-1))], \quad (7.48)$$

where $\partial_\parallel := \xi_\sigma^{-1}\partial_\sigma$. Here we have used Fick's law to write $\partial_\parallel \mathcal{C}(i)$ in terms of the parallel flux component. From here we let $a/\lambda \to 0$ to obtain

$$J_\parallel = -D\partial_\parallel C^{\text{eq}} = -\frac{DC_s}{k_B T}\partial_\parallel \mu, \quad (7.49)$$

which is identical to the macroscale longitudinal flux derived for $p = 0$ in Chapter 5. Again we emphasize the following

Result 7.2.1. *Step permeability affects only the transverse flux component, via the boundary conditions (7.1),(7.2), while the longitudinal flux remains unchanged for nonzero p.*

The relations (7.47), (7.49) can be combined into the matrix equation $\mathbf{J} = -C_s\mathbf{M}\cdot\nabla\mu$, where $\mathbf{M} = \mathbf{M}(\nabla h)$ is the same surface mobility tensor derived in Chapter 5 (diagonal when expressed in local coordinates). Writing $\mathbf{M} = m_{\eta\eta}\mathbf{e}_\eta\mathbf{e}_\eta + m_{\sigma\sigma}\mathbf{e}_\sigma\mathbf{e}_\sigma$, we observe that only the matrix element $m_{\eta\eta}$ is affected by the permeability rate p, which enters through the nondimensional parameter q_{eff}. We obtain

a PDE for h by combining (7.47), (7.49) with the mass conservation law (5.44) and formula (5.39) for the macroscale step chemical potential. The resulting evolution law is essentially (5.45), with $\mathbf{M}$ modified to account for step permeability through the renormalized kinetic parameter k.

7.3 Discussion and interpretation

In this chapter, we found the macroscale limit of the step flow equations in the case of transparent steps with permeability coefficient p. For each of the step geometries studied, only the transverse flux experiences the effect of step transparency, through a renormalized kinetic parameter in the macroscale analog of Fick's law.

Unchanged in this chapter are the relation between chemical potential and local slope, Eq. (5.39), and the mass conservation law, Eq. (9.11). These two ingredients, along with an appropriate macroscale analog of Fick's law, constitute a closed set of equations for the macroscale surface relaxation. Here we observe that only the macroscale analog of Fick's law needs to be modified, just as in Chapter 6 with the introduction of anisotropic diffusivity on terraces. This modification of Fick's law in the macroscale limit is required whenever the adatom concentration satisfies a different boundary value problem. In Chapter 6 we assumed a tensor diffusivity and retained the usual linear kinetic boundary conditions; here we considered a scalar diffusivity and extended the boundary conditions to include a dependence on neighboring terrace adatom concentrations. In general we can modify both the terrace diffusion equation and the boundary conditions at step edges, which leads

to an extension of the mobility $\mathbf{M}$ in the resulting macroscale analog of Fick's law.

The simple result of this chapter has possible limitations. Negative values of p have been suggested to explain electromigration-induced step pairing on Si(111). The case $p < -k/2$ challenges our macroscale limit by allowing q_{eff} to take on negative values, leading to a singularity in the equations at slopes $|\nabla h| = -1/q_{\text{eff}}$. Since the slope smoothly approaches zero near facet edges or local height extrema, the singularity where $|\nabla h| = -1/q_{\text{eff}}$ can only be avoided by imposing unwarranted restrictions on the magnitude of the slope. However, if the permeability rate p is large and positive, we expect the adatoms to jump without difficulty from one terrace to the next, being limited in their motion only by the finite terrace diffusivity. The macroscale limit derived here ought to hold in this case of diffusion-limited kinetics.

We might also interpret the renormalized kinetic rate in the macroscale equations as a result of homogenization. Instead of seeing a crystal surface as terraces separated by sharp steps, the *two-region model* treats the surface as a layered medium, with two types of regions distinguished by their diffusivities and their widths [125]. Since surface reconstruction might take place more readily near a line defect, it is natural to postulate the existence of a tubular region around each step, in which the adatom diffusivity differs from that of terraces. The effective rate of adatom transport over a *mesoscale* consisting of many terraces is now seen to depend on the different diffusivity D_a due to reconstruction in the tubular region corresponding to a step, and the width l_a of this region relative to the typical terrace width l; see Figure 7.2. We appeal to the calculation of [70] to find the averaged (or effective) diffusivity D_{av} for a train of N terraces spanning a total transverse distance L. This

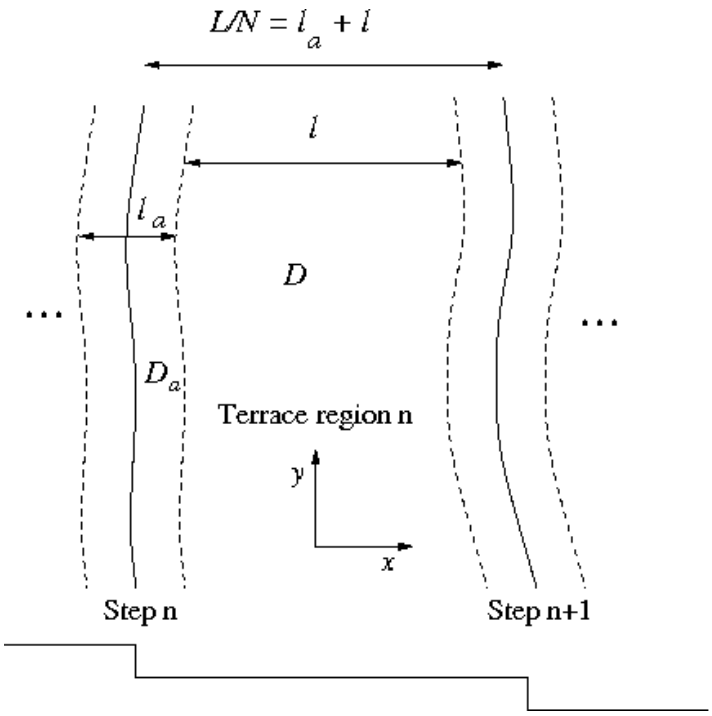

Figure 7.2: Illustration of the two-region model in contrast to the sharp step picture it replaces (adapted from [125]).

D_{av} is given by

$$D_{av} = \frac{1}{\frac{1}{L}\left(\frac{l_a}{D_a} + \frac{l}{D}\right)} = \frac{D}{1 + \left(\frac{D}{D_a} - 1\right)\frac{l_a}{a} m_0}, \tag{7.50}$$

where m_0 is the local slope in the mesoscale region. In hindsight, the same result can be derived by mapping the two-region model to an electric circuit consisting of resistors in series. The effective conductance $\sigma_{\text{eff}} = 1/R_{\text{eff}}$ of a two-resistor unit is given by the harmonic average of the two conductances, i.e.,

$$\frac{1}{\sigma_{\text{eff}}} = \frac{1}{\sigma} + \frac{1}{\sigma_a}. \tag{7.51}$$

We identify the conductance σ with the terrace diffusivity per unit length, D/l, while σ_a corresponds to the "step region" diffusivity per unit length, D_a/l_a. Equation (7.50) ensues.

Zhao, Weeks and Kandel [125] obtained (7.50) without recourse to homogenization theory or electric circuit analogies. Their interpretation allows for different sign of the coefficient $(D/D_a - 1)l_a/a$ depending on which inequality holds between the diffusivities in the two regions. Faster diffusion in the step region ($D_a > D$) leads to a negative coefficient of m_0. Similarly, a permeability coefficient p satisfying $p < -k/2$ leads to a negative q in the macroscale limit of this chapter. Evidently, the two-region model and the picture of permeable sharp steps both have enough flexibility in the choice of parameters to match a range of coefficients in the slope-dependent mobility. The agreement between these two nanoscale models at the level of macroscale equations is noteworthy, in view of the strikingly different pictures they present at the nanoscale. The persistence of a slope-dependent mobility with (possibly negative) material parameter q indicates just how robust

the macroscale limit is, emerging in the same form out of two conceptually distinct nanoscale models.

Our interpretation of permeability, as an additive renormalization of the kinetic rate in the macroscale equations, is simple enough to allow meaningful comparisons between predictions of the macroscale PDE (chapter 10) and Monte-Carlo simulations of stepped surfaces. An alternative interpretation by O. Pierre-Louis [89], in which the equilibrium concentration of the step flow equations is renormalized through a suitable combination of the boundary conditions, also admits direct comparison with atomistic simulations. The question of whether step transparency itself is exhibited by realistic surfaces cannot be addressed without a further understanding of the physical mechanisms which combine with permeability to produce different morphological changes. Our discussion of electromigration in Chapter 8 helps complete the picture of possible nanoscale physics, in order to categorize the kinetic regimes under which a stepped surface can evolve. By studying those regimes where permeability would couple with electromigration to yield a qualitatively different evolution, we might in principle be able to detect the presence and strength of step transparency for realistic materials.

Chapter 8

Electromigration and desorption[1]

In this chapter, we consider another set of extensions to the BCF picture of terrace adatom diffusion. First we introduce an electric field, which biases the motion of adatoms in a prescribed direction. Next we allow desorption of adatoms into the vapor phase. Combined with our results for anisotropic terrace diffusion and step edge diffusion, the inclusion of electromigration and desorption provides a comprehensive model of the mass transport processes over terraces and steps.

Our analysis aims to complement previous works in surface electromigration; see, e.g., [12, 15, 27, 28, 35, 52, 53, 55, 59, 60, 61, 72, 74, 88, 90, 92, 101, 102, 103, 111, 112, 124, 125]. These focus on the development of instabilities (e.g. step meandering and bunching) across scales, often from a dynamical system viewpoint. We, on the other hand, place electromigration in the context of connecting discrete schemes for interacting steps to global PDE laws and variational principles in 2+1 dimensions [16, 64, 66, 78, 80, 96, 98, 106, 109, 123]. The PDE we derive can be studied using local analysis, to see the possible control that an electric field might have on the spatial dependence of the slope profile near a facet. Investigating the possible *global* control of the surface evolution by an electric field is within the scope of our numerical method, as we discuss in Chapter 10.

[1] Parts of this chapter appeared previously in Quah and Margetis, *Macroscopic Electromigration on Stepped Surfaces*, submitted to SIAM Multiscale Modeling and Simulation.

The study of electromigration began with the observation by Latyshev et al. [59] that direct current heating of stepped Si(111) resulted in a step bunching instability. The appearance of step bunches depends both on the direction of the applied current and on the surface temperature. An early model by Stoyanov [111] offered a possible explanation for the link between electromigration current and step bunching. Stoyanov's model works only up to 850 °C, above which temperature the direction of electric current required for step bunching undergoes two distinct reversals. In particular, direct current in the step-down direction produces step bunching at temperatures around 935 °C and 1275 °C, but at 1190 °C step bunching requires current in the step-up direction.

More recent proposals to address the relation between electromigration and step bunching (although not directly relevant to our focus here) include but are not limited to the work by Pierre-Louis and Métois [88, 90], and by Zhao, Weeks, and Kandel [124, 125]. Experimental studies found the bias in adatom motion—the *drift velocity*—to be always parallel to the imposed electric field $\mathbf{E}$. This drift velocity $\mathbf{v}$ is related to $\mathbf{E}$ by [15, 28]:

$$\mathbf{v} = \frac{D\,(Z^*e)\,\mathbf{E}}{T}, \tag{8.1}$$

where D is the adatom diffusivity, Z^*e is the effective adatom charge,[2] and T is the Boltzmann energy[3]. At the level of steps, the electric field amounts to the addition of a convective (linear in the density gradient) term in the diffusion equation for the

[2]Here, we follow the notation of [15]. The symbol Z^* (with an asterisk) should not be confused with the usual symbol for the conjugate of a complex number.

[3]In this chapter *only* we use units where $k_B = 1$, thus replacing by T the k_BT of other chapters.

adatom density; see (8.35). Regarding (8.1), $|Z^*|$ is larger than unity for metals but can be much smaller than unity for semiconductors [15]. We note in passing that $\mathbf{E}$ influences the temperature in an experimental setup, since it directly controls the electric current that flows through and eventually heats up the sample.

In addition to electromigration, we will allow adatoms to desorb into the vapor with characteristic time τ. So, the term C/τ is added in the adatom diffusion equation where C is the adatom density. We study if and how this addition at the BCF level influences the macroscopic limit. Note that a phenomenological approach to desorption in crystal morphological evolution is offered by Villain [119]. We derive τ-dependent corrections of the large-scale flux, and describe how large τ needs to be so that desorption can be neglected in the macroscopic laws.

8.1 Macroscale limit and assumptions

The macroscopic limit aims to describe a continuous surface at sufficiently large scales. Previous studies of electromigration and desorption apparently have not focused on global evolution laws for the surface height, and hence carry a perspective different from ours. These works (i) focus mainly on stability issues, (ii) make use primarily of nanoscale models where steps are everywhere parallel, and (iii) allow steps to interact mainly through terrace diffusion (with less emphasis on step-step entropic or elastic dipole interactions).

Our derivation uses the multiscale expansion reviewed in Chapter 5, which handles a fully (2+1)-dimensional geometry just as easily as a straight-step geom-

etry. The expansion parameter is the step height, a. This formulation relies on the separation of local variables for interacting steps into fast and slow, and can encompass additional physical effects such as desorption and electromigration. As a result, we derive a fully continuum model in 2+1 dimensions that extends the model of Chapter 5 to a greater variety of experimentally relevant situations. The additional effect of anisotropic terrace diffusion can also be incorporated subsequently, following the calculation of Chapter 6.

We recall the geometric assumptions underlying the macroscopic limit. The (microscale) terrace width is assumed to be of the order of the step height, a, and small compared to: (i) the step radius of curvature; (ii) the length over which the step curvature varies; and (iii) the macroscopic length over which the step density varies. A step train satisfying these conditions is referred to as 'slowly varying', cf. Sections 5.3 and 6.1. The macroscopic limit is reached formally as $a/\lambda \to 0$ where λ is a macroscopic length. The step density is fixed and approaches the surface slope. We assume that the initial (at $t = 0$) ordering of steps is preserved by the flow (for $t > 0$),[4] and that step trains are *monotonic* (say, with descending steps in the direction of increasing transverse coordinate).

Furthermore, we require that certain kinetic parameter groups involving the step height, a, remain $\mathcal{O}(1)$ (as $a/\lambda \downarrow 0$). In particular, we take $D/(ka) = \mathcal{O}(1)$ where k is any relevant kinetic rate for attachment-detachment of adatoms at a step edge.

[4]This property should be derivable from microscale physics, such as the entropic repulsions that enforce the non-crossing condition. This aspect is not studied here.

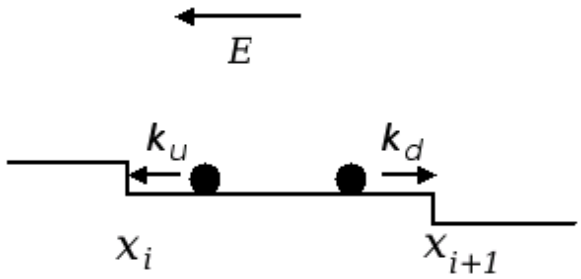

Figure 8.1: Schematic of 1D steps (cross section) with an applied electric field, E. Steps are descending with increasing x; E is shown to be in the step-up direction ($E < 0$); and k_u (k_d) is the kinetic rate for atom attachment-detachment from a terrace to an up- (down-) step edge.

8.2 One-dimensional step models

In this section, we review briefly ingredients of step motion, including *repulsive* entropic and elastic dipole step interactions, for 1D geometries: straight and concentric circular steps. Related versions of the adatom diffusion equation with either an electric field or desorption are solved explicitly.

The step configuration is shown in Figure 8.1. Both the diffusion of adatoms (density gradient) and electric field (drift velocity) contribute to the flux in each terrace. Each step advances or retreats in response to the net (normal) flux from the neighboring terraces. The surface evolves as the steps move, lowering its free energy.

8.2.1 Straight steps

The position of the ith step is denoted by $x_i(t)$ (t is time), where $x_{i+1} > x_i$ for all t, and $C_i(x,t)$ is the adatom density on the ith terrace, i.e., the region $x_i < x < x_{i+1}$. A *constant* electric field is applied externally in the x direction (perpendicular to steps), introducing a drift velocity v according to (8.1). The diffusion equation satisfied by $C_i(x,t)$ is

$$D\partial_x^2 C_i - v\partial_x C_i - \tau^{-1} C_i = \partial_t C_i \approx 0 \qquad x_i < x < x_{i+1} \ , \tag{8.2}$$

where τ is the characteristic desorption time. We use the quasi-steady approximation, $\partial_t C_i \approx 0$, by assuming that step motion is much slower than diffusion.

The adatom flux on the ith terrace, $J_i(x,t)$, is defined by Fick's law with drift:

$$J_i(x,t) = -D\partial_x C_i + vC_i \ . \tag{8.3}$$

Linear kinetics prescribes the familiar boundary conditions at the step edges:

$$-J_i = k_u(C_i - C_i^{\rm eq}) \qquad x = x_i \ , \tag{8.4}$$

$$J_i = k_d(C_i - C_{i+1}^{\rm eq}) \qquad x = x_{i+1} \ ; \tag{8.5}$$

k_u (k_d) is the kinetic rate for an up- (down-) step edge, and $C_i^{\rm eq}$ is the equilibrium adatom density at the ith step.

This $C_i^{\rm eq}$ expresses step interactions via the relation

$$C_i^{\rm eq} = C_s \exp\left(\frac{\mu_i}{T}\right) \sim C_s\left(1 + \frac{\mu_i}{T}\right) \ , \qquad |\mu_i| \ll T \ , \tag{8.6}$$

where μ_i is the ith-step chemical potential and C_s is the equilibrium adatom density at an isolated step. In Section 8.5.1 we consider the consequences of *not* linearizing

the exponential dependence on μ_i.[5]

To illustrate some simple computations, we next distinguish the limits (i) $\tau \to \infty$ (no desorption) and constant nonzero v, and (ii) $v = 0$ with finite τ. The combination of finite τ and nonzero v can be described explicitly, but to keep the presentation uncluttered we postpone this calculation until Section 8.5.2 on 2D geometry.

8.2.1.1 Electric field with no desorption

Solving (8.2) for $\tau \to \infty$ yields

$$C_i(x) = A_i e^{vx/D} + B_i \qquad x_i < x < x_{i+1} \ . \tag{8.7}$$

The adatom flux on the ith terrace, $J_i(x)$, is computed by (8.3):

$$J_i(x) = vB_i \ . \tag{8.8}$$

Substituting for C_i and J_i in (8.5) via (8.7) and (8.8) leads to the system

$$\begin{pmatrix} e^{vx_i/D} & 1 + v/k_u \\ e^{vx_{i+1}/D} & 1 - v/k_d \end{pmatrix} \begin{pmatrix} A_i \\ B_i \end{pmatrix} = \begin{pmatrix} C_i^{\mathrm{eq}} \\ C_{i+1}^{\mathrm{eq}} \end{pmatrix} . \tag{8.9}$$

This matrix equation is solved explicitly to yield

$$J_i(x) = J_i(x_i) = -v \frac{C_{i+1}^{\mathrm{eq}} - e^{v(\delta x_i)/D} C_i^{\mathrm{eq}}}{e^{v(\delta x_i)/D}(1 + v/k_u) - (1 - v/k_d)} \ , \tag{8.10}$$

where $\delta x_i := x_{i+1} - x_i = \mathcal{O}(a)$ is the terrace width.

[5]This extension also applies to the macroscale limits of previous chapters, but the formal manipulations used here are better motivated by first calculating the macroscale limit with electromigration.

8.2.1.2 Desorption with no electric field

Now consider diffusion equation (8.2) with $v = 0$ and finite τ. The solution reads

$$C_i(x) = A_i e^{bx} + B_i e^{-bx} \ , \qquad b := (D\tau)^{-1/2} \ . \tag{8.11}$$

The mass flux is $J_i(x) = -D\partial_x C_i = -Db(A_i e^{bx} - B_i e^{-bx})$. Boundary conditions (8.5) yield the matrix equation

$$\begin{pmatrix} e^{bx_i}(1-\theta_u) & e^{-bx_i}(1+\theta_u) \\ e^{bx_{i+1}}(1+\theta_d) & -e^{-bx_{i+1}}(1-\theta_d) \end{pmatrix} \begin{pmatrix} A_i \\ B_i \end{pmatrix} = \begin{pmatrix} C_i^{\rm eq} \\ C_{i+1}^{\rm eq} \end{pmatrix} \ , \tag{8.12}$$

where $\theta_l := Db/k_l$ ($l = u,\, d$). The mass flux on the ith terrace at $x = x_i$ is

$$J_i(x_i) = -Db\, \frac{C_{i+1}^{\rm eq} - [\cosh(b\,\delta x_i) + \theta_d\, \sinh(b\,\delta x_i)] C_i^{\rm eq}}{(1+\theta_u\theta_d)\sinh(b\,\delta x_i) + (\theta_u + \theta_d)\cosh(b\,\delta x_i)} \ . \tag{8.13}$$

The flux at $x = x_{i+1}$ can be obtained by the interchanges $u \leftrightarrow d$ and $C_i^{\rm eq} \leftrightarrow -C_{i+1}^{\rm eq}$.

Remark 8.2.1. *The fluxes in* (8.10) *and* (8.13) *are not simply proportional to* $C_{i+1}^{\rm eq} - C_i^{\rm eq}$ *(which in the macroscopic limit,* $\delta x_i = x_{i+1} - x_i = \mathcal{O}(a) \downarrow 0$*, becomes proportional to the gradient of the macroscale chemical potential,* μ*). In section* 8.4 *we argue more generally that* (8.10) *and* (8.13) *reduce to different macroscopic laws for the flux: The electric-field drift has a distinct macroscopic signature in the resulting Fick's law; in contrast, the desorption effect is of higher order (in the expansion parameter* a*), and is deemed negligible for a broad class of materials and conditions.*

8.2.2 Concentric circular steps

In this section, we apply the BCF formulation to an axisymmetric setting. Our goal is to study the interplay of drift and step curvature. So, consider steps

that are concentric circles of radii $r_i(t)$ with $r_{i+1} > r_i$. The external electric field $\mathbf{E}$ is taken to be radial, viz., $\mathbf{E} = e_r E$ (e_r: radial unit vector) where E may vary with the polar coordinate, r. To simplify the exposition, we set $E = \mathcal{E}(r)/r$.[6]

The electric field produces the radial drift velocity $\mathbf{v} = e_r v = e_r \mathcal{V}/r$ according to (8.1), where $\mathcal{V} = D\, Z^* e\, \mathcal{E}/T$. The radial adatom flux, $J_i(r) = e_r \cdot \mathbf{J}_i(r)$, is

$$J_i(r) = -D\partial_r C_i + vC_i \qquad r_i < r < r_{i+1} \ . \tag{8.14}$$

The terrace diffusion equation under the quasi-steady approximation thus reads

$$0 \approx -\mathrm{div}\, \mathbf{J}_i - \tau^{-1} C_i = D(\partial_r^2 C_i + r^{-1}\partial_r C_i) - r^{-1}\mathcal{V}\partial_r C_i - r^{-1}(\partial_r \mathcal{V})\, C_i - \tau^{-1} C_i \tag{8.15}$$

[where $r^{-1}(\partial_r \mathcal{V}) C_i = (\mathrm{div}\, \mathbf{v})\, C_i$]. In the following, we neglect the term $r^{-1}(\partial_r \mathcal{V}) C_i$ assuming that, for $v \neq 0$, $|\partial_r \mathcal{V}| C_i \ll |\mathcal{V}\partial_r C_i|$; this holds, for example, if $\mathcal{V}(r)$ varies sufficiently slowly.[7] Hence, (8.15) simplifies to

$$0 \approx D(\partial_r^2 C_i + r^{-1}\partial_r C_i) - r^{-1}\mathcal{V}\partial_r C_i - \tau^{-1} C_i \ . \tag{8.16}$$

In Section 8.5.2.2 we discuss the effect of retaining $(\mathrm{div}\mathbf{v})C_i$ in the diffusion equation.

Boundary conditions analogous to (8.5) that complement (8.16) follow from linear kinetics at the step edges:

$$-J_i(r_i) = k_u[C_i(r_i) - C_i^{\mathrm{eq}}] \ , \quad J_i(r_{i+1}) = k_d[C_i(r_{i+1}) - C_{i+1}^{\mathrm{eq}}] \ . \tag{8.17}$$

[6] In experimental setups, $\mathbf{E}$ must of course be generated and sustained by feasible charge distributions. The issue of sources for $\mathbf{E}$ is not addressed here. These practical concerns suggest the view that this radial case serves as a *toy model* for studying the interplay of drift and step curvature.

[7] This condition is also expected to hold for $\mathcal{V}$ of the form $\mathcal{V} = c\, r^{\omega}$ with sufficiently large r.

The difference of fluxes from neighboring terraces at the ith step edge yields the step velocity $\dot{r}_i = \frac{\mathrm{d}r_i}{\mathrm{d}t}$ according to mass conservation,

$$\dot{r}_i = \frac{\Omega}{a}[J_{i-1}(r_i) - J_i(r_i)] \ . \tag{8.18}$$

The coupled step flow equations with drift and desorption form an extension of the axisymmetric model by Israeli and Kandel [37] and Fok [25].

By analogy with section 8.2.1, we distinguish the cases with (i) $\tau \to \infty$, and (ii) $v = 0$, where explicit solutions are relatively simple.

8.2.2.1 Electric field with no desorption

First, we solve (8.16) for $\tau \to \infty$. By successive integrations we obtain the formula

$$C_i(r) = B_i + A_i \int_{r_i}^{r} \frac{1}{z} \exp\left[D^{-1} \int_{r_i}^{z} v(r')\,\mathrm{d}r'\right]\mathrm{d}z \qquad r_i < r < r_{i+1} \ . \tag{8.19}$$

By (8.14), we compute the corresponding (radial) flux:

$$\begin{aligned} J_i(r) = A_i \Bigg\{ & -\frac{D}{r} \exp\left[D^{-1} \int_{r_i}^{r} v(r')\,\mathrm{d}r'\right] \\ & + v(r) \int_{r_i}^{r} \frac{1}{z} \exp\left[D^{-1} \int_{r_i}^{z} v(r')\,\mathrm{d}r'\right]\mathrm{d}z \Bigg\} + v(r) B_i \ . \end{aligned} \tag{8.20}$$

Substituting (8.19) and (8.20) for C_i and J_i in conditions (8.17), we find

$$\begin{pmatrix} -\dfrac{D}{k_u r_i} & 1 + \dfrac{v_i}{k_u} \\ \left(1 - \dfrac{v_{i+1}}{k_d}\right) \displaystyle\int_{r_i}^{r_{i+1}} \phi_i(z)\,\mathrm{d}z + \frac{D}{k_d}\phi_i(r_{i+1}) & 1 - \dfrac{v_{i+1}}{k_d} \end{pmatrix} \begin{pmatrix} A_i \\ B_i \end{pmatrix} = \begin{pmatrix} C_i^{\mathrm{eq}} \\ C_{i+1}^{\mathrm{eq}} \end{pmatrix} \ , \tag{8.21}$$

where $v_j := v(r_j)$[8] and

$$\phi_i(r) := \frac{1}{r} \exp\left[D^{-1} \int_{r_i}^{r} v(r') \, \mathrm{d}r' \right] . \tag{8.22}$$

Solving for A_i and B_i we have

$$A_i = \frac{\mathcal{D}_A}{\mathcal{D}^v} , \qquad B_i = \frac{\mathcal{D}_B}{\mathcal{D}^v} , \tag{8.23}$$

$$\begin{aligned} \mathcal{D}^v := \frac{D}{k_u r_i}\left(1 - \frac{v_{i+1}}{k_d}\right) + \left[\frac{D}{k_d}\phi_i(r_{i+1}) + \left(1 - \frac{v_{i+1}}{k_d}\right)\int_{r_i}^{r_{i+1}} \phi_i(z) \, \mathrm{d}z\right] \\ \times \left(1 + \frac{v_i}{k_u}\right) , \end{aligned} \tag{8.24}$$

$$\mathcal{D}_A := \left(1 + \frac{v_i}{k_u}\right) C_{i+1}^{\mathrm{eq}} - \left(1 - \frac{v_{i+1}}{k_d}\right) C_i^{\mathrm{eq}} , \tag{8.25}$$

$$\mathcal{D}_B := \frac{D}{k_u r_i} C_{i+1}^{\mathrm{eq}} + \left[\frac{D}{k_d}\phi_i(r_{i+1}) + \left(1 - \frac{v_{i+1}}{k_d}\right)\int_{r_i}^{r_{i+1}} \phi_i(z) \, \mathrm{d}z\right] C_i^{\mathrm{eq}} . \tag{8.26}$$

The above formulas are simplified considerably if rv is treated as a constant.

For $r = r_i$ the radial flux reads

$$J_i(r_i) = -\frac{D A_i}{r_i} + v_i \, B_i . \tag{8.27}$$

The value $J_{i-1}(r_i)$ can be obtained similarly. The step velocity $\dot{r}_i$ is written explicitly by substituting the values for the integration constants into (8.27) and evaluating the net flux at r_i; cf. (3.33)–(3.36).

We conclude this subsection by noting in passing that the term $(\operatorname{div} \mathbf{v}) C_i$, which was neglected above, can be included in the diffusion equation without difficulty (although the algebra is lengthier and less transparent). An idea is to treat the term in question as a forcing, apply Duhamel's principle and thus derive an integral

[8] This distinction is not necessary if $v(r)$ is macroscopic, i.e., it varies slowly.

equation for C_i, which can be solved via a Born-Neumann series by iteration. This approach is undertaken in Section 8.5.2 for 2D. Alternatively, C_i can be expressed in terms of confluent hypergeometric functions [18].

8.2.2.2 Desorption with no electric field

Next, we turn our attention to (8.16) with $v = 0$ and finite τ. The solution reads

$$C_i(r) = A_i\, I_0(br) + B_i\, K_0(br)\ , \quad b = (D\tau)^{-1/2}\ , \qquad r_i < r < r_{i+1}\ , \tag{8.28}$$

where I_0 and K_0 are modified Bessel functions [19]. The flux at the ith terrace is

$$J_i(r) = -D\,\partial_r C_i(r) = -Db[A_i\, I_0'(br) + B_i\, K_0'(br)] \qquad r_i < r < r_{i+1}\ . \tag{8.29}$$

By applying boundary conditions (8.17) we find the matrix equation

$$\begin{pmatrix} I_0(br_i) - \dfrac{Db}{k_u}\, I_0'(br_i) & K_0(br_i) - \dfrac{Db}{k_u}\, K_0'(br_i) \\ I_0(br_{i+1}) + \dfrac{Db}{k_d}\, I_0'(br_{i+1}) & K_0(br_{i+1}) + \dfrac{Db}{k_d}\, K_0'(br_{i+1}) \end{pmatrix} \begin{pmatrix} A_i \\ B_i \end{pmatrix} = \begin{pmatrix} C_i^{\mathrm{eq}} \\ C_{i+1}^{\mathrm{eq}} \end{pmatrix}. \tag{8.30}$$

The microscale flux on the ith terrace at $r = r_i$ is

$$J_i(r_i) = Db\,\frac{\mathcal{M}_i\, C_i^{\mathrm{eq}} - (br_i)^{-1}\, C_{i+1}^{\mathrm{eq}}}{\mathcal{P}_i}\ , \tag{8.31}$$

where

$$\begin{aligned} \mathcal{M}_i =& I_0'(br_i)K_0(br_{i+1}) - K_0'(br_i)I_0(br_{i+1}) \\ &+ \frac{Db}{k_d}[I_0'(br_i)K_0'(br_{i+1}) - K_0'(br_i)I_0'(br_{i+1})]\ , \end{aligned} \tag{8.32}$$

$$\begin{aligned}\mathcal{P}_i =& I_0(br_{i+1})K_0(br_i) - I_0(br_i)K_0(br_{i+1}) \\ &+ \frac{Db}{k_u}[I_0'(br_i)K_0(br_{i+1}) - I_0(br_{i+1})K_0'(br_i)] \\ &+ \frac{Db}{k_d}[I_0'(br_{i+1})K_0(br_i) - I_0(br_i)K_0'(br_{i+1})] \\ &- \frac{(Db)^2}{k_u k_d}[I_0'(br_{i+1})K_0'(br_i) - I_0'(br_i)K_0'(br_{i+1})] \ . \end{aligned} \tag{8.33}$$

In the above relations, the prime denotes differentiation with respect to argument. The step velocity is expressed in terms of $(r_{i-2}, r_{i-1}, r_i, r_{i+1}, r_{i+2})$ via (3.33)–(3.36).

8.3 2-dimensional step geometry

In this section, we consider steps of reasonably arbitrary shape and formulate their equations of motion under a macroscopic electric field $\mathbf{E}$ without desorption ($\tau = \infty$, i.e., $b = (D\tau)^{-1/2} = 0$). Of particular interest are unidirectional electric fields with magnitudes that vary over a length scale large compared to the scale over which the adatom density varies. So, we impose

$$|(\operatorname{div} \mathbf{v})\, C_i| \ll |\mathbf{v} \cdot \nabla C_i| \ . \tag{8.34}$$

Condition (8.34) is satisfied trivially (by $\operatorname{div}\mathbf{v} \equiv 0$) if $\mathbf{E}$ is constant, which corresponds to many experimentally relevant situations.[9] With regard to the actual steps, we assume that their edges are represented by sufficiently smooth, closed curves on the reference plane (x, y), which do not cross or self-intersect, as ensured physically by the step-step repulsive (entropic and elastic dipole) interactions.

[9] If the three-dimensional $\mathbf{E}$ depends only on (x, y), (8.34) is trivially satisfied (by $\operatorname{div}\mathbf{v} \equiv 0$) in the absence of charge distribution.

8.3.1 Step geometry and formulation

We remind the reader of our notation for the geometry of 2D steps given in Chapter 5. The step train is monotonic, with steps descending outward from a top terrace (surface peak). Their edges are numbered $1, 2, ..., N$, starting from the topmost step. The local coordinates (η, σ) measure the distances transverse and parallel to steps, respectively, with η increasing in the step-down direction and σ increasing counterclockwise (top view). The unit vectors $\mathbf{e}_\eta, \mathbf{e}_\sigma$ are orthogonal, in the direction of increasing η, σ, respectively. The relevant metric coefficients ($\mathbf{r}$: position vector) are defined by

$$\xi_\eta := |\partial_\eta \mathbf{r}| \ , \qquad \xi_\sigma := |\partial_\sigma \mathbf{r}| \ .$$

In the following, ξ_η and ξ_σ are treated as $\mathcal{O}(1)$ and slowly varying with σ.

8.3.2 Equations of motion

In view of (8.34) and the quasi-steady approximation, the adatom density field C_i in the ith-terrace region ($\eta_i < \eta < \eta_{i+1}$) solves

$$0 \approx \partial_t C_i = \ \mathrm{div}(\mathbf{D} \cdot \nabla C_i) - \mathbf{v} \cdot \nabla C_i \ , \qquad \nabla = (\partial_x, \partial_y) = (\xi_\eta^{-1}\partial_\eta, \xi_\sigma^{-1}\partial_\sigma) \ , \quad (8.35)$$

where $\mathbf{D}$ is in principle a tensor function of position $\mathbf{r}$. Here, we consider a scalar constant, $\mathbf{D} = D$; anisotropic terrace diffusion is a straightforward application of the methods outlined in Chapter 6.[10] The (vector-valued) adatom flux $\mathbf{J}_i$ is

$$\mathbf{J}_i = -D\nabla C_i + \mathbf{v} C_i \ . \quad (8.36)$$

[10]The details of this extension are given in [97].

Robin-type boundary conditions for (8.35) inform C_i of: (i) attachment and detachment of atoms at steps; and (ii) step energetics, especially step-step interactions, via the equilibrium concentration, $C_i^{\rm eq}$. These boundary conditions read

$$-J_{i,\perp}(\eta_i,\sigma) = k_u[C_i(\eta_i,\sigma) - C_i^{\rm eq}(\sigma)] \ , \tag{8.37}$$

$$J_{i,\perp}(\eta_{i+1},\sigma') = k_d[C_i(\eta_{i+1},\sigma') - C_{i+1}^{\rm eq}(\sigma')] \ ; \quad J_{i,\perp} := \mathbf{e}_\eta \cdot \mathbf{J}_i \ , \ k_u/k_d = \mathcal{O}(1) \ . \tag{8.38}$$

8.3.3 Approximate solution of diffusion equation

By use of the local coordinates (η,σ), diffusion equation (8.35) for $C_i(\eta,\sigma)$ reads

$$0 = \frac{D}{\xi_\eta \xi_\sigma}\left[\partial_\eta\left(\frac{\xi_\sigma}{\xi_\eta}\partial_\eta C_i\right) + \partial_\sigma\left(\frac{\xi_\eta}{\xi_\sigma}\partial_\sigma C_i\right)\right] - v_\perp \xi_\eta^{-1}\partial_\eta C_i - v_\parallel \xi_\sigma^{-1}\partial_\sigma C_i \ , \tag{8.39}$$

where $\eta_i < \eta < \eta_{i+1}$; $v_\perp := \mathbf{e}_\eta \cdot \mathbf{v}$ and $v_\parallel := \mathbf{e}_\sigma \cdot \mathbf{v}$.

By analogy with the case of zero electric field [66], we solve (8.39) with recourse to the following proposition (which puts the derivations of Chapters 5,6, and 7 on a more rigorous footing).

Proposition 8.3.1. *Consider the boundary value problem consisting of PDE* (8.39) *on the terrace* $U_i = \{(\eta,\sigma)\,|\,\eta_i < \eta < \eta_{i+1}\}$, *and conditions* (8.37), (8.38) *on the boundary,* ∂U_i, *of* U_i. *Suppose that: (i) the boundary data exhibits a scale separation in the sense that, for some geometric parameter* $\epsilon \ll 1$, $C_i^{\rm eq}$ *is a fixed,* $\mathcal{O}(1)$ *function of the slow variable* $\overline{\sigma} := \epsilon\sigma$, *i.e.,* $C_i^{\rm eq} = C_i^{\rm eq}(\overline{\sigma})$, *while the rates* k_u, k_d *are* ϵ*-independent; (ii) the metric coefficients* ξ_η, ξ_σ *depend on* $(\eta,\overline{\sigma})$ *and are* $\mathcal{O}(1)$ *as*

$\epsilon \downarrow 0$*; and (iii)* $\operatorname{curl} \mathbf{v} = 0$ *(i.e.,* $\partial_x v_y = \partial_y v_x$*)*[11] *and* $\min\{k_u, k_d\} > (1/2)|\mathbf{v}|$*. Let* C_i *be a* C^2 *(twice continuously differentiable) function on* U_i *and* C^1 *(continuously differentiable) function on* $\overline{U}_i$*, the closure of* U_i*. Then, for* $\eta = \mathcal{O}(1)$*,* $C_i(\eta, \sigma) = C_i^{(0)}(\eta, \overline{\sigma}) + o(1)$ *where*

$$C_i^{(0)}(\eta, \overline{\sigma}) = B_i(\overline{\sigma}) + A_i(\overline{\sigma}) \int_{\eta_i}^{\eta} dz \; \frac{\xi_\eta|_z}{\xi_\sigma|_z} \exp\left[\int_{\eta_i}^{z} \frac{(v_\perp \, \xi_\eta)|_{\eta'}}{D} \, d\eta'\right] ; \tag{8.40}$$

$o(1) \to 0$ *as* $\epsilon \downarrow 0$*. The integration constants* A_i, B_i *are given by*

$$A_i(\overline{\sigma}) = \frac{(1 + v_\perp|_{\eta_i}/k_u) C_{i+1}^{\mathrm{eq}} - (1 - v_\perp|_{\eta_{i+1}}/k_d) C_i^{\mathrm{eq}}}{\dfrac{D}{k_u \xi_\sigma|_{\eta_i}} \left(1 - \dfrac{v_\perp|_{\eta_{i+1}}}{k_d}\right) + \left(1 + \dfrac{v_\perp|_{\eta_i}}{k_u}\right) \left[\dfrac{D}{k_d \xi_\eta} \partial_\eta f_i|_{\eta_{i+1}} + \left(1 - \dfrac{v_\perp}{k_d}\right) f_i|_{\eta_{i+1}}\right]} , \tag{8.41}$$

$$B_i(\overline{\sigma}) = \left(1 + \frac{v_\perp|_{\eta_i}}{k_u}\right)^{-1} \left[C_i^{\mathrm{eq}}(\overline{\sigma}) + \frac{D}{k_u \xi_\sigma|_{\eta_i}} A_i(\overline{\sigma})\right] , \tag{8.42}$$

where $f_i(\eta, \sigma)$ *is defined by*

$$f_i(\eta, \sigma) := \int_{\eta_i}^{\eta} \frac{\xi_\eta|_z}{\xi_\sigma|_z} \exp\left[\int_{\eta_i}^{z} \frac{(v_\perp \xi_\eta)|_{\eta'}}{D} \, d\eta'\right] dz \qquad (\eta, \sigma) \in U_i \; . \tag{8.43}$$

In the above, $Q|_z$ denotes the value $Q(\eta = z)$. The role of parameter ϵ is to express small variations of the step edge curvature, which in turn cause slow variations of $C_i = C_i^\epsilon(\eta, \sigma)$ with respect to σ, permitting a perturbative treatment. In the limit $\epsilon \downarrow 0$, the step edges become 1D, approaching concentric circles or straight lines (depending on limits of ξ_η, ξ_σ). We also assume that k_u and k_d are positive (as is typical in crystalline materials). For comments on the condition $|\mathbf{v}|/k_l < 2$ where $l = u, d$, see Remark 8.3.2.

Proof. For convenience and notational economy, in this proof we set $D = 1$ (or, define the inverse length $\widehat{\mathbf{v}} := \mathbf{v}/D$ and drop the hat) and suppress the terrace

[11] Alternatively, it can be assumed that $\mathbf{v}(\mathbf{r})$ varies slowly, e.g., $\mathbf{v} = \mathbf{v}(\epsilon_1 \eta, \epsilon_1 \sigma)$, $\epsilon_1 \ll \epsilon$.

index i unless noted otherwise. Assuming that a solution $C(\mathbf{r}) = C^\epsilon(\mathbf{r})$ exists and is unique, as implied below, we partly separate scales in PDE (8.39) for $\eta = \mathcal{O}(1)$. So, we expand formally $C^\epsilon(\mathbf{r})$ in an ϵ-power series; each coefficient, $C^{(j)}$, is allowed to be a function of $(\eta, \sigma, \overline{\sigma})$, which are treated as independent variables:[12]

$$C^\epsilon(\eta,\sigma) = C^{(0)}(\eta,\sigma,\overline{\sigma}) + \sum_{j\geq 1} \epsilon^j\, C^{(j)}(\eta,\sigma,\overline{\sigma}) = C^0(\eta,\sigma,\overline{\sigma}) + o(1)\ , \tag{8.44}$$

where the remainder approaches 0 as $\epsilon \downarrow 0$, assuming continuity of the solution with ϵ.[13] In addition, the operator ∂_σ is replaced by the linear combination

$$\partial_\sigma \Rightarrow \partial_\sigma + \epsilon\, \partial_{\overline{\sigma}}\ .$$

By dominant balance of $\mathcal{O}(\epsilon^0)$ terms, (8.39) entails the (zeroth-order) PDE

$$\left\{ \frac{1}{\xi_\eta \xi_\sigma} \left[\partial_\eta \left(\frac{\xi_\sigma}{\xi_\eta} \partial_\eta \right) + \partial_\sigma \left(\frac{\xi_\eta}{\xi_\sigma} \partial_\sigma \right) \right] - v_\perp \frac{\partial_\eta}{\xi_\eta} - v_\parallel \frac{\partial_\sigma}{\xi_\sigma} \right\} C^{(0)} = 0 \qquad (\mathbf{r} \in U)\ , \tag{8.45}$$

which must be solved under conditions (8.37), (8.38) for $C^{(0)}$ (for ϵ-independent k_u, k_d).

Next, we show that, for given continuous $C^{\mathrm{eq}}(\overline{\sigma})$, the above boundary value problem for $C^{(0)}$ has at most one solution. We apply a standard energy method [24]; the same argument carries through for proving uniqueness of C^ϵ. First, by the transformation $C^{(0)} = \breve{C} e^{(1/2)\int_{\mathbf{r}_i}^{\mathbf{r}} \mathbf{v}\cdot \mathrm{d}\mathbf{r}'}$, PDE (8.45) is converted to the Helmholtz equation $\Delta_{\mathbf{r}} \breve{C} - \frac{1}{4}(|\mathbf{v}|^2 - 2\mathrm{div}\mathbf{v})\breve{C} = 0$ ($\mathbf{r} \in U$: terrace), where $\breve{C}$ obeys the Robin

[12] The use of the extra slow variable $\overline{\eta} = \epsilon\eta$, although formally justifiable, is not deemed necessary.

[13] This physical property is invoked in conjunction with the assumption that eliminating the curvature variation (as $\epsilon \downarrow 0$) results in a well-defined adatom density, as suggested by Section 8.2.

boundary condition $-\nu\cdot\nabla\breve{C} =: -\partial_\nu\breve{C} = K(\mathbf{r})\,\breve{C} - k(\mathbf{r})\,C^{\rm eq}\,e^{-(1/2)\int_{\mathbf{r}_i}^{\mathbf{r}}\mathbf{v}\cdot{\rm d}\mathbf{r}'}$ ($\mathbf{r}\in\partial U$); ν is the unit outward normal vector, $K(\mathbf{r}) := k(\mathbf{r}) - (1/2)\nu\cdot\mathbf{v}$, and $k(\mathbf{r}) = k_u$ for an up-step edge ($\eta = \eta_i$ where $\nu = -\mathbf{e}_\eta$) while $k(\mathbf{r}) = k_d$ for a down-step edge ($\eta = \eta_{i+1}$ where $\nu = \mathbf{e}_\eta$). Consider sufficiently small $|\mathbf{v}|$ so that $K(\mathbf{r}) > 0$, yet $|\mathbf{v}|^2 \geq 2{\rm div}\,\mathbf{v}$, consistent with the neglect of the term $({\rm div}\,\mathbf{v})C^\epsilon$ in the diffusion equation. Now suppose there exist two solutions, say $\breve{C}_1$ and $\breve{C}_2$, of the boundary problem for $C^{(0)}$, with $\varphi := \breve{C}_1 - \breve{C}_2$; this φ satisfies the given Helmholtz equation with boundary condition $-\partial_\nu\varphi = K\,\varphi$. Second, define the non-negative energy $\mathcal{E}[\varphi] = \frac{1}{2}\int_U |\nabla\varphi|^2 + \varpi^2\varphi^2$ where $\varpi^2 := (1/4)(|\mathbf{v}|^2 - 2{\rm div}\,\mathbf{v})$. By Green's identity, $\mathcal{E}[\varphi] = \int_{\partial U}(\nu\cdot\nabla\varphi)\varphi = -\int_{\partial U} K\,\varphi^2 \leq 0$; thus, $\varphi\equiv 0$ which entails $C_1\equiv C_2$.

Based on this uniqueness assertion, we construct solution (8.40)–(8.42). The $\overline{\sigma}$-dependence of $C^{\rm eq}$ in the boundary data suggests that we look for a $C^{(0)}(\mathbf{r})$ that depends on η and $\overline{\sigma}$ (but not σ). Such a $C^{(0)}(\mathbf{r})$, if it can be constructed plausibly, is interpreted as the leading-order, unique solution of the boundary value problem.

Hence, we solve (8.45) by dropping the σ-derivatives. Two successive integrations with respect to the variable η immediately yield

$$C^{(0)}(\eta,\overline{\sigma}) = B(\overline{\sigma}) + \hat{A}(\overline{\sigma})\int_{\eta_i}^{\eta}\exp\left\{-\int_{\eta_i}^{z}\left[\frac{\xi_{\eta'}}{\xi_\sigma}\,\partial_{\eta'}\left(\frac{\xi_\sigma}{\xi_{\eta'}}\right) - \frac{(v_\perp|_{\eta'})\xi_{\eta'}}{D}\right]{\rm d}\eta'\right\}{\rm d}z\,, \quad (8.46)$$

where $\hat{A}$ and B are integration constants. Equation (8.46) readily reduces to (8.40) by direct integration (in η') of the first term in the exponent and the subsequent substitution $A(\overline{\sigma}) := (\xi_\sigma/\xi_\eta)|_{\eta_i}\hat{A}(\overline{\sigma})$.

The coefficients $A(\overline{\sigma})$ and $B(\overline{\sigma})$ are determined through boundary conditions

(8.37), (8.38) with $\sigma = \sigma'$. Accordingly, we obtain the system

$$\begin{pmatrix} -\dfrac{D}{k_u \xi_\sigma|_{\eta_i}} & 1 + \dfrac{v_\perp|_{\eta_i}}{k_u} \\ \dfrac{D}{k_d \xi_\eta} \partial_\eta f|_{\eta_{i+1}} + \big(1 - v_\perp/k_d\big) f|_{\eta_{i+1}} & 1 - \dfrac{v_\perp|_{\eta_{i+1}}}{k_d} \end{pmatrix} \begin{pmatrix} A \\ B \end{pmatrix} = \begin{pmatrix} C_i^{\mathrm{eq}} \\ C_{i+1}^{\mathrm{eq}} \end{pmatrix} ,$$

where $f(\eta, \sigma)$ is defined by (8.43). Solving this system leads to (8.41) and (8.42).

□

Henceforth, we drop the dependence of $v_\perp = \mathbf{v} \cdot \mathbf{e}_\eta$ (and $v_\parallel = \mathbf{e}_\sigma \cdot \mathbf{v}$) on i, since $\mathbf{v}$ is considered macroscopic and $\mathbf{e}_\eta$, $\mathbf{e}_\sigma$ vary slowly with η. It can be verified that (8.40) reduces to the solutions for 1D settings of sections 8.2.1.1 and 8.2.2.1.

Remark 8.3.2. *Thus far, we invoked the condition* $|\mathbf{v}|/k_\ell < 2$ *(*$\ell = u, d$*). By definition* (8.1) *for* $\mathbf{v}$*, this restriction amounts to imposing*

$$\frac{|\mathbf{v}|}{2k_\ell} = \frac{D}{2k_\ell a} \frac{|Z^* e|\,|\mathbf{E}| a}{T} < 1 , \qquad \ell = u, d .$$

In typical experimental situations, $D/(2k_\ell a)$ *is of the order of* 10^2 *or smaller* [43]*,* $|e\mathbf{E}|a/T$ *is of the order of* 10^{-5}*, and for semiconductors* $|Z^*|$ *ranges from* 10^{-4} *(or even smaller values) to about* 10 [15, 28]*. Hence,* $|\mathbf{v}|/k_\ell$ *would not exceed values of the order of* 10^{-2}*.*

From the perspective of perturbation theory adopted here, $D/(k_\ell a)$ *is treated as an* $\mathcal{O}(1)$ *quantity whereas* $|\mathbf{v}|/k_\ell$ *will be considered as* $o(1)$ *(see Proposition* 8.4.1*) when* $a \downarrow 0$*. This view furnishes the distinct physical contribution of drift in the large-scale surface flux. Practically, setting* $|\mathbf{v}| \ll k_\ell$ *seems to more closely describe semiconductor surfaces, where* $|Z^*|$ *can be much smaller than unity* [28]*. Mathematically, this view is a choice for obtaining the distinguished-limit contribution of* $\mathbf{v}$ *as* $a \downarrow 0$*.*

In Section 8.4.1 we impose $|\mathbf{v}|/k_l \ll 1$; as a result, Fick's law for the large-scale flux does not distinguish between up- and down-step edges, being symmetric in k_u and k_d.

8.4 Evolution equations at the macroscale

In this section we find the evolution equations for the macroscale height in the presence of an electric field. The modification of Fick's law (8.36) at the nanoscale leads to a convective term in the constitutive relation between the macroscale flux and chemical potential, as we show in Proposition 8.4.1. Unchanged from Chapters 5,6, and 7 are the mass conservation law and the formula for the macroscale chemical potential.

The law of mass conservation, in the absence of edge atom diffusion and material deposition from above, reads

$$\partial_t h + \Omega \, \mathrm{div} \mathbf{J} = 0 \; ; \tag{8.47}$$

see (5.44).

The macroscale chemical potential μ is regarded as a smooth interpolation, through a suitable Taylor expansion, of the microscale step chemical potential μ_i. The presence of an electric field is not expected to change the surface energy due to steps, which experience the same line tensions and repulsive interactions as in the case of zero electric field. We adopt the formula from Chapter 5, which reads

$$\mu = -\Omega \, \mathrm{div} \left\{ \partial_m [m(g_1 + g_3 \, m^2)] \frac{\nabla h}{|\nabla h|} \right\} \; , \quad m := |\nabla h| \; . \tag{8.48}$$

8.4.1 Macroscopic Fick's law with drift

In this section, we derive the constitutive relation between macroscale flux and chemical potential in full 2D. The restrictions to 1D geometries then follow as special cases. We choose units where the macroscopic length λ is unity ($\lambda = 1$) for convenience.

Proposition 8.4.1. *Suppose that in the macroscopic limit, $a \downarrow 0$, the step density $m_i = a/(\xi_\eta \delta\eta_i)$ and the kinetic parameters $D/(k_l a)$ are $\mathcal{O}(1)$ while $v/k_l = o(1)$, where $l = u$, d and $\delta\eta_i := \eta_{i+1} - \eta_i$. Then, the solution to diffusion equation* (8.39)*, under boundary conditions* (8.37)*,* (8.38)*, gives rise to the macroscale constitutive relation*

$$\mathbf{J} = \begin{pmatrix} J_\perp \\ \\ J_\parallel \end{pmatrix} = -C_s \mathbf{M} \cdot \left[\nabla\mu - \frac{T}{D}\,\mathbf{v}\left(1 + \frac{\mu}{T}\right)\right] \qquad \left(\mathbf{v} = \frac{D\,Z^* e\,\mathbf{E}}{T}\right) \ , \tag{8.49}$$

*where the (**E**-independent) mobility* $\mathbf{M}$ *(with units of length* ^{2}*/energy/time) is a second-rank tensor. In the coordinate system (η, σ), this* $\mathbf{M}$ *has the familiar representation of Chapter 5, namely,*

$$\mathbf{M} = \frac{D}{T}\,\frac{1}{1 + q|\nabla h|} \begin{pmatrix} 1 & 0 \\ \\ 0 & 1 + q|\nabla h| \end{pmatrix} \ , \qquad q := \frac{2D}{ka} \ , \quad k := \frac{2}{k_u^{-1} + k_d^{-1}} \ . \tag{8.50}$$

Proof. The starting point is the solution $C_i^{(0)}$ derived in Proposition 8.3.1; see (8.40). We drop the superscript (denoting perturbation order) in $C_i^{(0)}$ for ease of notation. The microscale adatom flux components are obtained by the formulas

$$J_{i,\parallel} = -D\xi_\sigma^{-1}\partial_\sigma C_i + v_\parallel C_i \ ,$$

$$J_{i,\perp} = -D\xi_\eta^{-1}\partial_\eta C_i + v_\perp C_i \ .$$

The plan is to consider the restrictions of these components to $\eta = \eta_i$, and view these restrictions as interpolations of (continuous) smooth functions, $J_\perp(\mathbf{r}, t)$ and $J_\parallel(\mathbf{r}, t)$.

First, we compute the requisite derivatives of C_i by (8.40):

$$\partial_\sigma C_i \sim \partial_\sigma B_i + \partial_\sigma A_i \int_{\eta_i}^{\eta} \frac{\xi_\eta|_z}{\xi_\sigma|_z} \exp\left[\int_{\eta_i}^{z} \frac{\xi_{\eta'}\, v_\perp|_{\eta'}}{D}\, \mathrm{d}\eta'\right] \mathrm{d}z \ ,$$

$$\partial_\eta C_i = A_i \frac{\xi_\eta}{\xi_\sigma} \exp\left[\int_{\eta_i}^{\eta} \frac{\xi_{\eta'}(v_\perp|_{\eta'})}{D}\, \mathrm{d}\eta'\right] \ .$$

It follows that

$$J_{i,\parallel} = -D\xi_\sigma^{-1}\partial_\sigma B_i + v_\parallel B_i \ , \tag{8.51}$$

$$J_{i,\perp} = -D\xi_\sigma^{-1} A_i + v_\perp B_i \qquad \eta = \eta_i \ . \tag{8.52}$$

Consider (8.41), (8.42) (in Proposition 8.3.1) for A_i, B_i. In the limit $a \downarrow 0$, or $\delta\eta_i \downarrow 0$ with $\xi_\eta \delta\eta_i = \mathcal{O}(a)$, these formulas simplify via the expansion $\int_{\eta_i}^{\eta_{i+1}} F(\eta)\, \mathrm{d}\eta = F(\eta_i)\, \delta\eta_i + o(\delta\eta_i)$, where $F(\eta)$ is any continuous function. After some algebra and neglect of $o(\delta\eta_i)$ terms, (8.51) and (8.52) become

$$J_{i,\parallel}|_{\eta_i} \sim \frac{v_\parallel\left[\dfrac{D}{\xi_\eta\delta\eta_i}\left(\dfrac{C_i^{\mathrm{eq}}}{k_d} + \dfrac{C_{i+1}^{\mathrm{eq}}}{k_u}\right) + C_i^{\mathrm{eq}}\right] - D\left[\partial_\parallel C_i^{\mathrm{eq}} + \dfrac{D}{\xi_\eta\delta\eta_i}\left(\dfrac{\partial_\parallel C_i^{\mathrm{eq}}}{k_d} + \dfrac{\partial_\parallel C_{i+1}^{\mathrm{eq}}}{k_u}\right)\right]}{\dfrac{D}{\xi_\eta\delta\eta_i}\left(\dfrac{1}{k_u} + \dfrac{1}{k_d}\right) + \left(1 + \dfrac{v_\perp}{k_u}\right)} \ , \tag{8.53}$$

$$J_{i,\perp}|_{\eta_i} \sim \frac{\dfrac{D}{\xi_\eta\delta\eta_i}(C_i^{\mathrm{eq}} - C_{i+1}^{\mathrm{eq}}) + v_\perp C_i^{\mathrm{eq}}}{\dfrac{D}{\xi_\eta\delta\eta_i}\left(\dfrac{1}{k_u} + \dfrac{1}{k_d}\right) + \left(1 + \dfrac{v_\perp}{k_u}\right)} \qquad \text{as } \delta\eta_i \downarrow 0 \ ; \quad \partial_\parallel := \xi_\sigma^{-1}\partial_\sigma \ . \tag{8.54}$$

In the above, all variables are evaluated at (the same) σ along the ith step edge.

We seek further simplification of (8.53) and (8.54). In the macroscopic limit, we invoke the (assumed as well defined) C^1 function $C^{\mathrm{eq}}(\mathbf{r})$ where $C^{\mathrm{eq}}(\mathbf{r})|_{\eta_i} \equiv C_i^{\mathrm{eq}}$,

$C^{\rm eq}_{i+1} \equiv C^{\rm eq}(\mathbf{r})|_{\eta_i} + (\partial_\eta C^{\rm eq})|_{\eta_i}\delta\eta_i + o(\delta\eta_i)$ and $\partial_\parallel C^{\rm eq}|_{\eta_i} \equiv \partial_\parallel C^{\rm eq}_i = \partial_\parallel C^{\rm eq}_{i+1} + O(\delta\eta_i)$. We keep only those combinations of microscopic parameters that remain $O(1)$. For example, the step density $m_i = a/(\xi_\eta\delta\eta_i)$ approaches the positive surface slope, i.e., $\lim_{a\downarrow 0} m_i = |\nabla h|$. On the other hand, the ratio $v_\perp/k_u$, involved in the denominator of $J_{i,\parallel}$ and $J_{i,\perp}$, is treated as negligibly small (compared to unity) by virtue of our hypothesis; see also Remark 8.3.2.

Without further ado, we make the substitutions $C^{\rm eq}_{i+1} - C^{\rm eq}_i = (\partial_\perp C^{\rm eq})\,\xi_\eta\delta\eta_i + o(\delta\eta_i)$ and $C^{\rm eq} \sim C_s(1+\mu/T)$ ($|\mu| \ll T$), where $\partial_\perp := \xi_\eta^{-1}\partial_\eta$. The resulting limits for the flux components read

$$\lim_{a\downarrow 0} J_{i,\parallel}|_{\eta_i} =: J_\parallel(\mathbf{r})|_{\eta_i} = -\frac{C_s D}{T}\,\partial_\parallel\mu(\mathbf{r}) + C_s v_\parallel\left[1 + \frac{\mu(\mathbf{r})}{T}\right]\,, \tag{8.55}$$

$$\lim_{a\downarrow 0} J_{i,\perp}|_{\eta_i} =: J_\perp(\mathbf{r})|_{\eta_i} = -\frac{C_s D}{T}\,\frac{\partial_\perp\mu - \dfrac{T}{D}\,v_\perp\left(1+\dfrac{\mu}{T}\right)}{1+q|\nabla h|} \qquad \eta = \eta_i\ . \tag{8.56}$$

These relations are identified with (8.49) under definition (8.50) for the mobility $\mathbf{M}$.

□

It can be verified directly that the same limits emerge if the evaluation point of fluxes is at $\eta = \eta_{i+1}$ [66]. Two remarks on the results of Proposition 8.4.1 are in order.

Remark 8.4.2. *In the absence of electromigration ($\mathbf{v} = 0$), we recover the relation $\mathbf{J} = -C_s\mathbf{M}\cdot\nabla\mu$ of Chapter 5. For nonzero drift ($\mathbf{v} \neq 0$), the additional term derived above is affine with μ. This new relation is recast to the zero-drift form via an exponential transformation of μ; see Section* 8.4.3.

Remark 8.4.3. *An alternate proof of Proposition* 8.4.1 *makes direct use of the*

adatom concentration, C_i, and the normal flux component, $J_{i,\perp}$, avoiding entirely the use of integration constants A_i and B_i. This approach treats boundary conditions (8.37), (8.38) *for $\sigma' = \sigma$ as a system of equations for $C_i(\eta_i)$ and $J_{i,\perp}(\eta_i)$. This argument is also applicable to situations where the boundary conditions couple densities of different terraces, e.g., in the case with step permeability (see Chapter 7).*

By Proposition 8.4.1, we state the following corollary for cases of symmetry.

Corollary 8.4.4. *Consider 1D settings with $\mathbf{v} \neq 0$, where translational or rotational symmetry causes all dependent variables to have zero σ-derivatives. The macroscopic surface flux corresponding to* (8.49) *is*

$$\mathbf{J} = J(\chi)e_\chi \ , \quad J(\chi) = -\frac{C_s D}{T}\,\frac{\partial_\chi \mu}{1+q|\partial_\chi h|} + \frac{C_s v}{1+q|\partial_\chi h|}\left(1+\frac{\mu}{T}\right) \ , \tag{8.57}$$

where $\chi = x$ for straight steps and $\chi = r$ for concentric circular steps; $q = 2D/(ka)$.

Recall that, in the microscale model underlying the limit of this section, the contribution $(\operatorname{div}\mathbf{v})C_i$ is left out from the terrace diffusion equation (see Section 8.2.2). For a discussion on a correction to the macroscopic limit, see Remark 8.5.4.

8.4.2 Evolution equation in Cartesian system

In this section, we describe the PDE for the surface height by combining ingredients (8.47) and (8.48)–(8.50) and making use of Cartesian coordinates, (x, y).

First, we recall the non-singular orthogonal matrix $\mathbf{S}$, Eq. (5.26).

$$\mathbf{S}(\partial_x h, \partial_y h) = (\mathbf{e}_\eta \ \mathbf{e}_\sigma) = \frac{1}{|\nabla h|}\begin{pmatrix} -\partial_x h & \partial_y h \\ -\partial_y h & -\partial_x h \end{pmatrix} \qquad (\nabla h \neq 0) \ . \tag{8.58}$$

The mobility tensor $\mathbf{M}$, which is defined by (8.49) in the (η, σ) coordinate system, is now expressed in the Cartesian coordinate system (x, y) by

$$\mathbf{M}_{(x,y)} = S\,\mathbf{M}_{(\eta,\sigma)}\,S^T\ ; \tag{8.59}$$

as usual, S^T denotes the transpose of S ($S^T = S^{-1}$). The Cartesian components of the surface flux (8.49) read (e_ℓ: orthonormal vectors, $\ell = x,\ y$):

$$\begin{aligned} J_x = &-\frac{C_s}{1+q|\nabla h|}\left\{\frac{D}{T}\left[\left(1+q\,\frac{(\partial_y h)^2}{|\nabla h|}\right)\partial_x\mu - q\,\frac{(\partial_x h)(\partial_y h)}{|\nabla h|}\partial_y\mu\right]\right. \\ &\left. -\left(1+\frac{\mu}{T}\right)\left[\left(1+q\,\frac{(\partial_y h)^2}{|\nabla h|}\right)v_x - q\,\frac{(\partial_x h)(\partial_y h)}{|\nabla h|}\,v_y\right]\right\}\ , \end{aligned} \tag{8.60}$$

$$\begin{aligned} J_y = &-\frac{C_s}{1+q|\nabla h|}\left\{\frac{D}{T}\left[\left(1+q\frac{(\partial_x h)^2}{|\nabla h|}\right)\partial_y\mu - q\frac{(\partial_x h)(\partial_y h)}{|\nabla h|}\partial_x\mu\right]\right. \\ &\left. -\left(1+\frac{\mu}{T}\right)\left[\left(1+q\,\frac{(\partial_x h)^2}{|\nabla h|}\right)v_y - q\,\frac{(\partial_y h)(\partial_x h)}{|\nabla h|}\,v_x\right]\right\}\ ;\ v_\ell = e_\ell\cdot\mathbf{v}\quad(\ell = x,\ y)\ . \end{aligned} \tag{8.61}$$

The PDE for the surface height follows from the mass conservation statement. Using the Cartesian representation of (8.47), we have

$$\partial_t h = -\Omega(\partial_x J_x + \partial_y J_y)\ . \tag{8.62}$$

This relation leads to a nonlinear, fourth-order parabolic PDE for h after substitution for J_x, J_y, and μ from (8.60), (8.61), and (8.48).

8.4.3 Change of variables

We show that law (8.49) is recast to the form

$$\mathbf{J} = -c\,\mathbb{M}\cdot\nabla\vartheta \qquad (c = \text{const.})\ , \tag{8.63}$$

leading to the PDE

$$\partial_{\tilde{t}}\tilde{h} = \operatorname{div}_\alpha[\mathbb{M}\cdot\nabla_\alpha\vartheta] \ , \tag{8.64}$$

with suitable choices of the tensor $\mathbb{M}$ and variable $\vartheta[\tilde{\mu}]$, the transformed chemical potential; the dimensionless variables $\tilde{t}$, $\tilde{h}$, $\tilde{\mu}$ and operators $\operatorname{div}_\alpha$, ∇_α are defined in Appendix B.

Constitutive relation (8.49) for the surface flux reads

$$\mathbf{J} = -\frac{C_s D}{\lambda_x}\,\widetilde{\mathbf{M}}\cdot[\nabla_\alpha\tilde{\mu} - \mathbf{u}(1+\tilde{\mu})] \ , \tag{8.65}$$

where the dimensionless mobility $\widetilde{\mathbf{M}}$ – in the (x,y) representation – and drift velocity $\mathbf{u}$ are defined by

$$\widetilde{\mathbf{M}}_{(x,y)} := \widetilde{\mathbf{S}}\cdot\begin{pmatrix} \dfrac{1}{1+\tilde{q}\,|\nabla_\alpha\tilde{h}|} & 0 \\ 0 & 1 \end{pmatrix}\cdot\widetilde{\mathbf{S}}^T \ , \ \mathbf{u} := \frac{\lambda_x}{D}\,\mathbf{v} \ ; \quad \tilde{q} := \frac{qh_0}{\lambda_x} \ . \tag{8.66}$$

The corresponding change-of-basis matrix, $\widetilde{\mathbf{S}}$, is $\widetilde{\mathbf{S}} \equiv \mathbf{S}(\partial_{\tilde{x}}\tilde{h}, \alpha\partial_{\tilde{y}}\tilde{h})$; cf. (8.58).

Consequently, the PDE for the nondimensional height, $\tilde{h}$, reads

$$\partial_{\tilde{t}}\tilde{h} = \operatorname{div}_\alpha\{\widetilde{\mathbf{M}}\cdot[\nabla_\alpha\tilde{\mu} - \mathbf{u}(1+\tilde{\mu})]\} \ . \tag{8.67}$$

Next, we show (8.63) and (8.64). By inspection, we start with the transformation

$$\vartheta = (1+\tilde{\mu})\,f^\vartheta \ , \tag{8.68}$$

where the (nonzero) $f^\vartheta = f^\vartheta(\tilde{x},\tilde{y})$ is to be determined. By virtue of $\mathbb{M}\cdot\nabla_\alpha\vartheta = (\mathbb{M}f^\vartheta)\cdot[\nabla_\alpha\tilde{\mu} + (\nabla_\alpha f^\vartheta/f^\vartheta)(1+\tilde{\mu})]$ and (8.65), we have the consistency relations

$$\mathbb{M}\,f^\vartheta = \widetilde{\mathbf{M}} \ , \qquad (\nabla_\alpha f^\vartheta)/f^\vartheta = -\mathbf{u} \ ,$$

the second one of which yields

$$f^{\vartheta}(\tilde{x},\tilde{y}) = A\, e^{-\mathbf{u}\cdot(\tilde{x},\tilde{y}/\alpha)} \;\Rightarrow\; \mathbb{M} = A^{-1}\widetilde{\mathbf{M}}(\nabla_\alpha \tilde{h})\, e^{\mathbf{u}\cdot(\tilde{x},\tilde{y}/\alpha)} \;, \quad A = \text{const.} \neq 0 \;. \tag{8.69}$$

Relations (8.63), (8.64) ensue. For definiteness, take $A = 1$.

The transformed chemical potential ϑ and mobility $\mathbb{M}$ are

$$\vartheta(\tilde{x},\tilde{y}) = \left\{1 - \tilde{\mu}_0 \,\mathrm{div}_\alpha\left[\tilde{g}\,\frac{\nabla_\alpha \tilde{h}}{|\nabla_\alpha \tilde{h}|} + |\nabla_\alpha \tilde{h}|\,\nabla_\alpha \tilde{h}\right]\right\} e^{-(u_x\tilde{x}+u_y\tilde{y}/\alpha)} \;, \tag{8.70}$$

$$\mathbb{M}_{(x,y)} = e^{u_x\tilde{x}+u_y\tilde{y}/\alpha}\widetilde{\mathbf{S}}\cdot\widetilde{\mathbf{M}}\cdot\widetilde{\mathbf{S}}^T = e^{u_x\tilde{x}+u_y\tilde{y}/\alpha}\,\widetilde{\mathbf{S}}\cdot\begin{pmatrix} \dfrac{1}{1+\tilde{q}\,|\nabla_\alpha \tilde{h}|} & 0 \\ 0 & 1 \end{pmatrix}\cdot\widetilde{\mathbf{S}}^T \;. \tag{8.71}$$

The finite element scheme introduced in Chapter 2 can easily accommodate the transformed chemical potential and mobility. The change-of-variables is not deemed likely to introduce numerical instability if the grid Peclet number $P_e = |\mathbf{v}|\Delta x/D$ is much less than 1 [77].[14] For easier readability of the code, however, we opted to include the convective term directly when simulating the macroscopic effect of an electric field. A thorough comparison of the two methods is still lacking.

8.5 Extensions of macroscopic limit

In an attempt to formulate a reasonably general theory of macroscopic surface relaxation, we enrich the BCF model with additional microscale effects. These are: (i) the exponential law $C_i^{\mathrm{eq}} = C_s \exp(\mu_i/T)$ in the place of its linearization, and (ii) atom desorption. Our broader goal with these extensions is to reconcile the macroscopic theory with realistic situations where an electric field is present.

[14] P_e compares the relative importance of convection to diffusion; Δx : mesh size.

We show that (i) can modify significantly the constitutive relation between surface flux and chemical potential. In contrast, effect (ii) arguably has vanishingly small influence on the macroscopic evolution law.

8.5.1 Exponential law for step chemical potential

To derive the constitutive relation between large-scale flux and chemical potential, we approximated the difference of equilibrium concentrations $C_i^{\rm eq}$ by use of the linearized form (8.6). The quantitative justification for this approximation is not clear in the literature, particularly since the chemical potential μ_i is not measured directly. However, the PDE is easily modified to accommodate the complete, exponential law. For a similar modification in 1+1 dimensions with $v = 0$ and long-range step interactions, see [123].

By skipping details irrelevant to the modification at hand, we start from (8.54). By setting $\mu_i = \mu(\mathbf{r})|_{\eta_i}$ we expand the difference $C_{i+1}^{\rm eq} - C_i^{\rm eq}$ as follows:

$$\begin{aligned} C_{i+1}^{\rm eq} - C_i^{\rm eq} &= C_s \left[\exp\left(\frac{\mu_{i+1}}{T}\right) - \exp\left(\frac{\mu_i}{T}\right) \right] \\ &= \frac{aC_s}{|\nabla h|} \exp\left(\frac{\mu(\check{\eta})}{T}\right) \frac{\partial_\perp \mu(\check{\eta})}{T} , \qquad \check{\eta} \in [\eta_i, \eta_{i+1}] . \end{aligned}$$

Hence, the normal flux component $J_{i,\perp}$ at (η_i, σ) becomes

$$J_{i,\perp}|_{\eta_i} = \frac{-\dfrac{D}{\xi_\eta \delta\eta_i} \dfrac{aC_s}{|\nabla h|} \exp\left(\dfrac{\mu(\check{\eta})}{T}\right) \dfrac{\partial_\perp \mu(\check{\eta})}{T} + v_\perp C_s \exp\left(\dfrac{\mu(\eta_i)}{T}\right)}{\dfrac{D}{\xi_\eta \delta\eta_i}\left(\dfrac{1}{k_u} + \dfrac{1}{k_d}\right) + \left(1 + \dfrac{v_\perp}{k_u}\right)} . \tag{8.72}$$

Similarly, the σ-derivative of $C_i^{\rm eq}$ appearing in (8.53) for the longitudinal flux com-

ponent, $J_{i,\parallel}$, now acquires exponential factors when expressed in terms of μ_i :

$$J_{i,\parallel}|_i = \left[-\frac{D}{\xi_\eta \delta\eta_i}\left(\frac{1}{k_u}+\frac{1}{k_d}\right)-1\right]^{-1}\left\{-\frac{C_s D}{\xi_\eta \delta\eta_i} v_\parallel \left[\frac{1}{k_d}\exp\left(\frac{\mu_i}{T}\right)\right.\right.$$
$$\left. + \frac{1}{k_u}\exp\left(\frac{\mu_{i+1}}{T}\right)\right] - v_\parallel C_s \exp\left(\frac{\mu_i}{T}\right) + C_s D \exp\left(\frac{\mu_i}{T}\right)\frac{\partial_\parallel \mu_i}{T}$$
$$\left. + \frac{D^2 C_s}{k_d \xi_\eta \delta\eta_i}\exp\left(\frac{\mu_i}{T}\right)\frac{\partial_\parallel \mu_i}{T} + \frac{D^2 C_s}{k_u \xi_\eta \delta\eta_i}\exp\left(\frac{\mu_{i+1}}{T}\right)\frac{\partial_\parallel \mu_{i+1}}{T}\right\} . \quad (8.73)$$

The coarse-graining procedure carries through as in Proposition 8.4.1. The components of the flux $\mathbf{J}(\mathbf{r})$ are found to satisfy the equations

$$J_\perp(\mathbf{r})\left(\frac{2}{k}+\frac{a}{D|\nabla h|}\right) = \exp\left[\frac{\mu(\mathbf{r})}{T}\right]\left\{-\frac{aC_s}{|\nabla h|}\frac{\partial_\perp \mu(\mathbf{r})}{T} + v_\perp \frac{aC_s}{D|\nabla h|}\right\} , \quad (8.74)$$

$$C_s \exp\left[\frac{\mu(\mathbf{r})}{T}\right]\frac{\partial_\parallel \mu(\mathbf{r})}{T} = -\frac{1}{D}\left\{J_\parallel(\mathbf{r}) - v_\parallel C_s \exp\left[\frac{\mu(\mathbf{r})}{T}\right]\right\} . \quad (8.75)$$

The last two equations result in the effective constitutive relation

$$\mathbf{J} = -C_s\, e^{\mu/T}\mathbf{M}\cdot\left(\nabla\mu - \frac{T}{D}\,\mathbf{v}\right) . \quad (8.76)$$

By inspection of (8.76), we have the following remark:

Remark 8.5.1. *The modified constitutive relation for the macroscopic surface flux results from the invariant under the law* $C^{\mathrm{eq}} = C^{\mathrm{eq}}[\mu]$ *form* (8.64) *and the definition*

$$\vartheta(\mathbf{r}) := e^{\mu(\mathbf{r})/T - \mathbf{v}\cdot\mathbf{r}/D} , \quad (8.77)$$

which is a direct extension of the linearized version, (8.68) *or* (8.70)*.*

8.5.2 Adatom desorption

The effect of desorption is expected to affect only the relation between the large-scale surface flux and chemical potential. In this section, we show that, under

certain conditions, desorption does not appear in the macroscopic laws to leading order in a.

8.5.2.1 Solution for microscale diffusion

Following the rationale of slow and fast step variables of section 8.3.3, we write the (quasi-steady) diffusion equation on the ith terrace with desorption time τ and a drift velocity $\mathbf{v}$ ($v_\perp = \mathbf{e}_\eta \cdot \mathbf{v}$) as

$$\partial_\eta \left(\frac{\xi_\sigma}{\xi_\eta} \partial_\eta C_i \right) - \frac{v_\perp \xi_\sigma}{D} \partial_\eta C_i \sim \frac{\xi_\eta \xi_\sigma}{\tau D} C_i \qquad (\eta_i < \eta < \eta_{i+1}) \ . \tag{8.78}$$

A first observation is that, for $v_\perp \neq 0$ and $\tau \neq \infty$, this equation does not admit a relatively simple solution, i.e., in terms of elementary functions. (The radial case of Section 8.2.2 certainly alludes to the same conclusion.)

It is of interest to note that there are at least two ways of solving (8.78). First, it can be converted to a canonical ordinary differential equation (ODE) solvable by confluent hypergeometric functions [18]. This route is not particularly informative. Alternatively, (8.78) can be recast to a Volterra integral equation, which can be solved by iterations through a (convergent) Born-Neumann series [116].

We now focus on the (simpler) integral-equation formulation for (8.78).[15]

Proposition 8.5.2. *Suppose C_i is a solution of the PDE* (8.78)*. Then, C_i satisfies the following Volterra equation on $\eta_i < \eta < \eta_{i+1}$:*

$$C_i(\eta, \sigma) = [B_i(\sigma) + A_i(\sigma) f_i(\eta, \sigma)] + [u_{i,1}(\eta, \sigma) + u_{i,2}(\eta, \sigma)\, f_i(\eta, \sigma)] \ , \tag{8.79}$$

[15] For notational simplicity, we use σ in the place of the slow variable $\overline{\sigma}$.

where

$$u_{i,1}(\eta,\sigma) = u_{i,1}[C_i] = -(\tau D)^{-1}\int_{\eta_i}^{\eta} \frac{f_i(\eta',\sigma)\xi_{\eta'}^2 C_i(\eta',\sigma)}{\mathcal{W}(\eta')}\, d\eta' \,, \tag{8.80}$$

$$u_{i,2}(\eta,\sigma) = u_{i,2}[C_i] = (\tau D)^{-1}\int_{\eta_i}^{\eta} \frac{\xi_{\eta'}^2\, C_i(\eta',\sigma)}{\mathcal{W}(\eta')}\, d\eta' \,, \tag{8.81}$$

$$\mathcal{W}(\eta) = \partial_\eta f_i = \frac{\xi_\eta}{\xi_\sigma}\, \exp\left[D^{-1}\int_{\eta_i}^{\eta} \xi_{\eta'}\,(v_\perp|_{\eta'})\, d\eta'\right] \,, \tag{8.82}$$

$f_i(\eta,\sigma)$ is defined by (8.43)*, and the coefficients $A_i(\sigma)$ and $B_i(\sigma)$ are determined through boundary conditions* (8.37)*,* (8.38) *for atom attachment-detachment at $\eta = \eta_i, \eta_{i+1}$. Note that $\mathcal{W}(\eta)$ is the Wronskian of the two homogeneous (for $\tau = \infty$) solutions of ODE* (8.78)*, namely, the functions 1 and $f_i(\eta,\cdot)$.*

Proof. We provide a sketch of the proof since this relies on standard techniques for linear ODEs and PDEs. Consider the (τ-dependent) term in the right hand side of (8.78) as a forcing. Apply Duhamel's principle (or the method of "variation of parameters") to construct a particular solution of the ODE. This approach yields C_i as a sum of: (i) a linear combination of the two homogeneous solutions, 1 and f_i; and (ii) a τ^{-1}-scaled particular solution, which involves two distinct integrals of C_i/τ (one for each homogeneous solution). The coefficients A_i and B_i in the aforementioned linear combination are determined via enforcement of the boundary conditions. □

The integral equation (8.79) can be solved by the conventional iteration (Born-Neumann) scheme [116]: First, set $C_i = 0$ under the integral (in $u_{i,1}$ and $u_{i,2}$) and obtain $C_i \sim B_i + A_i f_i$; second, replace C_i by $B_i + A_i f_i$ under the integral; next, repeat successively with the updated C_i. Because the kernel is L^2 and smooth, the

series generated by iterations converges to the solution C_i for all $\tau > 0$, and yields a sufficiently smooth C_i. Since the kernel is proportional to τ^{-1}, the procedure yields a power series in $1/\tau$, whose convergence rapidity is thus enhanced by increasing τ.

The value of the Born-Neumann scheme becomes evident for $\eta - \eta_i \ll 1$. Since $\int_{\eta_i}^{\eta} F(\eta')\,\mathrm{d}\eta' = F(\eta_i)\,(\eta - \eta_i) + o(\eta - \eta_i)$ for any continuous F, the associated iterated integrals contribute respective ascending powers of $\eta - \eta_i$. So, evidently, in the limit $\max_i \delta\eta_i = \max_i\{\eta_{i+1} - \eta_i\} \downarrow 0$, constructing a solution to (8.79) via a Born-Neumann series corresponds to producing a Taylor series in $\eta - \eta_i$ for $C_i(\eta, \sigma)$. This result is directly applicable to the macroscopic limit of the step system.

8.5.2.2 Limit $a \downarrow 0$

Next, we derive a macroscopic Fick's law with desorption and external electric field. We follow the main procedure of Proposition 8.4.1 by use of formula (8.79) (in Proposition 8.5.2) for C_i. Suppressing the σ dependence, we define

$$C_i^v(\eta) := B_i + A_i\, f_i(\eta)\ , \tag{8.83}$$

which is the solution *form* without desorption.[16] Thus, C_i satisfies

$$C_i(\eta) - C_i^v(\eta) = (\tau D)^{-1} \int_{\eta_i}^{\eta} \xi_{\eta'}^2\, \frac{f_i(\eta) - f_i(\eta')}{\partial_{\eta'} f_i}\, C_i(\eta')\ \mathrm{d}\eta'\ . \tag{8.84}$$

By differentiation of (8.84) with respect to η we obtain the normal flux component, $J_{i,\perp} = \mathbf{e}_\eta \cdot (-D\nabla C_i + \mathbf{v} C_i)$:

$$J_{i,\perp} - J_{i,\perp}^v = -\frac{\partial_\perp f_i}{\tau} \int_{\eta_i}^{\eta} \frac{\xi_{\eta'}^2\, C_i(\eta')}{\partial_{\eta'} f_i}\ \mathrm{d}\eta' + \frac{v_\perp}{\tau D} \int_{\eta_i}^{\eta} \xi_{\eta'}^2\, \frac{f_i(\eta) - f_i(\eta')}{\partial_{\eta'} f_i}\, C_i(\eta')\ \mathrm{d}\eta'\ , \tag{8.85}$$

[16] A_i and B_i entering C_i^v in principle depend on τ via boundary conditions at step edges.

where $J^v_{i,\perp} := -D\partial_\perp C^v_i + v_\perp C^v_i$; recall that $\partial_\perp = \xi_\eta^{-1}\partial_\eta$.

Now consider the limit $\delta\eta := \eta - \eta_i \downarrow 0$. By Taylor expanding the right hand sides of (8.84) and (8.85), we readily obtain

$$C_i(\eta) - C^v_i(\eta) = (2D\tau)^{-1}\, C^v_i(\eta_i)\, \xi^2_{\eta_i}\, \delta\eta^2 + \mathcal{O}(\delta\eta^3)\ , \tag{8.86}$$

$$J_{i,\perp}(\eta) - J^v_{i,\perp}(\eta) = -\tau^{-1} C^v_i(\eta_i)\, \xi_{\eta_i}\, \delta\eta + \mathcal{O}(\delta\eta^2) \qquad \text{as } \delta\eta \downarrow 0\ . \tag{8.87}$$

Next, we apply conditions (8.37) and (8.38) for $\sigma' = \sigma$. With recourse to $C^v_i(\eta_{i+1}) = C^v_i(\eta_i) + (\partial_\eta C^v_i)|_{\eta_i}\delta\eta_i + o(\delta\eta_i)$, and likewise for $J_{i,\perp}(\eta_{i+1})$, we find

$$-k_u^{-1}\, J^v_{i,\perp} = C^v_i - C^{\mathrm{eq}}_i\ , \tag{8.88}$$

$$\begin{aligned} k_d^{-1}\left[\left(1 + \frac{k_d}{D}\delta w_i\right) J^v_{i,\perp} + (\partial_\perp J^v_{i,\perp})\delta w_i\right] \\ \sim \left[1 + \left(\frac{v_\perp}{D} + \frac{1}{k_d\tau} + \frac{\delta w_i}{2D\tau}\right)\delta w_i\right] C^v_i - C^{\mathrm{eq}}_{i+1}\ , \end{aligned} \tag{8.89}$$

where $\delta w_i := \xi_{\eta_i}\,\delta\eta_i$, and C^v_i, $J^v_{i,\perp}$ and $\partial_\perp J^v_{i,\perp}$ are evaluated at η_i. Note that (8.88) does not involve τ explicitly. In contrast, (8.89) manifests desorption terms in the right hand side. If these, τ^{-1}-scaled, terms can be neglected appropriately, the resulting system becomes identical to that without desorption; the corresponding terms in C_i and $J_{i,\perp}$ can then be dropped.

Remark 8.5.3. *By inspection of the (attachment-detachment) boundary conditions* (8.88) *and* (8.89) *for the adatom flux and density, sufficient conditions for neglecting the desorption effect in the macroscopic limit* [*assuming* $k/k_\ell = \mathcal{O}(1)$, $\ell = u, d$] *are*

$$\frac{|\mathbf{v}|}{D} \gg \frac{1}{k\tau} \qquad \text{and} \quad \frac{a}{k\tau} \ll 1\ . \tag{8.90}$$

Then, the large-scale adatom flux is not affected by τ uniformly in space coordinates. Both of these conditions are expected to be met in a wide range of physical situations. In particular, the first condition amounts to having $|\mathbf{v}|\tau \gg a$ when $D/(ka) = \mathcal{O}(1)$. From the viewpoint of coarse graining and perturbation theory, formulas (8.90) *simply state that the effect of desorption is of higher order (in a).*

We conclude this section with the following observation.

Remark 8.5.4. *The (thus far neglected) term* $(\operatorname{div}\mathbf{v})C_i$ *in the terrace diffusion equation for the adatom density C_i can be treated on the same footing as the desorption term C_i/τ. Hence, in assessing the validity of dropping the former, it is reasonable to repeat the above procedure with τ^{-1} being replaced by* $\operatorname{div}\mathbf{v}$*, in an appropriate sense.*

8.6 Conclusions

Starting with the BCF model of step flow, we derived macroscopic evolution laws for the surface height in settings with an electric field. We considered microscopic processes of isotropic adatom diffusion on terraces, attachment and detachment of atoms at step edges with an Ehrlich-Schwoebel barrier, and desorption of atoms to the surrounding vapor. Energetic effects such as entropic and elastic dipole step interactions were included.

Our central contribution is Fick's law (8.49) relating surface flux $\mathbf{J}$, chemical potential μ, and drift velocity $\mathbf{v}$. The linear combination of μ and $\nabla\mu$ of this law is consolidated into a single variable, ϑ, by an exponential transformation. Accord-

ingly, the PDE for the macroscale height is recast to form (8.64), which has the same structure as the evolution law $\partial_t h = \Omega C_s \, \mathrm{div}\{\mathbf{M} \cdot \nabla \mu\}$ derived in the absence of an electric field. We showed that desorption is a higher-order effect in a sense dictated by multiscale expansions in the step height, a.

Many effects are absent from our analysis. For instance, time-dependent, coupled electromagnetic fields are not accounted for. In the same vein, the *control* of *evolving* surface morphologies by electric fields was barely touched upon. Our assumption of a slowly-varying step train restricts the validity of the PDE to regions where the steps do not experience drastic instabilities. We also leave out long-range step interactions, e.g., interactions mediated by bulk stress. We postpone until Chapter 9 a more thorough discussion of the appropriate boundary conditions for the derived PDE, and the effect of an electric field on the height profile near this boundary.

Chapter 9

Facets and boundary layers

In this chapter, we discuss analytical aspects of faceted relaxation of crystal surfaces. As we see in the next chapter, the results of applying the finite element method to the previously derived PDEs have been validated only in the limiting case $g_1/g_3 \ll 1$. For larger values of g_1/g_3, our numerical scheme is challenged by the appearance of facets, which expand during the surface relaxation. The variational approach on which our numerics are based still offers a possible connection with the physically realistic case of nonzero line tension. To see this connection, we turn to analytical methods, focusing on the local behavior of the height profile near a facet edge. We study how the slope far from the facet approaches continuously its boundary value ($|\nabla h| = 0$ at the facet edge), for different values of the material parameters and the electric field. This *local analysis* of this chapter complements the global analysis we used to derive decay rates for approximately separable PDE solutions, which are assumed to exist based on experimental observations and 1D step simulations. Our analysis is based on a conjecture (or ansatz) about the separability of space and time dependence of the slope profile, which entails a locally factorizable solution of the PDE.

9.1 Faceting on crystal surfaces

The presence of facets indicates clearly that a given surface orientation is below roughening, which is the context we assume when deriving a PDE for h from the motion of steps. However, strictly speaking the domain of this PDE does not include the facet itself, where the surface energy is singular due to the vanishing slope $|\nabla h|$.[1] We then face the problem of determining the appropriate boundary conditions at the facet edge. Analysis of the PDE and the boundary conditions near the facet edge provides insight into the local behavior of the slope profile. This analytically predicted behavior could be experimentally testable [115].

9.2 Formulation of faceted relaxation as a free-boundary problem

Spohn [109] first studied facet evolution as a free-boundary problem for nonlinear PDEs. Here, we summarize the main idea and extensions. The moving boundary is the facet edge, a curve we denote by $\mathbf{r}_{\rm f}(t) \in L_0(t)$. More precisely, for a train of descending steps in the vicinity of a facet with height $h_{\rm f}$ (Fig. 9.1), we identify the facet with the set $\{\mathbf{r} = (x, y) : h(x, y, t) = h_{\rm f}(t)\}$, and $\mathbf{r}_{\rm f}(t) \in L_0(t)$ is the boundary of this set. (Recall that L_i was used in Chapter 5 to denote the ith step edge. Although, strictly speaking, the facet edge does not correspond to the topmost step, we use L_0 for lack of a more suggestive notation.)

[1] The reason for this pathology is that step positions near the facet edge do *not* satisfy the usual assumptions of the macroscopic limit. Mathematically, the PDE can be extended on the facet by the "subgradient (subdifferential) formulation" [24], as outlined below.

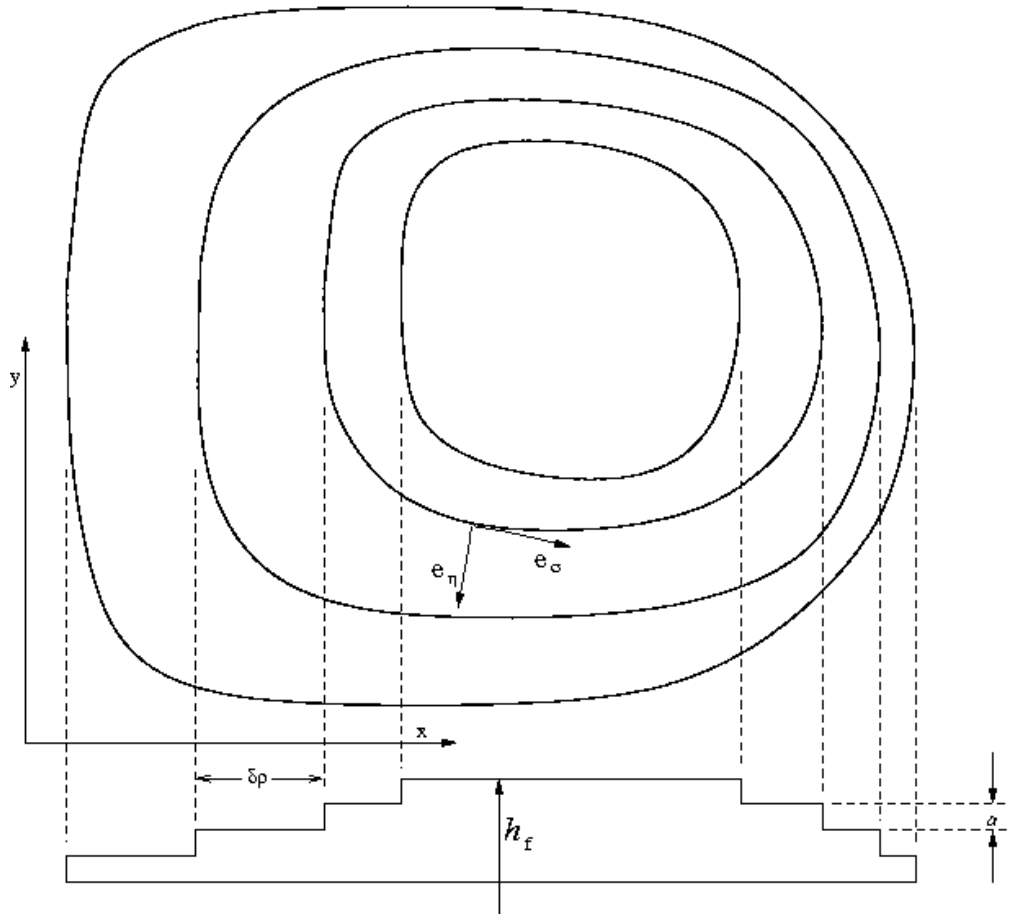

Figure 9.1: Orthogonal projection of a 2D step train in the vicinity of a facet.

The motion of the facet edge is found by imposing the requisite boundary conditions on the PDE solution. The slope profile at perpendicular distance $d_\perp$ from the facet edge has a (characteristic) $d_\perp^{1/2}$ behavior related to a Pokrovsky-Talopov phase transition, as predicted by Jayaprakash et al. [41, 42] for equilibrium crystal shapes. Margetis, Aziz and Stone [64] applied the free-boundary approach in an axisymmetric setting (circular steps) to determine how the width of a boundary layer near the facet edge scales with the ratio g_3/g_1 of step interaction strength to the step line tension, when $g_3/g_1 \ll 1$. In the case of straight steps, Odisharia used the free-boundary approach to establish the time decay of self-similar profiles [79]. Shenoy et al. applied nonlinear Galerkin schemes to incorporate facets into a variational formulation of surface relaxation [108].

9.3 Natural boundary conditions of the variational problem for periodic profiles

To investigate the effect of the free energy coefficients g_1 and g_3 on the observed slope profile near a facet, one must in principle write down the boundary conditions at the facet edge. A complete set of boundary conditions emerges "naturally" by considering the variational approach in more detail. We alert the reader that not all of the natural boundary conditions play a role in our subsequent local analysis. For the sake of completeness, we present the full set of natural boundary conditions, so that the numerical results of Chapter 10 with $g_1 \neq 0$ can be interpreted from the perspective of strong PDE solutions informed by conditions at

the free boundary. Not all of these boundary conditions are physically meaningful, but they possess the advantage of being enforced automatically by any numerical scheme based on the variational formulation. An "unphysical" condition is that the chemical potential extends continuously across the facet edge. In fact, this latter condition can be replaced by a boundary condition respecting the discrete sequence of collapse times for the top step [37]. *In this case, the resulting set of boundary conditions, while consistent with the microstructure of the crystal surface, unfortunately requires feedback from discrete step simulations to implement a numerical solution of the free-boundary problem.*

We now develop a brief argument for the natural boundary conditions arising from the variational formulation for evolution of a spatially periodic profile h. This approach follows closely the presentation of [79] in 1+1 dimensions. We restrict our attention to diffusion-limited kinetics, where the mobility $M = C_s D/(k_B T)$ is a scalar constant. To address ADL kinetics we would need to invoke the semi-implicit time stepping of Chapter 2, which yields a weighted H^{-1} inner product in the extended gradient (subgradient) formulation. By using the height profile at a previous time step in the evaluation of the tensor mobility $\mathbf{M}$, we determine explicitly the inner product through which the surface evolution is interpreted as a subgradient flow. This issue has been addressed in the doctoral dissertation by Odisharia [79].

The macroscale equations have the familiar structure of three key relations: (i) mass conservation, (ii) Fick's law for surface diffusion, and (iii) the equation for chemical potential in terms of slope. We restate these three ingredients under the

assumption of diffusion-limited kinetics.

$$\begin{aligned}\frac{\partial h}{\partial t} &= -\Omega\,\mathrm{div}\mathbf{J},\\ \mathbf{J} &= -\frac{C_s D}{k_B T}\nabla\mu,\\ \mu &= \Omega g_3 \frac{\delta\mathcal{E}}{\delta h} = \frac{\Omega g_3}{\lambda_x}\,\mathrm{div}_\alpha\mathbf{N},\end{aligned}$$

where div_α is the divergence operator with respect to nondimensional spatial variables[2], λ_x is a characteristic length in the basal plane, and $\mathcal{E} = \int \gamma(\nabla h)\mathrm{d}\mathbf{x}$ with $\gamma(\nabla h) = \frac{g_1}{g_3}|\nabla h| + \frac{1}{3}|\nabla h|^3$. To emphasize the importance of the *ratio* g_1/g_3, we choose to treat $\mathcal{E}$ and $\mathbf{N}$ as nondimensional; the chemical potential acquires the correct units through the prefactor $\Omega g_3/\lambda_x$. The auxiliary vector $\mathbf{N}$ is introduced to write the variation of $\mathcal{E}$ more explicitly: outside the facet the formula $\mathbf{N} = \frac{g_1}{g_3}\frac{\nabla h}{|\nabla h|} + |\nabla h|\nabla h$ holds. We take the height h to be a periodic function of the nondimensional spatial variables x, y, which entails

$$[0,1]\times[0,1]\times[0,\infty) \ni (x,y,t) \mapsto h(x,y,t) \in (-h_0-\varepsilon, h_0+\varepsilon);$$

see Appendix B.[3]

Because the surface energy density $\gamma(\nabla h)$ has a corner singularity at $\nabla h = 0$, we need to make use of a generalized notion of differentiation when combining the three ingredients of the macroscopic theory to incorporate facets. This generalization of a gradient flow begins with the definition of subgradient for a real-valued

[2]Following the notation of Appendix B; in the calculations below we drop the subscript α for the sake of readability.

[3]The range for h is chosen to accommodate the transient behavior in which the height slightly exceeds its initial amplitude $\max h(\cdot,\cdot,0) = h_0$ at the beginning of a relaxation experiment.

function on $\mathbb{R}^2$. Here we follow the presentation of Odisharia [79] to introduce the subgradient in the context of surface relaxation. We use $\langle \cdot, \cdot \rangle$ to denote the Euclidean inner product in the following

Definition 9.3.1. *The* subgradient *of* $\gamma : \mathbb{R}^2 \to \mathbb{R}$*, denoted* $\partial\gamma$*, is the set*

$$\partial\gamma = \{a \in \mathbb{R}^2 : \langle a, \delta \rangle \leq \gamma(\nabla h + \delta) - \gamma(\nabla h) \quad \forall \delta \in \mathbb{R}^2\}.$$

To illustrate this definition, we consider first the singular case $\nabla h = 0$. Then

$$\partial\gamma = \{a \in \mathbb{R}^2 : \langle a, \delta \rangle \leq \frac{g_1}{g_3}|\delta| + |\delta|^3/3\},$$

which is the ball of radius g_1/g_3 around 0.

In the smooth case ($\nabla h \neq 0$), we have

$$\partial\gamma = \{a \in \mathbb{R}^2 : \langle a, \delta \rangle \leq \frac{g_1}{g_3}|\nabla h + \delta| - \frac{g_1}{g_3}|\nabla h| + \frac{|\nabla h + \delta|^3}{3} - \frac{|\nabla h|^3}{3}\},$$

which reduces to the single element

$$a = \frac{g_1}{g_3}\frac{\nabla h}{|\nabla h|} + |\nabla h|\nabla h,$$

after expanding the norms in Taylor series about $\delta = 0$.

Evidently, the subgradient agrees with the usual notion of gradient when the free energy density is smooth enough. We note that the calculation of a subgradient depends on which inner product $\langle \cdot, \cdot \rangle$ is used in the definition. For the free energy density γ, the natural choice for $\langle \cdot, \cdot \rangle$ is the Euclidean inner product. For a *functional* such as $\mathcal{E}[\nabla h]$, we must use the inner product of the H^{-1} Sobolev space [24]. The essential property of the H^{-1} inner product is an identity that follows (formally)

from integration by parts:

$$\langle u, v\rangle_{H^{-1}} = -\langle \Delta^{-1} u, v\rangle_{L^2}, \tag{9.1}$$

where $\langle \cdot, \cdot \rangle_{L^2}$ denotes the usual inner product of square-integrable functions: $\langle f, g\rangle_{L^2} = \int_{[0,1]^2} fg \mathrm{d}A$. The idea of the H^{-1} inner product becomes more transparent by using the Fourier transform $\hat{u}$ of periodic u with zero mean.

The variation of $\mathcal{E}$ must be expressed using the language of subgradients so that the chemical potential μ can be defined in the case of facets. In this vein, we compute the subgradient of the functional $\mathcal{E}[h] = \int \gamma(\nabla h) \mathrm{d}\mathbf{x}$ with respect to the H^{-1} inner product. By definition,

$$u \in \partial_{H^{-1}} \mathcal{E} \Leftrightarrow \mathcal{E}[h + \delta] - \mathcal{E}[h] \geq \langle u, \delta\rangle_{H^{-1}} \quad \forall \delta. \tag{9.2}$$

Having at our disposal the calculation of $\partial\gamma(\nabla h)$ in both the smooth and the non-smooth cases, we let $\mathbf{N}(x, y) \in \partial\gamma(\nabla h)$ and consider $u = \Delta \operatorname{div}\mathbf{N}$.

For such $\mathbf{N}$ we have

$$\gamma(\nabla h + \nabla\delta) - \gamma(\nabla h) \geq \langle \mathbf{N}(x, y), \nabla\delta\rangle \tag{9.3}$$

pointwise, which can be integrated to obtain

$$\mathcal{E}[h + \delta] - \mathcal{E}[h] \geq \int \langle \mathbf{N}(x, y), \nabla\delta\rangle \mathrm{d}\mathbf{x} = -\int \langle \operatorname{div}\mathbf{N}, \delta\rangle \mathrm{d}\mathbf{x} \tag{9.4}$$

$$= -\langle \operatorname{div}\mathbf{N}, \delta\rangle_{L^2} \tag{9.5}$$

$$= \langle \Delta \operatorname{div}\mathbf{N}, \delta\rangle_{H^{-1}}. \tag{9.6}$$

Therefore $u = \Delta \operatorname{div}\mathbf{N} \in \partial_{H^{-1}} \mathcal{E}$. In fact, the subgradient of the functional E consists precisely of these elements [47]; i.e.,

$$\partial_{H^{-1}} \mathcal{E} = \{\Delta \operatorname{div}\mathbf{N} : \mathbf{N}(x, y) \in \partial\gamma(\nabla h) \text{ for each } (x, y)\}.$$

Returning to the problem of surface evolution, with DL kinetics we have

$$\partial_t h = -\frac{C_s D \Omega^2 g_3}{k_B T} \Delta \, \mathrm{div}\mathbf{N} \quad \text{globally}, \tag{9.7}$$

where $\mathbf{N}$ is the canonical restriction of the subgradient $\partial_{H^{-1}}\mathcal{E}$, i.e., the element "nearest" to the origin with respect to the H^{-1} norm. As we observed above, for $\nabla h \neq 0$ the subgradient consists of a single element, and the canonical restriction does not come into play. Only in the singular case $\nabla h = 0$ do we need to invoke the canonical restriction to determine h_t uniquely. The auxiliary function $\mathbf{N} \in \partial_{H^{-1}} E$ can be found by solving the minimization problem

$$\min_{\mathbf{N}\in\partial\gamma} \|\Delta \, \mathrm{div}\mathbf{N}\|^2_{H^{-1}} \Leftrightarrow \min_{\mathbf{N}\in\partial\gamma} \|\nabla \, \mathrm{div}\mathbf{N}\|^2_{L^2}. \tag{9.8}$$

The canonical restriction $\mathbf{N}$ which solves the minimization problem (9.8) must have a square integrable derivative $\nabla \, \mathrm{div}\mathbf{N}$. *This condition implies that* $\mathbf{N}$ *and* $\mu = \Omega g_3 \, div\mathbf{N}$ *are continuous on* $[0,1]^2$. We are now in a position to state the natural boundary conditions arising from the variational formulation.

The first boundary condition states that the slope $|\nabla h|$ approaches zero at the facet edge $L_0(t)$. Since $\mathbf{N}$ is restricted to the ball of radius g_1/g_3 on the facet, while $|\mathbf{N}| = \frac{g_1}{g_3}(1 + |\nabla h|^2)$ outside the facet, continuity of $\mathbf{N}$ dictates that $|\nabla h| \to 0$ as $\mathbf{r} \to \mathbf{r}_\mathrm{f} \in L_0$, i.e.,

$$\nabla h = 0, \quad (x, y) \in L_0. \tag{9.9}$$

The second boundary condition in DL kinetics follows from enforcing continuity of surface flux ($\nabla \, \mathrm{div}\mathbf{N}$ in the discussion above) at the facet edge. Outside the

facet, we have a surface flux given by

$$\mathbf{J} = -\frac{C_s D}{k_B T}\nabla\mu = \frac{C_s D\Omega g_3}{k_B T}\nabla\,\mathrm{div}\left(\frac{g_1}{g_3}\frac{\nabla h}{|\nabla h|} + |\nabla h|\nabla h\right). \tag{9.10}$$

The flux on the facet follows from mass conservation, $\dot{h}_f + \Omega\,\mathrm{div}\mathbf{J}_f = 0$, where $h_f(t)$ is the facet height. Solving for the divergence of $\mathbf{J}_f$, we write

$$\mathrm{div}\mathbf{J}_f = -\frac{\dot{h}_f}{\Omega} \quad \text{on the facet.} \tag{9.11}$$

Fix t, and integrate (9.11) over the interior of $L_0(t)$. We apply the divergence theorem to conclude

$$\oint_{L_0(t)} \mathbf{J}_f \cdot \nu \mathrm{d}s = -\Omega^{-1}\dot{h}_f A_f(t), \tag{9.12}$$

where $A_f(t)$ is the area of the facet at time t.

Now we invoke continuity of $\mathbf{J}$ at $L_0(t)$ to replace $\mathbf{J}_f$ in (9.12) with its counterpart (9.10) restricted at $L_0(t)$. The result is

$$\dot{h}_f A_f(t) = -\oint_{L_0(t)} \frac{C_s D\Omega^2 g_3}{k_B T}\nabla\,\mathrm{div}\left(\frac{g_1}{g_3}\frac{\nabla h}{|\nabla h|} + |\nabla h|\nabla h\right)\cdot\nu\mathrm{d}s. \tag{9.13}$$

The next boundary condition follows from continuity of the surface height $h = h(x, y, t)$ at the facet edge. The height continuity dictates

$$h_f(t) = h(x, y, t)|_{\mathbf{r}\in L_0(t)}. \tag{9.14}$$

We now differentiate with respect to t to obtain

$$\dot{h}_f(t) = \frac{\mathrm{d}}{\mathrm{d}t}h(\mathbf{r}, t) = \left.\frac{\partial h}{\partial t}\right|_{\mathbf{r}\in L_0(t)^+} - \nabla h|_{\mathbf{r}}\cdot\frac{\partial \mathbf{r}}{\partial t}. \tag{9.15}$$

The value of $\partial_t h$ as $(x, y) \to L_0(t)$ from outside the facet is governed by the relaxation PDE for DL kinetics.

$$\frac{\partial h}{\partial t} = -\frac{C_s D\Omega^2 g_3}{k_B T}\Delta\,\mathrm{div}\left(\frac{g_1}{g_3}\frac{\nabla h}{|\nabla h|} + |\nabla h|\nabla h\right). \tag{9.16}$$

Using (9.16) together with $\nabla h|_{L_0(t)} = 0$, we have the third boundary condition,

$$\dot{h}_f = -\frac{C_s D \Omega^2 g_3}{k_B T} \Delta \operatorname{div} \left(\frac{g_1}{g_3} \frac{\nabla h}{|\nabla h|} + |\nabla h| \nabla h \right) \Big|_{L_0(t)}. \tag{9.17}$$

We now elaborate on the boundary conditions stemming from continuity of the chemical potential μ and the vector field $\mathbf{N}$. These quantities have physical meaning outside the facet, where $\nabla h \neq 0$ and the step positions satisfy the usual assumptions conducive to a macroscale limit. Following Spohn [109], to determine how $\mathbf{N}$ and μ should be defined on the facet, we reverse the calculations that lead to surface flux outside the facet. In this vein, we start with the mass conservation law, $\dot{h}_f = -\Omega \operatorname{div} \mathbf{J}_f$, assuming that $\dot{h}_f$ is a known function of t. Extending the constitutive relation (9.10) to the facet, we want to solve

$$\mathbf{J}_f = -\frac{C_s D}{k_B T} \nabla \mu_f$$

for μ_f. Due to the scalar proportionality constant in DL kinetics, the solution for μ_f can be given as a line integral of $\mathbf{J}_f$ over a path contained in the facet:

$$\mu_f(x, y, t) = \mu_0 - \frac{k_B T}{C_s D} \int_{(x_0, y_0)}^{(x,y)} \mathbf{J}_f \cdot \mathrm{d}\mathbf{x}. \tag{9.18}$$

Then, continuity of μ implies $\mu_f(\mathbf{r}_\mathrm{f}(t), t) = \mu(\mathbf{r}_\mathrm{f}(t), t)$, or

$$\mu_0 - \frac{k_B T}{C_s D} \int_{(x_0, y_0)}^{(x,y)} \mathbf{J}_f \cdot \mathrm{d}\mathbf{x} = -\Omega g_3 \operatorname{div} \left[\frac{g_1}{g_3} \frac{\nabla h}{|\nabla h|} + |\nabla h| \nabla h \right], \quad (x, y) \in L_0(t). \tag{9.19}$$

Outside the facet we have $\mu = \Omega g_3 \operatorname{div} \mathbf{N}$, so the natural extension of $\mathbf{N}$ to the facet is a vector field $\mathbf{N}_f$ satisfying

$$\frac{C_s D \Omega^2 g_3}{k_B T} \Delta \operatorname{div} \mathbf{N}_f = \dot{h}_f. \tag{9.20}$$

Continuity of $\mathbf{N}$ at the facet edge gives us Dirichlet boundary conditions to complement the third-order PDE (9.20):

$$\mathbf{N}_f = -\left[\frac{g_1}{g_3}\frac{\nabla h}{|\nabla h|} + |\nabla h|\nabla h\right], \quad (x, y) \in L_0(t). \tag{9.21}$$

Conditions (9.9), (9.13), (9.14), (9.19), (9.20), and (9.21) for $\mathbf{J}$, μ, $\mathbf{N}$, and h follow naturally from the treatment of macroscopic height evolution in terms of the variational framework. With this perspective, the smoothing of the height profile is described by a path of steepest descent for the energy with respect to the H^{-1} inner product. At the risk of redundancy, we emphasize that conditions (9.19), (9.20), and (9.21), for continuity of μ and $\mathbf{N}$ at the facet edge, *rely on a nonphysical chemical potential defined on the facet*.[4] Implementation of the weak formulation for $g_1 \neq 0$ must therefore be interpreted cautiously, since the boundary conditions it enforces are not entirely consistent with the discrete character of processes occurring on a facet [37].

9.4 Scaling of the boundary layer width

While studying numerical simulations of relaxing axisymmetric steps, Margetis, Aziz and Stone [64] noticed a rapid variation of the slope in the vicinity of the top facet (in contrast to the slowly varying slope farther away, in the bulk of the step train). This observation prompted them to investigate the possibility of a *boundary layer* near the facet edge. Intuitively, one might argue for the existence of a boundary layer by noting that a slowly varying slope profile outside the facet must

[4]This inconsistency has been reported previously by Israeli and Kandel [37].

still connect continuously with the slope $|\nabla h| = 0$ at the facet edge, for any solution that respects the boundary conditions given above. In the boundary layer, the step interaction (g_3) term plays the role of a perturbation, influencing the slope profile through the balance among derivatives of different orders. This local analysis uses only the PDE for h and continuity of slope, *not the other boundary conditions at the facet edge*. As a result, the scaling we obtain is not altered if we replace μ-continuity by a more physical, microscale condition. To quantify the perturbation effect of the g_3 term, Margetis et al. [64] introduced a small parameter

$$\epsilon = \frac{g_3}{g_1} \ll 1. \tag{9.22}$$

The slope profile $F := \nabla h \cdot \mathbf{e}_\eta$ that solves the boundary value problem is then a function of space, time and ϵ. The PDE for F is found by computing the directional derivative of (9.16) along the local normal:

$$\frac{\partial F}{\partial t} = \frac{C_s D \Omega^2 g_1}{k_B T} \nabla \big(\Delta \, \mathrm{div} \nabla \left[\mathbf{e}_\eta + \epsilon F^2 \mathbf{e}_\eta \right] \big) \cdot \mathbf{e}_\eta. \tag{9.23}$$

Assuming a long-time similarity solution, which depends separately on t and the rescaled local coordinate, Margetis et al. found that the boundary layer width δ scales as $\epsilon^{1/3}$, independently of the axisymmetric initial conditions.

In this section we expand the details of this calculation to accommodate geometries in 2+1 dimensions. Allowing the facet to evolve in time, we assume that a boundary layer of (possibly time-dependent) width δ moves with the facet edge. Within this boundary layer, the slope profile is assumed to have an approximate factorization, which then leads to an ODE in the "fast" spatial variable. The re-

sults we obtain for the boundary layer width take the form of inspired conjectures or speculations, awaiting verification by experiments and rigorous analysis.

The fully 2-dimensional geometry is handled using local analysis, which separates the spatial coordinates into slow (σ) and fast (η). The terminology reflects the separation of scales (short distances along the step normal direction, larger distances along the step tangential direction) over which comparable variations in the slope profile are observed. Suppose that the rapid variation of the slope F, from 0 at the facet edge $\eta = w(t)$ to its value where step interactions are less important, takes place within a boundary layer of width $\delta(t)$. We then define a rescaled transverse coordinate $\overline{\eta}$ according to

$$\overline{\eta} = \frac{\eta - w(t)}{\delta(t)}, \tag{9.24}$$

so that $\overline{\eta}$ remains $\mathcal{O}(1)$ inside the boundary layer. We express the spatial dependence of the slope profile in terms of this rescaled coordinate:

$$F(\eta, \sigma, t; \epsilon) = \mathcal{F}(\overline{\eta}, \sigma, t; \epsilon) = \mathcal{F}\left(\frac{\eta - w(t)}{\delta(t)}, \sigma, t; \epsilon\right). \tag{9.25}$$

By substituting $\mathcal{F}$ for F in the PDE, we explicitly account for the rapid variation of the slope within the boundary layer. The time derivative $\partial_t F$ is replaced by

$$\partial_t F = -\left(\frac{\overline{\eta}\dot{\delta}}{\delta} + \frac{\dot{w}}{\delta}\right)\partial_{\overline{\eta}}\mathcal{F} + \partial_t \mathcal{F}, \tag{9.26}$$

while the normal derivative is replaced by

$$\partial_\eta F = \partial_{\overline{\eta}}\mathcal{F} \cdot \frac{\partial \overline{\eta}}{\partial \eta} = \frac{1}{\delta}\partial_{\overline{\eta}}\mathcal{F}. \tag{9.27}$$

Motivated by analogy with observations of the step density from axisymmetric step simulations, we make the conjecture of a long-time solution that obeys the

following local ansatz to leading-order in ϵ: [5]

$$\mathcal{F}(\overline{\eta}, \sigma, t; \epsilon) \sim a_0(\sigma, t) \cdot f_0(\overline{\eta}; \epsilon), \quad |\eta - w| < \mathcal{O}(\delta). \tag{9.28}$$

Outside the boundary layer ($\overline{\eta} \gg 1$), we expect that the slope becomes independent of the distance from the facet, i.e., $f_0(\overline{\eta}) \to 1$ and $\mathrm{d}f_0/\mathrm{d}\overline{\eta} \to 0$ as $\overline{\eta} \to \infty$.

We compute the required derivatives of $\mathcal{F}$ and then substitute into the PDE (9.23). Thus, we have

$$\partial_t \mathcal{F} - \left(\frac{\overline{\eta}\dot{\delta}}{\delta} + \frac{\dot{w}}{\delta} \right) \partial_{\overline{\eta}} \mathcal{F} = -B \nabla \big(\Delta \, \mathrm{div} \left[\mathbf{e}_\eta + \epsilon \mathcal{F}^2 \mathbf{e}_\eta \right] \big) \cdot \mathbf{e}_\eta, \tag{9.29}$$

where $B = C_s D \Omega^2 g_1 / (k_B T)$.

If we neglect σ derivatives in accordance with slow-fast variable separation, then the PDE becomes

$$\partial_t \mathcal{F} - \left(\frac{\overline{\eta}\dot{\delta}}{\delta} + \frac{\dot{w}}{\delta} \right) \partial_{\overline{\eta}} \mathcal{F} \;=\; -\frac{B\epsilon}{\xi_\eta \delta^4} \partial_{\overline{\eta}} \frac{1}{\xi_\eta \xi_\sigma} \partial_{\overline{\eta}} \left(\frac{\xi_\sigma^2}{\xi_\eta} \partial_{\overline{\eta}} \frac{1}{\xi_\eta \xi_\sigma} \partial_{\overline{\eta}} [(\epsilon^{-1} + \mathcal{F}^2) \xi_\sigma] \right). \tag{9.30}$$

There are two small parameters in (9.30): the ratio ϵ of step interactions to step line tension, and the boundary layer width δ, which is assumed to scale as a power of ϵ. To decide systematically which terms dominate the PDE for small ϵ, we multiply (9.30) by $\delta^4/(B\epsilon)$ and expand the nested derivatives to retain only the highest derivative of $\mathcal{F}^2$. This calculation yields

$$\frac{\delta^3 \dot{w}}{B\epsilon} \partial_{\overline{\eta}} \mathcal{F} - \frac{1}{\xi_\eta^4} \partial_{\overline{\eta}}^4 \mathcal{F}^{\in} = \mathcal{O}\left(\frac{\delta^4 \mathcal{F}_t}{B\epsilon}, \frac{\delta^3 \dot{\delta}}{B\epsilon} \right), \tag{9.31}$$

where the terms on the right-hand side are shown to be negligible [64].

[5] By $\sim$ we mean asymptotic equivalence as $\epsilon \to 0$, i.e., $\mathcal{F} \sim g \Leftrightarrow \lim_{\epsilon \to 0} \frac{\mathcal{F} - g}{g} = 0$.

Now the separation ansatz (9.28) indicates that f_0 satisfies an ordinary differential equation, whose coefficients are time-independent. We substitute (9.28) into (9.31) to obtain

$$\frac{\dot{w}\delta^3}{B\epsilon a_0}\partial_{\overline{\eta}} f_0 - \frac{1}{\xi_\eta^4}\partial_{\overline{\eta}}^4(f_0^2) = \mathcal{O}\left(\frac{\delta^4\mathcal{F}_t}{B\epsilon}, \frac{\delta^3\dot{\delta}}{B\epsilon}\right) \tag{9.32}$$

Considering the left-hand side of 9.32, the requirement of time-independent coefficients for the ODE satisfied by f_0 implies

$$\delta = \mathcal{O}(\epsilon^{1/3}). \tag{9.33}$$

The same local analysis can be applied in the case of a fixed drift velocity u, the macroscale effect of an electric field (see Chapter 8). Again, the dominant balance of terms as $\epsilon \to 0$ would involve only the highest derivatives of f_0 with respect to $\overline{\eta}$. In particular, the drift term could be made negligible in comparison to the other terms by taking $\eta - w$ small enough. This asymptotic treatment is complementary to the analysis of the next section, in which we discuss the local behavior of the slope itself when a fixed drift velocity is present.

We emphasize that the power-law scaling of the boundary layer width $\delta(t)$ with ϵ arises only from the form of the PDE and the condition of a long-time similarity solution satisfying (9.28). The existence of a solution with this particular form is not easily established for an arbitrary facet shape.

Further studies of step-flow models in 2+1 dimensions should be pursued to support the scaling ansatz assumed above. We would then have graphical confirmation that even a weak step-step interaction strength can lead to a rapid variation of step density in the neighborhood of a facet edge. Far away from the facet, line ten-

sion is expected to dominate so that the step density varies much more slowly. These remarks generalize the observations found for axisymmetric step flow simulations, as reported by [64].

9.5 Effect of an electric field on the slope profile near a facet

Another question that we might treat using local analysis concerns the application of a direct current through a faceted crystal shape. The destabilizing effect of an electric field on a uniform step train, producing either step bunching or step meandering, is well-known [15, 28, 125]. For a faceted material, even in the simple geometry of straight steps, the effect of an electric field has received far less attention. We conclude this chapter with a brief discussion of this effect, bringing together the local analysis of the previous section and the macroscale PDE with a drift term from Chapter 8. Our derivation assumes diffusion-limited kinetics in order to facilitate an approximate solution of the macroscale PDE, i.e., we take $q|\nabla h| \ll 1$ and replace $1 + q|\nabla h|$ by 1 wherever possible.

9.5.1 Straight-step morphology

We consider the continuous graph $y = h(x)$ with the facet $\{(x, y) \in \mathbb{R}^2 \,|\, h = \text{const.}\}$ in $x \leq 0$, while $\partial_x h < 0$ in $x > 0$; so the facet edge is at $x = 0$ as shown in Figure 9.2. We seek to characterize stationary solutions of the macroscale evolution equation. Setting $\partial_t h \equiv 0$ in the conservation law $\partial_t h + \Omega \partial_x J = 0$, where

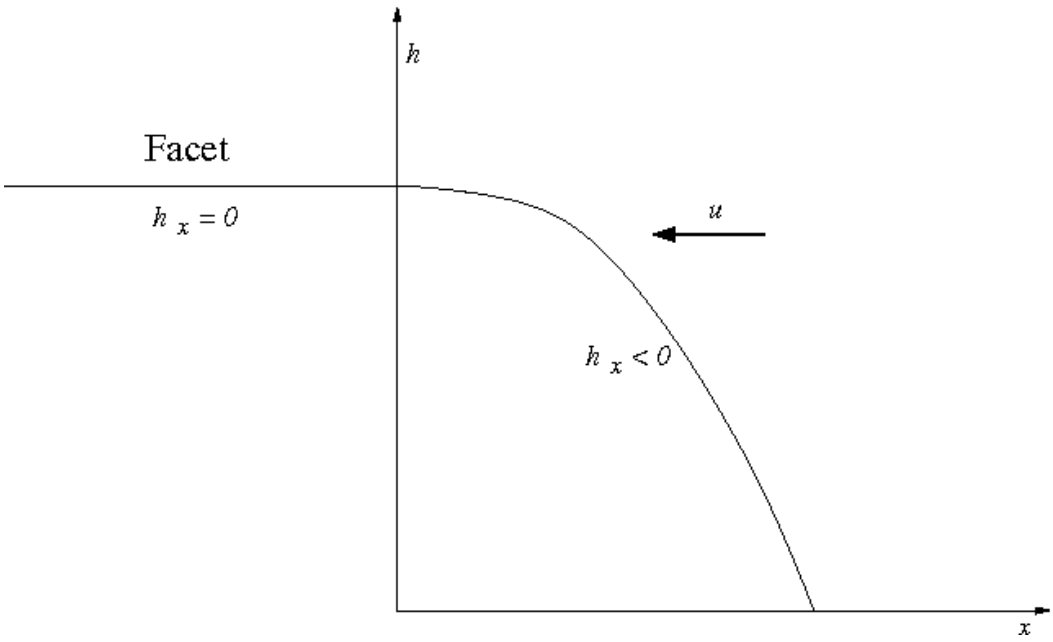

Figure 9.2: Cross-section of a facet and a descending train of straight steps.

$J = -[\partial_x \mu - D^{-1} v k_B T(1 + \mu/(k_B T))]$ entails the ODE

$$\partial_x \mu - l_v^{-1}\mu = l_v^{-1} k_B T - \mathcal{J}_0 \Rightarrow \mu(x) = (\mu_0 + k_B T - l_v \mathcal{J}_0) e^{x/l_v} - (k_B T - l_v \mathcal{J}_0) \quad x > 0 \; ; \tag{9.34}$$

where $l_v := D/v$, $\mathcal{J}_0 := J(0)$ and $\mu_0 := \mu(0)$. By substituting $\mu = -\Omega g_3 \partial_x(|\partial_x h|\partial_x h)$, $g_3 > 0$, we obtain the relation

$$\hat{g}_3(\partial_x h)^2 = (-k_B T + l_v \mathcal{J}_0)x + l_v(\mu_0 + k_B T - l_v \mathcal{J}_0)\big(e^{x/l_v} - 1\big) \quad x > 0 \; ; \; \hat{g}_3 = \Omega g_3 \; . \tag{9.35}$$

The above formula is simplified for $0 < x \ll |l_v|$ (weak drift) and for $x \gg |l_v|$ (strong drift). Accordingly, we obtain the approximation

$$|\partial_x h| \sim \hat{g}_3^{-1/2} \begin{cases} \sqrt{\mu_0 x} \; , & x \ll |l_v| \; , \\ \sqrt{l_v(\mu_0 + k_B T - l_v \mathcal{J}_0)}\, e^{x/(2l_v)} \; , & x \gg l_v > 0 \; , \\ \sqrt{(-|l_v|\mathcal{J}_0 - k_B T)x} \; , & x \gg -l_v > 0 \; . \end{cases} \tag{9.36}$$

For $x \gg -l_v > 0$, a compatibility condition is

$$-D\mathcal{J}_0 > k_B T|v| \ . \tag{9.37}$$

By (9.36), changes of the electric field magnitude and direction can cause a drastic qualitative change in the slope behavior. In particular, a strong electric force $Z^* eE$ in the step-down direction causes an increase of the slope, as steps tend to bunch. (Ultimately, of course, m approaches $\mathcal{O}(\sqrt{x})$ as $x \downarrow 0$.) This behavior is reversed by a strong electric force in the step-up direction, which restores the familiar $\mathcal{O}(\sqrt{x})$ behavior.

9.5.2 Axisymmetric structure

The radial case provides a model for the interplay of step edge curvature and electric field. Suppose the surface is axisymmetric, $h = h(r)$, with the facet $\{(r,h) \in \mathbb{R}^+ \times \mathbb{R} \,|\, h = \text{const.}\}$ in $0 \le r \le r_f$ while $\partial_r h < 0$ for $r > r_f$; so, the facet edge is at $r = r_f$. Consider a constant drift velocity v. The ODE for $\mu(r)$ is $\partial_r \mu - l_v^{-1}\mu = l_v^{-1} k_B T - r_f \mathcal{J}_0 / r$, with solution

$$\mu = (\mu_0 + k_B T) e^{(r-r_f)/l_v} - k_B T - r_f \mathcal{J}_0 \int_{r_f}^{r} \frac{e^{(r-r')/l_v}}{r'} \, \mathrm{d}r' \qquad r > r_f \ , \tag{9.38}$$

where $\mu_0 := \mu(r_f)$, $\mathcal{J}_0 := J(r_f)$. Taking into account that $\Omega^{-1}\mu = g_1/r + g_3 r^{-1} \partial_r [r(\partial_r h)^2]$, by direct integration we have

$$\begin{aligned} \hat{g}_3 (\partial_r h)^2 \sim {} & [l_v r_f \mathcal{J}_0 \, (1 - l_v/r_f) - \hat{g}_1 - r_f k_B T](r - r_f) + (k_B T + \mu_0) l_v \big[(r - l_v) e^{(r-r_f)/l_v} \\ & - r_f + l_v \big] - l_v (r_f \mathcal{J}_0) \, (r - l_v) \int_{r_f}^{r} \frac{e^{(r-r')/l_v}}{r'} \, \mathrm{d}r' \ , \qquad 0 < \frac{r - r_f}{r_f} \ll 1 \ ; \end{aligned} \tag{9.39}$$

$\hat{g}_l := \Omega g_l$ ($l = 1, 3$). Here, we consider distances $r - r_f$ from the facet boundary that are small compared to the facet radius of curvature. By analogy with Section 9.5.1, we simplify the formula for $\partial_r h$ by imposing weak or strong drift:

$$|\partial_r h| \sim \hat{g}_3^{-1/2} \begin{cases} \sqrt{(\mu_0 - \hat{g}_1/r_f)(r - r_f)} \,, & 0 < r - r_f \ll |l_v| \,, \\ [l_v(\mu_0 + k_B T - l_v \mathcal{J}_0)]^{1/2} \, e^{(r-r_f)/(2l_v)} \,, & r - r_f \gg l_v > 0 \,, \\ \sqrt{(|l_v||\mathcal{J}_0| - k_B T - \hat{g}_1/r_f)(r - r_f)} \,, & r - r_f \gg -l_v > 0 \,, \end{cases} \tag{9.40}$$

The approximation for $r - r_f \gg -l_v > 0$ is compatible with the condition

$$-D\mathcal{J}_0 > (k_B T + \hat{g}_1/r_f)|v| \,. \tag{9.41}$$

Approximations analogous to the radial case can be worked out in 2D by invoking the separation of local variables into fast (η) and slow (σ). Variations with respect to η are dominant in the vicinity of the facet, which allows us to find stationary solutions by solving an ODE in η. This approach provides formulas that directly generalize the radial case and is not further discussed here.

9.6 Conclusions

In this chapter, we considered the inclusion of facets in a weak solution of the macroscale evolution equation. A weak solution with one or more facets can be interpreted as a strong solution of the PDE informed by *natural boundary conditions* at the moving facet edge. These natural boundary conditions include continuity of slope, continuity of flux, and continuity of chemical potential across the facet edge.

To satisfy the boundary condition that the positive surface slope $|\nabla h|$ approaches zero at the facet edge, while varying more slowly away from the facet, we

hypothesized the existence of a boundary layer near the edge of the facet. Under the assumption that the slope profile in this boundary layer satisfies a separability ansatz, we derived a scaling of the boundary layer width in terms of the ratio g_3/g_1 of step interactions to step line tension.

Finally, we discussed the effect of an electric field on stationary solutions of the evolution equation in 1D step geometries. This approach yields qualitatively different slope profiles near the facet edge, depending on the strength and direction of the external electric field.

Chapter 10

Numerical results[1]

In this chapter, we illustrate numerically the rich variety of relaxation behaviors corresponding to solutions of the macroscale PDEs derived above. Of particular interest are the simulations that demonstrate a morphological transition, from a 2-dimensional profile at the start to an essentially 1-dimensional profile at finite times. Factors affecting the onset time of this transition include (i) the material parameter $q = D/ka$, (ii) the aspect ratio $\alpha = \lambda_x/\lambda_y$ of the initial *sinusoidal* profile, where λ_x and λ_y are the wavelengths in x and y, respectively, and (iii) the presence of an external electric field. By varying these three factors independently, we tentatively conclude that transition phenomena can be explained as the result of longitudinal fluxes comparable in size to the transverse fluxes. We alert the reader, however, that we still lack a complete understanding of the reason for this behavior. Also, some of the results we obtain might not apply to more general periodic profiles. Initial data with additional harmonics superimposed on the fundamental sinusoidal profile might exhibit nonlinear mode coupling effects, which could destroy the separable behavior reported below.

[1]Material in this chapter appeared previously in Bonito, Nochetto, Quah and Margetis 2009, Phys. Rev. E **79**, 050601 (R), and relies heavily on the finite element algorithms and codes graciously contributed by Andrea Bonito and Ricardo Nochetto.

The height evolution is governed by the PDE

$$\frac{\partial h}{\partial t} = \Omega C_s \operatorname{div}\left\{\mathbf{M}\cdot\left[\nabla\mu - \frac{k_B T}{D}\mathbf{v}\left(1+\frac{\mu}{k_B T}\right)\right]\right\},$$
$$\mu = -\Omega \operatorname{div}\left\{g_1\frac{\nabla h}{|\nabla h|} + g_3|\nabla h|\nabla h\right\},$$

which we nondimensionalize prior to numerical implementation. This nondimensionalization (carried out in Appendix B) serves two main purposes: (i) to focus on the structure of the equations without the distraction of dimensional coefficients, and (ii) to isolate the relevant combinations of material parameters, in particular those that have significant temperature dependence. The second purpose furnishes five combinations of parameters to describe the experimental setting. These parameter combinations are:

- $q = \frac{D}{ka}$, which compares diffusion and attachment/detachment rates;
- g_1/g_3, which compares the step line tension to step-step interactions;
- $\alpha = \lambda_x/\lambda_y$, the aspect ratio of the initial data;
- h_0/λ_x, the amplitude of the initial data;
- $\mathbf{u} = \mathbf{v}\lambda_x/D$, the nondimensional drift velocity (in the presence of an electric field).

The last three parameters can in principle be adjusted independently for any given material and temperature. On physical grounds we expect some restrictions on the physically attainable profile dimensions and drift velocity magnitude. For example, a corrugated surface with aspect ratio $\lambda_x/\lambda_y = 1/10000$ might be indistinguishable

from a one-dimensional profile, if imperfections in the patterning process ended up obscuring the long-wavelength period. Also, a sufficiently strong electric field will heat the sample, thereby changing the temperature unless the material is kept in contact with a suitably cold reservoir. The latter practical consideration is not accounted for in our simulations.

The first two parameters depend strongly on the temperature and the choice of material. The parameter q is the ratio of two thermally-activated quantities with different energetic barriers. If the energy barrier for adatom diffusion is larger (smaller) than that of attachment/detachment, then q is expected to increase (decrease) as temperature increases. The inequality between these energetic barriers need not be consistent from one material to another. In principle we can have one material where q increases with temperature, and another material where q decreases with temperature. Even two different orientations of the same material might exhibit contrasting temperature dependence of q. A good starting point for enumerating these possibilities is the table of energy barriers in [43] and the references cited therein.

The ratio g_1/g_3 of line tension to step interactions is also sensitive to the choice of material and temperature. Roughly speaking, the line tension decreases as temperature increases, reaching $g_1 = 0$ precisely at the roughening transition temperature. A more precise description of the temperature dependence of g_1 is given by invoking the Ising model [73]. The strength of repulsive step interactions, quantified by g_3, has two different contributions. Entropic repulsions become stronger as temperature increases, because steps have a greater tendency to wander and

collision distance is shorter. The strength of elastic dipole interactions, which are mediated through the crystal, varies with temperature mainly through the temperature dependence of the Young modulus for the material. Entropic repulsions tend to dominate at higher temperatures. As T approaches T_R from below, we therefore expect g_3 to increase. A formula for the step-step interaction coefficient g_3 is given in [43].

We note that a meaningful connection with experiments requires physically attainable values for the material parameters. In particular, crystal surfaces well below the roughening transition temperature typically fail to satisfy $g_1/g_3 \ll 1$. To obtain a numerically reliable result, and to circumvent the difficulty of enforcing boundary conditions at the moving facet edge, we were forced to consider only $g_1/g_3 = 0$ or $g_1/g_3 = \mathcal{O}(10^{-8})$ in our simulations. Note that small ($\mathcal{O}(10^{-8})$) values of g_1/g_3 *were* used in the numerical simulations in order to check the continuity of the observed phenomena with g_1, as discussed below. Our preliminary investigations with $g_1/g_3 \ll 1$ merit careful scrutiny, in order to avoid erroneous conclusions about the relaxation of real materials.

10.1 Review of the finite element method

With these limitations in mind, we now describe our numerical method, starting from the introductory material of Chapter 2. After nondimensionalization (see

Appendix B), the PDE we want to solve is

$$\partial_t h = \text{div}\mathbf{M} \cdot \nabla\mu, \tag{10.1}$$

$$\mu = \frac{\delta E}{\delta h} \tag{10.2}$$

for some appropriate mobility $\mathbf{M}$ and surface energy E. The spatial domain of this PDE is taken to be a rectangular region $\mathcal{B} = [0,1] \times [0,1]$, and h, μ at each time t are required to be *spatially periodic*. Given the initial data $h(\cdot, t)$ at $t = 0$, we want to determine the height profile at $t > 0$.

We exploit the variational structure of (10.1),(10.2) to simulate surface relaxation by using the FEM in space [9] and finite differences in time. The fourth-order PDE for h is conveniently written as two second-order equations: one for the height h, using mass conservation and the constitutive law for $\mathbf{J}$, and another for the chemical potential μ, which is essentially the variation with respect to h of the energy functional $E[h]$. We apply a semi-implicit Euler scheme [77] to express (10.1),(10.2) as a system in the updated variables (h^{n+1}, μ^{n+1}) where $h^n \approx h(\cdot, n\tau^n)$ and τ^n is the (adaptive) time step. The mobility $\mathbf{M}$ and the energy $E[h]$ are evaluated by use of (h^n, μ^n) to ensure *linearity* of the finite difference equations with (h^{n+1}, μ^{n+1}).

The equations for h^{n+1} and μ^{n+1} are recast to their "weak form" via multiplication by a periodic test function ϕ and integration by parts over $\mathcal{B}$. Restricting h^{n+1}, μ^{n+1}, and ϕ to the finite-dimensional space $\mathbb{V}_{\mathcal{T}}$ of continuous piecewise linear functions associated with the triangulation $\mathcal{T}$, we obtain the FEM equations for (h^{n+1}, μ^{n+1}), which are required to hold for all $\phi \in \mathbb{V}_{\mathcal{T}}$:

$$\int_{\mathcal{B}} \left(\frac{g_1}{g_3} \frac{\nabla h^{n+1}}{|\nabla h^n|} + |\nabla h^n| \nabla h^{n+1} \right) \cdot \nabla \phi = \int_{\mathcal{B}} \mu^{n+1} \phi, \tag{10.3}$$

$$\int_{\mathcal{B}} \left[h^{n+1} \phi + \tau^n \mathbf{M}^{\varepsilon}(\nabla h^n) \nabla \mu^{n+1} \cdot \nabla \phi \right] = \int_{\mathcal{B}} h^n \phi. \tag{10.4}$$

One major concern is the singularity of the g_1 term and the similarity transformation $\mathbf{M}_{x,y} = \mathbf{S}\mathbf{M}_{\eta,\sigma}\mathbf{S}^{-1}$, Eqs. (5.24)–(5.26), when $|\nabla h| = 0$. Computing the fraction $\nabla h^{n+1}/|\nabla h^n|$ which multiplies g_1/g_3 is numerically unstable when $|\nabla h^n|$ is close to zero. The elements of the change-of-basis matrix $\mathbf{S}$ given by (5.26) have $|\nabla h|$ in the denominator; consequently, the computation of $\mathbf{S}$ near $\nabla h = 0$ is also numerically unstable. We eliminate the singularity in these terms by adding a small regularization parameter so that the problematic denominators remain nonzero as $\nabla h \to 0$; see Table 10.1 for possible regularization schemes. Mathematically it can be argued that the mobility becomes a scalar (identity tensor) wherever $\nabla h = 0$. Ideally, this limit should be respected by the regularization we choose, in order to avoid any spurious results arising from a mathematically inconsistent mobility. However, we do note that in a particular instance where one of our regularization schemes did not respect this limit, the numerical results were practically the same, as we discuss below.

10.2 Software and computers

Our implementation of (10.3),(10.4) uses the FreeFem++ program, http://www.freefem.org/ff++/, developed by Olivier Pironneau, Frédéric Hecht, and Jacques Morice. The code specific to our PDE (10.3),(10.4) was written by Andrea

Bonito following the algorithm suggested by Ricardo Nochetto. Simulations were performed on a Dell desktop PC with 2.0GHz Intel Core 2 processor, 1GB of RAM, running Fedora Core 7 and Linux kernel 2.6.21.

The following auxiliary libraries and programs were also used:

- The UMFPACK library, http://www.cise.ufl.edu/research/sparse/umfpack, was used for direct solvers. UMFPACK implements the Unsymmetric Multi Frontal Method to solve unsymmetric sparse linear systems.

- The utility Gnuplot http://www.gnuplot.info/ was used to plot graphs. Gnuplot offers a command-line interface for visualizing data and functions in 2D and 3D plots.

- The MATLAB software suite, http://www.mathworks.com/, was used for post-processing the FreeFem++ output files, when Gnuplot did not offer the needed capabilities for certain plots.

10.3 Zero line tension ("ideal" case)

The macroscale equation we simulate for the height evolution has been shown in Chapter 5 to stem from the motion of steps, which exist as stable objects only below the surface roughening temperature. Temperatures below roughening dictate $g_1 > 0$; otherwise there would be no free energy cost to create surface defects, and these would appear and disappear spontaneously. However, once we have found a PDE consistent with step flow, we are free to ask how its solutions behave in certain limiting cases. As a test case, we take $g_1 = 0$ to circumvent the difficulty of treating

height evolution as a free boundary problem; see Chapter 9 for a discussion of the open problems in this direction. We also alert the reader that the case $g_1 \neq 0$ with sufficiently high g_1/g_3 leads to an ill-conditioned linear system for our numerical method [6], which makes the results of a simulation unreliable. Thus far, we have not been able to overcome the numerical hurdles of larger values for g_1/g_3.

The limit $g_1 \to 0$ is a starting point, with the same capacity to illustrate the contributions of our model as the plausibly more physical choice with $g_1/g_3 = \mathcal{O}(1)$. In this limiting case we can see the effect of a tensor mobility and an electric field. One major concern addressed within this perspective is whether observables of the macroscopic theory (e.g., height, surface energy) are continuous solutions as functions of g_1. In particular, we want to check whether the numerically observed transition for 2D to almost 1D profiles persists for nonzero (even small) g_1/g_3. In other words, we want to make sure that no "spurious" singular behavior is developed by the macroscale theory as $g_1 \to 0$. We begin this section by contrasting our tensor mobility predictions with the scalar mobility simulations of [108], both with $g_1 = 0$. By analogy with 1D macroscale models, these simulations set

$$M = \frac{D}{k_B T} \frac{1}{1 + q|\nabla h|}, \tag{10.5}$$

i.e., a *scalar mobility* which does not distinguish between step-normal and step-parallel fluxes. Our purpose in conducting these tests is to see whether our finite element code generates height profiles consistent with the results of previous variational methods, namely the Fourier series expansions within a Galerkin scheme used by Shenoy et al [107, 108].

10.3.1 Simulations with zero E-field

Our first test of the finite element implementation of the relaxation PDE used a scalar mobility, in order to validate our code against previously published results [107, 108]. In [107], Shenoy and co-authors outline their method of Galerkin expansions of the surface height profile. They start from a variational formulation of the height evolution equation and derive a system of ODEs for the coefficients in the Galerkin expansion of h. They simulate the relaxation with different values for the material parameters q and g_1/g_3, finding approximately separable solutions which decay either exponentially or algebraically in time when the initial height profile is a perfect sinusoid [107, 108].

We simulated a decaying bidirectional modulation, with different wavelengths in x and y. The height profiles from this simulation are plotted in Figure 10.1, with time increasing to the right.

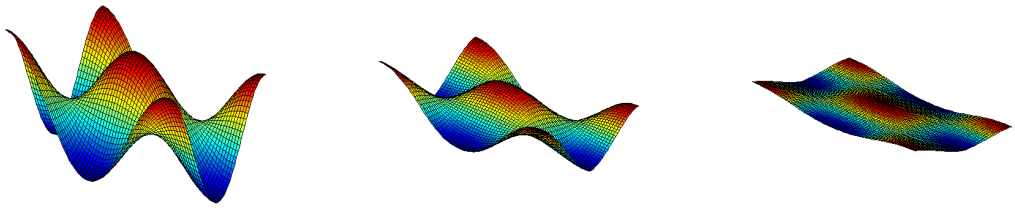

Figure 10.1: Height profiles computed using scalar mobility $M = \frac{D}{k_B T} \frac{1}{1+q|\nabla h|}$, for initial data $h = h_0 \cos(k_1 x) \cos(k_2 y)$, $h_0/\lambda_x = 0.03$, $k_2/k_1 = 11/24$, and material parameters $q = 10^4$, $g_1/g_3 = 0$.

The biperiodicity of the initial sinusoidal profile evidently persists throughout the relaxation, suggesting that the spatial dependence can be factored from the height in the approximate sense of (5.47). Assuming this factorization holds, a plot of the height peak versus time would reveal which decay law is exhibited by the solution. We plot in Figure 10.2 the evolution of energy and height peak using data from the same numerical experiment as Figure 10.1.

With logarithmic axes for height and energy, the two decay curves in Figure 10.2 are well-approximated by straight lines for most of the relaxation. To the eye, this trend is enough to classify the decay law as exponential. This finding is qualitatively consistent with [107, 108]. We are inclined to interpret their agreement with our plots as good evidence that Bonito's code [7] is reliable for the parameters under consideration. However, we have not carried out comparisons of our finite element-based numerical results with Shenoy's Fourier series-based numerics. Thus, our discussion here is restricted to qualitative (rather than precise quantitative) features of simulations.

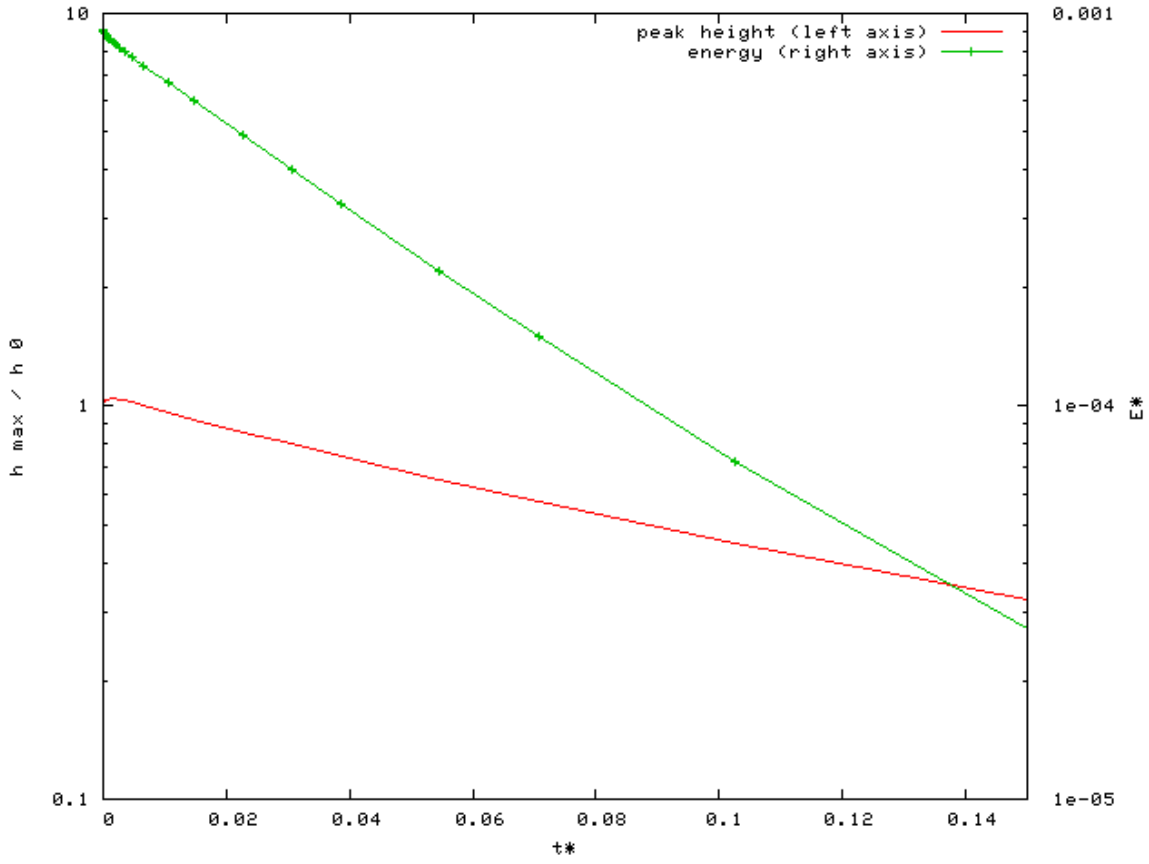

Figure 10.2: Decay of height peak and energy computed using scalar mobility, for initial data $h = h_0 \cos(k_1 x)\cos(k_2 y)$, $h_0/\lambda_x = 0.03$, $k_2/k_1 = 11/24$, and material parameters $q = 10^4$, $g_1/g_3 = 0$. t^* and E^* are measured in units where $\frac{k_B T \lambda_x^5}{C_s D g_3 \Omega^2 h_0}$ and $\frac{g_3 h_0^3 \lambda_y}{\lambda_x^2}$ are taken to be 1.

Table 10.1: Different regularization schemes for the tensor mobility. The first ("naïve") scheme was originally coded by Bonito. To respect the limit of scalar mobility as $|\nabla h| \to 0$, we discussed and implemented scheme 2. Nochetto suggested scheme 3, which takes a convex combination of the identity with the unregularized $\mathbf{M}$.

1. $$\mathbf{M}^\varepsilon = \frac{1}{|\nabla h|^2 + \varepsilon^2} \begin{pmatrix} \frac{h_x^2}{1+q|\nabla h|} + h_y^2 & -\frac{q|\nabla h| h_x h_y}{1+q|\nabla h|} \\ -\frac{q|\nabla h| h_x h_y}{1+q|\nabla h|} & \frac{h_y^2}{1+q|\nabla h|} + h_x^2 \end{pmatrix}$$

2. $$\mathbf{M}^\varepsilon = \begin{pmatrix} \frac{(h_x+\varepsilon)^2 + (1+q|\nabla h|)(h_y+\varepsilon)^2}{(1+q|\nabla h|)(|\nabla h|+\sqrt{2}\varepsilon)^2} & \frac{-q|\nabla h|(h_x+\varepsilon)(h_y+\varepsilon)}{(1+q|\nabla h|)(|\nabla h|+\sqrt{2}\varepsilon)^2} \\ \frac{-q|\nabla h|(h_x+\varepsilon)(h_y+\varepsilon)}{(1+q|\nabla h|)(|\nabla h|+\sqrt{2}\varepsilon)^2} & \frac{(h_y+\varepsilon)^2 + (1+q|\nabla h|)(h_x+\varepsilon)^2}{(1+q|\nabla h|)(|\nabla h|+\sqrt{2}\varepsilon)^2} \end{pmatrix}$$

3. $$\mathbf{M}^\varepsilon = (1-\lambda^2) I + \lambda^2 \mathbf{M}, \qquad \lambda = \min(\varepsilon, |\nabla h|)/\varepsilon.$$

We now present the results of implementing a tensor mobility in the finite element code. Because the tensor mobility distinguishes between step-normal and step-parallel fluxes, its representation in a fixed coordinate system relies on the change-of-basis matrix $\mathbf{S}$ given by (5.26), which is singular at $\nabla h = 0$ as discussed above. We ran the simulations with different choices of regularization for the tensor mobility (see Table 10.1) , finding good agreement even between regularizations that gave different limits for $\mathbf{M}$ as $\nabla h \to 0$ [8]. This robustness with respect to regularization suggests that the novel phenomena reported below are insensitive to the exact behavior of fluxes around peaks and valleys. We expand on this interpretation after showing a few more plots.

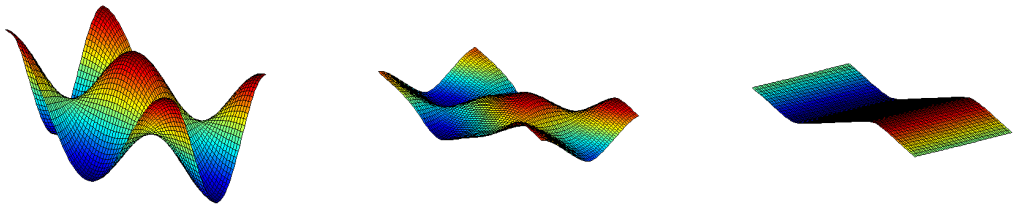

Figure 10.3: Height profiles computed using tensor mobility, starting from the initial data $h = h_0 \cos(k_1 x) \cos(k_2 y)$, $h_0/\lambda_x = 0.03$, $k_2/k_1 = 11/24$, and material parameters $q = 10^4$, $g_1/g_3 = 0$.

Figure 10.3 shows the computed height profiles at three selected times during a relaxation with tensor mobility. The initial data is identical to that of Figure 10.1, biperiodic with different wavelengths in x and y. At later times (middle and right surface plots), the x-dependence becomes less pronounced. Even before the height peak decays to 1% of its initial amplitude, the computed height profile looks essentially like a 1-dimensional modulation.

Because the spatial dependence of the height profile does not remain the same throughout the simulation, we suspect that a different separation ansatz $h \approx H(x, y)A(t)$ is obeyed for different time intervals, e.g.,

$$\begin{aligned} h &\approx H_1(x, y)A(t), \qquad 0 < t < t_1 \\ h &\approx H_2(x, y)A(t), \qquad t_1 < t < t_2 \\ &\vdots \end{aligned}$$

We find it instructive to show the decay of height peak and energy. These curves, we hope, would give us a clue about what time scales are relevant for observing the transition.

In Figure 10.4 we compare the predictions for decay of peak height using scalar and tensor mobilities. The simulation with tensor mobility appears to exhibit an exponential decay of the height peak until we reach $t^* \approx 0.1$, after which the height peak drops sharply into another decay regime. This sharp drop on the graph of height peak vs. time coincides with the onset of a transition, as confirmed visually by plotting the height profiles for t^* before and after $t^* = 0.1$.

To give the reader a feel for what physical time might correspond to $t^* = 0.1$, we compute the magnitude of the time unit $\frac{k_B T \lambda_x^5}{C_s D g_3 \Omega^2 h_0}$ for the *hypothetical* material that has an extremely small value of g_1/g_3, corresponding to the simulation above. To this end we set $h_0/\lambda_x = 0.03$ as dictated by the simulation, and choose $D/(ka) = q = 10^4$ and $g_1/g_3 = 0$. The other parameters we take from Si(001) at 700 K, which Erlebacher et al. used in the first demonstration of nonclassical smoothing [20]. We originally considered Si(001) because of its large q value, but the non-negligible ratio g_1/g_3 makes it unsuitable for a simulation using finite elements. For now its main purpose is to furnish plausible values for the undetermined parameters in our time unit.

The possibility of constructing the "metamaterial" which agrees with *all* of the parameters of our simulation is not addressed here. One promising direction is to look for materials that exhibit a preroughening transition, such as GaAs, in which $g_1/g_3 \to 0$ before the BCF theory becomes inapplicable [85]. Based on the meager literature, it appears that kinetic parameters such as k_u,k_d, and D are difficult to determine for GaAs, due to the high deposition flux needed to keep a sample under observation [85]. Accordingly, we fall back on the more fully-documented Si material

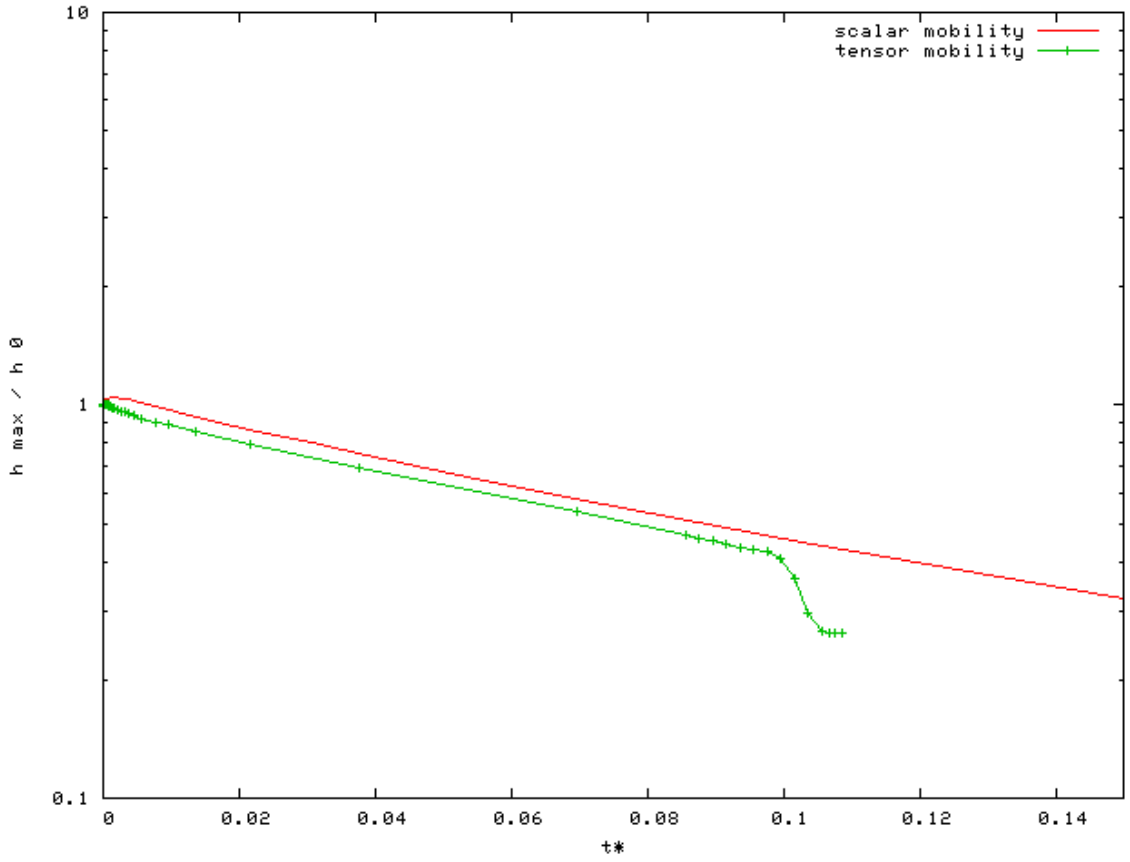

Figure 10.4: Decay of height peak, as computed using scalar and tensor mobilities, starting from initial data $h = h_0 \cos(k_1 x) \cos(k_2 y)$, $h_0/\lambda_x = 0.03$, $k_2/k_1 = 11/24$, with material parameters $q = 10^4$ and $g_1/g_3 = 0$. t^* is measured in units where $\frac{k_B T \lambda_x^5}{C_s D g_3 \Omega^2 h_0}$ is taken to be 1.

in order to calculate a possibly reasonable time unit.

After substituting the values from [20, 39], we determine our time unit to be $\frac{k_B T \lambda_x^5}{C_s D g_3 \Omega^2 h_0} = 3 \times 10^{-8} (\lambda_x / \mathring{A})^4$ seconds. The wavelength λ_x of the surface feature is still free to vary, which allows an appreciably large range of time scales that this one simulation can address. In particular, if we could pattern a bidirectional corrugation in our hypothetical material with 100 nm wavelength along the shorter direction, then relaxation at 700 K would need to proceed for at least 45 minutes before our predicted transition could occur. However, a wavelength of 100 nm might not comprise enough steps for the macroscale limit to be justified. Biperiodic profiles with larger period (e.g., 363 nm [20]) would need to be observed much longer: at least 12 hours to see the transition computed by our simulation above.

If the height profile did indeed decay in a separable manner until about $t^* = 0.1$, then the surface energy $E = \int_{\mathcal{B}} g_1 |\nabla h| + \frac{g_3}{3} |\nabla h|^3$ should also show an exponential dependence on time. Since g_1/g_3 was taken to be zero for this simulation, a globally approximately factorizable solution $h(x, y, t) = H(x, y) A(t)$ would entail $E = A(t)^3 \int_{\mathcal{B}} \frac{g_3}{3} |\nabla H|^3$, whose time dependence is exponential precisely when $A(t)$ is exponential. We plot in Figure 10.5 the decay of surface energy as predicted by simulations with scalar and tensor mobilities. Note that this factorizability of E is strictly speaking spoiled if both g_1 and g_3 are nonzero.

With E^* plotted on a logarithmic axis in Figure 10.5, the curve corresponding to either mobility appears as a straight line at least until $t^* = 0.1$. The slope of this line is approximately three times as large as the slope in Figure 10.4, which is what we would expect from an exactly separable solution. However, after $t^* = 0.1$, the curve corresponding to tensor mobility deviates from a straight line, dropping sharply into another decay law. The simulation described here does not continue long enough to say anything definitive about this second decay law, owing to the stopping criterion that terminated the simulation after an essentially 1D profile had been reached [7]. Earlier simulations, without such a stopping criterion in place, indicate that the 1D profile after the transition follows another separable, exponential decay.

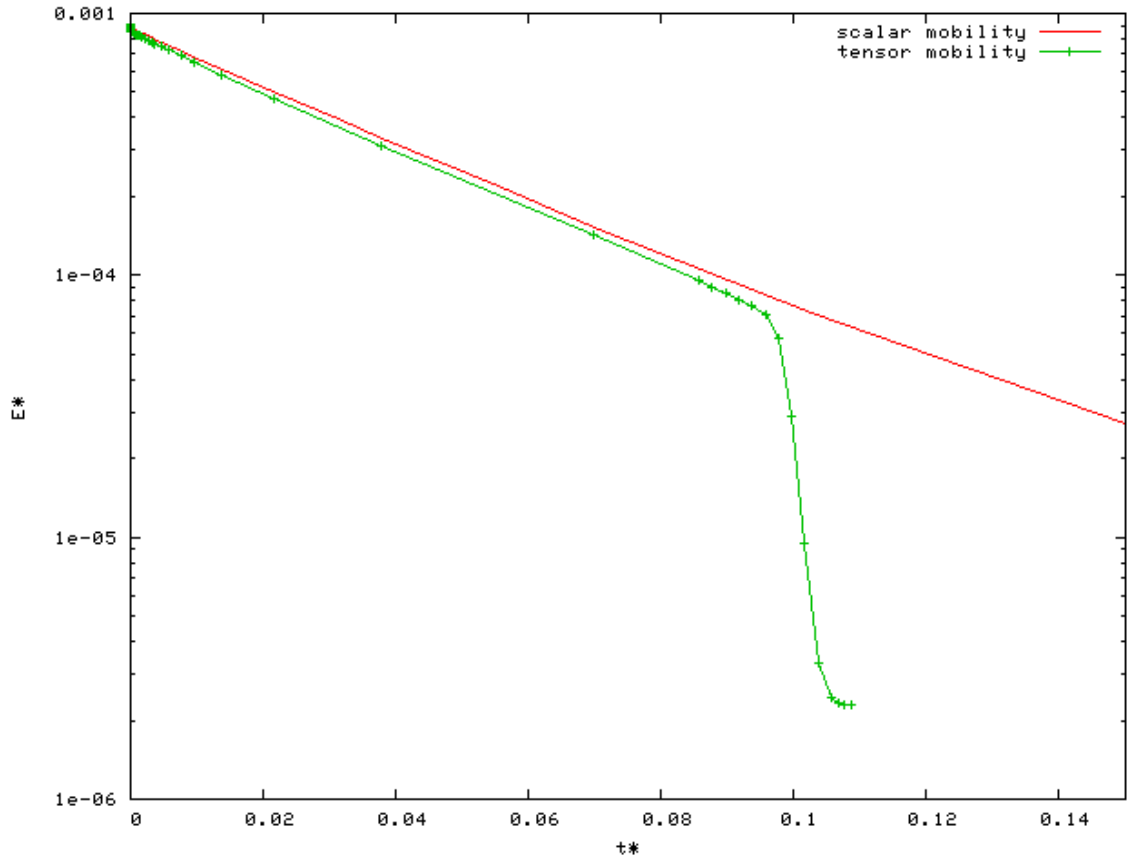

Figure 10.5: Decay of surface energy, as computed using scalar and tensor mobilities, starting from initial data $h = h_0 \cos(k_1 x) \cos(k_2 y)$, $h_0/\lambda_x = 0.03$, $k_2/k_1 = 11/24$, with material parameters $q = 10^4$ and $g_1/g_3 = 0$. t^* and E^* are measured in units where $\frac{k_B T \lambda_x^5}{C_s D g_3 \Omega^2 h_0}$ and $\frac{g_3 h_0^3 \lambda_y}{\lambda_x^2}$ are taken to be 1.

We now show contour plots of the height profile at various stages of the relaxation, in order to elucidate a possible mechanism for the appearance of a transition. Figure 10.6 shows level sets of height (top row) and streamlines for the vector adatom flux (bottom row) at four different times during the transition. The *streamlines* are defined by the property of being tangent to the vector adatom flux at each point in $\mathcal{B}$. Our use of streamlines is adopted from fluid mechanics, where they serve as a visual aid in describing the velocity field of a fluid. To plot the streamlines at a given time t, we first compute the height profile and macroscale chemical potential, which yields by (8.49) the vector-valued flux $\mathbf{J}$. We then solve Poisson's equation for ψ, i.e., $\Delta\psi = \partial_x J_y - \partial_y J_x$, so that $\mathbf{J} = (J_x, J_y)$ is orthogonal to $\nabla\psi = (\partial_x\psi, \partial_y\psi)$. Level sets of ψ then correspond to streamlines.

In contrast to the case of scalar mobility, the adatom flux is *not* orthogonal to the level sets, but instead has an appreciable component in the longitudinal direction. This longitudinal component can be comparable in size to the transverse component of flux, despite the slower variation of the chemical potential along the former direction than the latter. Again, this effect can be traced back to the tensor mobility, which for $q \gg 1$ inhibits the macroscale flux in the transverse direction but not in the longitudinal direction. To illustrate the effect of smaller q (and hence a lower energy barrier for uphill and downhill mass transport), we show in Figure 10.7 the height level sets and the streamlines corresponding to $q = 5000$. The other parameters from the previous simulation are kept unchanged.

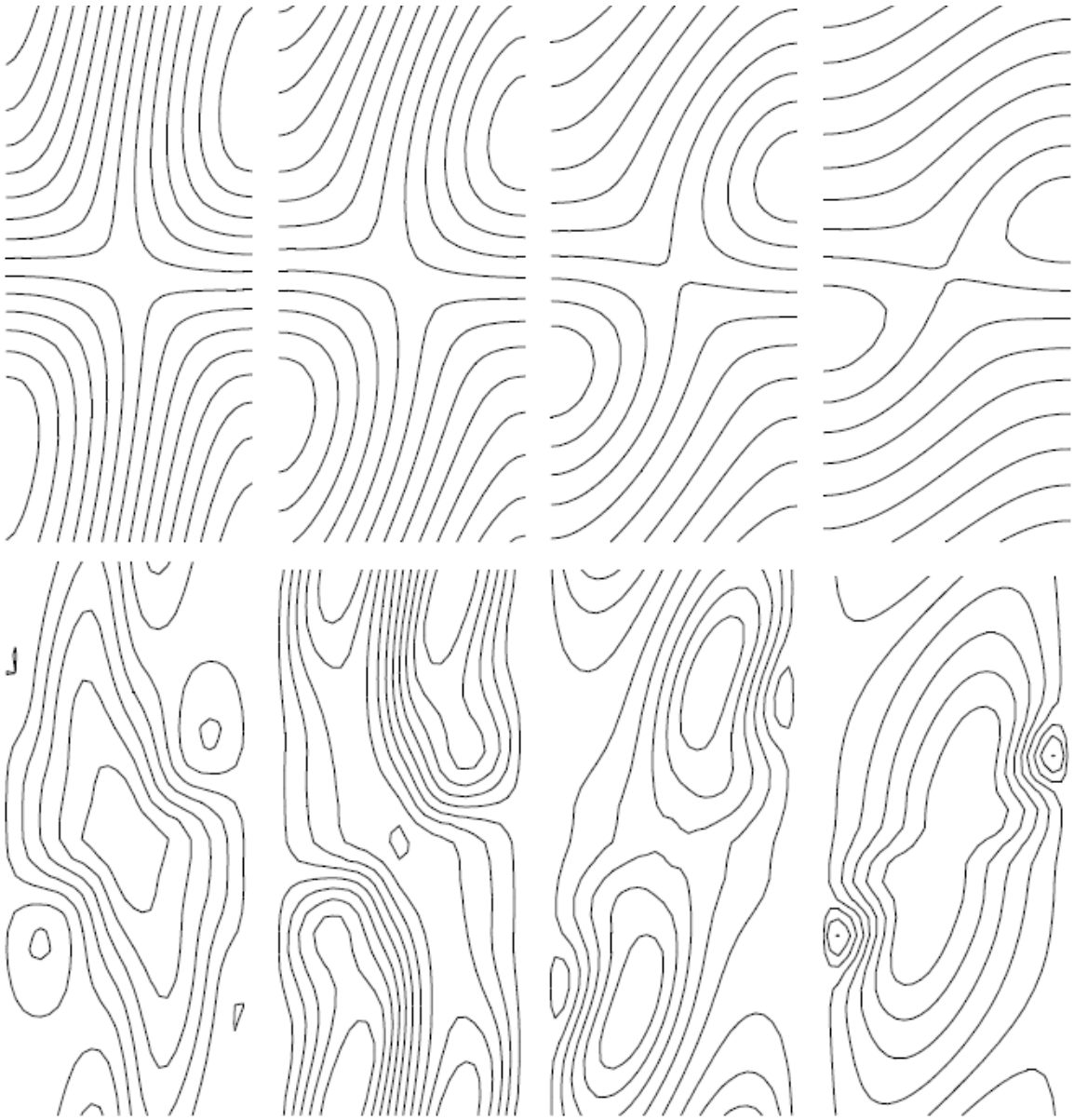

Figure 10.6: Snapshots during the transition from the initial data $h = h_0 \cos(k_1 x) \cos(k_2 y)$, $h_0/\lambda_x = 0.03$, $k_2/k_1 = 11/24$ to an eventually 1D profile, taken from [7]. The simulation uses tensor mobility and material parameters $q = 10^4$, $g_1/g_3 = 0$. Top row: level sets of height. Bottom row: streamlines, which are locally tangent to the vector adatom flux. Plot window is $[0, \lambda_x/2] \times [0, \lambda_y/2]$.

As q is increased, the transverse flux is diminished, and downhill mass transport proceeds more slowly. The decay of height peak would then be expected to take longer, as confirmed in Figure 10.8. Meanwhile, the longitudinal flux now has a greater relative contribution, since adatoms flowing along level sets of height encounter the same energetic barrier as for smaller q. This flow of adatoms along the step-parallel direction happens fast enough that steps with large perimeter have a chance to straighten, eventually aligning themselves with the x-axis as more mass flows downhill (uphill) from the peaks (valleys). We now have a possible explanation for the robustness of a transition with respect to regularization of the mobility. If the transition results from sizable contributions of the longitudinal adatom flux on terraces of large perimeter, then the fluxes on smaller-perimeter terraces near $|\nabla h| = 0$ are of secondary importance, serving only to transport mass downhill (or uphill) from peaks (or valleys). As long as the tensor mobility yields an adatom flux at peaks of the surface profile that points approximately downhill (and flux at valleys that points uphill), then the accurate calculation of flux at other points is sufficient to induce a transition.

The error in the computed flux arising from the regularized mobility can be quantified by comparing the regularization parameter ε with the computed denominator $|\nabla h|$ to which it is added. If the mesh size is 10^{-2}, then the height difference between neighboring gridpoints, say $|h(x_i, y_j) - h(x_{i+1}, y_j)|$, must be much greater than $10^{-2}\varepsilon$ in order to avoid an inaccurate flux calculation. In practice, this inequality is only violated very close to the peaks and valleys of a profile, or for very flat profiles. We find that an "outward-pointing" flux is respected by all of the

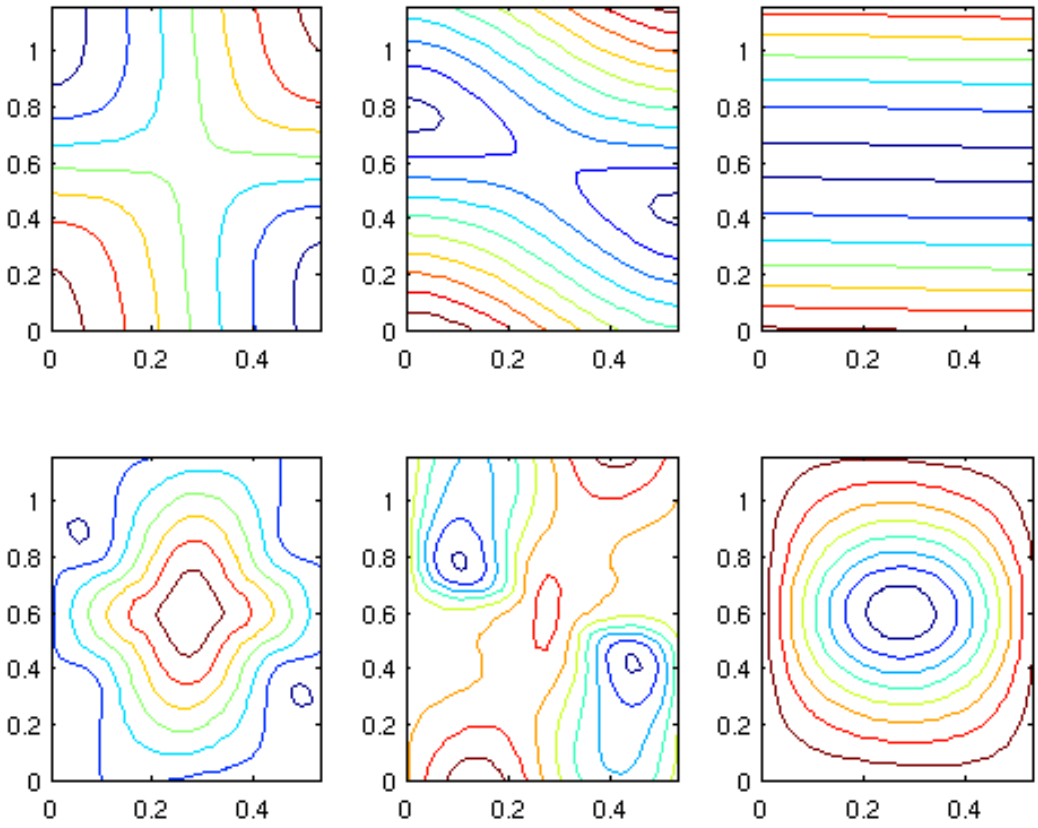

Figure 10.7: Snapshots during the transition from the initial data $h = h_0 \cos(k_1 x) \cos(k_2 y)$, $h_0/\lambda_x = 0.03$, $k_2/k_1 = 11/24$ to an eventually 1D profile. The simulation uses tensor mobility and material parameters $q = 5000$, $g_1/g_3 = 0$. Top row: level sets of height. Bottom row: streamlines, which are locally tangent to the vector adatom flux. Plot window is $[0, \lambda_x/2] \times [0, \lambda_y/2]$.

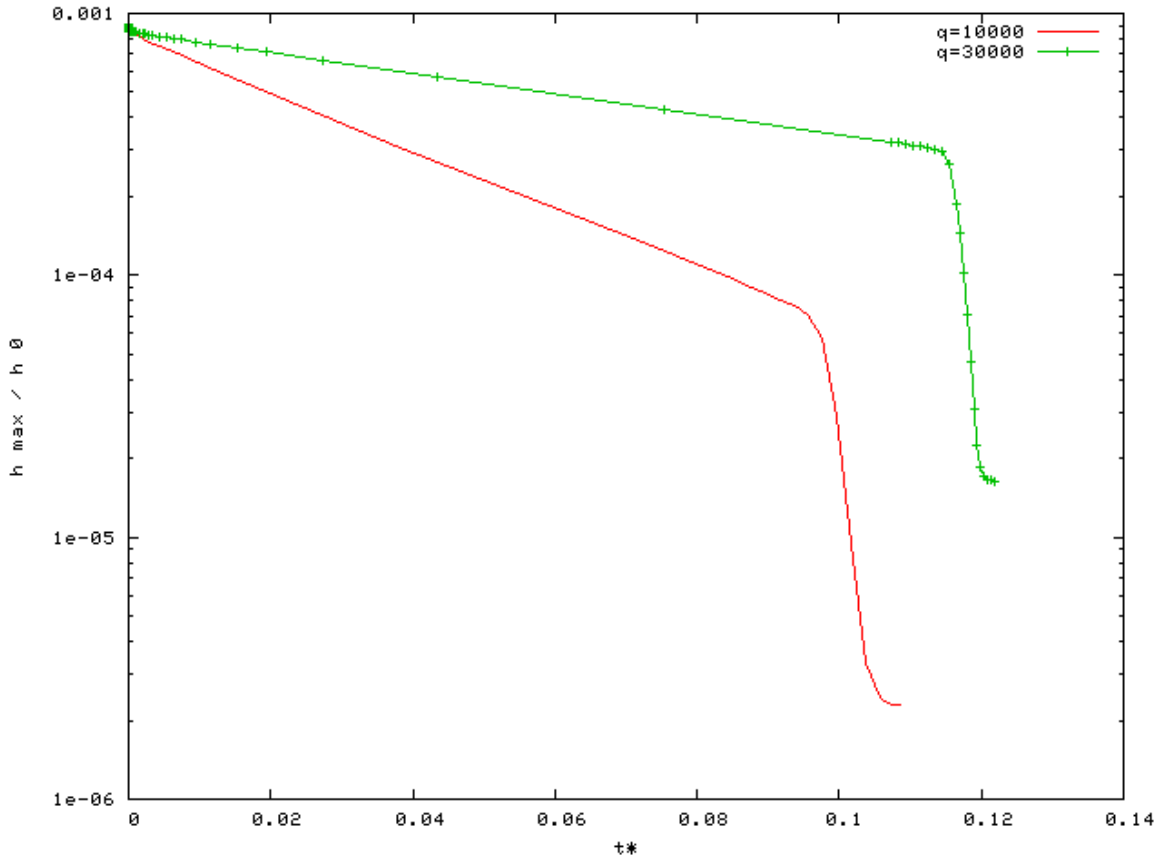

Figure 10.8: Decay of the height peak happens more slowly as q is increased, due to the increased attachment-detachment barrier that must be surmounted for mass to be transported uphill or downhill.

regularization schemes we tried, and they all predicted a transition event. We infer that the tensor mobility manifests a transition more through the fluxes on level sets close to the mean height, than through the fluxes on terraces of shorter perimeters.

10.3.2 Simulations with nonzero E-field

We were fortunate to have finished calculating the macroscale limit of step flow in the presence of an electric field, just when the numerical results of implementing the tensor mobility were available. The presence of an electric field at the BCF level, as we saw in Chapter 8, leads to a convective term in the macroscale adatom flux, Eq. (8.49). The evolution equation is given by modifying (10.3),(10.4) with the addition of a convective term in (10.3). We solve numerically the following system within the space of piecewise linear functions on $\mathbb{V}_{\mathcal{T}}$ (cf. Section 2.2):

$$\int_{\mathcal{B}} \left(\frac{g_1}{g_3} \frac{\nabla h^{n+1}}{|\nabla h^n|} + |\nabla h^n| \nabla h^{n+1} \right) \cdot \nabla \phi = \int_{\mathcal{B}} \mu^{n+1} \phi, \tag{10.6}$$

$$\int_{\mathcal{B}} \left[h^{n+1} \phi + \tau^n \mathbf{M}^{\varepsilon}(\nabla h^n) \big(\nabla \mu^{n+1} + (1 + \mu^{n+1}) \mathbf{u} \big) \cdot \nabla \phi \right] = \int_{\mathcal{B}} h^n \phi; \tag{10.7}$$

see Appendix B for a nondimensional interpretation of these equations. Again, the relevant geometric ratios and parameter combinations are λ_x/λ_y, h_0/λ_x, $\mathbf{u} = \lambda_x D^{-1}\mathbf{v}$, q, and g_1/g_3.

By tuning the electric field (and hence the drift velocity $\mathbf{u}$), we hoped to gain some control over the relative contributions of transverse and longitudinal fluxes, which were hypothesized as the driving mechanisms behind a transition. This control would allow us to inhibit or accelerate a transition, by reinforcing the fluxes along a specified direction. We find that by choosing a drift velocity in the direction of the *longer* wavelength, the time to observe a transition is drastically *reduced*.

In Figure 10.9 we plot the decay of the height peak and surface energy, computed with Bonito's finite element code using tensor mobility, with and without an electric field. The exponential transformation of Chapter 8 is *not* implemented

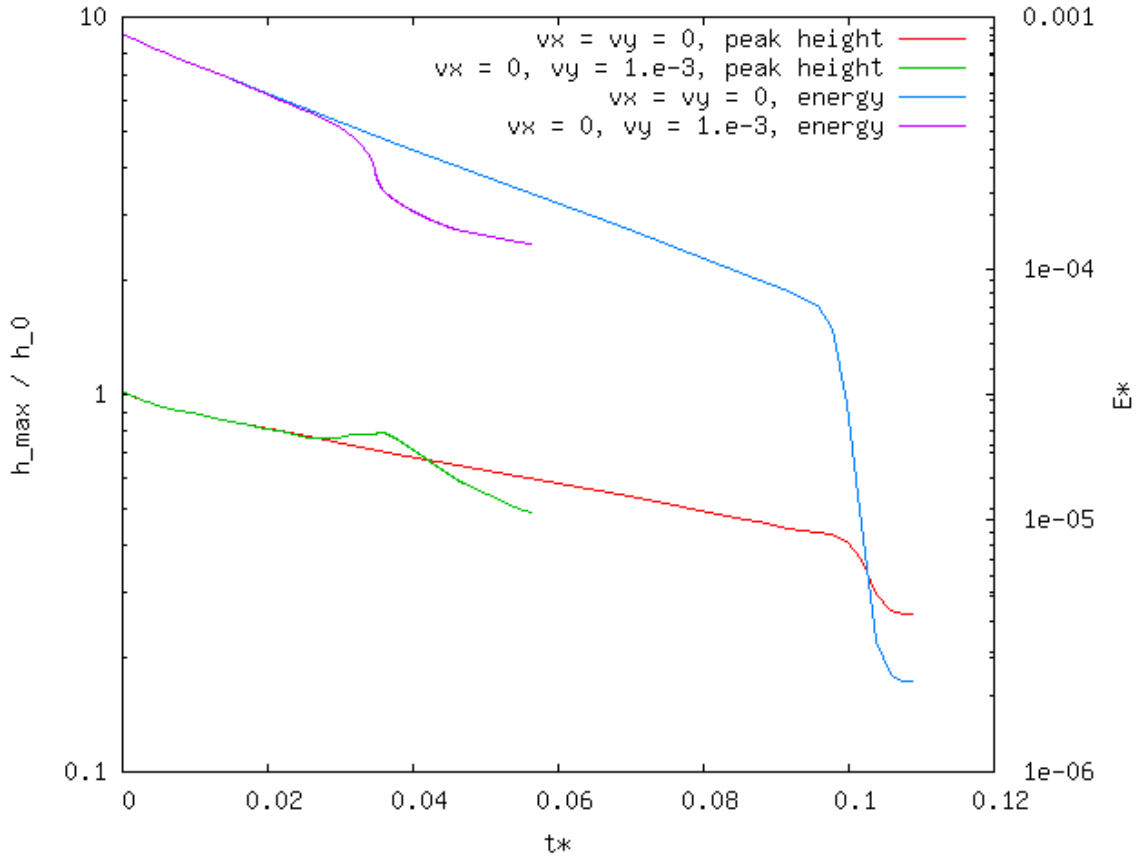

Figure 10.9: Decay of the height peak and surface energy using tensor mobility, with and without an electric field. The electric field is aligned with the y-axis and appears to accelerate a transition.

in this code, due to unresolved issues with the validation. We see that the height peak and surface energy follow an exponential decay in both cases, until the sudden drop corresponding to a transition. The transition happens earlier in the presence of an electric field, suggesting that the reinforced adatom fluxes are a plausible explanation for this phenomenon. The nondimensional time of the transition is now $t^* \approx 0.05$ in the presence of an electric field, corresponding to about half of the previously indicated time for the hypothetical material above.

For completeness we also show in Figure 10.10 the contour plots and streamlines computed with the electric field. Again we see that fluxes are *not* normal to level sets of height, so that large-perimeter steps have a chance to elongate before downhill or uphill mass transport causes them to collapse. In addition, the presence of an electric field seems to direct the fluxes into a pattern more conducive to straightening the large-perimeter steps than the $\mathbf{u} = 0$ simulation presented above. The reinforcement of adatom fluxes in the y-direction eventually assists the uphill and downhill mass transport as the profile tends to become 1-dimensional.

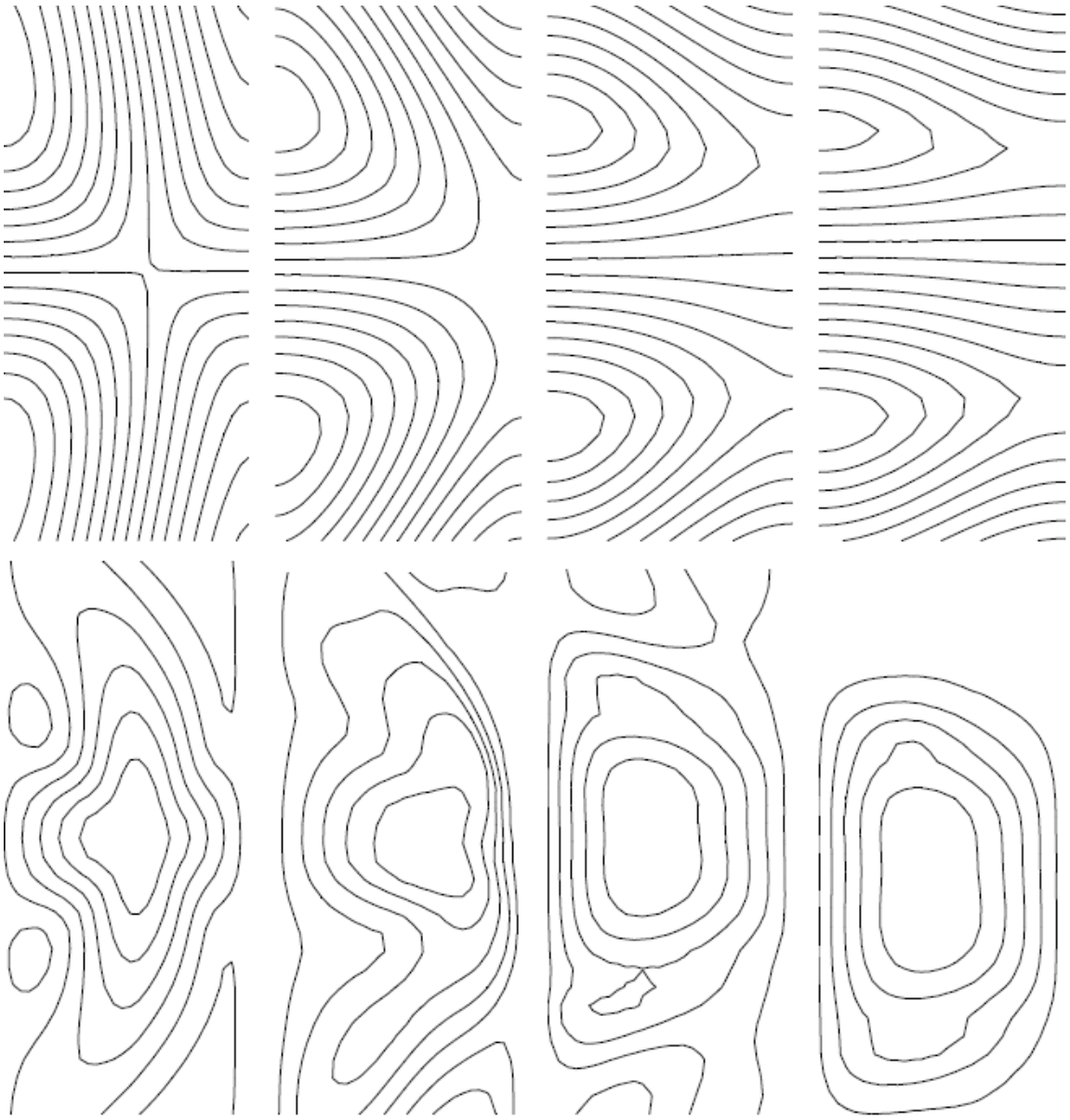

Figure 10.10: Snapshots during the transition from the initial data $h = h_0 \cos(k_1 x) \cos(k_2 y)$, $h_0/\lambda_x = 0.03$, $k_2/k_1 = 11/24$ to an eventually 1D profile, calculated using tensor mobility, drift velocity $(u_1, u_2) = (0, 10^{-3})$, and material parameters $q = 10^4$, $g_1/g_3 = 0$. Top row: level sets of height. Bottom row: streamlines, which are locally tangent to the vector adatom flux. Plot window is $[0, \lambda_x/2] \times [0, \lambda_y/2]$.

10.4 Continuous dependence on line tension of the 2D to 1D transition

Now that we have a basic idea of the macroscale surface evolution in the limiting case $g_1 = 0$, we address the question of whether our observations carry over to the case of *nonzero* g_1. Another possibility is that some of our observations arise only as a singular limit for $g_1 \to 0$, while others do persist and vary continuously with g_1.

The disappearance of facets at $g_1 = 0$ has been interpreted as a singular limit, prompting some materials scientists to view g_1 as an $\mathcal{O}(1)$ parameter that determines whether the Mullins above-roughening theory or the BCF step-based framework should be adopted [107]. Our perspective is more inclusive, treating the PDE derived from step flow as a tool with predictive value over a large range of g_1. The reliability of these predictions, however, depends in large part on the accuracy of our numerics.

In our approach, the $g_1 = 0$ case serves as a testbed from which to draw tentative conclusions about $g_1 > 0$, where simulations are currently incomplete. In addition, the PDE simulated here is the limit of step motion. Thus, the limit $g_1 \to 0$ of the macroscopic theory is essentially the $\lim_{g_1 \to 0} \lim_{a \to 0}$ of the step flow equations. In principle, this limit is expected to be different from $\lim_{a \to 0} \lim_{g_1 \to 0}$, in which the BCF theory is questionable or not valid.

While the results for $g_1/g_3 = 0$ were still being collected and discussed, we also began preliminary trials with g_1/g_3 nonzero. Returning to the idea of partitioning

the parameter space into regions based on their eventual evolution, we wondered about the shape of the separatrix between transition-supporting and transition-suppressing regions. One cross-section that we considered trying to plot was the restriction of this separatrix by keeping fixed the aspect ratio λ_x/λ_y, the initial amplitude h_0/λ_x, and the drift velocity $\mathbf{u}$. The resulting cross-section would be a curve in the $q - g_1/g_3$ plane, which we hypothesized to look something like Figure 10.11.

We conjectured a threshold q that *increases* with g_1/g_3, because the facet size grows more quickly for larger g_1/g_3, which would increase the contribution of transverse fluxes in the steeply-sloped regions between facets. The longitudinal fluxes can still be given time to effect a transition, if a larger value of q is used to slow down the uphill and downhill mass transport. The threshold q has been determined only for the smallest values of g_1/g_3 in Figure 10.11. The trend of threshold q for larger g_1/g_3 is merely speculated. As it turned out, the calculation of these threshold q values for larger g_1/g_3 was never completed, due to the enormous computational time our algorithm seemed to require. After further investigation, we attributed the uncharacteristically slow convergence of the method to an ill-conditioned linear system [6]. Work to address this ill-conditioning and to extend confidently our finite element implementation in the case of large g_1/g_3 is still an open problem [6, 77].

The more modest goal of considering only a single nonzero value of g_1/g_3, small enough for the numerical method to yield reliable results, led us to take $(g_1/g_3)(\lambda_x/h_0)^2 = 10^{-4}$. We simulated the relaxation using both (i) scalar and tensor mobilities, (ii) zero and nonzero drift velocities. Again the use of a tensor mobility produced a transition, which is marked by the abrupt change from pure

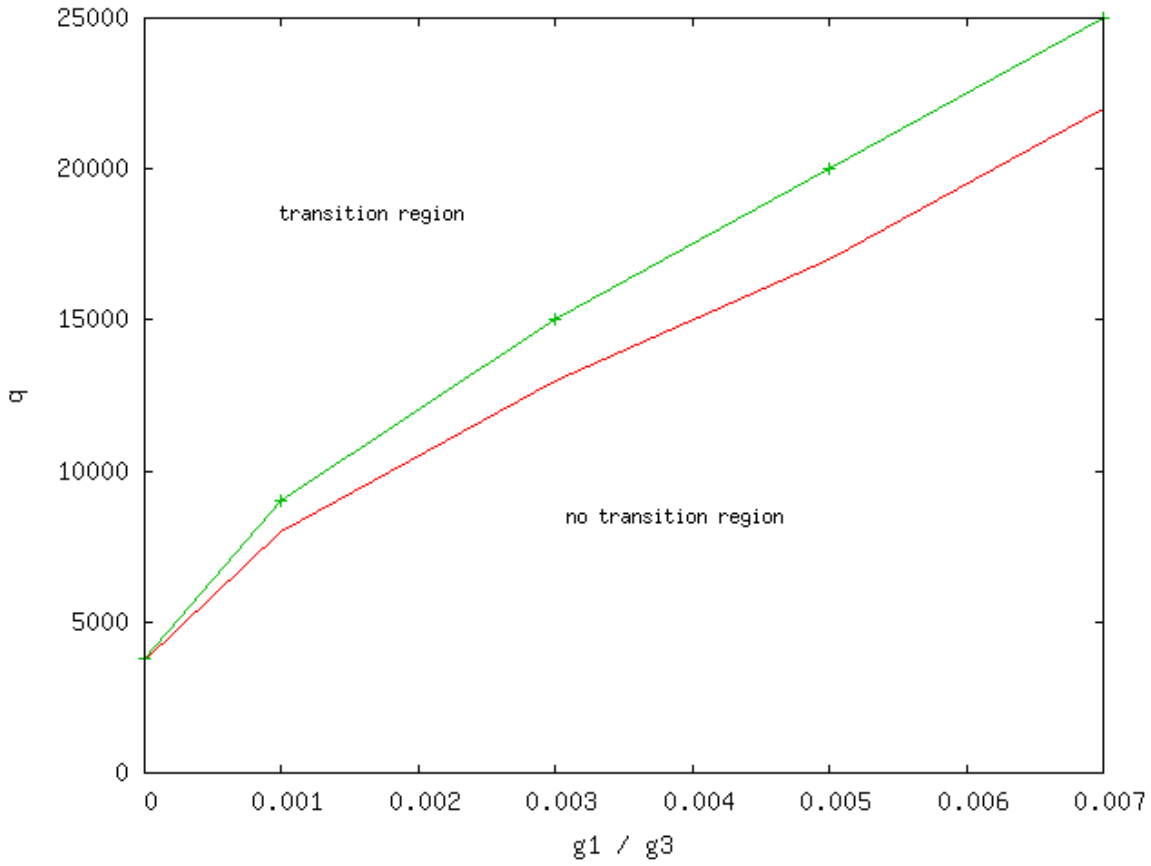

Figure 10.11: Speculation for the separatrix between transition-supporting and transition-suppressing regions, with fixed aspect ratio $\alpha = 2/3$, initial amplitude $h_0/\lambda_x = 0.03$, and drift velocity $\mathbf{u} = 0$. The upper (lower) curve would connect the computed $(g_1/g_3, q)$ pairs for which a transition does (does not) occur. The uncertainty (vertical distance between the two curves) of the separatrix ordinates can in principle be decreased using bisection. In practice, a good preconditioner is needed to stabilize the numerics when g_1/g_3 is large [6].

exponential behavior in the height peak and energy curves; see Figure 10.12. Note also that the presence of an electric field accelerates the transition. Evidently, the two major observations we made for zero g_1 are also true for this particular choice of nonzero g_1. It is tempting to conjecture that the transition and its acceleration by an electric field are *not* singular limits as $g_1/g_3 \to 0$.

10.5 Conclusions and open issues

The two major contributions of our modeling in this thesis are (i) a tensor mobility, which distinguishes between step-parallel and step-normal components of the macroscale flux $\mathbf{J}$, and (ii) an electric field, which leads to a convective term in the constitutive relation for $\mathbf{J}$. These contributions inspired and led directly to the (hopefully) novel phenomena predicted here by finite element simulations of the macroscale evolution equation. A tensor mobility, which for ADL kinetics makes longitudinal fluxes predominant, leads to a transition from initially biperiodic data to an eventually one-dimensional profile. The inclusion of an electric field reinforces adatom fluxes along a specified direction, thereby causing the transition to be observed earlier. These two effects appear to persist continuously as g_1/g_3 is allowed to take nonzero values.

The connection between our simulations and real materials is still elusive. The first reason is computational: at larger values of g_1/g_3 corresponding to real materials, our finite element implementation tries to solve an ill-conditioned matrix problem. The second reason is physical: the boundary conditions enforced by ap-

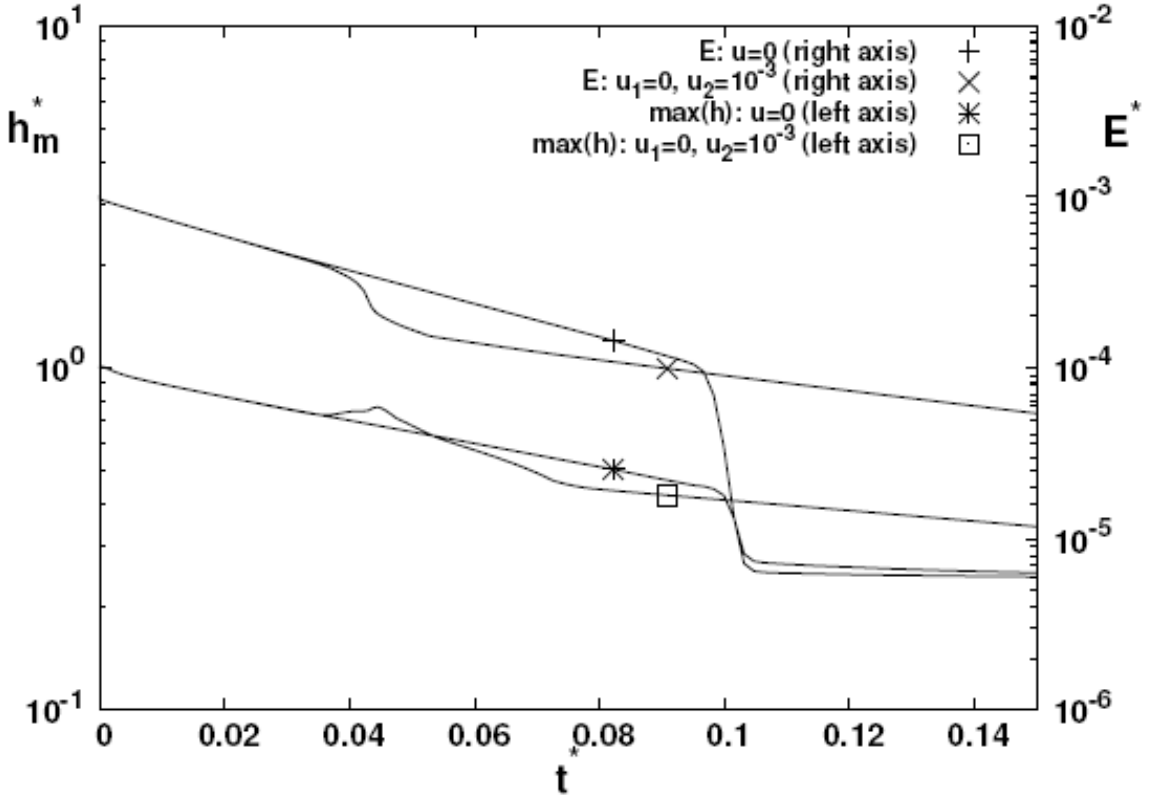

Figure 10.12: Log plots for maximum height $h_m^* = \max h/h_0$ (left axis) and surface energy E^* (right axis), taken from [7]. These simulations used tensor mobility, material parameters $(g_1/g_3)(\lambda_x/h_0)^2 = 10^{-4}$, $q = 10^4$, and initial data $h = h_0 \cos(k_1 x)\cos(k_2 y)$, $k_2/k_1 = 11/24$, $h_0/\lambda_x = 0.03$. A transition still occurs in the presence of a facet.

plying the finite element method over the entire domain $\mathcal{B}$ are *incompatible* with the boundary conditions stemming from the flow of steps [65]. Even if we had trustworthy numerical results for larger values of g_1/g_3, the weak formulation itself would be questionable.

We leave it for future numerical work to characterize how the predicted phenomena vary with increasing g_1/g_3. Pending issues include (i) finding a good preconditioner, so that the matrix problem given by our finite element equations is well-posed; (ii) enforcing more realistic boundary conditions, by restricting the domain of the PDE and informing the solution of microscale effects at the facet edge; and (iii) developing a numerical scheme for step flow in 2+1 dimensions, in order to determine the discrete sequence of collapse times for the top step [37].

The most promising route for connecting our macroscale theory to experiments is analytical, at least until the ill-conditioning problem is resolved and a hybrid scheme is adopted to incorporate step collapse times into the weak formulation. We also hope that ongoing research in metamaterials might lead to an engineered material with the precise set of parameters that numerical constraints forced us to use in our simulations. Lacking a suitable experimental setting that can be simulated reliably by our numerics, we leave it for future research to make a more specific connection with real materials. For now we can only report the noteworthy numerical results for a hypothetical material, which appear precisely because of the novel contributions of our macroscale model; namely, a tensor mobility and the macroscale drift due to electromigration.

Chapter 11

Epilogue: conclusions and open questions

In this thesis we have studied the macroscale consequences of different physical processes at the nanoscale, deriving PDEs to describe macroscopic surface relaxation in the absence of material deposition. Our main result is a macroscale analog of Fick's law relating surface flux to the chemical potential. We revisit these results by discussing correspondences between the terms of this relation and the underlying nanoscale processes. For convenient reference, we give once again the macroscale analog of Fick's law in the most general form found so far.

$$\mathbf{J} = -C_s \mathbf{M} \cdot \left[\nabla \mu - k_B T D^{-1} \mathbf{v} \left(1 + \frac{\mu}{k_B T} \right) \right] \tag{11.1}$$

Energetic considerations yield the formula for the macroscale step chemical potential, which remains invariant under changes of the nanoscale kinetic processes considered in this thesis:

$$\mu = -\Omega \operatorname{div} \left\{ g_1 \frac{\nabla h}{|\nabla h|} + g_3 |\nabla h| \nabla h \right\}. \tag{11.2}$$

The inclusion or suppression of the different possible nanoscale processes is reflected in the macroscale equation (11.1) by a linear superposition of effects, or a renormalization of parameters. As an example, consider the effect of step edge diffusion. By allowing for adatoms to diffuse along the step edge, we saw in chapter 6 that the $\sigma\sigma$ mobility element acquired an additional term proportional to the edge

Table 11.1: Macroscale consequences of several physical processes at the nanoscale. An asterisk next to "none" alerts the reader that the macroscale effects are deemed negligible, being of higher order in the expansion parameter a.

nanoscale process	**effect on M**	**effect on v**
isotropic diffusion	tensor character distinguishes between transverse and longitudinal fluxes, with diagonal form in the local coordinate representation	none
anisotropic diffusion	tensor form even in the local coordinate representation	none
step edge diffusion	additional term in the $m_{\sigma\sigma}$ element	none
step transparency	kinetic parameter $q = 2D/(ka)$ renormalized via $k \mapsto k + 2p$	none
electric field $\mathbf{E}$	none	proportional to $\mathbf{E}$
adatom desorption	none*	none*

diffusivity. Later, when studying the results of electromigration current, we saw that the macroscale equation acquired a convective term featuring the drift velocity $\mathbf{v}$. These correspondences are summarized in Table 11.1.

Although the description of step flow below roughening can vary appreciably depending on which nanoscale processes we include in the model, the macroscale limit is much more robust, taking the form of a standard conservation equation together with (11.1) and (11.2). Finding the same macroscale limit via homogenization theory [70] serves as further confirmation of the coarse-graining results shown here.

11.1 Summary of contributions

One macroscale PDE, with appropriate modification of the parameters, encompasses a wide range of step flow models within the BCF framework. We have studied representative versions of the macroscale evolution equation both numerically and analytically. These complementary approaches address different regimes in the parameter space, and different questions about the evolving surface morphology.

Numerically, we have simulated the macroscale PDE using a semi-implicit time scheme and the finite element method in space. We observe a 2D→1D transition under ADL kinetics, indicating that the tensor mobility distinguishes between step-normal and step-parallel fluxes. This transition appears to be accelerated by the application of an electric field in the direction of the longer initial wavelength. Our understanding of the transition phenomena is incomplete, but we hypothesize that a key contribution is the initially enhanced magnitude of longitudinal fluxes relative to transverse fluxes under ADL kinetics. The relevance of our numerical results to real materials is not immediate, owing to the restricted subset of the parameter space ($g_1/g_3 \ll 1$) that the finite element method could handle reliably. Preliminary computations with *nonzero* but *small* g_1/g_3 suggest that the 2D→1D transition persists continuously as g_1/g_3 is allowed to take on small positive values. This continuous dependence on g_1/g_3 offers the promise of an eventual connection with real materials, or even engineered *metamaterials*.

Analytically, we have looked for approximately separable solutions of the macroscale PDE for surface height, predicting novel decay laws for some regions

of the parameter space. We have studied the possibility of a boundary layer near a facet edge, finding a boundary layer width that scales as a power of g_1/g_3 in the regime where g_1/g_3 is large. We have also characterized the effect of an electric field on the slope profile near a facet. These latter two predictions offer the most promising connection with real materials, whose parameter values challenge the reliability of our numerical method.

11.2 Open questions

An ambitious research program inevitably raises more questions than it answers. We list below some of the pending issues that this thesis could not address.

- **Stabilizing the numerics for larger values of** g_1/g_3. As indicated in Chapter 10, we lack a reliable simulation of the macroscale PDE for values of the parameter g_1/g_3 of the order of unity. The usual way to address this numerical instability is by means of a preconditioning matrix. An open problem is to develop an accurate and efficient preconditioner for the matrix equation given by the finite element method.

- **Higher-order time stepping.** Much of the discrepancy between different simulations could be attributed to the choice of adaptive time step [6]. In contrast, the calculated decay of height peak and energy were rather robust with respect to mesh size [6]. Perhaps a fruitful direction to pursue is the modification of our algorithm to reduce the time discretization errors.

- **Comparison of macroscale simulations with step flow in 2D.** Valida-

tion of the macroscale theory is commonly done by comparing its predictions with those of an atomistic simulation, as in the work of Shenoy et al. [107, 108]. Since our derivation of the macroscale PDE begins with the generalized BCF model rather than atomistic physics, it might be instructive to compare a step flow simulation with the results of this thesis. The step-flow model of Weeks et al. [122], which has been implemented numerically by Kan et al. [45], offers a promising means of comparison. A crucial question is whether the material parameters used in simulations of Weeks' model are within the scope of our finite element method. (Note that extensive comparisons of step flow with PDEs have been carried out for one-dimensional geometries [25, 79].)

- **Boundary conditions at facet edges.** As discussed in Chapter 9, the variational formulation of our evolution equation does not respect the boundary conditions arising from the microstructure at a facet edge. An open problem is the development of a *hybrid approach*, which would couple the variational implementation of a fully continuum PDE with collapse time data from the flow of steps near facets.

- **Further analysis of the macroscale PDE.** All of our numerics assumed a spatially periodic solution whose period remained unchanged throughout the simulation. The analytical justification of this assumption is still lacking. Other qualitative features of the computed surface morphology, such as the non-monotonic decay of height peak, could likewise be subject to analysis. The question of backwards uniqueness in time is also of physical significance,

as indicated in the following.

- **Inverse problem.** To make our modeling more attractive to the materials engineering community, we might want to analyze whether a desired surface pattern can emerge from self-organization of an initial profile, which relaxes near equilibrium according to the flow of steps below roughening. This question is an obvious analog for our macroscale PDE of the backwards uniqueness property for the heat equation. We essentially want to characterize which "final data" can successfully be evolved backward in time by our fourth-order nonlinear PDE. This characterization might involve the Fourier components of the final data (as in the case of the heat equation), or perhaps a more restrictive set of conditions. If we manage by analytical means to address backwards uniqueness satisfactorily, we might then try to implement a numerical algorithm to approximate the solution of the inverse problem.

- **Stochastic effects.** In this thesis we performed coarse-graining for a completely *deterministic* BCF-type model. Stochastic effects (especially the effect of noise at the nanoscale) were *not* studied. A more realistic picture of the nanoscale physics would allow for the fluctuation of step edges by adding noise terms to the step flow equations. An interesting problem is then to derive the macroscale limit from these stochastic differential equations.

- **Far-from-equilibrium conditions.** Throughout this thesis we assumed the surface to evolve near equilibrium. In this vein we have focused entirely on relaxation phenomena, omitting the effect of material deposition. The under-

standing we gain from studying relaxation is expected to carry through to far-from-equilibrium conditions, because relaxation by surface diffusion is always present in evolving surfaces. However, the far-from-equilibrium setting is found to yield qualitatively different macroscale equations [11, 68, 69], which are of interest in their own right and for the connection they promise with modern experiments in epitaxial growth.

Appendix A
Brief review of the Mellin transform

In this Appendix, we introduce the Mellin transform starting from the more familiar Laplace integral transform. Motivated by the eventual use of the Mellin transform in asymptotic expansion of integrals, we include only those technical details needed to facilitate this application. The extension to iterated integrals and inversion formulas in higher dimensions are not needed for our purposes; the reader is directed to [100] for a more thorough discussion of these issues.

Many problems in engineering and applied mathematics are cumbersome to solve when expressed in the relevant physical variables. Integral transforms were developed to address this difficulty. The role of an integral transform is to map an equation from the original domain (e.g., physical space or time) into another domain (e.g., wavenumber or frequency space) where the computations are simpler. The solution in the transformed domain is then pulled back to the physical domain by the inverse transform.

The Laplace transform is well-known for its use in ordinary differential equations (ODEs): by taking the Laplace transform of a linear ODE, we obtain an algebraic equation for the transform of the ODE solution. After solving the resulting algebraic equation, we can apply the inverse Laplace transform to express the solution in the original variable. This idea is made rigorous by the following

Definition A.0.1. *For a function* $f : \mathbb{R} \to \mathbb{R}$*, the* two-sided Laplace transform $\hat{f}(s)$ *is given by:*

$$\hat{f}(s) = \int_{-\infty}^{\infty} f(t)e^{-st}dt. \tag{A.1}$$

The original function $f(t)$ is recovered from $\hat{f}(s)$ by the inverse Laplace transform*:*

$$f(t) = \frac{1}{2\pi\imath} \int_{\gamma-\imath\omega}^{\gamma+\imath\omega} \hat{f}(s) e^{st} ds, \tag{A.2}$$

where γ is a real number so that the integration path lies in the region of convergence of $\hat{f}(s)$.

For asymptotic expansion of integrals, it turns out to be more convenient to use an integral transform whose kernel is a power function rather than an exponential. In this vein, we let $x = e^t$, $\mathrm{d}x = x\mathrm{d}t$ in (A.1), which yields

$$\hat{f}(s) = \int_0^\infty f(\ln x) x^{-s} \frac{\mathrm{d}x}{x}. \tag{A.3}$$

We introduce $F(x)$ to denote the composite function $f(\ln x)$, and $-\zeta = -s - 1$ to denote the power of x. The resulting integral, viewed as a function of ζ, is called the *Mellin transform* and written $\hat{F}(\zeta)$, i.e.,

$$\hat{F}(\zeta) = \int_0^\infty F(x) x^{-\zeta} \mathrm{d}x. \tag{A.4}$$

We break up the integral (A.4) into two parts when studying its convergence properties:

$$\hat{F}(\zeta) = \left(\int_0^1 + \int_1^\infty \right) F(x) x^{-\zeta} \mathrm{d}x. \tag{A.5}$$

The restrictions on ζ for convergence of (A.5) emerge from enforcing boundedness of the two integrals separately. We have a bound for the first integral,

$$\left| \int_0^1 F(x) x^{-\zeta} \mathrm{d}x \right| \leq \int_0^1 |F(x)| x^{-\mathrm{Re}\zeta} \mathrm{d}x, \tag{A.6}$$

where $\mathrm{Re}\zeta$ denotes the real part of ζ. Suppose that $F(x) = \mathcal{O}(x^p)$ as $x \to 0$. This first integral converges if $p - \mathrm{Re}\zeta > -1$, or $\mathrm{Re}\zeta < 1 + p$.

On the other hand, we have for the second integral

$$\left| \int_1^\infty F(x) x^{-\zeta} \mathrm{d}x \right| \leq \int_1^\infty |F(x)| x^{-\mathrm{Re}\zeta} \mathrm{d}x. \tag{A.7}$$

If $F(x) = \mathcal{O}(x^q)$ as $x \to \infty$, then the convergence of the second integral requires $q - \mathrm{Re}\zeta < -1$, or $1 + q < \mathrm{Re}\zeta$. Together with the first condition on ζ, we find the *fundamental strip* $1 + q < \mathrm{Re}\zeta < 1 + p$, which indicates the region in the complex ζ plane where the integral defining the Mellin transform converges.

The *inverse Mellin transform* is obtained from $\hat{F}(\zeta)$ by the same contour integral as (A.2):

$$F(x) = f(\ln x) = \frac{1}{2\pi\imath} \int_{\gamma-\imath\omega}^{\gamma+\imath\omega} \hat{F}(\zeta) x^{\zeta-1} \mathrm{d}\zeta. \tag{A.8}$$

For the asymptotic evaluation of integrals, where $F(x)$ is defined by an integral with a "large" or "small" variable x, this formulation is useful when the Mellin transform $\hat{F}(\zeta)$ is *meromorphic*. Then the only singularities of $\hat{F}$ are poles in the complex ζ plane, and an asymptotic expansion for F can be calculated by applying the Cauchy residue theorem. Care must be taken to ensure that the integration path is deformed to account for the sign of $\ln x$ and the strip of convergence.

The Mellin transform is useful when $F(x)$ is defined by a definite integral with "large" or "small" parameter x, and the main contribution to this integral cannot be attributed to isolated values of the integration variable. Indeed, classical asymptotic approaches, such as the steepest descent or the stationary phase methods, are usually sufficient in such cases. When the contribution to $F(x)$ comes from an extended interval in the domain of integration, the Mellin transform helps by mapping this contribution to an isolated singularity in the transformed ζ space. The required

calculation is often easier in the transformed domain, as we see in Chapter 4 when studying the integral for elastic interaction energy.

Appendix B
Nondimensionalization of the evolution equations

In this chapter we rewrite the evolution equations for the macroscale surface height in nondimensional form. These equivalent representations allow for a more systematic numerical treatment of relaxation experiments. We find that for relaxation of initially sinusoidal profiles, any collection of material and geometric parameters can be thought of as a point $\mathbf{p}$ in $\mathbb{R}^6$, with coordinates λ_x/λ_y, h_0/λ_x, $\lambda_x D^{-1}\mathbf{v}$, q, g_1/g_3. If a certain crystal surface is specified, then q and g_1/g_3 are not independent; both quantities are related through the temperature T. If the crystal surface is not specified, then varying q and g_1/g_3 independently has the same effect as considering many different possible materials over a wide range of temperatures.

The subset of $\mathbb{R}^6$ corresponding to physically realizable parameters can be further partitioned according to the distinct morphological changes that the macroscale PDE allows. One such partition, distinguishing between initial data that supports a 2D $\rightarrow$ 1D transition and initial data that prohibits such a transition, has been illustrated in [7] as cross-sections in the q, α plane, where $\alpha = \lambda_x/\lambda_y$ is the aspect ratio. To extract from these plots the initial conditions for an experimental comparison with real materials, we need to undo the nondimensionalization of the simulated equations. Undoing this nondimensionalization will determine all the terms of the

original macroscale PDE, rewritten here in the universal form

$$\frac{\partial h}{\partial t} = \Omega C_s D \operatorname{div}\left\{\mathbf{\Lambda}\cdot\left[\frac{\nabla\mu}{k_BT} - D^{-1}\mathbf{v}\left(1+\frac{\mu}{k_BT}\right)\right]\right\}, \tag{B.1}$$

$$\mu = -\Omega g_3 \operatorname{div}\left\{\frac{g_1}{g_3}\frac{\nabla h}{|\nabla h|} + |\nabla h|\nabla h\right\}, \tag{B.2}$$

where $\mathbf{\Lambda}$ is the dimensionless mobility tensor.

The initial data has characteristic lengths λ_x, λ_y in the basal plane, and h_0 in the vertical direction. Accordingly, we define nondimensional spatial variables by

$$\tilde{x} = x/\lambda_x, \tag{B.3}$$

$$\tilde{y} = y/\lambda_y, \tag{B.4}$$

$$\tilde{h} = h/h_0. \tag{B.5}$$

To compute spatial derivatives, we define the operators ∇_α and $\operatorname{div}_\alpha$ by

$$\nabla_\alpha = (\partial_{\tilde{x}}, \alpha\partial_{\tilde{y}}), \tag{B.6}$$

$$\operatorname{div}_\alpha = \partial_{\tilde{x}} + \alpha\partial_{\tilde{y}}, \tag{B.7}$$

which are related to the usual operators ∇ and div in an obvious way:

$$\nabla_\alpha = \lambda_x\nabla \quad \text{and} \quad \operatorname{div}_\alpha = \lambda_x \operatorname{div}. \tag{B.8}$$

The nondimensional chemical potential $\tilde{\mu}$ and drift velocity $\mathbf{u}$ are defined as

$$\tilde{\mu} = \frac{\mu}{k_BT}, \tag{B.9}$$

$$\mathbf{u} = \lambda_x D^{-1}\mathbf{v}. \tag{B.10}$$

Applying (B.3)–(B.8) to (B.2), we find

$$\mu = -\frac{\Omega g_3 h_0^2}{\lambda_x^3}\operatorname{div}_\alpha\left(\frac{g_1\lambda_x^2}{g_3h_0^2}\frac{\nabla_\alpha\tilde{h}}{|\nabla_\alpha\tilde{h}|} + |\nabla_\alpha\tilde{h}|\nabla_\alpha\tilde{h}\right). \tag{B.11}$$

The prefactor in (B.11) requires us to find $\tilde{\mu}$ by solving

$$\tilde{\mu} = -\frac{\Omega g_3 h_0^2}{k_B T \lambda_x^3} \operatorname{div}_\alpha \left(\frac{g_1 \lambda_x^2}{g_3 h_0^2} \frac{\nabla_\alpha \tilde{h}}{|\nabla_\alpha \tilde{h}|} + |\nabla_\alpha \tilde{h}| \nabla_\alpha \tilde{h} \right). \tag{B.12}$$

Substituting (B.3)–(B.10) into the PDE (B.1), we find

$$\frac{\partial \tilde{h}}{\partial t} = \frac{\Omega C_s D}{\lambda_x^2 h_0} \operatorname{div}_\alpha \{ \mathbf{\Lambda} \cdot [\nabla_\alpha \tilde{\mu} - \mathbf{u}(1 + \tilde{\mu})] \}. \tag{B.13}$$

The prefactor in (B.13) suggests that we choose a time unit t_0 given by

$$t_0 = \frac{h_0 \lambda_x^2}{\Omega C_s D}, \tag{B.14}$$

so that $\tilde{t} = t/t_0$ is nondimensional.

In light of (B.12), (B.13), the numerical implementation of the macroscale height evolution with drift $\mathbf{u} \neq 0$ requires that we rescale *three* coefficients in the code: the line tension coefficient g_1/g_3, the material parameter q appearing in $\mathbf{\Lambda}$, and the prefactor in (B.12). The nondimensional time can absorb only the prefactor in (B.13). In contrast, for $\mathbf{u} = 0$ the nondimensional time can also absorb the prefactor of (B.12), thereby reducing the number of rescaled coefficients to two: g_1/g_3 and q. This procedure is adopted in Chapter 10, where our time unit is chosen as $t_0 = \frac{k_B T \lambda_x^5}{\Omega^2 C_s g_3 D h_0}$.

Bibliography

[1] Abramowitz M and Stegun I 1964, *Handbook of Mathematical Functions with Formulas, Graphs, and Mathematical Tables*, (10th ed., National Bureau of Standards, 1972).

[2] Atkinson C and Wilmott P 1994, *Interactions of continuous distributions of ledges*, Proc. Roy. Soc. London Ser. A **446**, 277–287.

[3] Balykov L and Voigt A 2006, *A 2+1 -dimensional terrace-step-kink model for epitaxial growth far from equilibrium*, Multiscale Model. Simul. **5**, 45–61.

[4] Blakely J, Umbach C and Tanaka S 1997, *Atomic steps in the decay of 1- and 2-dimensional gratings*, in Dynamics of Crystal Surfaces and Interfaces, ed. Duxbury P and Pence T, Plenum, New York, NY.

[5] Boas M L 1984 *Mathematical Methods in the Physical Sciences*, Wiley, New York, NY.

[6] Bonito A 2007–2009, private discussions.

[7] Bonito A, Nochetto R, Quah J and Margetis D 2009, *Self-organization of decaying surface corrugations: A numerical study*, Phys. Rev. E. **79**, 050601/1–4.

[8] Bonito A, Nochetto R, Margetis D, in preparation.

[9] Braess D 2001, *Finite Elements: Theory, Fast Solvers, and Applications in Solid Mechanics*, Cambridge University Press, Cambridge, UK.

[10] Burton W K, Cabrera N, and Frank F C 1951, *The growth of crystals and the equilibrium structure of their surfaces*, Philos. Trans. R. Soc. London, Ser. A **243** 299–358.

[11] Caflisch R E, E W, Gyure M F, Merriman B and Ratch C 1999, *Kinetic model for a step edge in epitaxial growth*, Phys. Rev. E **3**, 6879–6887.

[12] Chang J, Pierre-Louis O and Misbah C 2006, *Birth and morphological evolution of step bunches under electromigration*, Phys. Rev. Lett., **96**, 195901/1–4.

[13] Danker G, Pierre-Louis O, Kassner K and Misbah C 2004, *Peculiar effects of anisotropic diffusion on dynamics of vicinal surfaces*, Phys. Rev. Lett. **93**, 185504/1–4.

[14] Degawa M, Minoda H, Tanishiro Y and Yagi K 2001, *In-phase step wandering on Si(111) vicinal surfaces:Effect of direct current heating tilted from the step-down direction*, Phys. Rev. B **63**, 045309/1–8.

[15] Dufay M, Frisch T and Debierre J-M 2007, *Role of step-flow advection during electromigration-induced step bunching*, Phys. Rev. B **75**, 241304/1–4.

[16] E W and Yip N K 2001, *Continuum theory of epitaxial crystal growth I*, J. Statist. Phys. **104**, 221–253.

[17] Ehrlich G and Hudda F 1966, *Atomic view of surface self diffusion: Tungsten on tungsten*, J. Chem. Phys. **44**, 1039–1099.

[18] Erdélyi A 1981, ed., *Bateman Manuscript Project: Higher Transcendental Functions, Vol. I*, Krieger, Malabar, FL.

[19] Erdélyi A 1981, ed., *Bateman Manuscript Project: Higher Transcendental Functions, Vol. II*, Krieger, Malabar, FL.

[20] Erlebacher J, Aziz M J, Chason E, Sinclair M B and Floro J A 2000, *Nonclassical smoothening of nanoscale surface corrugations*, Phys. Rev. Lett. **84**, 5800–5803.

[21] Eshelby J D 1956, *The continuum theory of lattice defects*, Solid State Phys. **3**, 79–144.

[22] Evans J W, Thiel P A and Bartelt M C 2006, *Morphological evolution during epitaxial thin film growth: Formation of 2D islands and 3D mounds*, Surf. Sci. Reports **62** 1–128.

[23] Evans J W 2008, *Step dynamics modeling of multilayer growth*, minisymposium 55, SIAM conference Philadelphia, PA.

[24] Evans L C 2002, *Partial Differential Equations*, AMS, Providence, RI.

[25] Fok P-W 2006, *Simulation of Axisymmetric Stepped Surfaces with a Facet*, MIT Ph.D. thesis.

[26] Fok P-W, Rosales R R, and Margetis D 2007, *Unification of step bunching phenomena on vicinal surfaces*, Phys. Rev. B **76**, 033408/1–4.

[27] Frisch T and Verga A 2005, *Kinetic step bunching instability during surface growth*, Phys. Rev. Lett., **94**, 226102/1–4.

[28] Fu E S, Liu D-J, Johnson M D, Weeks J D, and Williams E D 1997, *The effective charge in surface electromigration*, Surf. Sci. **385**, 259–269.

[29] Ghez R and Iyer S S 1988, *The kinetics of fast steps on crystal surfaces and its application to the molecular beam epitaxy of silicon*, IBM J. Res. Develop. **32**, 804–818.

[30] Gruber E E and Mullins W W 1967, *On the theory of anisotropy of crystalline surface tension*, J. Phys. Chem. Solids **28**, 875–887.

[31] Hager J and Spohn H 1995, *Self-similar morphology and dynamics of periodic surface profiles below the roughening transition*, Surf. Sci. **324**, 365–372.

[32] Hecht F, Pironneau O, Le Hyaric A and Ohtsuka K 2008, *FreeFem++* (online documentation), accessed May 2008 at `http://www.freefem.org/ff++/ftp/freefem++doc.pdf`.

[33] Herring C 1949, *Effect of change of scale on sintering phenomena*, J. Appl. Phys. **21**, 301.

[34] Herring C 1951, *Surface tension as a motivation for sintering*, in The Physics of Powder Metallurgy, ed W E Kingston, McGraw Hill, New York, NY, 143–179.

[35] Ho P S and Kwok T 1989, *Electromigration in metals*, Rep. Prog. Phys. **52**, 301–348.

[36] Israeli N and Kandel D 1998, *Profile scaling in decay of nanostructures*, Phys. Rev. Lett. **80**, 3300–3303.

[37] Israeli N and Kandel D 1999, *Profile of a decaying crystalline cone*, Phys. Rev. B **60**, 5946–5962.

[38] Israeli N and Kandel D 2000, *Decay of one-dimensional surface modulations*, Phys. Rev. B **62**, 13707–13717.

[39] Israeli N and Kandel D 2002, *Comment on "Nonclassical smoothening of nanoscale surface corrugations"*, Phys. Rev. Lett. **88**, 169601.

[40] Jackson J D 1999, *Classical Electrodynamics*, Wiley, New York, NY.

[41] Jayaprakash C, Saam W F, and Teitel S 1983, *Roughening and facet formation in crystals*, Phys. Rev. Lett. **50**, 2017–2020.

[42] Jayaprakash C, Rottman C, and Saam W F 1984, *Simple model for crystal shapes: Step-step interactions and facet edges*, Phys. Rev. B **30**, 6549–6554.

[43] Jeong H-C and Williams E D 1999, *Steps on surfaces: Experiments and theory*, Surf. Sci. Reports **34**, 171–294.

[44] Joós B, Einstein T L, and Bartelt N C 1991, *Distribution of terrace widths on a vicinal surface within the one-dimensional free-fermion model.* Phys. Rev. B **43**, 8153–8162.

[45] Kan H-C, Kwon T and Phaneuf R J 2008, *Effect of length scales in directing step bunch self-organization during annealing of patterned vicinal Si(111) surfaces: Comparison with a simple near-equilibrium model*, Phys. Rev. B **77**, 205401/1–6.

[46] Kandel D and Kaxiras E 1996, *Microscopic theory of electromigration on semiconductor surfaces*, Phys. Rev. Lett. **76**, 1114–1117.

[47] Kashima Y 2005, *A subdifferential formulation of fourth order singular diffusion equations*, Adv. Math Sci. Appl. **14**, 49–74.

[48] Keefe M E, Umbach C C and Blakely J M 1994, *Surface self-diffusion on Si from the evolution of periodic atomic step arrays*, J. Phys. Chem. Solids **55**, 965–973.

[49] Kevorkian J and Cole J D 1996, *Multiple scale and singular perturbation methods*, Springer, New York, NY.

[50] Kosevich A M 1972, *Osnovy mechaniki kristallicheskoĭ* (Fundamentals of Crystal Lattice Mechanics), Nauka, Moscow.

[51] Krug J 1997, *On the shape of wedding cakes*, J. Statist. Phys. **87**, 505–518.

[52] Krug J 2005, *Introduction to step dynamics and step instabilities*, in Multiscale Modeling of Epitaxial Growth, ed A Voigt, International Series of Numerical Mathematics **149**, Birkhäuser, Basel, Switzerland, 69–96.

[53] Krug J, Tonchev V, Stoyanov S, and Pimpinelli A 2005, *Scaling properties of step bunches induced by sublimation and related mechanisms*, Phys. Rev. B, **71**, 045412/1–15.

[54] Krug J 2007, private communication.

[55] Krug J 2009, *Nonlinear dynamics of surface steps*, preprint, cond-math.mtrl-sci/arXiv:0810.5749.

[56] Kubo R and Nagamiya T 1969, *Solid State Physics* ed R S Knox, McGraw Hill, New York, NY.

[57] Kukta R V, Peralta A, and Kouris D 2002, *Elastic interaction of surface steps: Effect of atomic-scale roughness*, Phys. Rev. Lett. **88**, 186102/1–4.

[58] Landau L D and Lifshitz E M 1965, *Teoriya uprugosti*, Nauka, Moscow. (Theory of Elasticity, 2nd ed., Pergamon Press, Oxford, 1970).

[59] Latyshev A V, Aseev A L, Krasilnikov A B, and Stenin S I 1989, *Transformations on clean Si(111) stepped surface during sublimation*, Surf. Sci. **213**, 157–169.

[60] Liu D-J and Weeks J D 1998, *Quantitative theory of current-induced step bunching on Si(111)*, Phys. Rev. B **57**, 14891–14900.

[61] Liu D-J, Weeks J D, and Kandel D 1998, *Current-induced step bending instability on vicinal surfaces*, Phys. Rev. Lett. **81**, 2743–2746.

[62] Lo T S and Kohn R V 2002, *A new approach to the continuum modeling of epitaxial growth: slope selection, coarsening, and the role of the uphill current*, Physica D **161**, 237–257.

[63] Marchenko V I and Parshin A Ya 1980, *Elastic properties of crystal surfaces*, Soviet Phys. JETP **52**, pp 129–131.

[64] Margetis D, Aziz M J and Stone H 2005, *Continuum approach to self-similarity and scaling in morphological relaxation of a crystal with a facet*, Phys. Rev. B **71**, 165432/1–22.

[65] Margetis D, Fok P-W, Aziz M J and Stone H A 2006, *Continuum theory of nanostructure decay via a microscale condition*, Phys. Rev. Lett. **97**, 096102/1–4.

[66] Margetis D and Kohn R V 2006, *Continuum relaxation of interacting steps on crystal surfaces in 2+1 dimensions*, Multiscale Model. Simul. **5**, 729–758.

[67] Margetis D 2007, *Unified continuum approach to crystal surface morphological relaxation*, Phys. Rev. B **76**, 193403/1–4.

[68] Margetis D and Caflisch R E 2008, *Anisotropic step stiffness from a kinetic model of epitaxial growth*, Multiscale Model. Simul. **7**, 242–273.

[69] Margetis D and Kohn R V, *Continuum theory of material deposition on stepped surfaces in 2+1 dimensions*, in preparation.

[70] Margetis D 2009, *Homogenization of reconstructed crystal surfaces: Fick's law of diffusion*, Phys. Rev. E **79**, 052601/1–4.

[71] Margetis D 2009, *Steps in 2D*, lecture notes.

[72] Métois J J, Heyraud J C, and Stoyanov S 2001, *Step flow growth of vicinal (111) Si surface at high temperatures: step kinetics or surface diffusion control*, Surf. Sci. **486**, 95–102.

[73] Michely T and Krug J 2004, *Islands, Mounds and Atoms, Patterns and Processes in Crystal Growth Far from Equilibrium*, Springer, Heidelberg.

[74] Misbah C and Pierre-Louis O 1996, *Pulses and disorder in a continuum version of step-bunching dynamics*, Phys. Rev. E, **53**, R4318–R4321.

[75] Mullins W W 1957, *Theory of thermal grooving*, J. Appl. Phys. **28** 333–339.

Mullins W W 1959, *Flattening of a nearly plane solid surface due to capillarity*, J. Appl. Phys. **30** 77–83.

[76] Najafabadi R and Srolovitz D J 1994, *Elastic step interactions on vicinal surfaces of fcc metals*, Surf. Sci. **317**, 221–234.

[77] Nochetto R H 2007–2009, private discussions.

[78] Nozières P 1987, *On the motion of steps on a vicinal surface*, J. Phys. (France) **48**, 1605–1608.

[79] Odisharia I V 2006, *Simulation and Analysis of the Relaxation of a Crystalline Surface*, NYU Ph.D. thesis.

[80] Ozdemir M and Zangwill A 1990, *Morphological equilibration of a corrugated crystalline surface*, Phys. Rev. B **42**, 5013–5024.

[81] Ozdemir M and Zangwill A 1992, *Morphological equilibration of a facetted crystal*, Phys. Rev. B **45**, 3718–3729.

[82] Paulin S, Gillet F, Pierre-Louis O and Misbah C 2001, *Unstable step meandering with elastic interactions*, Phys. Rev. Lett. **86**, 5538–5541.

[83] Pedemonte L, Bracco G, Boragno C, Buatier de Mongeot F and Valbusa U 2003, *Smoothing of nanoscale surface ripples studied by He atom scattering*, Phys. Rev. B **68**, 115431/1–6.

[84] Pfeiffer R S and Mahan G D 1993, *Mean-field theory of elastic dipoles on a face-centered-cubic lattice*, Phys. Rev. B **48**, 669–671.

[85] Phaneuf R 2007–2009, private discussions.

[86] Pierre-Louis O, Misbah C, Saito Y, Krug J and Politi P 1998, *New nonlinear evolution equation for steps during molecular beam epitaxy on vicinal surfaces*, Phys. Rev. Lett. **80**, 4221–4224.

[87] Pierre-Louis O 2001, *Continuum model for low temperature relaxation of crystal steps*, Phys. Rev. Lett. **87**, 106104/1–4.

[88] Pierre-Louis O 2003, *Step bunching with general step kinetics: stability analysis and macroscopic models*, Surf. Sci. **529**, 114–134.

[89] Pierre-Louis O 2003, *Phase field models for step flow*, Phys. Rev. E **68**, 021604/1–19.

[90] Pierre-Louis O and Métois J 2004, *Kinetic step pairing*, Phys. Rev. Lett. **93**, 165901/1–4.

[91] Pierre-Louis O 2005, *Dynamics of crystal steps*, Comptes Rendus Physique, **6**, 11–21.

[92] Pierre-Louis O 2006, *Local electromigration model for crystal surfaces*, Phys. Rev. Lett. **96**, 135901/1–4.

[93] Pimpinelli A and Villain J 1998, *Physics of Crystal Growth*, Cambridge University Press, Cambridge, UK.

[94] Politi P and Villain J 1996, *Ehrlich-Schwoebel instability in molecular-beam epitaxy: A minimal model*, Phys. Rev. B **54**, 5114–5129.

[95] Politi P and Misbah C 2006, *Nonlinear dynamics in one dimension: A criterion for coarsening and its temporal law*, Phys. Rev. E **73**, 036133/1–15.

[96] Quah J and Margetis D 2008, *Anisotropic diffusion in continuum relaxation of stepped crystal surfaces*, J. Phys. A: Math. Theor. **41**, 235004/1–18.

[97] Quah J and Margetis D 2009, *Electromigration in macroscopic relaxation of stepped surfaces*, submitted to Multiscale Model. Simul.

[98] Rettori A and Villain J 1988, *Flattening of grooves on a crystal surface: A method of investigation of surface roughness*, J. Phys. (France) **49**, 257–267.

[99] `http://www.sandia.gov/surface_science/stm`

[100] Sasiela R J and Shelton J D 1993, *Integral evaluation using Mellin transform methods*, J. Math. Phys. **34**, 2572–2617.

[101] Sato M, Uwaha M, Saito Y, and Hirose Y 2002, *Step wandering induced by the drift of adatoms in a conserved system*, Phys. Rev. B, **65**, 245427/1–6.

[102] Sato M, Uwaha M, and Saito Y 2005, *Evaporation and impingement effects on drift-induced step instabilities on a Si(001) vicinal surface*, Phys. Rev. B **72**, 045401/1–9.

[103] Schimschak M and Krug J 1997, *Surface electromigration as a moving boundary value problem*, Phys. Rev. Lett. **78**, 278–281.

[104] Schulze T P and E W 2001, *A continuum model for the growth of epitaxial films*, J. Cryst. Growth **222**, 414–425.

[105] Schwoebel R L and Shipsey E J 1966, *Step motion on crystal surfaces*, J. Appl. Phys. **37**, pp 3682–3686.

[106] Shenoy V B and Freund L B 2002, *A continuum description of the energetics and evolution of stepped surfaces in strained nanostructures*, J. Mech. Phys. Solids **50**, 1817–1841.

[107] Shenoy V B, Ramasubramaniam A, Freund L B 2003, *A variational approach to nonlinear dynamics of nanoscale surface modulations*, Surf. Sci. **529**, 365–383.

[108] Shenoy V B, Ramasubramaniam A, Ramanarayan H, Tambe D T, Chan W-L and Chason E 2004, *Influence of step-edge barriers on the morphological relaxation of nanoscale ripples on crystal surfaces*, Phys. Rev. Lett. **92**, 256101/1–4.

[109] Spohn H 1993, *Surface dynamics below the roughening temperature*, J. Phys. I **3**, 69–81.

[110] Stangl J, Holý V, and Bauer G 2004, *Structural properties of self-organized semiconductor nanostructures*, Rev. Mod. Phys. **76**, 725–783.

[111] Stoyanov S 1991, *Electromigration induced step bunching on Si surfaces — How does it depend on the temperature and heating current direction?*, Jpn. J. Appl. Phys. **30**, 1–6.

[112] Stoyanov S 2000, *Scaling properties of step bunches formed on vicinal crystal surfaces during MBE growth*, Surf. Sci. **464**, L715–L718.

[113] Tanaka S, Bartelt N C, Umbach C C, Tromp R M and Blakely J M 1997, *Step permeability and the relaxation of biperiodic gratings on Si(001)*, Phys. Rev. Lett. **78**, 3342–3345.

[114] Tersoff J, Johnson M D and Orr B G 1997, *Adatom densities on GaAs: Evidence for near-equilibrium growth*, Phys. Rev. Lett. **78**, 282–285.

[115] Thürmer K, Reutt-Robey J E, Williams E D, Uwaha M, Emundts A, and Bonzel H P 2001, *Step dynamics in 3D crystal shape relaxation*, Phys. Rev. Lett. **87**, 186102/1–4.

[116] Tricomi F G 1985, *Integral Equations*, Dover, New York, NY.

[117] Uwaha M 1988, *Relaxation of crystal shapes caused by step motion*, J. Phys. Soc. Japan **57**, 1681–1686.

[118] Uwaha M and Watanabe K 2000, *Decay of an island on a facet via surface diffusion*, J. Phys. Soc. Japan **69**, 497–503.

[119] Villain J 1991, *Continuum models for crystal growth from atomic beams with and without desorption*, J. Phys. I **1**, 19–42.

[120] Vvedensky D D, Zangwill A, Luse C N and Wilby M R 1993, *Stochastic equations of motion for epitaxial growth*, Phys. Rev. E **48**, 852–862.

[121] Vvedensky D D 2004, *Multiscale modeling of nanostructures*, J. Phys.: Condens. Matter **16**, R1537–R1576.

[122] Weeks J D, Liu D-J, and Jeong H-C 1997, *Two-dimensional models for step dynamics* in Dynamics of Crystal Surfaces and Interfaces, ed. Duxbury P and Spence T, Plenum, New York, NY.

[123] Xiang Y 2002, *Derivation of a continuum model for epitaxial growth with elasticity on vicinal surface*, SIAM J. Appl. Math., **63**, 241–258.

[124] Zhao T, Weeks J D, and Kandel D 2004, *Unified treatment of current-induced instabilities on Si surfaces*, Phys. Rev. B, **70**, 161303/1–4.

[125] Zhao T, Weeks J D, and Kandel D 2005, *From discrete hopping to continuum modeling on vicinal surfaces with applications to Si(001) electromigration*, Phys. Rev. B **71**, 155326/1–9.

Zhao T and Weeks J D 2005, *A two-region diffusion model for current-induced instabilities of step patterns on vicinal Si(111) surfaces*, Surf. Sci. **580**, 107–121.